DSE - Small Satellites Constellation for Earthquake Precursors

Designing a System of CubeSats to Search for Indicators of Oncoming Earthquakes

H.E. Bayer	4232569	A.S. Nevinskaia	1520237
B. Kool	4270738	S. Polydorou	4355903
J.C. Maene	4371275	C.M. Ricke	4367758
C.P. Marsman	4269918	C.E.I. Vakaet	4353099
Y.L. Neuteboom	1513079		

Final Report

Design Synthesis Exercise

Picture taken from: https://s-media-cache-ak0.pinimg.com/originals/5d/d1/ea/5dd1eaf0f196927ca157a2be940039ca.jpg

TUDelft

Aerospace Engineering

July 4, 2017

Small Satellites Constellation for Earthquake Precursors

Final Report - Version 2.0

by

H. E. Bayer, B. Kool, J. C. Maene, C. P. Marsman, Y. L. Neuteboom, A. S. Nevinskaia, S. Polydorou, C. M. Ricke, C. E. I. Vakaet

In Partial Fulfillment of the Requirements for the Degree of

Bachelor of Science
in Aerospace Engineering

at the Delft University of Technology,

Version	Date	Changes
1.0	23-06-2017	First draft version
1.1	28-06-2017	Implement feedback by tutor and coaches
2.0	04-06-2017	Implement feedback from peer reviews

Tutor: Dr. A. Menicucci,   TU Delft/SSE
Coaches: S. R. Kadathanad ,   TU Delft/AS
           P. J. Denissen,   TU Delft/NovAM

TUDelft Delft
University of
Technology

PREFACE

This document is the final report of the Small Satellites Constellation for Earthquake Precursors project in partial fulfilment of the requirements for the Design Synthesis Exercise (DSE) of the Faculty of Aerospace Engineering at the TU Delft. The report presents a design of a space mission with the objective to monitor the earth ionosphere to search for early warnings of major earthquakes, in which design choices are critically justified. It is the last of four reports written to document the design process of this mission. The previous reports are a project plan, baseline report and midterm report. The team would like to thank Dr. A. Menicucci for her professional advise and providing an answer to all questions. Also, the team would like to thank P. J. Denissen and S.R. Kadathanad for their assistance and guidance. The help of both tutor and coaches was indispensable during the design process. Likewise the team is grateful for Prof. P. Picozza's and his colleague professor L. Conti's, expert advise which provided great value. Furthermore, the team would like to acknowledge the valuable input given by J. Bouwmeester, F. Capogna, K. Kumar, J. Laifr, M. Langer, E. Mooij, P. Nielsen, A. Smith, S. Speretta, P. Sunderamoorthy, M. Uludağ , B. Zandbergen and the professionals from Hyperion and ISIS.

Delft, June 2017

CONTENTS

ABBREVIATIONS AND ACRONYMS

ADCS	Attitude Determinations & Control Subsystem		MISSE	Materials International Space Station Experiment
ACS	Attitude Control System		mNLP	Multi-Needlde Langmuir Probe
ACU	Array Conditioning Unit		MPPT	Maximum Power Point Tracker
ADS	Attitude Determination System		MTTF	Mean Time To Failure
AOP	Argument Of Perigee		N/A	Not Applicable
BCT	Blue Canyon Technologies		NASA	National Aeronautical and Space Administration
CAD	Computer Aided Design		NEN	Near Earth Network
C&DH	Command and Data Handling		NHB	NASA Handbook
COM	Communications		NOP	Nitrous Oxide Propane
COTS	Commercial Off The Shelf		NSS	New Space System
DOA	Dead-On-Arrival		OBC	On Board Computer
DoD	Depth of Discharge		OBDH	On Board Data Handling
DSE	Design Synthesis Exercise		PCB	Printed Circuit Board
EOL	End of Life		PID	Proportional-Integral-Derivative
EPD	Energy Particle Detector		PNZ	Percent Non-Zero
EPIC	Earthquake-Precursors-Ionospheric-Constellation		POCC	Payload Operations Control Centre
EPS	Electrical Power System		PSLV	Polar Satellite Launch Vehicle
ESA	European Space Agency		RAAN	Right Ascension of the Ascending Node
FFD	Functional Flow Diagram		RPA	Retarding Potential Analyser
GA	Genetic Algorithm		S/C	Spacecraft
GENSO	Global Educational Network for Satellite Operations		SF	Spacraft Fixed
GEO	Geosynchronous Orbit		SRP	Solar Radiation Pressure
GN&C	Guidance, Navigation and Control		SOCC	Satellite Operations Control Centre
GPS	Global Positioning System		SST	Space Surveillance and Tracking
ID	Identification Number		STELA	Semi-analytical Tool for End of Life Analysis
INMS	Ion-Neutral Mass Spectrometer		STK	Systems Tool Kit
ISC	International Seismological Centre		STK	Stakeholder
ISO	International Standardisation for Organisations		SWOT	Strengths, Weaknesses, Opportunities and Threats
ITAR	International Traffic in Arms Regulations		TA	True Anomaly
ITU	International Telecommunication Union		TDRSS	Tracking and Data Relay Satellite System
LAIC	Lithosphere-Atmosphere-Ionosphere Coupling		TT&C	Telemetry, Tracking & Command
LEO	Low Earth Orbit		T&V	Testing and Validation
LP	Langmuir Probe		TCS	Thermal Control System
MAI	Maryland Aerospace Institute		TU Delft	Delft University of Technology
MASTER	Meteoroid and Space Debris Terrestrial Environment Reference		UHF	Ultra High Frequency
MCC	Mission Control Centre		UV	UltraViolet
MEMS gyro	Microelectromechanical Systems Gyroscope		V&V	Verification and Validation
MLE	Mean Likelihood Estimation		VHF	Very High Frequency

LIST OF SYMBOLS

Symbol	Definition	Units & Constants
a	Semi-major axis	km
a	Apogee of orbit	m
a	Albedo Factor	-
A	Frontal area of the CubeSat	m^2
A_{eff}	Effective area	m^2
A_r	Ram area	m^2
A_{surf}	Total radiating surface of the spacecraft	m^2
c	Speed of light	m/s
C_0	Cost of the first product	€
C_D	Drag coefficient	2.2
C_n	Cost of the n-th product	€
$cp_a - cm$	Distance between centres of aerodynamic pressure and mass	m
$cp_s - cm$	Distance between the centres of solar radiation pressure and mass	m
D	Residual dipole moment	Am^2
D	Magnetic dipole	Am^2
e	Eccentricity	-
e	Error signal - difference between spacecraft attitude and the desired one	-
E	Energy stored	Wh
E	Eccentric anomaly	rad
E	Young's modulus of elasticity	Pa
F	Relative space between satellites in adjacent planes	-
F	Thrust force	N
g	Gravitational acceleration of Earth	9.81 ms^{-1}
h	Orbital height	km
h	Angular momentum stored by rotational objects	rad/s
$h_{a,store}$	Reaction wheel momentum storage capacity for meeting the pointing accuracy	Nm
$h_{d,store}$	Reaction wheel momentum storage capacity for disturbance torque resilience	Nm
H_c	Angular momentum	kgm^2/s
i	Inclination	rad
I	Moment of inertia	kgm^2
I_{sp}	Specific impulse	s
J_2	Second dynamic form factor of Earth	$1.08262668 \cdot 10^{-3}$
J_a	Albedo radiation	W/m^2
J_p	Planetary radiation	W/m^2
J_s	Direct solar radiation	W/m^2
k	Total number of operational satellites	-
K_d	Derivative gain	-
K_i	Integral gain	-
K_p	Proportional gain	-
L	Learning curve coefficient	0.85
L	Length of structural member	mm
m	Mass	kg
m	Minimum number of required operational satellites	-
m_0	Initial vehicle mass	kg
m_p	Propellant mass	kg
M	Mean anomaly	rad
M	Magnetic constant	$7.8 \cdot 10^{15}$
M_0	Mean anomaly at epoch	rad
M_w	Earthquake intensity	-
n	Total number of swarm satellites	-
N	Amount of random solutions	
p	Reliability of one CubeSat	-
P	Number of equally spaced planes in Walker constellation	-
P	Generated power	W
P	Orbital period	s
P_i	Probability of being in the ith state	-
P_{nom}	Nominal power	W
P_{sa}	Solar power generated during daylight	W
PNZ	Percent Non-Zero	-
q	transient matrix element	-

q_k	k_{th} quaternion	-
$\dot{q}_k$	k_{th} quaternion differentiated with respect to time	1/s
Q	Heat radiation	W
R	Reliability	-
r_1	Radius of the departure orbit	km
r_2	Radius of the arrival orbit	km
R_e	Radius of the Earth	6378.137 km
R_{orbit}	Orbit radius of satellite	km
t	Time	s
t_0	Epoch reference time	days
T	Temperature	K
T	Total number of satellites in Walker constellation	-
T	Torque	Nm
T_a	Atmospheric drag torque	Nm
T_d	Time spent in daytime	s
T_e	Time spent in eclipse	s
T_D	Maximum occuring disturbance torque	Nm
T_g	Gravity gradient components in the respective x, y and z directions in the spacecraft reference frame	
T_m	Magnetic torque	Nm
T_s	SRP torque	Nm
v	Velocity	ms^{-1}
V	Orbital velocity	m/s
z_i	Mean time spent in the ith state until absorption	days
α	Weibull shape parameter	-
α	Absorptivity	-
α_c	Coefficient of thermal expansion	1/K
β	Weibull shape parameter	-
ϵ	Emittance	-
ϵ	Strain	-
δ	Elevation angle	°
δ_T	Change in length due to thermal expansion/contraction	mm
Δv	Impulse needed to perform a manoeuvre	ms^{-1}
η	Weibull scale parameter	-
η	Efficiency	-
η_e	Path efficiency during eclipse	-
η_d	Path efficiency during daytime	-
η_T	Temperature efficiency	-
γ	Maximum angle before elevation angle is too low	°
λ	Failure rate	1/year
λ	Unitless function off the magnetic latitude	-
μ	Gaussian mean	-
μ	Standard gravitational parameter of the Earth	398,600 km^{3}s^{-2}
ρ	Atmospheric density	kgm^3
θ	Longitude	°
θ	True anomaly	rad
θ	Weibull scale parameter	s
θ	Rotational angle	rad
θ_a	Pointing accuracy	rad
ω	Argument of perigee	rad
ω	body angular velocity	rad/s
$\dot{\omega}$	rate of change of body angular velocity	rad/s^{-2}
ω_e	Central body's rotation rate of Earth	rad/s
Ω	Right ascension of ascending node	rad
$\dot{\Omega}_p$	Nodal precession rate	rads^{-1}
ϕ	Angle of incidence of solar flux	rad
ϕ	Longitude	°
Φ	Solar constant	-
σ	Stefan-Boltzmann constant	5.67·10^{-8} Wm^{-2}K^{-4}
σ	Stress	N/m^2
σ^2	Gaussian variance	-

SUMMARY

Earthquakes are natural geophysical phenomena. Their occurrence is caused by the release of natural stresses which build up in the Earth's uppermost mantle and crust (lithosphere), by relative movement of tectonic plates. When earthquakes affect human populated areas, they cause devastating disasters. On the 26th of December 2004, an earthquake hit the sea bed of the Indian Ocean with a magnitude of $M_w = 9.2$ on the moment magnitude scale, causing the Boxing Day Tsunami. This earthquake was documented as one of the deadliest natural disasters in recorded history, killing 280,000 people in 14 countries, and causing a crippling economic impact of over 15 billion USD. This is one of many examples of the devastating natures of earthquakes.

In the past centuries people have attempted to predict earthquakes, without success. Earthquake precursors are still not fully understood, yet in the recent years many improvements have been made since it has become known that the build up of earthquakes causes perturbations in the ionosphere. This connection is known as the lithosphere-ionosphere coupling. As such, space technology emerges with a large potential for the study of this lithosphere-ionosphere coupling. In the past 2 decades, several satellites have embarked on the mission to monitor the perturbations in the ionosphere and link them to the occurrence of earthquakes. One such example is the DEMETER satellite mission launched in 2004. These missions have all entailed the use of a single satellite or at most two satellites in formation flight. This has many limitations such as the coverage area of earthquake zones. For this reason, a constellation of small satellites is proposed to globally monitor the perturbations in the ionosphere, thereby providing an innovative solution for precursors of large earthquakes ($M_w > 7$).

In addition, the feasibility of such an earthquake precursor system using a satellite constellation, has been positively indicated by the DEMETER mission. Even more so, a small satellite constellation (consisting of CubeSats) would provide a low-cost and highly available system. Thus, a team of nine aerospace engineering students is challenged to design a CubeSat constellation for earthquake precursors in 10 weeks. The mission shall be referred to as the Earthquake-Precursors-Ionospheric-Constellation (EPIC), with the following mission statement:

> *'Provide a design for an early warning system for earthquakes, using a constellation of small satellites monitoring the earth ionosphere for earthquake precursors'.*

The purpose of this final technical design report is to provide detailed design of all CubeSat components and discuss all related analysis. The final layout and integration will be established and optimised. Furthermore, the overall mission overview and the design process are covered. After finishing this final design, the following mission objective was achieved:

> *'Make a design for a small satellites constellation mission which monitors the earth ionosphere to search for early warnings of major earthquakes, by nine students in ten weeks - DSE group 2 spring 2017'.*

The final technical design is the completing report and a direct follow-up of the midterm report, which selected the most suitable mission concept. Prior to that, the team was organised and performed a requirement study and concept identification during the project kick-off and baseline review respectively. As for project management and organisation, this report contains an explanation of the whole project design process and development logic. In addition, a look is taken into future actions that have to be performed to execute the mission. This is supported by a Gantt chart, supplying a chronological and specific way forward. The mission concept itself, discussed in detail in the midterm report, is elaborated upon further. For the concept, first a market research is performed to test if the mission is valuable, after which all the CubeSat subsystems are analysed. Further, the lay-out and configuration determines how these subsystems are integrated.

Before an engineering design mission is advanced to the detailed design phase, a market analysis should show a valid, profitable reason for the development. Global economic losses due earthquakes are estimated to amount to at least 38 billion USD annually, for which a precursors system could have a big impact. So, a reliable earthquake warning system can be worth multiple billions USD. Not to forget is that a warning system could prevent thousands of deaths that occur yearly, so a clear reason exists from a market point of view to develop this mission. However, the mission concept still needs to be proven, thus the scientific community will serve as first customer of the design. For this reason, the EPIC mission focuses on obtaining high quality data, which can be used to get a better understanding of involved phenomena. After proof of concept, governments or large infrastructure companies will be targeted.

The first design problem tackled is the scientific background of earthquake precursor phenomena and the necessary payload. The scientific theory supporting earthquake prediction is the so called lithosphere-atmosphere-ionosphere coupling. Geophysicists have found that a few days before an earthquake, physical and chemical changes occur in the Earth's crust (lithosphere). Some of these changes can affect the upper part of the Earth's atmosphere (ionosphere), which can be measured by satellites. As explained in the midterm report, two CubeSats fly in formation in each orbital plane. Each group consists of two CubeSats with partially different payload and will measure these effects. All Cube-Sats are equipped with a magnetometer and dosimeter. An electric and ion-neutral mass spectrometer is applied for the first CubeSat in the formation, and a retarding potential analyser and energy particle detector for the second CubeSat.

The assigned payload can only be used to its full potential of collecting precursor data if the coverage is adequate. The coverage considered consists of the historical earthquakes of M_W. A swath width of 800km is applied around the epicentres. The earthquake frequency for each location is subsequently used to determine a weighted coverage map, given higher priority to earthquake sensitive areas. The re-visit time of this coverage map is set to four hours, with a 99% coverage criterion. Next, a multi-objective genetic optimisation is used to minimise the revisit time, while maximising the amount of CubeSats per formation. For the optimisation, Walker-Delta constellations are considered. The final constellation is concluded by the optimisation algorithm as a 55:6/6/2 Walker constellation at 520km altitude. In order to get the constellation operational, the CubeSats shall be launched in batches of twelve by the Electron rocket by Rocket Labs. Initially, two launches ensure that the constellation is deployed within 6 months. Natural perturbations are used to drift the CubeSats at different altitude and inclination, which limits the necessary delta-v budget to 235m/s.

Provided the payload and constellation configuration, all other subsystems can be designed. An important step in providing the earthquake early warning system is to ensure the collected scientific data is transmitted in time. The maximum data rate generated by payload is 4594bits/s, which is transmitted at least every twelve hours. For this, the KSAT ground station network in combination with a S-band communication link is demanded. The communication network is modelled to investigate possible discrepancies over time. The simulation concludes a maximum communication gap of less than twelve hours and a necessary memory size of 400Mbit. Together with the revisit time of four hours, earthquake precursor data is therefore always available within sixteen hours. Uplinking data of command or software updates happens through a separate ultra high frequency (UHF) link.

Another key subsystem supporting ionospheric data collection is the attitude determination and control system. The payload requires at least a pointing accuracy of 1° for optimal measurements. Firstly, all different operational modes during the mission operation are investigated for the necessary attitude performance. Next, the control hardware is sized to be capable of counteracting various disturbance torques, while keeping a pointing accuracy of 1°. Next, a commercial of the shelf active attitude determination and control system is chosen. However, a sufficient pointing accuracy can only be achieved during solar minimum. The CubeSat responses due to disturbances are also modelled in a simulation, confirming stability. A large disturbance is damped out in less than 60s usign the reaction wheels and faster than the orbital period using the magnetotorquers.

All subsystems should provide sufficient power to operate. The electrical power subsystem for each

CubeSat will be based on four deployable solar panels. Each solar panel is covered with GaAs triple-junction solar panels from AzurSpace. The angles at which these panels are deployed are optimised through simulation. Furthermore, two battery packs of 106.4Wh in total ensure sufficient power supply during eclipse time.

As discussed before, the constellation deployment requires a delta-v budget of at least 235m/s. In the midterm report, it is demonstrated that liquid propulsion can ensure low burn times to meet the required deploy time of six months. Keeping this in mind, a trade-off concludes that a commercial of the shelf liquid bi-propellant shall be adopted for the final design. Furthermore, a customised propellant tank is integrated in the design such that the total propellant mass is 0.88kg.

The next analysed subsystem is the structural design of the CubeSat. A standardised 6U CubeSat structure is adopted and subjected to an analytical and finite element, checking for static and vibrational stresses. The maximum loads are provided by the Electron launcher specification. Using the finite element method, maximum static stresses are found to be 582kPa, while maximum stresses occur at 709Hz for the vibrational case. These values are confirmed with the analytical approach and meet the requirement of the launcher. Furthermore, also thermal stresses are evaluated, not indicating any issues. However, for thermal stability, an organic white paint surface finish is required for the CubeSat.

The last phase of the subsystem design is the integration and lay-out of the final CubeSat. During design, all subsystems are designed within certain budgets, such as mass, volume, power,. . . The integrated design has a mass of 9.2kg, while the total power budget is 14.2W. Next, a manufacturing plan describes how the final assembly, testing and qualification of the CubeSats takes place.

After the subsystems are designed, all used engineering tools are verified and validated. Assumptions of each model representing a physical phenomenon are stated. Next, verification is performed on the models using unit tests on parts of the code and higher-level system tests. During the design of the subsystem, also risk and sustainability are driving framework of the design. After the CubeSat design, these are reviewed including a performance analysis.

The a risk analysis is performed to identify risks and specify a risk mitigation strategy. The likelihood and criticality of the mission risk are assessed and summarised in a risk map. Subsequently, measures are taken to mitigate these risks. Next, the reliability, availability, maintainability and safety are analysed. The reliability of the CubeSats is determined from an analysis of historical data. The constellation reliability of the CubeSat constellation is assessed on a global level, using Monte Carlo simulations and component level using a Markov model. Using redundancy, the constellation has a 90% probability of full lifetime availability.

During the system engineering process, considerable attention went into the sustainability of the EPIC mission. Essentially, sustainability ensures a balance between the economic, social and environmental aspects of a system. An important sustainable aspect is the extensive use of commercial off the shelf components, reducing the amount of resources wasted, hence increasing the sustainability. Similarly, the production and material selection for CubeSats in general is discussed. Moreover, the spacecrafts should de-orbit within 25 years at end-of-life. By simulating natural decay, it is found that the spacecraft will decay without any design changes for the proposed constellation.

Finally, several driving design parameters such as cost budget, orbital height and solar flux are varied for the final design to understand the quality of the final design and possible design flaws. For example, an important conclusion discovered is that the mission should be operating during solar minimum to enhance scientific yield and ensure stability. Furthermore, if the mission altitude or inclination is altered too much, the deployment and decay times do not meet the requirements. Considering aforementioned reasons, it can be concluded that the design is valid for the mission purpose and is correctly iterated.

1

INTRODUCTION

Earthquakes are among the most dangerous natural phenomena. Every year earthquakes cost lives and cause damage. In an attempt to prevent these disasters, scientists have researched the prediction of earthquakes for many years.

More recently, space missions have been used to prove a link between the changes in electric and magnetic fields in the ionosphere and the occurrence of earthquakes. The ionosphere is a part of Earth's atmosphere, that starts at approximately sixty kilometres and goes up to an altitude around thousand kilometres. In the days before an earthquake scientist have found physical and chemical changes in the Earth's crust. Further on, this crust will be referred to as the lithosphere. Some of these changes could affect the ionosphere and measurements at that altitude can be done by satellites. The monitoring and comparison of the changes in the lithosphere and ionosphere can be used to predict earthquakes.

However, seismically active regions have to be monitored for a larger amount of time to provide a reliable precursor system. A system is needed that can provide reliable measurements of the ionosphere with a greater coverage. To fulfil this need, a team of aerospace engineering students is asked to design a mission as part of the DSE. This mission will be referred to as EPIC. The mission statement of EPIC is:

> 'Provide a design for an early warning system for earthquakes, using a constellation of small satellites monitoring the earth ionosphere for earthquake precursors'.

The purpose of this final report is to present a preliminary mission design, in which design choices are critically justified. Also, the performance of the design is evaluated to determine the feasibility and identify possible weaknesses in the design. This can be reckoned with in the detailed design phase of the mission. This final report is also meant as an outline for future research in the field of earthquake precursor constellations, which can advance science. An other purpose of the report is to provide confidence in the design by professional use of project management tools and displaying systems engineering skills. Since this report is part of the DSE of the TU Delft (Delft University of Technology), one should also take into account the educational purpose of this project. Nine students should not only gain knowledge on space missions and earth observation, but also improve their project management and system engineering skills. Lastly, the team would like to have a positive impact on the world, by providing a solid base for earthquake precursor missions and hopes to see a decrease in earthquake victims in the future. All this is done in order to achieve the project objective. The project objective is defined as:

> 'Make a design for a small satellites constellation mission which monitors the earth ionosphere to search for early warnings of major earthquakes, by nine students in ten weeks - DSE group 2 spring 2017'.

This final report starts off with a mission overview, Chapter 2, in which the scientific principles of earthquake precursors are presented. Also, this chapter contains a market analysis and a functional analysis. These three parts are the fundamentals on which the design is based. With this information the project management and system engineering can be introduced. This is done in Chapter 3. This chapter consists of a project design & development logic, the Gantt chart and a section on the logistics and external dependencies of the mission. In Chapter 4 the resource allocation can be found.

With all this in mind, the design of the constellation is done. In Chapter 5 the constellation and all its aspects are treated. This is done chronologically, starting with the launch of the CubeSats. Next,

in Chapter 6 the propulsion system, a very innovative concept for CubeSats, is discussed. The EPIC CubeSats are equipped with a propulsion system to make sure the necessary Δv can be provide. The following chapter, Chapter 7, the payload selection is done. In this chapter it is decided what instruments will be used and in what configuration these sensors will be implemented.

After a payload is chosen, the subsystems that support the spacecraft can be selected. First the attitude determination and control subsystem (ADCS) is treated in Chapter 8. This is followed by the telecommunications subsystem in Chapter 9. The next subsystem is the electrical power system (EPS) and can be found in Chapter 10. In this chapter both the solar arrays and the batteries are designed. Also, the EPS is visualised using block diagrams. After the EPS, the on-board data handling subsystem is discussed, which is one of the most important components of the CubeSat and can be found in Chapter 11.

This is followed by the thermal control subsystem. A thermal analysis of the spacecraft (S/C) is done, including thermal stress, which are closely connected to the material & structural characteristics. The thermal control subsystem can be found in Chapter 12 and the material & structural characteristics can be found in Chapter 13.

After all the subsystems are chosen and the lay-out of the satellites is presented. This is done for two types of CubeSats with different configurations and can be found in Chapter 14. Next to the CubeSats, other mission aspects need to be considered as well. First the technical risk management is treated. In this chapter, Chapter 15 the critical subsystems identified in order to make a risk map and do risk mitigation. The following chapter, Chapter 16, focuses on the reliability, availability, maintainability and safety (RAMS) analysis. These are discussed in this order.

Once the design of the EPIC mission has been presented, a plan has to be made to produce the CubeSat. This is presented in Chapter 17. Since the production goes hand in hand with the sustainable development strategy, the chapter on sustainability follows the production plan. This can be found in Chapter 18.

At this point the whole mission has been described, hence it should be verified that the design fits the budgets and to what extend the design complies to the requirements. This is done in Chapter 19.1. In this chapter a sensitivity analysis is done as well, in order to understand how certain parameters influence the design.

The report closes off with the conclusion and recommendations, in which is discussed to what extend the purposes of the report are realised. Also a summary of the findings and recommendations for future work are presented. Appendix A.1 gives the spacecraft system and astrodynamic characteristics of the EPIC mission.

2

MISSION OVERVIEW

This chapter covers the mission overview. Elements included are the scientific background of the mission, the market analysis and the functional analysis. Section 2.1 describes the scientific principles of earthquake prediction. Section 2.2 derives the effect of the market on the mission design. Lastly, Section 2.3 shows the visualisation of the activities performed during the mission.

2.1. IONOSPHERIC PRECURSORS OF EARTHQUAKES PRINCIPLES

In this section, the basic principles of earthquake prediction, required to select the sensors used in the project, are discussed. In the first three paragraphs the basics of seismology are discussed. In the next paragraph the earthquake precursors in the lithosphere are presented. The last paragraph describes the effect of the lithospheric precursors on the ionosphere.

An earthquake can be defined as a rupture in the Earth's crust [1]. These ruptures occur when the deformation of the crust exceeds its mechanical strength. The deformation is caused by crustal dynamics, also known as plate tectonics. Locally, the rupture occurs at faults, existing discontinuities from previous crustal movement [2]. The intensity of earthquakes can be determined using different scales. In this project, the scale first proposed by Kanamori [3] is used.

Early earthquake prediction methods focused on the periodicity of earthquakes and the seismic cycle [1]. However, this approach has not been proven to be reliable or accurate enough for relevant earthquake predictions. Instead, physical and chemical changes within the Earth's crust need to be considered. These changes are particularly pronounced during the thirty days before an earthquake. In this period, crack formation accelerates exponentially and an earthquake will happen in the near future.

The area in which deformation takes place prior to an earthquake, is called the earthquake preparation zone. The Lithospheric Earthquake precursors are generated in this zone. The radius of the zone is directly proportional to the magnitude of the earthquake (M_w). For the estimation of the size of this area, multiple methods are available. Most commonly the method proposed by Dobrovolsky is used [4]. The physical phenomena preceding an earthquake propagate from the crust to the atmosphere and ionosphere. The affected area in the ionosphere is assumed to be located above the surface projection of the earthquake preparation zone.

Scientific research has identified multiple earthquake precursors in the lithosphere. The behaviour of these precursors is well understood and described. Two types of precursors are of particular interest, as they affect the ionosphere. The first type comprises the concentration variations of the geochemical precursors such as radon, CO_2, aerosols and helium-enriched nitrogen. Radon is especially interesting, since it is a noble, radioactive gas [5]. It therefore does not react with other components and can easily be detected due to its beta-radiation. The second type is related to variations in the electromagnetic field. These variations are large and its propagation affects the electromagnetic field in the ionosphere.

The coupling between lithospheric and ionospheric precursor variations is called the Lithosphere-Atmosphere-Ionosphere Coupling (LAIC). LAIC has been proven to exist. However, no consensus has been reached about the exact method (model) [6]. Hence, the project will only focus on measuring parameters which have been proven as earthquake precursors. These include variations in plasma [7][8][9], particles, ionospheric structure [10][11] and electromagnetic field [12][13]. The measurements of these parameters are however influenced by natural disturbances such as solar flares, volcanic activity and the

weather. It is therefore believed that measurements from space will never provide enough certainty for reliable prediction. Instead the data should be used together with data from other sources. The scientific community expects that, by performing statistical analysis on the combined parameters and by using enough data, predictions will be sufficiently reliable.

2.2. MARKET ANALYSIS

An engineering product is only valuable if it is targeted at a considerably profitable and preferably growing market. Furthermore, it is desirable that the market is not saturated by strong competitors and that the market power is low, such that the market is not dictating the price. The following market analysis aims at describing the market and at identifying the most beneficial segment for EPIC. A SWOT and a Porter's five forces analysis will be conducted to support the targeted segment. To conclude, the effect of the market on the mission design is discussed.

2.2.1. MARKET DEFINITION, SIZE AND TRENDS

In this analysis, the market is defined as the collection of organisations who desire and are able to pay for scientific data on ionospheric properties such as electric and magnetic field fluctuations. This definition includes customers interested in the data for all purposes, so not only for an earthquake warning system, but also for weather and volcanic activity analysis. The system designed in this DSE is limited to generating ionospheric precursor data only. However, for the market analysis, the whole system of earthquake prediction is considered. This system combines the ionospheric precursors with ground survey data to make predictions about impending earthquakes.

Earthquakes have devastating economic and humanitarian effects around the globe. A recent study has estimated that the yearly global economic loss due to earthquakes ranges (± 1 standard deviation) between 38 and 50.2 billion USD [14]. By having an early warning system it is believed that a significant amount of these losses can be avoided. For example, in 2004 an earthquake in the Indian Ocean caused one of the deadliest tsunamis ever, resulting in 280 000 killed persons and a 15billion USD economic impact. Hence, a reliable earthquake warning system can be valued well into billions of dollars.

As for the market growth, it is estimated that the frequency of earthquakes has not increased in the past hundred years [15]. The market is however expected to change due to increasing population density and advancements in (more and earthquake resistant) infrastructure. In particular ageing infrastructure, which is a notorious problem in first world countries, can pose serious risks when earthquakes occur [16]. Moreover, the market is currently not addressed by anyone, which creates a promising opportunity.

Finally, it is also important to note the growth within the remote sensing market. Currently, the remote sensing market is valued at 8.9billion dollars, with a compound annual growth rate of 9.3% over the coming five years [17]. This indicates the interests of investors in the field of remote sensing, which will ease funding of the program. Furthermore, it is expected that the cost of operations will reduce over time as the market of remote sensing grows.

2.2.2. MARKET SEGMENTATION

In this section the first potential customers are listed and put into segments.

- **Governments:** Governments are responsible for the safety of its citizens. Hence, it is believed that governments around the globe have interest in an earthquake prediction system. Furthermore, the economic cost of earthquakes to the governments is significant in terms of infrastructure damage. Earthquake impact could be mitigated with an early warning system. This interest can be exemplified by the funding of space missions such as DEMETER by the french government.

- **Large infrastructure companies:** It is expected that economic losses of large infrastructure companies could be reduced with an earthquake prediction system. For example, pipelines could be emptied, reducing the potential contamination due to spillage. Next to that, the maritime industry and nuclear power plants can benefit by preparing for potential tsunamis.

- **Insurance companies:** Insurance companies can create a competitive advantage by better protecting the insured goods against an earthquake.
- **Scientific community:** The scientific community can use the data from the sensors to improve atmospheric models. Likewise, the data can be used to further the understanding of atmospheric coupling to seismic events.

From the list of customers, two customer segments are derived. The first segment is a combination of government, infrastructure and insurance companies. This segment needs earthquake predictions at a certain location. The predictions should be as early, cheap, accurate and reliable as possible. Here, accuracy is defined as the detectable magnitude of an earthquake and reliability as a combination of the probability of a false-negative or false-positive prediction and the ratio of these values. To optimally cater to this market a trade-off between these four parameters should be performed. A more detailed market analysis is required to better understand the relative importance of each parameter. However, this is beyond the scope of this report.

The second customer segment is the scientific community. This segment is often underfunded and is therefore less commercially interesting. Nevertheless, this market segment has different advantages. The scientific community increases the understanding of earthquake precursors, leading to better performance and understanding of the earthquake prediction system. Therefore, the scientific community needs extensive sensor data as well as relevant housekeeping data of the satellite.

2.2.3. STRENGTHS, WEAKNESSES, OPPORTUNITIES AND THREATS ANALYSIS

The strengths, weaknesses, opportunities and threats (SWOT) analysis, as depicted in Table 2.1, serves as an identifier of competitive advantages and necessary points of improvement. The lesson learned from the SWOT analysis is that sufficient resources have to be spent for improving the reliability of the CubeSat constellation. Besides, the currently inadequate knowledge of the scientific community on LAIC is an obstacle that is difficult to tackle. On the other side, a high opportunity is the powerful boost if the earthquake warning concept can be proven during the EPIC mission. Next to that, by using CubeSats, the current CubeSat community and space agencies shall likely gain interest in the mission and be of support.

2.2.4. PORTER'S FIVE FORCES ANALYSIS

The five forces or Porter's analysis is a frequently used tool in determination the business strategy development [18]. From this, the competitiveness of the industry together with the attractiveness of the proposed concept is assessed.

- **Threat of new entrants**: New entrants that want to measure ionospheric data need a considerable amount of resources and time to create a space mission. However, they may come up with new substitute products. Currently, no possible substitutes are known, so new entrants are considered to have a low market power.
- **Threat of substitute products or services**: There are several methods to observe oncoming earthquakes. Some earthquake prediction methods - like abnormal animal behaviour or earthquake foreshocks - cannot serve as a reliable predictor[1]. Substitutes are therefore evaluated to have low market power.
- **Bargaining power of buyers**: Currently, no other ionospheric satellite data can be provided. Initially, the bargaining power of the buyers will be high due to the risk of investment. The market power of the EPIC mission will increase as successful predictions are made.
- **Bargaining power of suppliers**: data gathered by EPIC only becomes valuable for earthquake prediction when combined with ground stations data. This interdependence reduces the market power of the constellation. Suppliers providing the satellite components have a medium market power. Only a few suppliers exist on the current market, but if they set the price too high, the team can choose to produce the components themselves. On the contrary, satellite launchers have higher bargaining power, since a custom launcher is unfeasible.

---

[1] http://www.yourarticlelibrary.com/earthquake/earthquakes-prediction-9-methods-to-predict-earthquake/13915/ [cited 27-05-2017]

Table 2.1: SWOT analysis on the group and project as a whole.

Strengths	Weaknesses
• Higher reliability (constellation) • Low costs (CubeSats) • Lower risk from redundancy and cheaper replacement • Highly motivated young team	• No proven concept of earthquake prediction using ionospheric data • Not all components are COTS available • Limited scientific understanding of ionospheric earthquake precursors • Lower reliability of CubeSats • Lower measurement accuracy
Opportunities	**Threats**
• High interest after proof of concept • Potential cooperation with space agencies • Innovative use of constellation for earthquake prediction • Extension of constellation for lower revisit times • Growing interest for remote sensing data	• Failure of one or more satellites • Limitations of earthquake precursors • Lack of potential customers and customer segments • Limited public funding and investment • Contributing to space debris

• **Rivalry among existing competitors**: Current missions collecting ionospheric data are in the conceptual or preliminary design phase[2]. No funding is found since the return for investors is too risky as the ionopheric effects of earthquakes are not yet fully scientifically proven. QuakeSat is the only launched mission and has no successors.

2.2.5. EFFECT OF THE MARKET ON THE MISSION DESIGN

From the market analysis several observations can be made which are taken into account for the design. Firstly from Section 2.2.1, it can be seen that the potential value of an earthquake prediction system is considerable. Therefore, a large budget can be devoted to such a system. From Section 2.2.2 it is found that the majority of the market is interested in complete, highly reliable earthquake predictions. From literature study it is found that this ionospheric earthquake prediction has not yet been proven feasible [19]. Therefore, at first, extensive research and testing is required in the field, proving the concept of a short term earthquake warning system.

For this reason, the mission focuses on providing the necessary data to the scientific community. Once the scientific understanding is sufficient, the constellation could expand and focus on effective earthquake predictions. As for funding, initially the capital will most likely come from the scientific community due to the involved risks. For that reason, the initial risks and investment costs need to be low. This is achieved by utilising mostly COTS components and by basing the design on experience of similar missions.

Finally in subsection 2.2.3, a table is provided with the strengths, weaknesses, opportunities and threats of the project. From this table important areas of focus for the design are identified. From subsection 2.2.4 it can be concluded that there is a low threat of new entrants, substitutes or rivalry. Attention

---

[2]`http://space.geocities.jp/SeismoSTAR/Missions.html` [cited 12-06-2017]

should instead be put on the buyers and suppliers which will have significant power over the mission design.

2.3. FUNCTIONAL ANALYSIS

"A function is a task or activity to be performed by people, equipment, hardware or software" [20]. In this section, two tools are used to visualise all functions the constellation should perform. The first tool is a functional flow diagram (FFD) which can be found in Subsection 2.3.1 and the second is a functional break-down diagram, which is found in Section 2.3.2. The numbering of both diagrams is done conform to each other.

2.3.1. FUNCTIONAL FLOW DIAGRAM

In order to visualise the chronological flow of activities during the mission, a FFD is made. The FFD for the EPIC mission can be found in Figure 2.1. Activities that take place at the same time are depicted parallel in the flow with an AND sign. Other actions depend on which choices will be made further on in the design process. At these points an OR sign is used to indicate alternative paths. Some parts of the system use a controlling loop to make sure values are between acceptable boundaries. If the values are acceptable, the path indicated with the letter G can be followed. If this is not the case, the path indicated with $\overline{G}$ will be followed.

The diagram is divided in three levels. At the top of the FFD, the top level functions are shown. These are the different phases of the mission, starting with the launch of the CubeSats and ending with the End of Life (EOL) approach. Every one of these functions can be split up in multiple functions that also should be performed chronologically, which form the level two functions. In case the level two functions consist of multiple tasks, these are depicted in the third level. The six main levels are shortly explained below.

- **1.0 Launch:** The satellites will be launched by an external launch contractor. After production and testing, the CubeSats will be transported to the launcher and will be inserted into a dispenser. Once the CubeSats are launched into space, the dispenser will eject them into the mission orbit.

- **2.0 Deploy satellite:** Once the satellite is in orbit, the first step is the detumbling of the S/C. Next, the booms and solar arrays are deployed, followed by the start-up of all other subsystems. With every part of the satellite in function, the constellation is ready for the half year deployment phase.

- **3.0 Deploy constellation:** In order to get the proper coverage of Earth, the satellites are distributed using drift caused by the second form factor of the Earth, or J_2-effect. Altitude is an important contributor to the drift rate, so to achieve different drift rates the satellites are transferred to higher and lower orbits using the propulsion system. During the deployment phase, commissioning is done. Also some ionospheric measurements can be performed, which will be continued in the next phase.

- **4.0 Acquire data:** The EPIC satellites are in orbit to perform their mission of searching for earthquake precursors. In the branch on data acquisition, the activities can be found that together describe the process of gathering and processing data on ionospheric changes.

- **5.0 Housekeeping:** One of the most vital functions of the spacecraft is housekeeping. Most subsystems are present in the S/C to support the task of performing the mission by obtaining data. These subsystem functions are visualised in the housekeeping part of the flow diagram.

- **6.0 End of life:** In case of failure of one of the EPIC satellites, it will continue orbiting as space debris. The constellation is designed such that all CubeSats will decay and burn in the atmosphere within the regulatory 25 years.

2.3.2. FUNCTIONAL BREAK-DOWN DIAGRAM

In a functional break-down the functions of a system are visualised in an AND-tree. This is a hierarchical structure in which the functions are not necessarily performed in chronological order. The functional break-down of the EPIC mission can be found in Figure 2.2. As can be seen, there are five main branches, that are labelled with the letters A to E. The functions that also appear in the FFD, Figure 2.1,
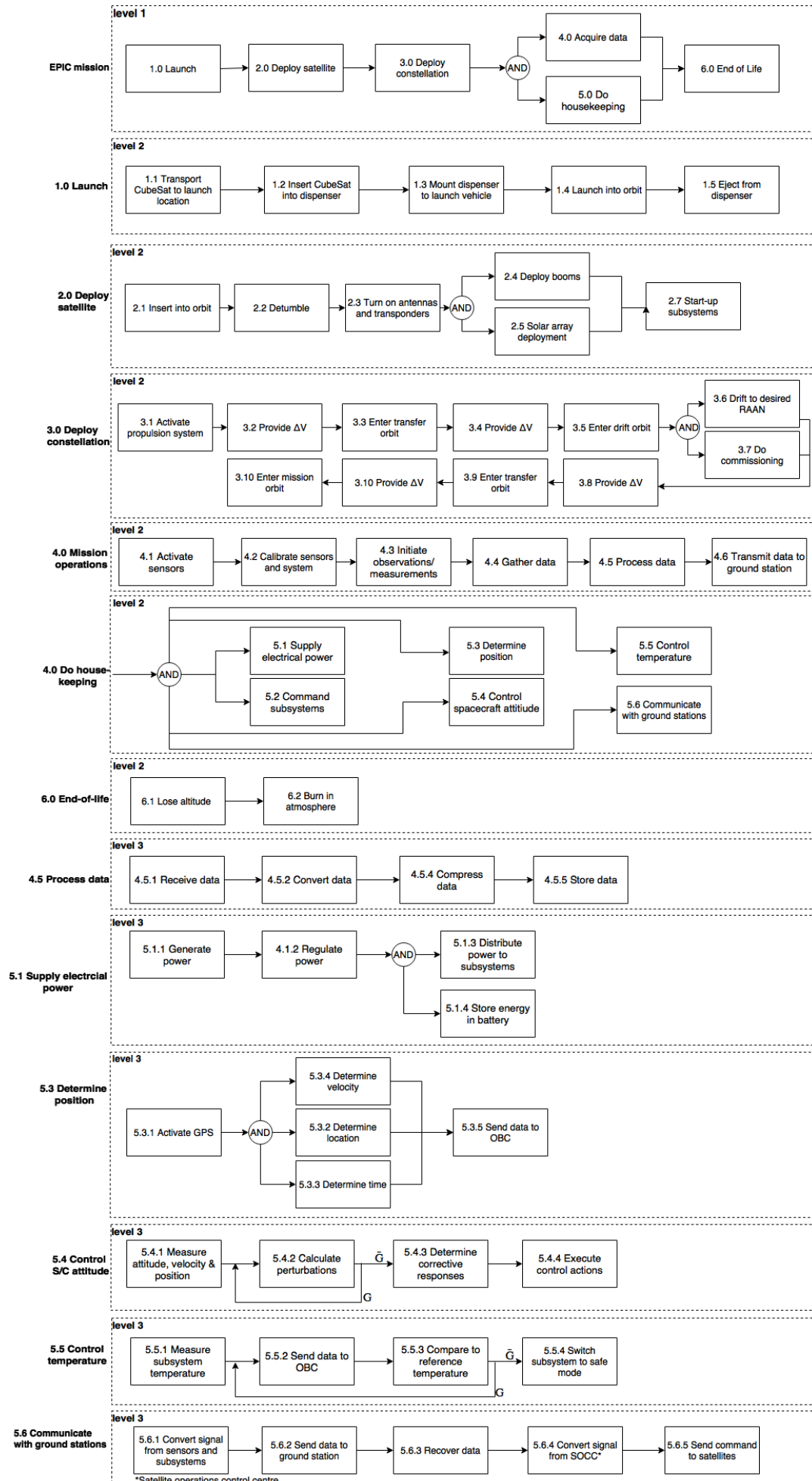
Figure 2.1: Functional flow diagram of the EPIC mission
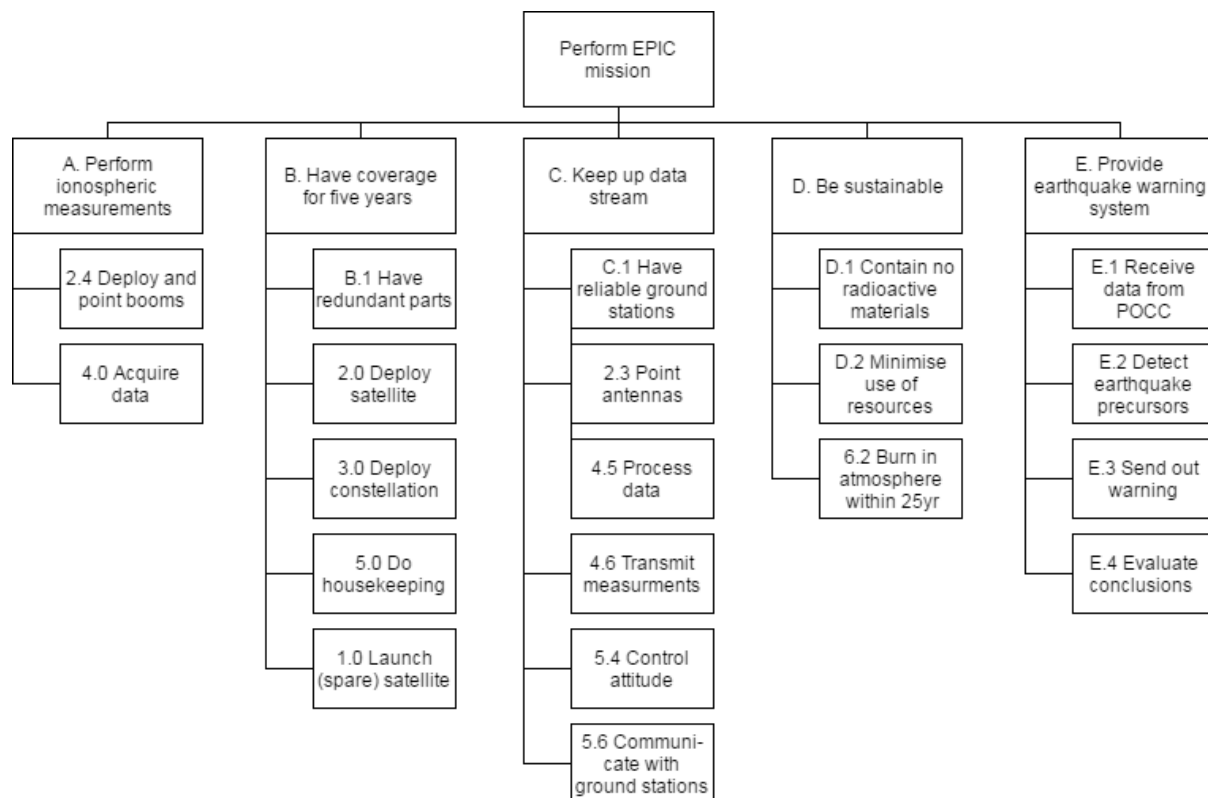
Figure 2.2: Functional break-down diagram of EPIC mission

are given the same numbering. Their sub-functions can be found in Figure 2.1 as well.

A short description of the five main branches can be found below.

- **Perform ionospheric measurements:** In order to perform the mission, measurements of earthquake precursors in the ionosphere are done. Therefore, instruments have to be pointed according to their pointing accuracy whilst data is acquired by these instruments. Both parts of this branch can also be found in the FFD.
- **Have coverage for five years:** A large part of the functions are executed to keep the constellation and the satellites functioning. In case of satellite failure, spares should be available.
- **Keep up data stream:** Exchange of data from the satellites to the ground stations should be done continuously. Measurements, housekeeping and location data are sent down, while the satellites receive commands when necessary by uplink.
- **Be sustainable:** Regulations regarding sustainability and space debris should be followed. Also safety of personnel during production and transport is taken into account.
- **Provide earthquake warning system:** Measurements in the ionosphere should be interpreted in order to comply with the mission statement.

3

PROJECT MANAGEMENT AND SYSTEMS ENGINEERING

This chapter focuses on the project management and systems engineering after the DSE. The first section, Section 3.1, shows the project design and the development logic, visualised by a flow chart. In Section 3.2 the Gantt chart is given, which provides a chronological overview of the mission, starting from the pre-DSE mission analysis & project definition and finishing at the end of the mission's operational life. The last section, Section 3.3 gives a chronological overview of the operations and logistics of the mission.

3.1. PROJECT DESIGN AND DEVELOPMENT LOGIC

Figure 3.1 shows the order of the activities that should be done during the post-DSE phase of the EPIC mission. During the design the concurrent engineering philosophy is used resulting in fast iterations. Concurrent engineering is the parallel running of separate phases during the product definition trajectory [21]. Furthermore, sustainability, risk mitigation and RAMS are taken into account through all stages of the design. To ensure accuracy of the design extensive verification and validation is performed on all programs and models used. Also, design decisions are checked with expert opinions and historical flight data.
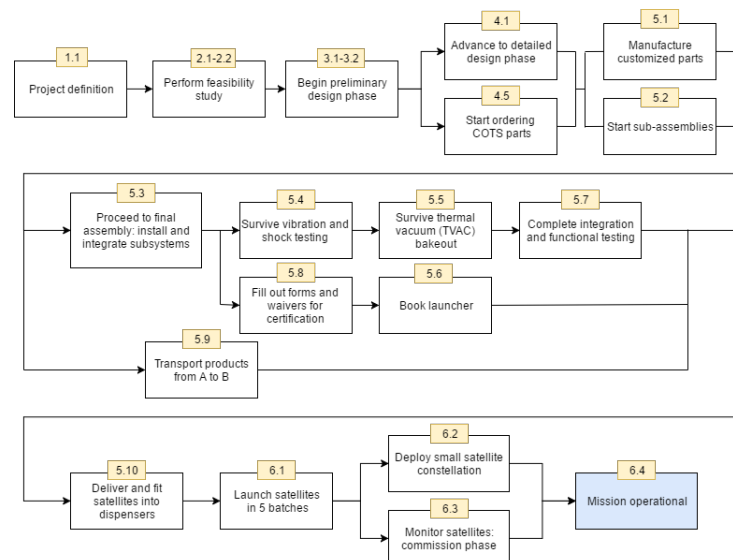
Figure 3.1: Flow chart of post-DSE phases of EPIC mission

3.2. PROJECT GANTT CHART

The Gantt chart included on page 13 provides an overview of the steps taken during, and after this DSE as elaborated in Section 3.1. Note that the mission operational time of five years is only partially shown, to have a clear overview on all the design stages. The design phases are based upon the design process of NASA [22]. Furthermore, for exact deadlines, a buffer is added; e.g. the booking of the launcher is uncertain, since it depends on previous design stages and qualification procedures.

ID		WBS	Task Name	Start	Finish
1		1	**Phase 0: Mission analysis, needs identification**	**Fri 24-3-17**	**Fri 21-4-17**
2		1.1	DSE project definition	Fri 24-3-17	Fri 21-4-17
3		2	**Phase A: Perform feasibility study**	**Mon 24-4-17**	**Tue 9-5-17**
4		2.1	DSE project plan	Mon 24-4-17	Fri 28-4-17
5		2.2	DSE baseline report	Mon 1-5-17	Tue 9-5-17
6		3	**Phase B: preliminary design definition**	**Wed 10-5-17**	**Fri 7-7-17**
7		3.1	DSE midterm report	Wed 10-5-17	Fri 2-6-17
8		3.2	DSE final report	Mon 5-6-17	Fri 7-7-17
9		4	**Phase C: Detailed design definition**	**Mon 10-7-17**	**Sat 30-6-18**
10		4.1	Post-DSE detailed design	Mon 10-7-17	Fri 25-5-18
11		4.2	Reserve bandwidth at ITU	Thu 6-7-17	Wed 18-10-17
12		4.3	Public relations campaign	Mon 18-9-17	Fri 29-12-17
13		4.4	Funding campaign	Mon 23-10-17	Fri 9-3-18
14		4.5	Order COTS parts	Thu 6-7-17	Wed 13-9-17
15		5	**Phase D: production, qualification**	**Mon 2-7-18**	**Fri 5-4-19**
16		5.1	Manufacture customised parts	Mon 2-7-18	Fri 28-9-18
17		5.2	Start sub-assemblies	Mon 1-10-18	Wed 24-10-18
18		5.3	Proceed to final assembly: integration	Thu 25-10-18	Wed 28-11-18
19		5.4	survive vibration and shock testing	Thu 29-11-18	Fri 21-12-18
20		5.5	survive thermal vacuum (TVAC) bakeout	Mon 24-12-18	Mon 28-1-19
21		5.6	Book launcher	Mon 6-8-18	Tue 16-10-18
22		5.7	Complete integration and functional testing	Tue 29-1-19	Wed 13-3-19
23		5.8	Fill out forms and waivers for certification	Fri 14-12-18	Wed 13-3-19
24		5.9	transportation of products	Mon 2-7-18	Fri 29-3-19
25		5.10	deliver CubeSats and put in dispensers	Mon 1-4-19	Fri 5-4-19
26		6	**Phase E: utilisation**	**Mon 8-4-19**	**Wed 8-1-20**
27		6.1	launch	Mon 8-4-19	Mon 8-4-19
28		6.2	constellation deployment	Tue 9-4-19	Thu 10-10-19
29		6.3	satellite monitoring: commission phas	Tue 9-4-19	Fri 31-5-19
30		6.4	mission operational	Fri 11-10-19	Wed 8-1-20

Project: FinalGanttChart
Date: Fri 23-6-17

Task		Project Summary	Inactive Milestone	Manual Summary Rollup	Deadline
Split		External Tasks	Inactive Summary	Manual Summary	Progress
Milestone		External Milestone	Manual Task	Start-only	
Summary		Inactive Task	Duration-only	Finish-only	

3.3. OPERATIONS AND LOGISTICS CONCEPT DESCRIPTION

In this chapter the operations & logistics concept description can be found. According to the Oxford dictionary, the definition of logistics is "the detailed coordination of a complex operation involving people, facilities, or supplies."[1] In the operations and logistics concept description this interaction is visualised in a flow diagram, Figure 3.2. The diagram is split up in three mission sections: pre-launch operations & logistics, mission operations & logistics and EOL operations & logistics. External factors are indicated with a bold lined box.

In the first section, the production process & operations up to the launch are shown. The process starts with the delivery of COTS parts. These should be assembled and integrated in the CubeSat structure. This should be done taking the safety of the personnel and the environment into account. The assembly and testing of the CubeSats will be done in the TU Delft clean room, hence this part of the process depends on this facility. Also, multiple tests are done, as prescribed by the launch company. Moving on, the CubeSats will be transported to the launch site, which is arranged by the launch company Rocket Lab. The pre-launch operations and logistics section of the mission closes off with the launch, when the CubeSats are launched and inserted in orbit.

The launch segment of the mission will be used for orbital maintenance by replacing broken satellites. In Chapter 16 the maintenance of the CubeSats is discussed. This way, the EPIC constellation can be functional for the required five years. Once in orbit, the satellites communicate with the mission control centre (MCC), the satellite operations control centre (SOCC) and the payload operations control centre (POCC). This is done via ground stations provided by the company KSAT. Space debris monitoring is done by the space surveillance and tracking (SST) division of the European space agency (ESA). Their data will be communicated to the EPIC team and in case of a risk of collision, actions can be taken.

After a CubeSat is shut down or broken, it will burn in the atmosphere within twenty five years. During the orbital decay, the CubeSat will be space debris and will be monitored accordingly.
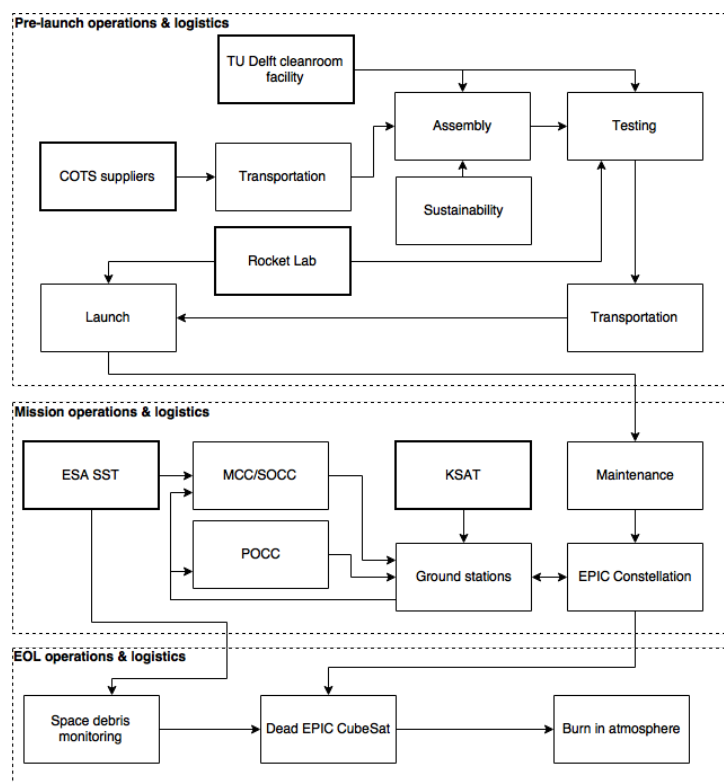

Figure 3.2: Operations and logistics concept flow diagram

---

[1] https://en.oxforddictionaries.com/definition/us/logistics [cited 14-06-17]

<div align="right">

4

</div>

RESOURCE ALLOCATION

In this chapter the allocation of resources is discussed. The chapter starts off with the cost analysis in Section 4.1. In this section a visualisation of the cost break down can be found as well. The next section discusses allocation of the budgets to the different subsystems. This includes price, mass, volume, power and temperature range.

4.1. COST ANALYSIS

A cost analysis aids any mission development execution to stay within budget. For EPIC however, this analysis also enables the calculation of the total number of S/C that can be produced. This section initiates with an assessment of the EPIC development and recurrent costs. The section concludes with an estimation of the total number of EPIC CubeSats that can be produced within the available budget of 50M€.

The development cost covers the design and the external operation expenses. Decker suggests a design manpower and an external operations cost, of roughly 2M€ and 1M€, respectively [23]. After an assessment of expert opinions from ISIS [24], Hyperion [25] and Menicucci [26] on Deckers calculations, his estimations are adopted.

The recurrent expenses comprise the satellite hardware, assembly & integration, Testing & Validation (T&V) and the launch cost. The hardware budget covers the S/C platform and payload. An overview of the costs for each of these subsystems is provided in Table 4.1. The launch cost (including insurance) per EPIC CubeSat shall be 0.55M€ (Chapter 6). EPIC CubeSats are mainly assembled from COTS components, hence the integration costs can be estimated to be 5-10% of the total CubeSat hardware costs [24] which is 40k€ per CubeSat. According to Uludağ [27], CubeSats are required to at least be tested for their performance in thermal-vacuum and vibrational characteristics. For one S/C, the duration of these tests is approximately one month. The price for renting test facilities in the Netherlands is approximately 20k€. For testing EPIC S/C a conservative estimate for the testing has been assumed, hence 100k€ is allocated for T&V per S/C.

With the assumed hardware, launch, assembly, integration and T&V cost per S/C, the total hardware budget per S/C is estimated to be 0.62M€. The number of S/C that can be produced within the cost budget, is by Equation 4.1, using a scale economy model. C_n represents the cost of the n-th product, C_0 the cost of the first product, L the learning-curve coefficient, and n the number of times that C_0 has doubled [28].

$$C_n = C_0 L^n \tag{4.1}$$

According to ISIS the learning-curve coefficient L for CubeSats is usually in the range of 0.7 and 0.9 [24]. According to Hyperion it must be kept in mind that there will be non-recurrent engineering cost in the form of adaptations of the COTS products. This extra cost post influences the life cycle constant in a negative way. After summarising the expert and the EPIC team opinions, a life cycle constant is adopted of 0.85. With this assumption, 46 EPIC S/C can be realised. An overview of the results is displayed in a cost break-down structure as seen in Figure 4.1.
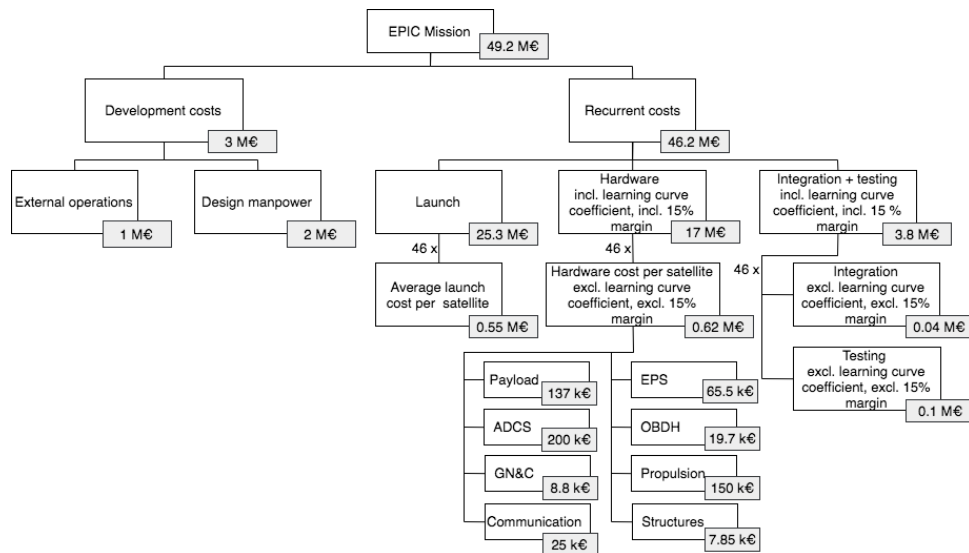
Figure 4.1: Cost break-down structure of the EPIC mission

4.2. HARDWARE BUDGETS

In Table 4.1, the allocated resources per subsystem of each satellite is described. The table also includes the total budgets per S/C for both payload configurations. A detailed budget breakdown for the different configurations, with payload A and payload B can be found in Chapter 7. Further in this section, the hardware budget consumption for the mass, volume, Δv and communication line are described.

MASS

Summing the mass of the detailed subsystem breakdown in Table 4.1 for configuration A and B results in 8924g and 9404g respectively. After performing an assessment of expert opinions, it is decided to include a margin of 20% to these results. This margin consists for 10% of the required integration components (e.g. bolts, cables) and for 10% out of an engineering design margin [29]. For the configuration A and B this results in a mass of 10.7kg and 11.3kg respectively. Since the maximum allowable mass of 6U CubeSats is 12kg [30], the mass including contingencies is still within the budget.

VOLUME

The volume parameters for each subsystem can again be found in Table 4.1. To ensure integration of the subsystems is possible, thus that all subsystems fit the structure, a simulation is executed in a CAD. During the design in the CAD program, space is taken into account for cabling. As explained in Chapter 14, after the integration is performed, a total volume of 0.8U and 0.3U is left over as contingency for configuration A and B respectively. Since almost only COTS components are used, the volume budget is not expected to change drastically. However, if components would be unavailable, this contingency volume can be used.

∆V BUDGET

The most important conclusion drawn in the report for the Δv budget can be found in Chapter 6. A total Δv of 270m/s is present on the CubeSat. This includes 15% contingency on top of the necessary Δv of 235m/s for the deployment as calculated in Section 5.2.

LINK BUDGET AND DATA RATES

The link budget for uplink and downlink budget calculation is discussed in detail in the midterm report [31]. The link closes, including a margin of 10dB, with 8.75dB and 6.15dB for the UHF and S-band link (Appendix A). Furthermore, the data rate that has to be send down is 5758 bit/s (Table 11.1). As explained in Chapter 9, a large margin is still available. The maximum data gathering rate that could be send down is 13676 bit/s. This data rate could also still be processed by the on-board computer as clarified in Chapter 11.

Table 4.1: Overview of all CubeSat subsystems and their assigned budgets (data rates in Table 11.1)

Subsystem	COTS Component	Manufacturer	Price [€]	Mass [g]	Storage volume [mm x mm x mm]/U	Nominal power [W]	Peak power [W]	min/max temperature [°C]	Location in report
Payload A	see Section 7.1	see Section 7.1	137000	1136	1.01U	4.11	4.11	-20/40	Chapter 7
Payload B	see Section 7.1	see Section 7.1	137000	1616	1.38U	3.63	3.63	-20/40	Chapter 7
ADCS	iADCS [25]	Hyperion	200000	1700	95.4x95.9x67.3	2.00	4.00	-20/40	Chapter 8
GNC	NAV-NG GPS/FM [32]	Skyfoxlab	6900	74	71.1×45.7×11	0.13	0.13	-40/85	Section 5.5
	piPATCH-L1/FM [32]	Skyfoxlab	1900	50	98x98x15.4	0.07	0.11	-40/85	
Communication	NanoCom TR-600 [33]	GOMSpace	25000	74.2	90x96x31	1.00	6.00	-40/85	Chapter 9
	NanoCom ANT2000 [34]	GOMSpace		110	98x98x20.1	0.60	10.70	-40/85	
	ANT-6F [35]	GOMSpace		100	N/A	2.00	10.00	-40/85	
	NanoCom AX100 [36]	GOMSpace		24.5	6.5x40x65	2.80	2.80	-40/85	
Electrical power	Solar panel with AzurSpace 3G30C cells (x119) [24]	ISIS	42250	1000.0	N/A	N/A	N/A	-120/150	Chapter 10
	BA0x 16 cells (x2) [24]	ISIS	11600	310.0	89x95x14	N/A	N/A	-60/120	
	NanoPower P60	GOMspace	8600	64.0	96x90x30.6	N/A	N/A	-30/40	
OBDH	iOCS (2x) [24]	ISIS	19700	200.0	96x90x12.4	0.40	0.40	-25/60	Chapter 11
Propulsion	PM200 [25]	Hyperion	150000	2820	200x100x100	0.10	6.00	0/40	Section 6.3
Thermal	White coating	AZ Technology Materials	3773	161.2	7mm thickness 0.2 m^2 area	N/A	N/A	0/40	Chapter 12
	NASA/GSFC S-311P827/01 (x8) [37]	QTI Sensing Solutions	16	0.16	N/A	1.00	1.00	-55/125	
Structures	6U CubeSat structure [24]	ISIS	7850	1100.00	100x226.3x340.5	N/A	N/A	-40/80	Section 13.3
Total Payload A			614589	8924		14.20	45.25		
Total Payload B			614589	9404		13.72	44.77		

LAUNCH, CONSTELLATION DEPLOYMENT AND CONSTELLATION DESIGN

The crucial novelty of the EPIC mission is making use of a constellation to acquire more scientific data to provide an earthquake precursor system. The launch, constellation deployment and constellation design are therefore extensively discussed in Section 5.1, Section 5.2 and Section 5.3 respectively. To ensure the orbital trajectories are correctly followed, a GN&C system is implemented as discussed in Section 5.5.

5.1. LAUNCH

In this section the launch option is chosen based on the trade-off from the midterm report [31]. From this trade-off, two possible options were chosen: piggyback and dedicated launcher. Since the midterm report, further analysis and conversations with launch providers [24] have provided sufficient knowledge to make an informed decision between the two.

Launch providers indicated that a dedicated launch is expected to be marginally more expensive, if at all, than a piggyback launch. Even when a dedicated launch is not fully loaded, the remaining space can be sold to secondary missions, reducing the costs significantly. The other trade criteria considered in the trade-off (flexibility, availability, reliability and sustainability) have also been confirmed as equally good or better for dedicated launches compared to piggyback launches.

For these reasons the dedicated launch option is chosen. Multiple companies provide dedicated launchers. However, most rockets are significantly larger and more expensive than required for the mission. Hence, the options were reduced to rockets with a cost below 15 million USD. This leads to the following two options: the polar satellite launch vehicle (PSLV) by the Indian department of space and the Electron by Rocket Lab (see Figure 5.1).

The Electron rocket is by far the cheaper of the two, with a launch cost of 5.5 million USD[1] over 15 million USD[2] for the PSLV. Based on the Electron user manual [38], the rocket is capable of launching a maximum of around 12 6U CubeSats to the orbits considered by EPIC. Furthermore, Rocket Lab is expected to have a high launch cadence, 50 per year, resulting in high availability. The smaller payload will result in less secondary cargo, reducing the dependency on others to finance the launch.

In contrast, PSLV is capable of launching more than 145 6U S/C to the intended orbit. This is one order of magnitude beyond the scale of this project. This rocket was only launched every other month in 2016. The downside of the Electron, however, is the reliability. The rocket has only been launched once and failed to reach orbit[3]. In contrast, PSLV has a reliability of 97%. Only the first rocket failed to reach orbit. But despite the reliability concerns, the Electron rocket is chosen due to the cost, flexibility and availability. It is expected that by the time the EPIC S/C will be deployed, the Electron will be sufficiently reliable.

---

[1]`https://www.space.com/34364-rocket-lab-small-satellite-launch-race.html` [cited 09-06-2017]
[2]`http://www.thehindubusinessline.com/news/science/pslvc21-sends-french-spot-6-japanese-satellite-into-orbit/article3877021.ece` [cited 09-06-17]
[3]`https://www.rocketlabusa.com/latest/rocket-lab-successfully-makes-it-to-space-2/` [cited 09-06-2017]
[4]`http://www.popularmechanics.com/space/rockets/news/a26506/rocket-lab-maiden-flight-electron-rocket/` [cited 12-06-2017]

Figure 5.1: Electron rocket by Rocket Labs[4]

5.2. CONSTELLATION DEPLOYMENT

This section aspires to clarify the constellation deployment strategy and to determine the required Δv budget for the deployment. Subsequently, Chapter 6 shall size the propulsion and particularise the Δv budget.

5.2.1. CONSTELLATION DEPLOYMENT STRATEGY

After the CubeSats are released by a launcher, they progress all in the same orbit, i.e. they have the same Kepler parameters. However, the global distribution of the earthquake areas requires a Walker distribution as explained in Section 5.3. The Walker distribution implies that the satellites already have the desired inclination, so they only have to be separated in the Right Ascension of the Ascending Node (RAAN) and the True Anomaly (TA).

As explained in the design trade-off [31], the chosen strategy for constellation deployment is based on natural orbital perturbations, since the required Δv for other methods can not be provided by Cube-Sats. The non-homogeneous gravity potential field of the Earth causes the so-called J_2-effect, which produces a precession in RAAN, depending on altitude (or semi-major axis a) and inclination (i) as in Equation 5.1. The constants are the radius of the Earth (R_e), eccentricity (e) and the geopotential coefficient J_2.

$$\dot{\Omega}_p = -\frac{3}{2}\left[\frac{R_e}{a\left(1-e^2\right)}\right]^2 \frac{2\pi}{P} J_2 \cos(i) \tag{5.1}$$

To make use of the natural perturbation for deployment, firstly the CubeSat will perform a Hohmann transfer and/or inclination change manoeuvre to achieve a different RAAN precession for each Cube-Sat. Secondly, the CubeSats drift during a certain period of time to reach the desired angular separation in RAAN. Eventually, a second transfer manoeuvre shall be performed, after which the satellites are positioned in the final $55:6/6/2$ Walker constellation at 520km altitude (Section 5.3).

The launch position and final positions in RAAN are illustrated in Figure 5.2. The first design iteration concluded that the Δv available by the CubeSat is insufficient to ensure deployment if only one launcher is used. For this reason, two separate launchers, at opposite RAAN position are utilised. As a result, the maximum drift that has to take place is 60° in RAAN. For further reference, the CubeSat drifting at the lower altitude is referred to as the lower CubeSat and the CubeSat drifting at higher altitude is the upper CubeSat. The final orbital position of each drifting orbit is indicated in Figure 5.2.

5.2.2. CONSTELLATION DEPLOYMENT OPTIMISATION

The problem remaining is to quantify the necessary altitude and inclination differences for the deployment of each CubeSat. These are determined by minimising the Δv, while keeping within the altitude constraints. The minimisation objective is mathematically expressed in Equation 5.2. The centre, upper
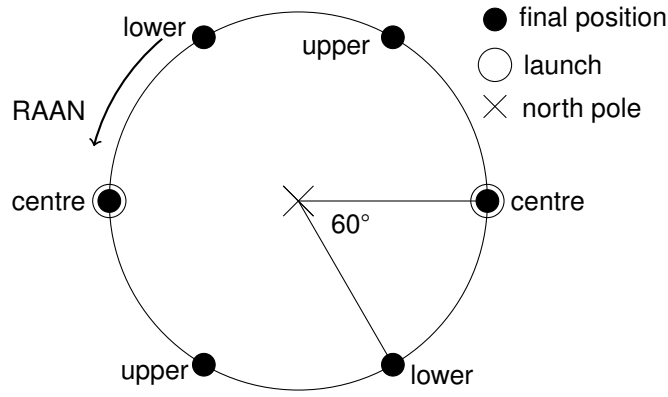
Figure 5.2: Distribution of the CubeSats in RAAN
after launch, top view on Earth

and lower satellites are defined in Section 5.2.1.

$$\min\left\{\max_{n\in[\text{centre,upper,lower}]}\left\{\Delta v_{h_{1,n}}(h_{\text{launch}}, h_{\text{lower}}, h_{\text{upper}}) + \Delta v_{h_{2,n}}(h_{\text{launch}}, h_{\text{lower}}, h_{\text{upper}}) + 2\Delta v_{inc,n}\right\}\right\} \quad (5.2)$$

The required deployment time of 6 months is added as a constraint together with the altitude bounds of 400km and 670km stemming from propulsion constraints and the sustainability requirements (Chapter 18) respectively. The final constellation configuration, as discussed in Section 5.3, shall be a $55:6/6/2$ Walker constellation at 520km altitude.

From Equation 5.2, it is known that a combination of altitude and inclination changes has to be optimised. Equation 5.3 gives the Δv required for Hohmann transfers. The first transfer Δv_{h_1} is for transferring from the launch altitude to the drifting orbit, while Δv_{h_2} is required to transfer from the lower altitude r_1 to the higher altitude $/r_2$ or vice versa. The Δv_h also depends one the Earth graviational parameter μ.

$$\Delta v_h = \sqrt{\frac{\mu}{r_1}}\left(\sqrt{\frac{2r_2}{r_1+r_2}}-1\right) + \sqrt{\frac{\mu}{r_2}}\left(1-\sqrt{\frac{2r_1}{r_1+r_2}}\right) \quad (5.3)$$

Next, the necessary Δv_{inc} to perform an inclination change is given by equation Equation 5.4. Here, the change depends on the current inclination (i), the semi-major Furthermore, since the drift can take up to 6 months, orbital decay has to be taken into account; i.e. the final drift altitude differs from the initial altitude. The difference in altitude each orbit caused by drag is estimated by Equation 5.5 [39]. Important is that no other effects such as solar pressure are considered, this assumption is verified in Section 5.4. Moreover, the worst case values for atmospheric density (ρ) are adopted from [39], as well as the standard value of 2.2 for C_D. The CubeSat mass is denoted as m and the frontal area is A.

$$\Delta v_{inc} = \sqrt{\frac{\mu}{a}}\sin\left(\frac{|\Delta i|}{2}\right) \quad (5.4) \qquad\qquad \Delta a = -2\pi\left(\frac{C_D A}{m}\right)\rho a^2 \quad (5.5)$$

As indicated in Equation 5.1, the precession in RAAN depends on both the inclination and altitude change. So, an increase in Δv used for inclination lowers the necessary Δv for altitude changes to acquire the necessary precession rate and vice verse. For the optimisation algorithm, first the precession rate due to the performed altitude change is calculated. Next, the inclination change (Δi) that is necessary to ensure the required precession rate is calculated using Equation 5.6. The period is given by P, the Earth radius is R_e and the semi-major axis is a.

$$\Delta i = \arccos\left(\frac{\left(\dot{\Omega}_{p,centre} + \dot{\Omega}_{p,req}\right)a^2\left(1-e^2\right)P}{2\pi J_2 R_e^2}\right) - i_{centre} \quad (5.6)$$

Given the required deployment time of six months, the required difference in precession rate is $\dot{\Omega}_{p,req} = \frac{\pi}{6}\cdot(t_{\text{deployment}})^{-1} = 6.64\cdot10^{-8}$ rad/s for the upper satellite and -6.64$\cdot10^{-8}$ rad/s for the lower satellite. The

precession rate of the centre CubeSat $\dot{\Omega}_{p,centre}$ can be determined using Equation 5.1.

Since the altitude and inclination inputs depend on each other, the necessary altitude cannot be solved analytically. Therefore, a numerical optimisation program is written in MATLAB based on genetic optimisation (see Section 5.3.4), using all interdependencies of aforementioned Δv manoeuvres. The optimisation algorithm is performed as in Figure 5.3; where the optimised variables are h_{launch}, h_{lower} and h_{upper}.
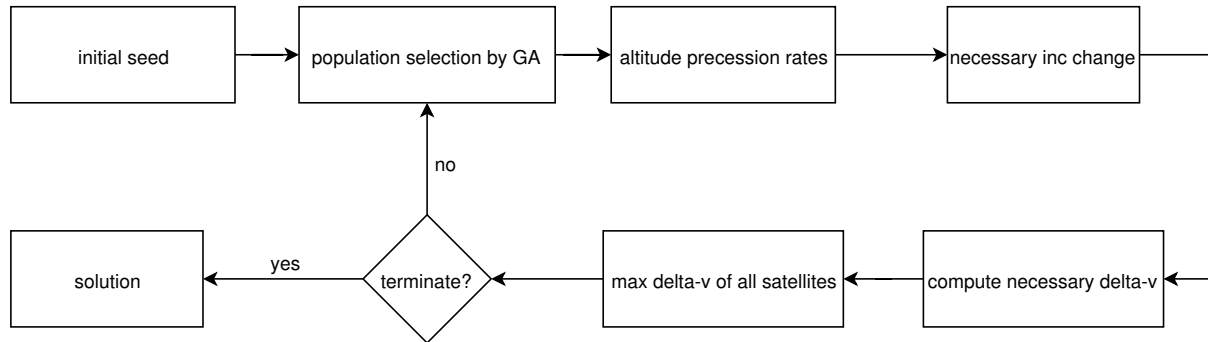

Figure 5.3: Flow diagram of the deployment optimisation algorithm

At first the initial seed of inputs are assumed, after which the genetic algorithm (GA) selects an initial solution population. For each solution, the altitude precession rates Equation 5.1 and the according Δv_{inc} of Equation 5.6 are calculated to meet the required precession difference. Finally, the total necessary Δv of all CubeSats is used to measure the fitness of the solution. The optimisation algorithm terminates if the solutions of the solution population converge as defined by the optimisation toolbox of MATLAB. The resulting optimal launch altitude is 530km, for which the required Δv as a function of lower and upper CubeSat altitude is presented in Figure 5.4. An optimal initial lower and upper altitude of 432km and 670km respectively are concluded. Furthermore, the upper CubeSat shall perform an inclination change of 0.37°. Take note that inclination changes take place at the highest possible altitude, since that requires less Δv (see Equation 5.4). An overview of all performed manoeuvres is presented in Table 5.1.

Table 5.1: Constellation deployment

Satellite	required Δv [m/s]	Deployment procedure after launch
lower	210.2	1. Hohmann transfer (530km→435km) 2. 6 month drifting 3. Hohmann transfer (350km→520km)
centre	1.6	1. 6 months drifting 2. Hohmann transfer (527km→530km)
upper	235.1	1. Hohmann transfer (520km→670km) 2. inclination change (55° → 55.37°) 3. 6 months drifting 4. inclination change (55.37° → 55°) 5. Hohmann transfer (669km→520km)

5.3. CONSTELLATION DESIGN

This chapter will cover the orbits and the constellation aspects of the EPIC mission. Firstly, in Section 5.3.1, the discussion focuses on the considered coverage. Then, Section 5.3.2 presents the propagation of the satellites and the coverage calculations. Next, the constellation design is proposed in Section 5.3.3. Results of the constellation configuration can be found in Section 5.3.5.
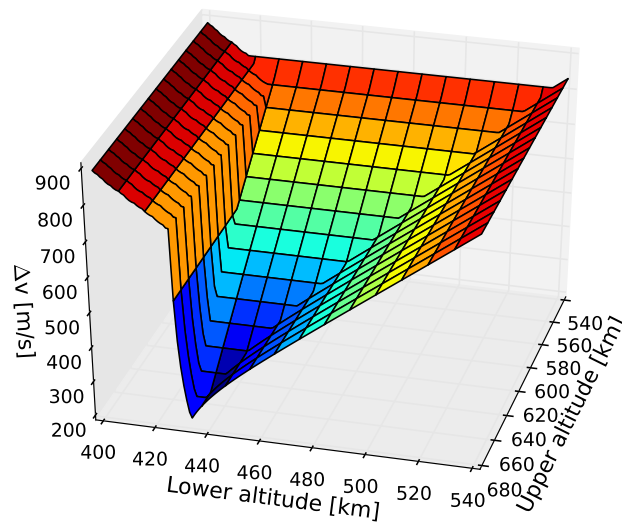
Figure 5.4: Required Δv as a function of lower and upper deployment altitude

5.3.1. COMPLEX COVERAGE AND REVISIT TIMES OF EARTHQUAKE AREAS

Before designing the satellite orbits, an indispensable step is to define what areas need to be covered by the satellite. As determined by the EPIC requirements, earthquakes with M > 7 shall be monitored [40]. Therefore the worldwide earthquake affected areas will be used as the coverage area. The publicly accessible database of the International Seismological Centre (ISC) with historical earthquake data (Version 4.0) filtered on M > 7 is adopted for constellation design of EPIC [41]. The earthquake events collected over 100 years from the ISC database provide a sufficient indication of future earthquake event locations, as also shown in literature [42]. The effected area around the earthquake epicentres is estimated to be 800 km including a contingency of 20% [40] [4]. A resulting coverage area as presented in Figure 5.5, is often referred to as a 'complex' coverage area since no simple geometries are discernible and no ready solutions are available [43]. The affected area is transformed into latitudes and longitudes and projected on the map using the Haversine method [44]. A mapping resolution of 1° latitude is used, which is an acceptable grid spacing [45].
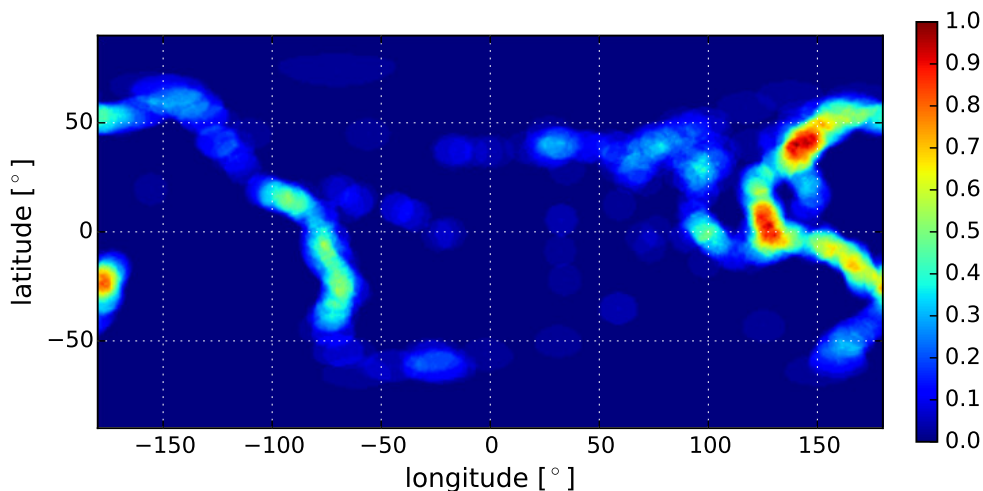

Figure 5.5: Area affected by historical earthquakes using a Miller cylindrical projection [41]

After identifying the earthquake affected areas, the coverage map used for EPIC is determined by assigning weights to important areas to cover. The weights are assigned according to the frequency of historical earthquake occurrence for each area, scaled to the area with the most earthquakes given a weight of 1. A weight of 0 is given to areas without historical earthquakes. The weighted coverage map that will be used for the constellation design is presented in Figure 5.5.

After the required coverage area is defined, it is important to consider that commonly a percentage of coverage per revisit is defined, since the revisit time is increased significantly when full coverage is needed. From Figure 5.6 a reasonable coverage of 99% is concluded for the EPIC constellation design as in agreement with the requirements [40]. Next to the required coverage area, also the required revisit time of 4 hours influences the constellation design to a great extent. Important to consider is that the revisit time is not constant due to the complexity of orbit propagation. For an extended amount of time, the revisit time can be modelled by a normal distribution, as also shown in Figure 5.7. For the EPIC constellation design, the mean revisit time plus two standard deviations is optimised to have a conservative approach; i.e. for 2.5% of the cases the revisit of the complex coverage is not satisfied.
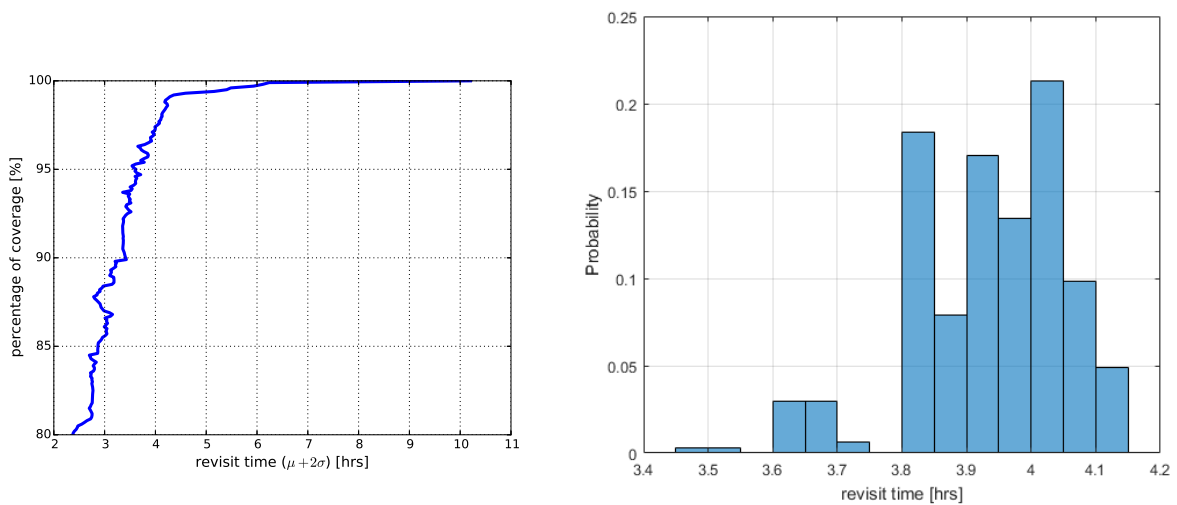

Figure 5.6: Percentage of coverage per revisit for a 55:6/6/2 Walker constellation at 520 km altitude

Figure 5.7: Percentage of coverage per revisit for a 55:6/6/2 Walker constellation at 520 km altitude

5.3.2. ORBITAL PROPAGATION
To design any satellite constellation, an orbital propagator for the satellite bodies must be selected. Currently, multiple industrial propagator software tools (STK) and open-source propagator tools (GMAT, GHOST, TUDAT, . . .) exist. However, since the evaluation of the satellite orbit trajectory is often too time-consuming for aforementioned software, a simplified Keplerian propagator tool is produced in MATLAB for this project. This propagator only takes the effects of the rotation of the earth, the rotation of the earth around the Sun, the J_2 effect and atmospheric drag into account. A simplified propagator is adequate to determine the optimal constellation configuration (Section 5.3.3). Next follows a short description of the developed tool.

Generally, a time-step propagation of the celestial body is used to determine the orbital trajectory. The mean anomaly (M) is calculated for each time step Δt using Equation 5.7 from which the eccentric anomaly (E) is obtained solving Equation 5.8 in an iterative process. Here, e is the orbital eccentricity. From the eccentric anomaly the true anomaly (θ) is realised using Equation 5.9 [39]. For these equations, t is the current time, while t_0 is the starting time.

$$M = M_0 + 2\pi P(t - t_0) \qquad (5.7)$$

$$M = E - e\sin E \qquad (5.8)$$

$$\tan\frac{\theta}{2} = \sqrt{\frac{1+e}{1-e}}\tan\frac{E}{2} \qquad (5.9)$$

Next, the Kepler elements influenced by disturbances are updated. Most important orbital perturbations are caused by irregularities of the gravitational field, third-body perturbations, solar pressure and atmospheric drag. The largest effect at altitudes of 500km or higher is due to the gravitational field, which is approximately 2 orders of magnitude larger than other effects [39]. Especially the J_2 effect will cause a radial acceleration to the spacecraft and is used for the propagator. The nodal precession $\dot{\Omega}_p$ can be expressed as in Equation 5.1. The Kepler elements shifted by the J_2 perturbation are the RAAN and argument of perigee (AOP), which are updated for each time-step as in Equation 5.10 and Equation 5.11 [39].

$$\Delta RAAN = 2\pi \dot{\Omega}_p (t - t_0) \quad (5.10) \qquad \Delta AOP = -2\pi \frac{\dot{\Omega}_p}{\cos(i)} \left(2 - \frac{5}{2} \sin(i)^2 \right) (t - t_0) \quad (5.11)$$

Lastly, the Keplerian orbital elements are transformed into latitude and longitude using Equation 5.12 and Equation 5.13 to compare to the coverage area. The effect of the rotation of the Sun on the longitudinal position of the satellites is included by the term ω_e, where $\omega_e = 360.99°$/solar day [46]. For these equations, θ is the true anomaly and i is the inclination.

$$\text{latitude} = \arcsin\left(\sin\left(AOP + \theta\right)\sin(i)\right) \quad (5.12)$$

$$\text{longitude} = \arctan\left(\frac{\sin\left(\text{latitude}\right)}{\tan(i)\cos(AOP + \theta)}\right) + RAAN - (t - t_0)\omega_e \quad (5.13)$$

For the use of the propagator tool, a time-step Δt and total propagation time of the satellites has to be carefully chosen to avoid discretisation errors. From Figure 5.8, a time-step of 0.0001 days (≈ 9s) and a propagation duration of 10 days is concluded.
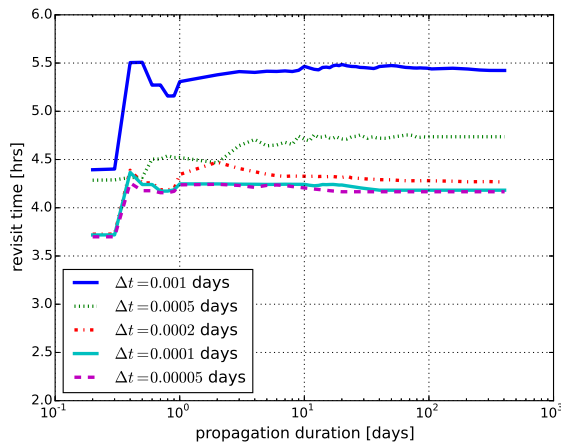

Figure 5.8: Time-step and propagation duration trade-off based on a $55.5 : 6/6/2$ Walker constellation at $520 km$ altitude
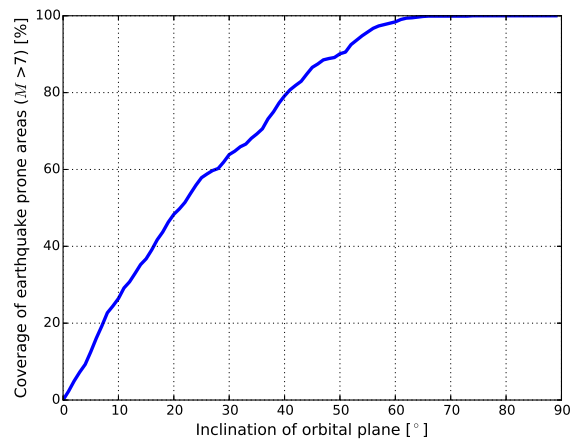
Figure 5.9: Occurrence of earthquakes as a function of latitude [41]

5.3.3. CONSTELLATION DESIGN USING TRADITIONAL WALKER METHODS

Constellation design has been recognised in many studies as a complex problem. The most commonly used constellation system is the Walker-Delta constellation; e.g. used for the Galileo Navigation system[5]. More recently, mainly due to the expansion of the CubeSat market, other constellation designs using optimisation have been proposed providing better results for complex coverage problems [47]. However, these come at a great computational expense, whilst not providing significantly better results [31]. Additionally, the symmetrical properties enhance the performance of e.g. the deployment of the constellation.

---

[5] http://www.esa.int/Our_Activities/Navigation/Galileo_and_EGNOS [cited 15-05-2017].

For the traditional, regular Walker constellation, all the orbital planes have the same inclination (i) and altitude. A Walker constellation can be reproduced using a set number scheme as defined by Walker. For T satellites evenly distributed over P orbital planes with a relative angular shift of $F(360°/T)$, the Walker constellation can be reproduced using the defined numbering scheme: $i : T/P/F$ [48].

The 5 unknown variables for the Walker constellation are the altitude and the 4 Walker design variables (i, T, P, F). Because of the complexity of orbit propagation, no analytic solution exists to determine the optimal satellite trajectories for each concept using Walker constellations. Therefore, the constellation design is generally subjected to an optimisation algorithm [45]. Commonly a genetic algorithm (GA) is applied [49] since other optimisation algorithms tend to find local optima [50]. A concise clarification of GA is given in Section 5.3.4.

To determine the 5 unknown variables, the performance parameter to be optimised needs a clear definition. The objective of the chosen concept in the design trade-off [31] is to maximise the quality of the scientific output of the mission. Therefore, the constellation's performance is optimised to maximise the amount of satellites in formation flight, given the minimal revisit time as specified by the requirements and budget constraints. However, since the revisit time depends on all 5 variables, first the revisit time has to be optimised, after which the necessary amount of satellites T of the Walker constellation are minimised. If T is minimal, automatically the amount of satellites per formation will be maximal.

This kind of multi-objective optimisation is typically done using a Pareto front. So, summarised, the optimisation problem can be conceived as in Equation 5.14. The Pareto front as well as the GA build-in function of MATLAB are utilised. A Pareto front is a set of potential optimal solutions, often used for engineering solutions. After the set of solutions is generated, a trade-off is performed by the engineer to decide on the final solution, as described in detail by Kim et al. [51].

$$\min\{t_{\text{revisit}}(h, i, T, P, F), T\}, i > 62° < 118°, 350km < h < 670km \tag{5.14}$$

Finally, before the optimisation can be executed, the constraints on the variables are examined. The latitude of the measurements for a satellite is limited by the inclination angle (i); e.g. an orbit with an inclination of $50°$ covers areas between latitude $50°$ and $-50°$. Therefore, the effect of the inclination of the orbit on the percentage coverage of earthquake areas is examined. At a $60°$ orbital inclination, 98.4% of the total amount of earthquake areas with magnitude larger than 7 are covered (see also Figure 5.9). By including the swath angle of 800km ($\approx 8°$ latitude), the inclination shall be larger than 52°.

Also, the altitude (h) is constrained between 350km and 670km. The lower limit is to lower the necessary Δv as explained in Section 5.2, while the upper limit stems from the EOL requirement (Section 18.2).

5.3.4. GENETIC OPTIMISATION ALGORITHM

A genetic algorithm is inspired by nature's population change over time. A population being a number of solutions, in which the strongest or best fit solutions are used to 'breed' a new population. Following 5 distinct steps are performed by the GA [52]:

- **Initialisation:** The GA starts by making a population of N amount of random solutions which are distributed between upper and lower bounds.
- **Selection:** The performance of all N members of the population is evaluated by a fitness function. The fitness of the member determines the selection that creates children.
- **Heredity:** The creation of these children can be seen as getting children in nature. The selected parents give their traits on to their children. This can be done individually for every child or the parents breed a group of children.
- **Mutation:** To ensure the solutions do not converge to a local solution, the children have a possibility of mutating. The trait of the child can be completely random within the initial constraints and the mutation will propagate if it results in a better solution.
- **Termination:** The loop is terminated either by a maximum number of generations, a maximum running time or convergence of the solution.

The optimisation toolbox of MATLAB contains a GA function which is adopted for this design[6]. The overall structure of the MATLAB algorithm is shown in Figure 5.10 and the code is available online[7].
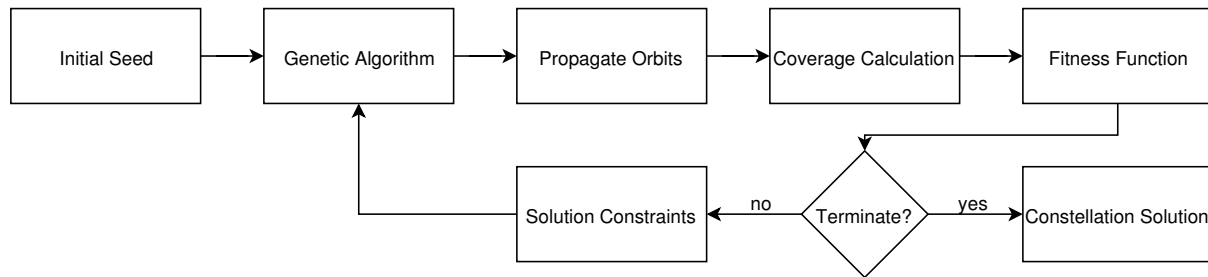

Figure 5.10: Algorithm flow diagram of constellation optimisation

5.3.5. CONSTELLATION RESULTS AND FORMATION FLIGHT

The resulting Pareto front of the multi-objective optimisation process is shown in Figure 5.11. The Pareto front analysis resolved that no solutions exist below six planes. Nevertheless, several solutions exists with six planes or higher. The set of Pareto frontier solutions, e.g. best solution as a function of P, is given in Table 5.2. The convergence speed is expressed in amount of generations. The objective of the optimisation problem is to minimise the revisit time and amount of planes. Keeping in mind the revisit time constraint of 4 hours mentioned in Section 5.3.1, the $55.5 : 6/6/2$ Walker constellation at 520km altitude is chosen as final orbital configuration. Figure 5.12 provides an STK visualisation of this constellation configuration.
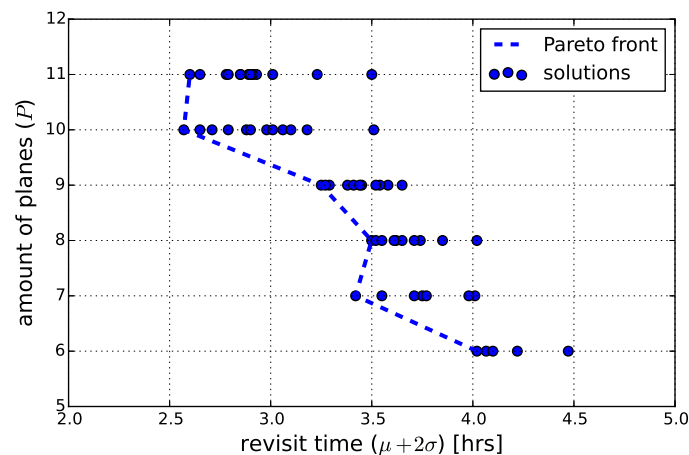

Figure 5.11: Pareto front of the multi-objective genetic optimisation

To maximise the scientific yield, in each orbital plane, at least two satellites fly in formation as determined in the concept trade-off [31]. During the detailed design phase, it is concluded that the €50 million budget only allows for two satellites in each plane, while still providing sufficient redundancy for a reliable constellation (see Chapter 16). The separation of the satellites flying in formation is mainly dictated by the scientific principles of ionospheric disturbances. Email correspondence with the TwinSat mission revealed that little is known about formation flight so far and the separation distance cannot be optimised yet [53]. However, if the separation would be too large (>800km), some major earthquake phenomena could be missed. On the other hand, if the separation is too small (<100km), the changes measured by both satellites would be too small. Therefore, an intermediate separation of 400km is concluded.

---

[6]https://nl.mathworks.com/discovery/genetic-algorithm.html [cited 18-05-2017]
[7]https://goo.gl/IdMUOC [cited 24-05-2017]

Table 5.2: Summary of constellation configuration with a 99% coverage criteria.

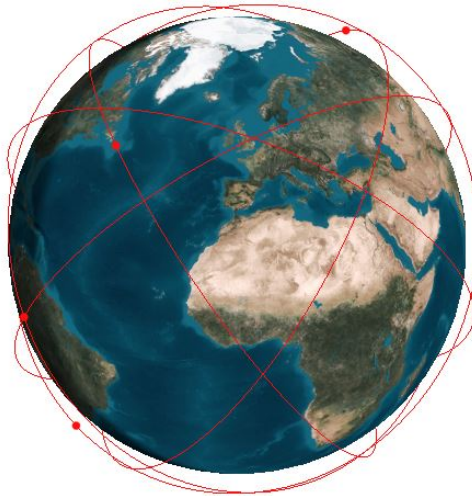| T	Revisit time [hrs]	Altitude [km]	i	P	F	Generations
1	23.97	559.3	52.0	1	0	21
2	12.14	519.6	89.5	2	0	3
3	7.51	516.8	86.6	3	1	17
4	6.41	509.7	54.0	4	0	18
5	5.27	511.5	53.4	5	4	10
6	4.02	519.2	55.5	6	2	9
7	3.26	551.5	87.5	7	0	17
8	3.49	559.8	53.2	8	7	20
9	3.25	544.1	81.9	6	8	10
10	2.57	510.5	53.8	10	4	8
11	2.60	555.3	57.1	11	10	7

Figure 5.12: Visualisation of the 55:6/6/2 walker constellation in STK

5.4. VERIFICATION AND VALIDATION

The verification and Validation of this Chapter is split in two sections. The first section describes the V&V of the constellation deployment. The second section discusses V&V of the constellation design.

5.4.1. CONSTELLATION DEPLOYMENT VERIFICATION AND VALIDATION

The verification of the constellation deployment optimisation was found to be challenging since deployment of CubeSat constellations is an innovative concept. A suggestion on the approach of such a constellation deployment is given by Crisp et al. [54]. The paper describes how nodal precession is used for CubeSat constellation deployment, while comparing to the FORMOSAT-3/COSMIC mission. This satellite mission deployed six satellites in equally spaced planes. The starting altitude was 515km altitude and the final orbit is at 800km [55]. However, the Δv for this mission was not optimised for these larger satellites, since Δv budget was not an issue as it is for the EPIC mission. Other design considerations such as calibration of scientific instruments are more important for FORMOSAT and drive the deployment strategy. In addition, no inclination changes are considered for this mission to perform an optimal set of manoeuvres, as is done for the EPIC mission.

The necessary Δv for the constellation deployment of FORMOSAT is calculated in Table 5.3. Since no optimisation is used for FORMOSAT, the used Δv is higher than for the EPIC mission, as is expected. Furthermore, to compare with the actual Δv computation and verify the Hohmann transfer Δv unit in the optimisation tool, the performed transfers by FORMOSAT are simulated, also shown in Table 5.3.

The slight deviations in necessary Δv to make the plane changes is due to the drift of the orbits due to drag and solar pressure. The actual orbital altitude at the time of the plane change of FORMOSAT is not stated by Fong et al. [55]. However, the difference is less than 1%, so that the Hohmann transfer calculations are validated by the the FORMOSAT mission and verified by the results of Crisp [54].

Table 5.3: Comparison of the optimised constellation Δv with reference literature

Satellite	Δv optimised	Analytical simulated Δv without optimisation	Δv by Crisp [54]	Actual Δv [55]
3C (FM5)	116.3	152.5	152.2	153.1
3F (FM2)	116.3	152.5	152.6	154.0
3A (FM6)	116.3	152.5	153.0	153.0

5.4.2. CONSTELLATION DESIGN VERIFICATION AND VALIDATINO

Firstly, the orbital propagator explained in Section 5.3.2 shall be verified and validated. The main assumption for the propagator is that only J_2 perturbations are present. However, many other perturbation forces like 3rd body perturbations, atmospheric perturbations, relativistic effects, etc. can be modelled for. These kind of perturbations are generally not important for scientific CubeSat missions, as the position determination is less demanding as for example global positioning system (GPS) satellites[8]. The effect of the made assumptions is assessed by propagating the same Keplerian elements in GMAT as used for the EPIC propagator. From Figure 5.13 it can be concluded that the orbital propagation is very similar to GMAT results.

Verification of the optimisation tool methodology is accomplished by comparing the results to reference papers as [47], [56] and [57] using the same inputs. A more detailed validation of the constellation is done by testing the optimisation tool to reproduce the GPS constellation. The GPS constellation is ought to provide full, continuous four-fold coverage of the Earth surface. Thus the constellation optimisation is tested for which Walker constellation this can be achieved, concluding on a 55.5:18/3/1 configuration. Thus, at least 18 satellites in 3 planes are necessary. Considering that the GPS constellation continuously uses 24 satellites, this is a satisfying results. The additional satellites used by GPS are probably used for redundancy or for other design considerations.
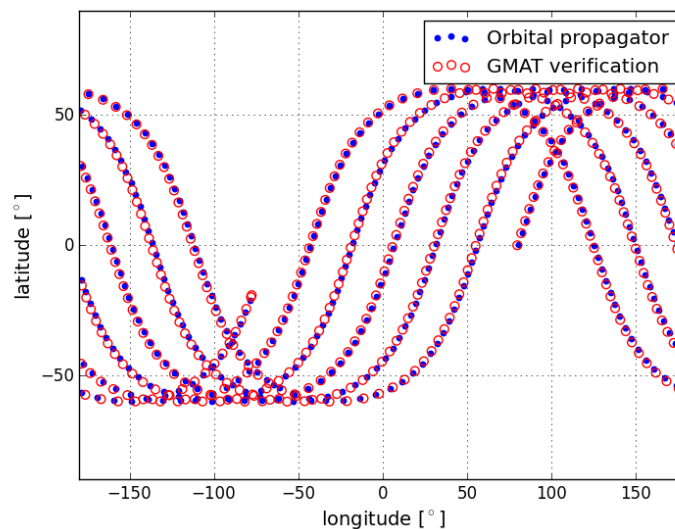

Figure 5.13: Comparison of the used propagation with GMAT, using a timestep of ≈ 90s

---

[8]http://www.dlr.de/rb/desktopdefault.aspx/tabid-10749/10536_read-23371/ [cited 15-05-2017]

5.5. GUIDANCE NAVIGATION & CONTROL

The guidance, navigation and control (GN&C) subsystem is required to measure the position and velocity vector of the CubeSat. This essential subsystem for the orbit determination provides accurate positions of the CubeSat, which is crucial to determine the location of earthquakes. Similarly, the GN&C subsystem is also implemented to provide accurate positions during deployment manoeuvres and for collision avoidance. Several COTS GN&C components are available, from which the NAV-NG GPS/FM by Skyfoxlab is chosen during the design trade-off [31], as shown in Figure 5.14. This ultra low power GPS receiver is ITAR-free and has excellent flight heritage. Moreover, the component provides a position accuracy up to 20m ($\pm 2\sigma$) and a velocity accuracy of 0.1m/s ($\pm 2\sigma$).

During nominal operations, no navigation control of the CubeSat is necessary. To ensure a sustainable design choice, (Chapter 18), the best EOL strategy is natural decay, so that no attitude maintenance occurs. Only for constellation deployment or collision avoidance, active navigation control is required.
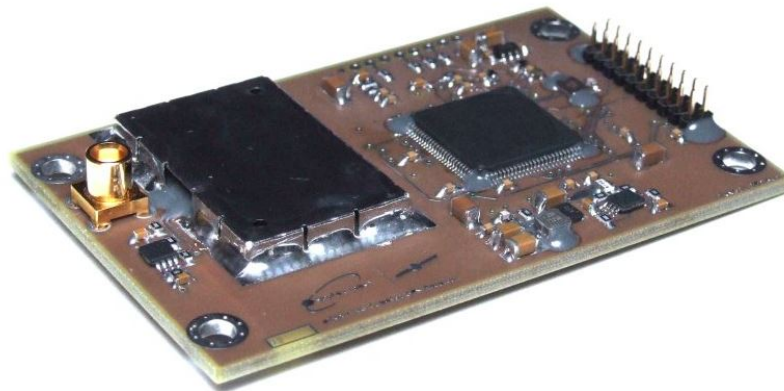

Figure 5.14: NAV-NG GPS/FM by Skyfoxlab

6

PROPULSION SUBSYSTEM

In order to establish the deployment of the constellation as discussed in Chapter 5, the EPIC CubeSats should be equipped with an appropriate propulsion system. The selection and considerations regarding propulsion will be discussed in this chapter. In the first section, Section 6.1, all available propulsion systems are presented. In Section 6.2 the use of Δv during the mission is discussed and a propulsion system is chosen to be part of the EPIC CubeSat mission. Section 6.3 is on the sizing and configuration of the fuel tank. Next, an overview of the characteristics of the chosen propulsion system is given, which can be found in Section 6.4. This is followed by a sensitivity analysis in Section 6.5. The chapter closes off with a conclusion in Section 6.6, in which key design choices and motivations are captured.

6.1. AVAILABLE CUBESAT PROPULSION SYSTEMS

The propulsion system that will be chosen for the EPIC mission, shall have to comply with a set of requirements. The parts of the different budgets that are allocated to the propulsion system, can be found in Table 6.1. The total system budget allocation and methods can be found in the midterm report [31].

Table 6.1: Budget allocated to the propulsion subsystem

Budget	Allocation to propulsion
Cost [€]	200,000
Weight [kg]	0.9
Volume [U]	2
Power [W]	6
Δv [m/s]	235

There are many companies, that are developing propulsion systems for CubeSats. In this trade-off it is assumed, that the companies that have already produced and tested a prototype of their propulsion system, will have the product ready in time for the production of the EPIC CubeSats. CubeSat propulsion systems that are still in the early phase of development are discarded. This is why only ten companies that make propulsion systems are investigated.

In Table 6.2 the list of propulsion systems can be found. Even though the use of CubeSat parts from the United States is strongly discouraged due to ITAR, these were still investigated. However, the high performance thrusters from the USA make use of the highly toxic propellant hydrazine, which is not accepted by the launch contractor and does not comply with the requirements on sustainability [38][40]. The performance of American thrusters with green propellants is equal to or less than their European equivalents, hence there is no need to include them in the trade-off. After discarding the propulsion systems from the USA, five systems are left to consider. These are the thrusters produced by AMR, GOMSpace, Hyperion and NanoAvionics. The characteristics of these propulsion systems can be found in Table 6.3.

---

[1] http://n-avionics.com/propulsion-systems/small-satellite-green-chemical-propulsion-system-epss/ [cited 12-06-17]

Table 6.2: Available CubeSat propulsion systems

Company	Product	Origin
Aerojet Rocketdyne	MPS-120XL	USA
Aerojet Rocketdyne	MPS-120XW	USA
Aerojet Rocketdyne	MPS-130	USA
AMR	IMF Nano Truster	Germany
Busek	BET1-mN	USA
Busek	Micro Resistojet	USA
Busek	BMP-220	USA
Busek	BGT-X5	USA
CUAerospace	PUC	USA
GOMSpace	Nanoprop 6U	Denmark
Hyperion	PM400	The Netherlands
Hyperion	PM200	The Netherlands
NanoAvionics	EPSS	Lithuania
Tethers	Hydros Thruster	USA
Vacco	Standard MiPS	USA

Table 6.3: Propulsion system characteristics for five potential propulsion systems

Company Product	AMR IFM Nano [58]	GOMSpace Nanoprop 6U [59]	Hyperion PM200 [25]	Hyperion PM400 [60]	NanoAvionics[1] EPSS
Propellant	Solid indium	Butane	NOP	NOP	ADN Blend
Δv [m/s]	525	12	110	230	220
Power [W]	40	2	6	6	9
Thrust [N]	0.35	0.04	0.3-0.8	0.5-1.5	0.3
I_{sp} [s]	5000	110	285	285	220
V [U]	0.6	1.0	1.0	2.0	2.0
Dry mass [kg]	0.75	0.77	1.10	1.40	-
Propellant mass [kg]	0.250	0.150	0.310	0.632	0. 388
Cost [€]	30,000	-	150,000	150,000	-
TRL	6	6	6	7	7

6.2. DELTA-V CONSIDERATIONS

With the required total Δv of 235 m/s and a power budget of 6W, both the GOMSpace Nanoprop 6U and the AMR Nano thruster are unsuitable for the EPIC mission. This means only the NanoAvionics EPSS, the Hyperion PM400 and the PM200 will be further analysed. An additional advantage of the NanoAvionics EPSS, is that the system will be tested in space on the LituanicaSAT-2, which will be launched as part of the QB50 mission on 23th of June 2017[2].

In order to establish the desired Walker constellation, the available Δv is the most critical property of a CubeSat propulsion system. The Δv of the Hyperion and the NanoAvionics thrusters were given for a 8kg and a 4kg CubeSat respectively. To calculate what Δv could be provided for a 9.5kg S/C, the rocket equation, Equation 6.1, is used. [39]

$$\Delta v = g \cdot I_{sp} \cdot ln\left(\frac{m_0}{m_0 - m_p}\right) \qquad (6.1)$$

In Equation 6.1, g is the gravitational acceleration of Earth in m/s^2, I_{sp} is the specific impulse of the propulsion system in s, m_0 is initial vehicle mass in kg and m_p is the propellant mass in kg. This gives a Δv of 84m/s and 173m/s for the Hyperion PM200 and Hyperion PM400 respectively. For the NanoAvionics system the equation yields a value of 81m/s, hence it can be concluded, that all three systems in the original configuration are not suitable for the EPIC mission. Both companies have been contacted

---

[2] http://n-avionics.com/projects/lituanicasat2-satellite-mission/ [cited 12-06-17]

in order to obtain additional information regarding customisation of the product. NanoAvionics was not able to disclose any information, hence their system has been discarded. The Hyperion PM200 system can be designed with additional fuel tank volume and can be produced in any possible configuration. Since all other properties fit the given budgets, it has been decided that the Hyperion PM200 propulsion system will be integrated in the EPIC CubeSats.

6.3. FUEL TANK SIZING AND CONFIGURATION DESIGN

In Chapter 5 it is determined, that in order to do reach full constellation deployment in six months, the propulsion system should provide a minimum Δv of 235m/s. A contingency of 15% is used, which gives a required Δv of 270m/s. From conversations with Hyperion Technologies, it is found that a larger fuel tank can be provided. The ratio of structural weight to propellant weight of the extra tank is 1.5. This means that, for example, a 10x10x10cm unit of extra propellant tank could be added, which would account for an extra 0.9kg of structural weight and 0.6kg of extra propellant. [25]

It should be taken into account, that with the mass of the extra propellant and extra structural weight, the available Δv decreases. By iterating the rocket equation, Equation 6.1, an total value for the propellant weight is found. The values are listed in Table 6.4.

Table 6.4: Propulsion subsystem mass break down

| Component	Mass [kg]
Initial structural mass	1.1
Initial propellant mass	0.31
Extra structural mass	0.85
Extra propellant mass	0.57
Total propulsion subsystem mass	**2.83**
Total CubeSat mass (no contingency)	**9.40**

The extra fuel mass of 0.57kg will need a fuel tank volume of 1016cm^3. With the standard propulsion system of 1U, the propulsion system would have a volume of 1833cm^3. This exceeds the the requirements stated in Table 6.1. However, it is possible to produce the system in any desired configuration using additive manufacturing, so it is a good option to store the extra fuel in otherwise unused space. [25] The customisation of the Hyperion PM200 propulsion system will bring on additional costs, but since the original costs of €150,000 are well within the budget of €200,000, this is still feasible.

It must be noted, that the mass budget of 0.9kg has not been realised. This is due to the fact, that this is not a realistic estimation. Since the total S/C mass does not exceed 12kg, this deficiency is accepted. In Section 6.5. In Figure 6.1 the standard 1U version of the propulsion system is shown and in Chapter 14, which is on the lay-out of the S/C, the configuration of the fuel tanks for the modified propulsion system can be found.

6.4. HYPERION PM200 PROPULSION SYSTEM CHARACTERISTICS

The Hyperion PM200 belongs to the category of miniature non-toxic nitrous oxide propane (NOP) propulsion systems. These are liquid bi-propellant thrusters for small satellites. The use of the green propellants nitrous oxide and propane makes the system safe and complying to the sustainability requirements. The 555g of nitrous oxide is stored in a cylindrical fuel tank. Inside this fuel tank, the 70g of propane is stored in a spherical tank. Both the nitrous oxide and the propane are operated and stored at their vapour pressure. The vapour pressure of N_2O is 45bar and the vapour pressure of propane is 7.3bar. [61]

The two reactions that are taking place in order to provide the energy for the propulsion are Equation 6.2 and Equation 6.3.
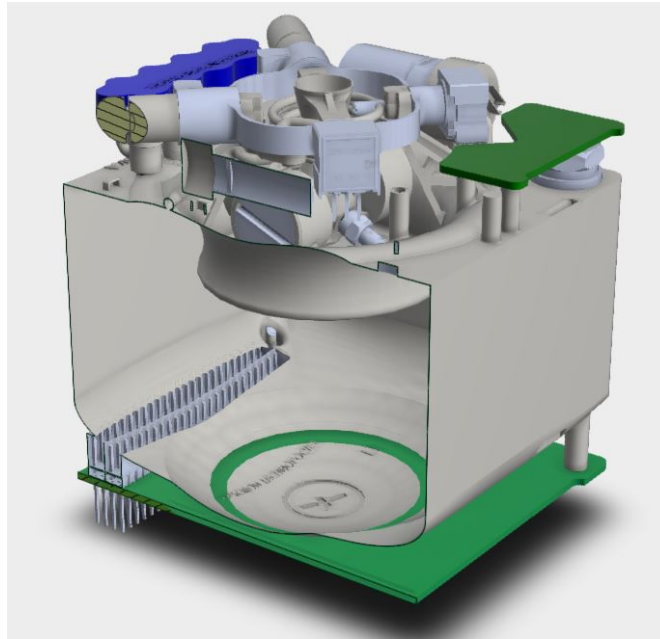
$$2N_2O \rightarrow 2N_2 + O_2 \tag{6.2}$$
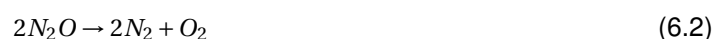
Figure 6.1: Illustration of PM200 1U unit, developed and produced by Hyperion

$$\Delta t = \frac{m}{g \cdot I_{sp} \cdot \dot{m}} \cdot \Delta v \qquad (6.4)$$

$$\dot{m} = \frac{F}{g \cdot I_{sp}} \qquad (6.5)$$

$$C_3H_8 + 5O_2 \rightarrow 3CO_2 + 4H_2O \qquad (6.3)$$

A spark plug provides a temperature of 520°C, which will decompose the nitrous oxide in nitrogen and oxygen. [62] The decomposition generates heat and thrust. This hot exhaust with high oxygen percentage can be used to initiate the propane combustion. NOP propulsion is an appropriate choice for small S/C like CubeSats, because of its high storage density and self pressurising properties. With a volume slightly higher than 2U, the PM200 in customised form, is suitable for the 6U CubeSat. In contrast to the electrical propulsion systems, which have a high power usage during longer periods, the PM200 uses less than 6W in a short period of time. This fits the power budget given in Table 6.1.

The maximum burn time for the required orbital manoeuvres can be calculated using Equation 6.4 and Equation 6.5. In this equation, Δt is the burn time in seconds and $\dot{m}$ is the mass flow in kg/s. F is the thrust provided by the propulsion systems, which is from 0.3N to 0.8N between -5°C and 40°C. For the calculation of the burn time, the worst case scenario values are used, which gives a Δt of 4402 seconds, hence to achieve the desired velocity change to perform one Hohmann transfer, the propulsion system should thrust for 2 hours, 33 minutes and 15 seconds continuously. From testing is found, that the system can fire for 15s. After this, a cooling time of 750s is necessary, which means the propulsion system requires 294 duty cycles of 765 seconds. [61] This means one Hohmann transfer will take approximately 2 days and 14 hours. This will not cause a problem in the constellation deployment time requirement.

The Hyperion PM200 propulsion system has a design life of more than five years, which is sufficient for the mission life set in the requirements. [61] All system parameters can be found in Table 6.3.

6.5. SENSITIVITY ANALYSIS

In this section a sensitivity analysis is done. The sensitivity analysis of parameters that influence more than one aspect of the mission is done in Chapter 19. In this section design modifications that have to be made in case of a change in specific impulse and safety factor of the propellant tanks are discussed.

Currently, the PM200 propulsion system has a specific impulse of 285s. If this parameter turns out to be 20% higher, i.e. 342s, this would positively influence the available Δv, using the same amount of fuel. With a specific impulse of 342s, it is also possible to scale down the fuel tank. In this case only 0.53kg of extra fuel should be added to the original configuration. This results in a total system mass of 10.75kg and a propulsion system volume of 1883cm^3.

With a specific impulse of 228s, which is 20% lower, the available Δv would decrease. This is not an option, so the fuel tank needs to be scaled up and more innovative fuel tank designs should be considered. In this case, 1.07kg of extra fuel should be stored, which results in a total system mass of 12.09kg and a propulsion system volume of 2783cm^3.

SAFETY FACTOR OF THE PROPELLANT TANK

The propellant tanks are designed to withstand two times the maximum operating pressure and are tested up to 1.5 times the maximum operation pressure. [61] This leads to a heavy structure with a structure to fuel ratio of 1.5. If this ratio is brought down with 20% to 1.2, only 0.7kg of extra fuel needs to be added to the standard 1U propulsion system, which leads to a total S/C mass of 10.9kg.

On the other hand a higher ratio can be used, although this is less likely. With a structure to fuel ratio of 1.8 an extra 0.76kg of fuel should be taken and the total CubeSat would have a mass of 11.54kg. In the detailed design phase of the mission, it would be recommendable to discuss with Hyperion if a lower safety factor would be a viable option.

6.6. CONCLUSION

The propulsion system, that is chosen for the CubeSats of the EPIC mission is the Hyperion PM200. This propulsion system has the advantage with respect to other available propulsion systems, that it can be produced in any desired fuel tank size and configuration. The EPIC mission requires a Δv of 235m/s. Although propulsion systems are available with such a high Δv, these propulsion system require a power that does not fit the power budget given in Chapter 4. The PM200 on the other hand requires a maximum operating power of 6W. Besides, the PM200 makes use of a green propellant, which fits the EPIC design philosophy regarding sustainable development.
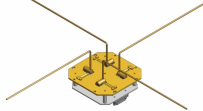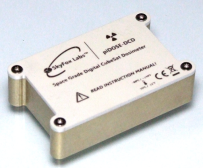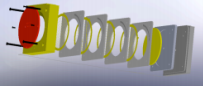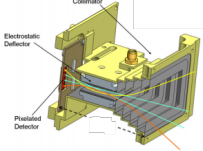
7

PAYLOAD

In the first section of this chapter, Section 7.1, specific sensor models are selected. The next section, Section 7.2, describes the methodology to configure the sensors into two payload packages. The last section, Section 7.3, presents and discusses the two configurations.

7.1. SENSOR SELECTION

In this section the specific model of each instrument type is selected. The feasible instrument types were determined in the midterm report [31]. Based on the information currently available, an existing model for each type of sensor is proposed, see Table 7.1. During the detailed design, beyond the scope of this project, the payload will still be adjusted. However, it is expected that the selected models will be sufficiently close to the final sensors. The methodology to determine the model of each type is discussed in the following list:

- **Langmuir probe:** The QB50 multiple needle Langmuir probe (mNLP) from the University of Oslo is the only flight proven, COTS Langmuir probe found. Furthermore, the project has existing relations with QB50 through the university. Therefore this model of the Langmuir probe is chosen.

- **Dosimeter:** Multiple COTS dosimeters are available, however the piDOSE-DCD from SkyFox Labs is chosen due to its performance. The sensor also does not accumulate charges and is ITAR (International Traffic in Arms Regulations) free. Integration documentation does not show any conflicts with the current S/C design.

- **Magnetometer:** During private conversations with ISIS the flight proven New Space System (NSS) Magnetometer was recommended for the mission [24]. The sensor is accurate, yet has a low volume, weight and power requirement compared to competitors. Furthermore due to the existing relationship with ISIS, this sensor is chosen. A magnetometer is affected by noise of the electronics on the S/C. Therefore the sensor will be mounted away from electronics, as discussed in the next section.

- **Electric field probe:** This type of sensor is very simple yet needs to be deployed on a boom of approximately four metres to measure sufficiently accurate. In this analysis the electric field sensor includes the deployment mechanism. Such a sensor, for a CubeSat, has only been found on the DICE mission. The sensor is called the DIME Double E-Field Probe and is made by ASTRA, a U.S. based company (ITAR-concerns). However due to the lack of alternatives this sensor is chosen, yet more research will be performed to gain more insight on the available options.

- **Ion-Neutral Mass Spectrometer (INMS):** The only COTS INMS for CubeSats found, is the QB50 INMS by University College London. Like the Langmuir probe existing relations are present with the QB50 project, affirming the decision to use this sensor.

- **Retarding Potential Analyser (RPA):** The thermal RPA model by the William B. Hanson Center for Space Sciences at the University of Texas at Dallas, is the only currently available RPA for CubeSat missions.

- **Energy Particle Detector (EPD):** The STEIN Particle Detector is again the only energy particle detector currently found on a CubeSat scale. The sensor has a high raw data rate ($1.92 \cdot 10^6$) and should be decimated by the on board computer (OBC) or by dedicated electronics.

Table 7.1: Payload instrumentation datasheet

Instrument	Model		Dimensions [mm]	Power [W]	Mass [g]	Operational temperature [°C]	Price [€]	Data rate [bit/s]	Source
Langmuir probe	QB50 m-NLP		100x100x36	1.18 [63]	225	-20 to +40	16,000[64]	2000 [65]	[66]
Dosimeter	piDOSE-DCD		53x32x14	0.5	47	-30 to +60	5,900^a	14.4[32]	[67]
Magnetometer	NSS Magnetometer		96x43x17	0.725	200	-25 to +70	15,130	720	b
Electric field probe	DIME Double E-Field Probe		95x95x15	0.1694	275	not available	50,000^c	560	[68]
Ion-neutral mass spectrometer	QB50 INMS		83x83x30.5	0.85	200	-20 to +40	50,000[64]	1300 [69]	[70]
Retarding potential analyser	Thermal RPA		96x96x63	0.45	600	-55 to +125	50,000^c	400	[71]
Energy Particle Detector	STEIN Particle Detector		95x86x75	0.46	350	not available	50,000^c	$1.92 \cdot 10^6$	[72]

[a] http://www.skyfoxlabs.com/product/16-cubesat-geiger-counter [cited 06-06-2017]
[b] https://www.cubesatshop.com/product/nss-magnetometer/ [cited 06-06-2017]
[c] Estimate based on advice [26]

7.2. CONFIGURATION SELECTION PROCESS

This section shows the selection process for the payload layout on the EPIC-A and the EPIC-B satellites. Power, mass, volume and instrument placement shall determine the outcome of the layouts.

The goal is to maximise the scientific yield by including as many types of instruments as possible on the satellites. In the midterm report [31] it was concluded that the magnetometer, dosimeter, Langmuir probe and the electric sensors scored very high in all aspects. Also, in order to facilitate the functioning of the formation flight, the aforementioned instruments are included on both the EPIC-A and EPIC-B satellites.

A number of instruments require placement on the ram face of the satellite. These include the mNLP, the RPA, INMS and the EPD. As mentioned before, the Langmuir probe is included on both EPIC-A and EPIC-B satellites. Each satellite allows placement for two ram-facing instruments. Thus a selection is made between the RPA, INMS and the EPD.

The considered aspects for the selection process include the type of measurements of the instrument, the performance of the instrument (in terms of mass, power and volume, see Table 7.1) and the source of the instrument (United States versus Europe).The RPA measures the plasma/ionic density, ionic temperature and ionic composition. The INMS determines the composition and structure of positive ions and neutral particles. The EPD measures the energy levels of the particles and distinguishes electrons, ions and neutrals. To have more distinct measurements, the RPA shall be included in the payload layout of one of the satellites. Also, the EPD originated from the United States and falls under the ITAR regulatory regime. Whereas the INMS is manufactured by a partner of TU Delft. Furthermore, the INMS has a greater flight heritage than the EPD. Considering the aforementioned aspects, the INMS is more favourable than the EPD, thus the INMS is included on one of the satellites.

Finally, some of the sensors such as the Langmuir probe and the magnetometers require adjustments. The mNLP probe by QB50 has been designed for a 3U CubeSat. Small adjustments to the sensor are needed, as seen in Figure 7.1, to ensure compatibility with a 6U. Next, the magnetometer is affected by noise from the S/C electronics. Hence for optimal measurements the sensor should be mounted away from the electronics. The required distance and mounting location is currently under investigation. However initial analysis has indicated the sensor could be mounted at the end of the solar panel, potentially combined with a boom. The sensor has therefore been given an extra mass of 100g to account for mounting. Lastly, also the non-COTS sensor, the RPA and electric field probe, are expected to be custom made for the EPIC mission.
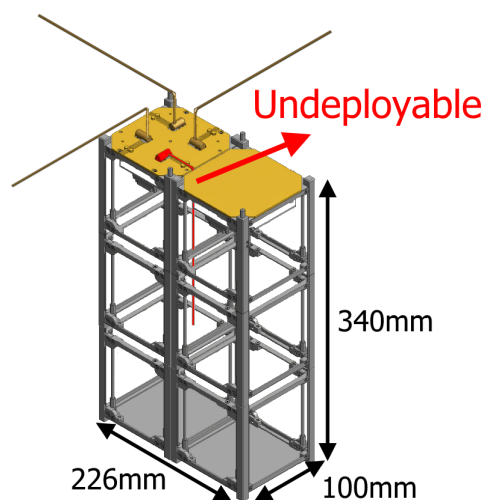

Figure 7.1: Deployment problem of the QB50 mNLP on a 6U CubeSat

7.3. RESULT

The sensor and configuration selection process results in the configurations given in Table 7.2 and Table 7.3. Due to the constraints discussed in the previous section only these two payloads are possible, hence no trade-off is made. The tables show the overall layout of the payload for both the EPIC-A and EPIC-B satellites. A contingency is added to the power, mass and volume of 5%, 10% and 10%, respectively. This contingency accounts for extra development and components required for the payload to interface with the on-board computer. with these contingencies, the power, mass, volume and cost are well within their initially assigned budgets [31].

The cost of each payload, given in the tables, is based largely on the price of the components. The payload will however require redesign and integration efforts, as discussed in the previous section. Hence a non-recurring cost has been added to the budget. The updated cost estimation of the payload will be used to improve the cost-break down structure, found in Section 4.1.

Table 7.2: EPIC-A payload layout and characteristics

Type	Power [W]	Mass [g]	Volume [U]	Cost [€]
Magnetometer	0.725	200	0.070	15,130
Dosimeter	0.5	47	0.023	5,900
Langmuir Probe	1.18	225	0.36	16,000
Electric sensors	0.4	80	0.11	50,000
INMS	0.85	200	0.21	50,000
Total	**3.42**	**947**	**0.92**	**137,030**
Total incl. contingency	**4.11**	**1136**	**1.01**	**N/A**

Table 7.3: EPIC-B payload layout and characteristics

Type	Power [W]	Mass [g]	Volume [U]	Cost [€]
Magnetometer	0.725	200	0.070	15,130
Dosimeter	0.5	47	0.023	5,900
Langmuir Probe	1.18	225	0.36	16,000
Electric sensors	0.4	80	0.11	50,000
RPA	0.45	600	0.55	50,000
Total	**3.02**	**1347**	**1.26**	**137,030**
Total incl. contingency	**3.63**	**1616**	**1.38**	**N/A**

<div align="right">

8

</div>

ATTITUDE DETERMINATION AND CONTROL SUBSYSTEM

The Attitude Determination and Control System (ADCS) stabilises, controls and positions a satellite in a desired orientation despite any external or internal disturbances acting on it [73]. It can be viewed as an angular momentum management system, and angular momentum as a commodity that can be acquired, dumped or stored [29]. Attitude solution design for S/C is an iterative process, and for the EPIC S/C this process is initiated in Section 8.1 with the specification of requirements. In Section 8.2 the mathematical attitude model is explained and quantified. The results of the first two sections enable the selection, sizing and an ADCS COTS product trade-off, which is executed in Section 8.3. Once the operational environment and the attitude hardware are determined, an assessment on commonly used ADCS algorithms is given in Section 8.4. Finally, the results of the subsequent sections of this chapter are synthesised in an attitude propagation simulation in Section 8.4, followed by a Verification, Validation & Recommendations assessment in Section 8.7.

8.1. OPERATIONAL MODES & REQUIREMENTS

The ADCS design requirements are derived from the mission goals. Since the EPIC mission is executed in different phases and therefore in different operational modes, the attitude requirements for each mode are analysed separately. The identified EPIC modes are the following:

- **Orbit insertion:** first phase after jettison. ADCS is not activated.
- **Acquisition:** initiation of power generation, attitude determination and stabilisation of S/C for enabling communication with ground stations. Can be used after power upsets and failures.
- **Drive:** for the realisation of the constellation - S/C shall propel to different altitudes (Chapter 5).
- **Normal:** payload is collecting scientific data, communication with ground stations is enabled.
- **Contingency:** safe mode, used if failures occur. Lower power requirements apply.

The assessed performance criteria are defined in the list below:

- **Pointing accuracy:** degree of control of S/C attitude - with respect to an inertial reference frame.
- **Range:** range of angular motion over which requirement must be acquired.
- **Transient response:** allowed settling time or attitude overshoot - in response to inputs.

Table 8.1 provides an overview of the EPIC ADCS operational modes and their respective requirements.

Table 8.1: EPIC ADCS operational modes and respective requirements.

Parameter	Acquisition	Drive	Normal	Contingency
Pointing accuracy [°]	-	30	1	-
Range [°/s]	all	0-30	0-1	all
Transient response [s]	17100	60s	60s	-

The most stringent pointing accuracy - which is 1°, is dictated by the RPA payload (Chapter 7). During the drive mode, the required pointing accuracy is 30°, which establishes communication maintenance between S/C and ground stations (Chapter 9). After a disturbance input these pointing requirements

must be met within one minute. The pointing accuracies that can be achieved depend on the radial velocity of the vehicle, and are 0-30 %/s and 0-1 %/s for the drive and normal modes, respectively. The S/C must be able to enter the acquisition and contingency modes at all realistic radial velocities for the EPIC vehicles. Acquisition of attitude stability must be attained within three orbits ($\pm$17100s), for the drive and the normal modes this is one minute.

8.2. MATHEMATICAL ATTITUDE MODEL

The S/C rotational motion can, in approximation, be seen as independent of its transnational motion [29]. There are however many other, often complex parameters that do influence the S/C attitude. In this section the mathematical model that correlates angular momentum and rotational motion is introduced, after which the attitude model parameters - the S/C geometric properties and the external disturbance torques - are quantified.

EQUATIONS OF ROTATIONAL MOTION

Angular momentum ($\mathbf{H}_c$ in kgm^2/s) is a vector quantity which is related to a body's angular velocity (ω in rad/s); it can be calculated with Equation 8.1 [29]. Here, $[I_c]$ represents the inertia matrix of a body referred to its centre of mass C and $\mathbf{h}$ the angular momentum stored by rotational objects (e.g. reaction wheels). Torque is the change of the angular momentum with time - as depicted in Equation 8.2. Equation 8.3 is the conservation equation of motion for rotational dynamics, as provided by the Newton-Euler law, obtained by applying the product rule of calculus to Equation 8.1 and rearranging the result.

$$\mathbf{H}_c = [I_c]\omega + \mathbf{h} \quad (8.1) \qquad \frac{d\mathbf{H}_c}{dt} = \mathbf{T} \quad (8.2) \qquad \mathbf{I}\dot{\omega} = \mathbf{T} - \dot{\mathbf{h}} - \dot{\mathbf{I}}\omega - \omega \times \mathbf{H} \quad (8.3)$$

With Equation 8.3 the rate of change of angular velocity ($\dot{\omega}$) of a body can be calculated. There are four aspects that influence its outcome. The first term on the right hand side indicates that the S/C attitude dynamics depend on the inputs of external torques. It also shows that attitude can be managed by creating external torques with certain actuators (e.g. magnetic torquers). The second term describes the influence of internal torques, it shows how the changes in rotational velocity of S/C components, such as reaction wheels, can affect the S/C rotational velocity. The third term needs to be taken into consideration when changes in mass distributions occur, e.g. when articulations of solar panels or antennae are executed. The fourth term indicates that the rotation of a S/C, when considered in the S/C reference frame, changes the direction of angular momentum, whilst the magnitude stays constant (commonly known as the gyroscopic stiffness) [74].

QUATERNIONS

Defining S/C attitude requires only three Euler angles. However, this methods is computationally intensive and includes singularities, which are certain orientations at which an angle is not defined. Quaternion representation is more common for S/C attitude simulations - it simplifies the kinematic and dynamic equations and it includes no singularities.

A quaternion representation is a 4×1 matrix. Using Euler's rotational theorem the quaternion can be defined with a rotational angle θ and a rotational axis as shown in Equation 8.4; vector $\mathbf{e} = (e_x, e_y, e_z)$ being a unit vector representing the axis of rotation.

The dynamic equation of motion in quaternion representation, as defined by Wertz [75], is depicted in Equation 8.5. In this equation a constant rotational rate is assumed over an infinitesimal time Δt.

The kinematic equation of motion in quaternion form is given by Equation 8.6. Here, the quaternion differentiated with respect to time $\dot{\mathbf{q}}$ is given as a function of the the previous quaternion $\mathbf{q_k}$ and the skew symmetric matrix Ω, which represents the angular velocity of the S/C.

$$\mathbf{q} = \begin{bmatrix} e_x \sin\frac{\theta}{2} \\ e_y \sin\frac{\theta}{2} \\ e_z \sin\frac{\theta}{2} \\ \cos\frac{\theta}{2} \end{bmatrix} \quad (8.4) \qquad \mathbf{q_{k+1}} = \mathbf{q_k} + \dot{\mathbf{q}}\Delta t \quad (8.5) \qquad \dot{\mathbf{q}} = \frac{1}{2} \begin{bmatrix} 0 & \omega_z & -\omega_y & \omega_x \\ -\omega_z & 0 & \omega_x & \omega_y \\ \omega_y & -\omega_x & 0 & \omega_z \\ \omega_x & -\omega_y & -\omega_z & 0 \end{bmatrix} \mathbf{q_k} \quad (8.6)$$

An elaborate explanation on mathematical quaternion operations, Direction Cosine Matrices and reference frame transformations between Earth-centred inertial, Earth-centred Earth-fixed and spacecraft fixed reference frames, is out scope of this report can be found (among others) in [75] and [76].

GEOMETRIC PROPERTIES
The quantification of disturbance and control torques requires an assessment of the centre of mass of the S/C body, which results from Equation 8.7. A centroid can be viewed as the average point of an area and as such, the application of a force through the centroid shall create no torque. When there exists an offset of distance between the two, the S/C shall rotate about its centre of mass.

$$\begin{bmatrix} C_x \\ C_y \\ C_z \end{bmatrix} = \frac{1}{\sum m} \begin{bmatrix} \sum m\bar{x} \\ \sum m\bar{y} \\ \sum m\bar{z} \end{bmatrix} \quad (8.7) \qquad \begin{aligned} I_{xx} &= \int (y^2 + z^2)dm \\ I_{yz} &= \int (yz)dm \end{aligned} \quad (8.8) \quad [I_c] = \begin{bmatrix} I_{xx} & -I_{xy} & -I_{zx} \\ -I_{xy} & I_{yy} & -I_{yz} \\ -I_{zx} & -I_{yz} & I_{zz} \end{bmatrix} \quad (8.9)$$

The equations of rotational motion depend on the changes in moments of inertia of a body (see Equation 8.3). For a body, the moment of inertia is defined as the second moment of mass about an axis and the product of inertia is viewed as a measure of the lack of symmetry in a mass distribution. For example for the x-axis, these two types of inertia can be calculated using Equation 8.8. The inertia matrix $[I_c]$ of an object is depicted in Equation 8.9. Using principal axes, which are a set of orthogonal axes of a body for which the products of inertia are zero, the mathematical models can be simplified [29]. For the EPIC S/C the mass moments of inertia for principle axes are depicted in Table 8.2.

Table 8.2: Moments of inertia for principal axes of the EPIC S/C.

Geometric property	I_{xx} [kg/m^2]	I_{yy} [kg/m^2]	I_{zz} [kg/m^2]
Magnitude	0.058	0.104	0.137

EXTERNAL DISTURBANCE TORQUES
The environment in which a S/C operates drives the ADCS design. For EPIC S/C, four major sources of disturbance torques are present: solar radiation pressure (SRP), aerodynamic drag, gravity-gradient effect and the Earth's magnetic field. Quantification of the disturbance torques is necessary for the selection and sizing of the attitude control hardware. These calculations are performed under the following assumptions:

- **Keplerian parameters:** the operational orbit is at an altitude of 520km and an inclination of 55°.
- **Earth geometry:** Earth is assumed to be a perfect sphere - thus flattening effects are neglected.
- **Disturbance torque model simplification:** disturbance torque quantification is performed with simplified mathematical models. As the variables that are used here are taken such that maximum torques are found, this simplification is justified for the ADCS design.
- **Contingency:** disturbance torques other than the four major once are neglected in calculations. These include e.g. infrared emission pressure, albedo effects and outgassing. These torques are, compared to the four major ones, relatively small and are covered in the design by including a margin of 20% - this method shall negate the contribution of these torques as well as other unforeseen events [74].

The maximum torque created by SRP can be estimated with Equation 8.10. Here, T_s is the SRP torque, Φ is the solar constant, c is the speed of light, A_s is the sunlit surface area, q is a unitless reflectance factor that can take the values between 0 and 1 (for maximum torque assume perfect reflection - take q as 1), ϕ is the angle of incidence of solar flux (for maximum torque assume 90°) and the term $cp_s\text{-}cm$ represents the distance between the centres of solar radiation pressure and mass.

The maximum torque created by aerodynamic drag on S/C can be estimated with Equation 8.11. Here, T_a is the atmospheric drag torque, C_d is the drag coefficient, A_r is the ram area, V is the orbital velocity and the term $cp_a\text{-}cm$ represents the distance between the centres of aerodynamic pressure and mass.

$$T_s = \frac{\Phi}{c} A_s (1+q)(cp_s - cm)cos(\phi) \qquad (8.10)$$

$$T_a = \frac{1}{2} C_d A_r V^2 (cp_a - cm) \qquad (8.11)$$

The maximum torque on S/C created by the Earth's magnetic field can be estimated with Equation 8.12. In this equation, T_m is the magnetic torque, D is the S/C's residual dipole moment and B is the magnetic field strength. B can in turn be obtained from the magnetic constant M, the distance between the Earth's and S/C's centre of mass R and λ, a unitless function of the magnetic latitude, which takes the value of 1 at the magnetic equator and 2 at the magnetic poles.

$$T_m = DB = D\left(\frac{M}{R^3}\lambda\right) \qquad (8.12)$$

$$\begin{bmatrix} T_{g_x} \\ T_{g_y} \\ T_{g_z} \end{bmatrix} = \frac{3\mu}{2R^3} \begin{bmatrix} |I_{zz} - I_{yy}|\sin(2\phi)\cos^2(\theta) \\ |I_{zz} - I_{xx}|\sin(2\theta)\cos(\phi) \\ |I_{xx} - I_{yy}|\sin(2\theta)\cos(\phi) \end{bmatrix} \qquad (8.13)$$

The gravity gradient force gets weaker with increasing altitude. The maximum torque components that can be created by this source are found using Equation 8.13. Here, T_g represents the gravity gradient components in the respective x, y and z directions, μ is the Earth's gravitational constant, R is the distance between Earth's and S/C's centre of mass, ϕ and θ refer to the roll (about the x-axis) and pitch (about the y-axis) angles respectively.

$$T_{g,total} = \sqrt{T_{g_x}^2 + T_{g_y}^2 + T_{g_z}^2} \qquad (8.14)$$

$$T_{total} = \sqrt{T_s^2 + T_a^2 + T_m^2 + T_g^2} \qquad (8.15)$$

The total gravity gradient and the total overall torques can then be found using the root sum squared method, as depicted in Equation 8.14 and Equation 8.15, respectively [29].

Initial disturbance torque calculations are then performed and a check with the constraints of reaction wheel storage capabilities is obtained. It is found that the reaction wheels available on the market for 6U CubeSats have a momentum storage capacity of less than 60mNms. With this in mind, iterations in calculations are performed. The findings in the results can be summarised and new requirements can be generated. These findings, and their respective sources, are the following:

- **Magnetic cleanliness**: Normally, S/C generate a magnetic field themselves, since magnetic materials are incorporated in the hardware and because electric currents produce magnetic fields as well. The interaction between Earth's and S/C's magnetic field then causes a magnetic torque. The magnetic torque has shown to be the largest one of the four major once in initial calculations for EPIC and without extra measures the pointing accuracy of 1° has proven to be unachievable. A 6U CubeSat typically has a magnetic residual dipole in the order of 0.1-0.5Am^2. However, the EPIC S/C shall have to be assembled under conditions that will ensure a 'magnetic cleanliness', where the S/C magnetic dipole shall be reduced to at least 0.013Am^2. A detailed assessment on how this can be achieved is out of scope of this project. But it can be noted that this will require a thorough analysis of the magnetic dipoles on subsystem level - these then can be integrated such that the overall S/C dipole is cancelled to some degree. The incorporation of permanent magnets can realise this requirement as well [77].

- **Solar activity:** solar activity has cycles of approximately 11 years and its magnitude greatly influences atmospheric density and thus the aerodynamic disturbance torque. For an average solar activity, assuming the MSISE-90 model[1] and a respective atmospheric density of 4.03·10^{-14}kg/m^3 at 520km, the EPIC satellites cannot achieve the 1° pointing requirement; this is only achievable above 530km (assuming the magnetic cleanliness requirement is satisfied). Below this limit, the atmospheric density increases and the reaction wheel momentum storage capacity is exceeded. However, requirements from Δv budget and constellation deployment dictate that the operational altitude shall initially be at 520km. The mission must therefore be planned such, that the S/C will operate during a period of low solar activity. The EPIC launch date has, as for now, been set up to be in 2019; sunspot Cycle 25, which entails a lower solar activity, is predicted to initiate at the end of 2019, with its sunspot maximum occurring in 2024[2]. It can therefore be concluded that a lower solar activity can be assumed in the calculations for EPIC ADCS sizing. If the EPIC orbit insertion is indeed to occur at solar minimum activity, the S/C shall decay only 10km in 3 years of operational life. At 520km the the atmospheric density can be assumed to be 4.03·10^{-14}kg/m^3 and at

---

[1] http://www.braeunig.us/space/atmos.htm [cited 26-06-17]
[2] https://en.wikipedia.org/wiki/Solar_cycle [cited 27-06-17]

510km to be $5.03 \cdot 10^{-14}$ kg/m^3 for the MSISE-90 model (which was the case for the NLRMSISE-00 model in mid January of 2010[3]).

The EPIC variables and results for the four major disturbance torques are provided in Table 8.3 [29]. Note that the solar and magnetic torques are the highest in magnitude - that is when the magnetic cleanliness requirement is complied with. The ADCS must at least be able to overcome the highest occurring disturbance torque [74] - it is therefore sized for the initial altitude of 520km and then checked for its performance at 510km. It must be noted that at a higher solar activity or atmospheric density than is assumed, the pointing accuracy can still be achieved. It will however, not be achieved continuously. For continuous achievement a atmospheric density of less than $2.7 \cdot 10^{-13}$ kg/m^3 is required.

Table 8.3: Inputs and results for the disturbance torque calculations for the EPIC mission; a 20% margin is included in the results [29].) [74].

T_s [Nm] $7.14 \cdot 10^{-7}$	Φ [W/m^2] 1367	c [m/s] $3 \cdot 10^8$	A_s [m^2] 0.18	ϕ [°] 90	q [-] 0.6	cp_s-cm [m] 0.34
T_a [Nm] $1.08 \cdot 10^{-7}$	C_d [-] 2.2	A_r [m^2] 0.175	V [m/s] $7.602 \cdot 10^3$	(cp_a-cm) [m] 0.34	-	-
T_m [Nm] $7.04 \cdot 10^{-7}$	D [Am^2] 0.013	B [T] $4.5 \cdot 10^{-5}$	M [Tm^3] $7.602 \cdot 10^{15}$	λ [-] 1.9	-	-
T_g [Nm] $1.46 \cdot 10^{-7}$	μ [m^3/s^2] $3.986 \cdot 10^{14}$	R [m] 6378137	ϕ[°] 45	θ [°] 45	-	-

8.3. ATTITUDE SOLUTION DESIGN

The ADCS consists of the Attitude Determination System (ADS), the Attitude Control System (ACS) and requires computational power from the OBC. The OBC processes the ADS sensor inputs, compares these with the desired attitude and generates an input for actuators - if necessary. The overall attitude performance shall be the product of both the knowledge determination and attitude control, thus of the combined performance of the attitude sensors and actuators. There exists a number of different ADCS solutions on the market [29]. The final attitude solution for EPIC shall mainly depend on the requirements and the currently available COTS attitude packages for 6U CubeSats.

SELECTION OF ATTITUDE CONTROL METHODS

Passive stabilisation techniques, using e.g. gravity gradient torques, have the advantage of lower power and mass budget consumption. However, the attitude control errors that they can provide are in the order of 5°; this does not suffice the EPIC requirements. Thus, an active attitude control system is required [78]. Three axes active attitude control techniques are much more common nowadays - even though they are more expensive and more complex - they have demonstrated comparable or even higher total reliability performance [74]. Widely used active ACS are magnetorquers; the incorporation of three magnetorquers improves the control errors for roll and yaw to 3° and 2°, respectively. An additional constant speed reaction wheel can decrease the control errors to less that 0.2° per axis [78]. The magnetorquers can then be used for accumulated momentum dumping, stored in the reaction wheels. In summary, the attitude control method for EPIC is selected to be active and to exist out of three-axis magnetorquers and three-axis reaction wheels - a widely used technique for S/C with comparable requirements, that can attain the required EPIC pointing accuracy of 1° and which is more reliable compared to passive control techniques [74].

SIZING OF CONTROL HARDWARE PERFORMANCE

Sizing S/C attitude actuator performance is based on an analysis of the maximum occurring disturbance torques and an evaluation of the slew and pointing accuracy requirements. Firstly, the reaction wheel sizing is executed. This must be done for two performance criteria: disturbance torque resilience and pointing accuracy achievement. Both performances can be quantified in terms of reaction wheel momentum storage capacity.

---

[3] https://ccmc.gsfc.nasa.gov/modelweb/models/nrlmsise00.php [cited 26-06-17]

The required reaction wheel momentum storage capacity h$_{D,store}$, for disturbance torque resilience can be calculated by integrating the worst-case occurring disturbance torque over a full orbit. A simplified expression can be used to simulate this sinusoidal phenomenon, as depicted in Equation 8.16. Here, the 0.707 is the root mean square average of a sinusoidal function, T$_D$ is the maximum occurring disturbance torque and P the period of a full orbit.

$$h_{D,store} = T_D P \frac{0.707}{4} \qquad (8.16) \qquad\qquad h_{a,store} = \frac{T_D}{\theta_a} \frac{P}{4} \qquad (8.17)$$

The required reaction wheel momentum storage capacity h$_{a,store}$, for meeting the most stringent pointing accuracy requirement of 1° (Chapter 7), can be calculated with a simplified mathematical model, as depicted in Equation 8.17. Here, θ_a is the required pointing accuracy in rad.

The maximum torque a reaction wheel must be capable of exerting, is dictated by the slew requirements and can be found using Equation 8.18. Here, I represents the moment of inertia about the rotational axis, θ the rotational angle in rad and t is the time span of the slew manoeuvre. Note here that no specific slew requirements - other than nadir pointing, are required for EPIC S/C. The momentum that needs to be stored during this slew can be found using Equation 8.19. The time span for the nadir slew must be considered for half an orbit (see next paragraph).

$$T_{slew} = 4\theta \frac{I}{t^2} \qquad (8.18) \qquad h_{slew,store} = T_{slew} \frac{t}{2} \qquad (8.19) \qquad D = \frac{T}{B} \qquad (8.20)$$

The working principles of magnetorquers are based on creating a magnetic dipole (D), by letting electric current run through their coils. In the vicinity of the Earth's magnetic field, a torque is then exerted on the S/C body, which results from Equation 8.20. Magnetorquers that are to be used for momentum dumping, must cover the maximum disturbance input and include an extra margin, which serves as a compensation for the lack of full directional control. The maximum dump torque is only two times available per orbit, because of the shape of Earth's magnetic field. As a rule of thumb, a S/C magnetorquer must be able to provide a magnetic moment of 3-10Am^2 for an output of 1Am^2 from Equation 8.20 [74]; for EPIC calculations are executed for the higher estimate.

An overview of the resulting quantified hardware performance required for EPIC ADCS is depicted in Table 8.4.

Table 8.4: Momentum storage, slew torque and magnetic dipole performance requirements for the EPIC ADCS hardware.

h$_{D,store}$ [Nms]	h$_{a,store}$ [Nms]	T$_{slew}$ [Nm]	h$_{slew,store}$ [Nms]	D [Am^2]
7e-4	6e-2	2e-7	2e-4	0.2

SELECTION OF ATTITUDE SENSORS

The total attitude control that can be obtained is the accumulated result of the errors provided by the accuracy determination and control. With its high 1° pointing accuracy requirement in two axes (yaw and pitch), the EPIC mission justifies the implementation of attitude determination sensors that can provide the highest accuracy determination, even though this comes at a higher cost, volume and mass budget. The sensor that can provide the highest determination accuracy, which is in the range of 0.0003° to 0.01°, is the star tracker. Nowadays more often called a star camera, this sensor creates an image by letting light fall onto its charge coupled device, creating an image (a working principle similar to the one of a digital camera) which is then compared to a built-in star catalogue, from which a three-axis attitude determination is obtained. Star trackers can however be highly sensitive to the intense radiation in the Van Allen belts of the Earth's magnetosphere and the EPIC S/C shall approach these during the constellation deployment phase (Chapter 5). Therefore a gyroscope - an inertial sensor which measures the angular rotation - can be added if fitting within budget. More commonly for CubeSats are microelectromechanical systems gyroscopes (MEMS gyros) [74] [25].

A market research is then performed to identify the currently available COTS ADCS for 6U CubeSats that can reach the EPIC mission objectives. Many not-integrated ADCS products are available on the market for CubeSats. However, only integrated ADCS packages are considered for the EPIC mission, since the assumption is made that the assembly, integration and testing of the various not-integrated components would require more budget resources and increase the design complexity, which in turn increases the development risk.

Only three ADCS packages are currently COTS available for 6U CubeSats that can comply with the EPIC requirements. Two of these are produced by USA companies Blue Canyon Technologies (BCT)[4] and Maryland Aerospace (MAI)[5], one is produced by Hyperion from Delft [25].

A trade-off of these products is performed, as shown in Table 8.5. The most driving trade-off criteria were selected: control accuracy, space lifetime, mass, volume, flight heritage and the regulations that these products may fall under. Other criteria have been discarded because off very similar performance parameters, which would not contribute to decision making, these were the following: cost, determination accuracy, slew rate and maximum torque. The selected criteria for which the characteristics of the three packages are comparable are given a relatively low weight of 1/20. Flight heritage is given a weight factor of 1/4 and whether the product is possibly subject to regulations is given a driving weight factor of 1/2. USA high tech state-of-the-art products may be subjected to ITAR regulations [26].

The obvious winner of this trade-off is the Hyperion ADCS package. It should be noted that this offers another advantage: the propulsion system for the EPIC mission is selected from the same company. This offers leaner integration and calibration possibilities between the ADCS and the propulsion system. A section cut of this product is depicted in Figure 8.1. Although the initial budget allocation for the ADCS was heavily underestimated, the system still fitted within the final design budget (Chpater 4).

Table 8.5: Trade-off of the three ADCS packages from Hyperion, Blue Mountain Tech and Maryland Aerospace. The winner is Hyperion. Green: excellent, exceeds the expectations; blue: good, meets the expectations; yellow: correctable or acceptable deficiencies; red: unacceptable deficiencies.

Criteria with weights								
Options	Accuracy (1/20)	Life (1/20)	Mass (1/20)	Volume (1/20)	Power (1/20)	Regulations (1/2)	FH (1/4)	
Required	1 °	3 years	196 g	0.15 U	1.2 W	no ITAR	Yes	Score [%]
1 HYP	green «1 °	blue 3	yellow 1700 g	yellow 0.7 U	yellow 2 W	green NL	yellow algorithms	51
2 BCT	green ±0.007 °	blue 3	yellow 1230 g	yellow 0.75 U	yellow 2 W	red USA	yellow algorithms	20
3 MAI	blue 1°	green 5	yellow 694 g	yellow 0.516 U	blue 1.13 W	red USA	green yes	29

After the trade-off has been performed, a sensitivity analysis was performed by firstly removing the trade-off criteria one by one and secondly, by adding and removing 1/10 weight factor to each criteria subsequently. The only factor that changed the results was the removal of the regulations criterion. In that case the MAI ADCS was the winner.

8.4. ATTITUDE ALGORITHMS

The working principle of an active ACS is based on tracking the error signals e - the difference between S/C attitude, as determined by the sensors, and the desired one - after which a corrective torque is calculated from a suitable algorithm in the OBC. For S/C mainly two algorithms are commonly applied for attitude control: Proportional-Integral-Derivative (PID) and Bdot. In this section these are discussed and applied to simulate the EPIC S/C stability characteristics.

---

[4] http://bluecanyontech.com/ [cited 28-06-17]
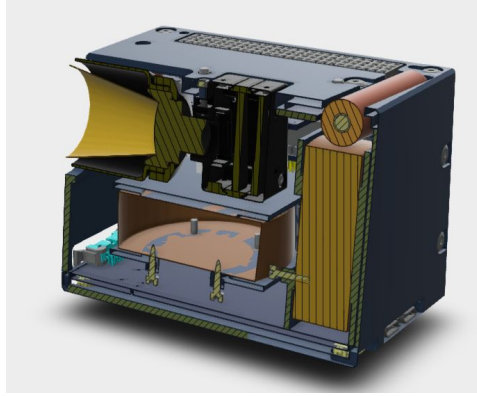[5] http://maiaero.com/ [cited 28-06-17]

Figure 8.1: Section cut view of iADCS400 by Hyperion

KALMAN FILTERS

The pointing accuracy that can be attained for the full S/C system is the sum of errors obtained in each step of determination and control. All attitude data, as determined by the sensors, shall have some degree of error. It has been shown in the previous sections of this chapter that obtaining the EPIC pointing accuracy is only just achievable, and only under low solar activity circumstances. Therefore, it is crucial to reduce the attitude errors in each and every step of the system - if this is possible within the budgets. For attitude determination a Kalman (type) filter is the widely used choice for S/C. It is a linear optimal estimator and is recursive, which means that new measurements can be processed as they arrive. The Kalman filter assumes that the input attitude states are random and Gaussian distributed, each state having a mean μ and an uncertainty - variance σ^2. It includes correlations between states in a covariance matrix, estimates the current state and predicts the next. In each iteration step the new best estimate is a prediction form the previous best estimate plus a correction for known external disturbances. The new uncertainty is determined derived from the previous uncertainty and includes additional uncertainty from the environment.

PROPORTIONAL-INTEGRAL-DERIVATIVE

The Proportional-integral-Derivative algorithm tracks e and computes its integral and derivative to form the output signal (u), a schematic overview of this principle is depicted in Figure 8.2. The output signal is a sum of e times the proportional gain K_p, the integral of e times the integral gain K_i and e times the derivative gain (K_d). The exerted control torque is calculated from u with Equation 8.21, here given as an example for the roll error (about the x-axis). Each of the gains has a different effect on the output signal u. K_p states the magnitude of control torque is to result from a unit of e. Increasing (K_d) has the effect of slowing down the response of the system - in other words, it has a damping effect on the attitude rate. A feedback system in which K_i is zero, shall always maintain a signal error as long as the disturbance torque is present: the steady-state error. Including K_i in the system can get rid of this error, as it makes the control torque increase gradually.
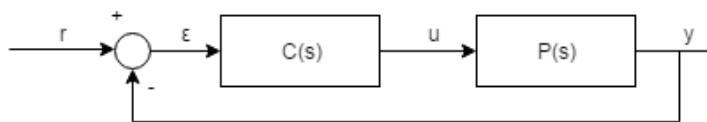
Figure 8.2: Unity feedback schematic for the PID algorithm. Here, the controller (C(s)) represents the OBC of an ADCS system; the plant (P(s)) represents both the ADS and the ACS combined.

$$T_{xc} = -K_p\phi - K_{xd}\dot{\phi} - K_{xi}\int \phi \, dt \quad (8.21)$$

BDOT

A common algorithm used for commanding the magnetorquers is the Bdot. It is widely used, effective, yet relatively simple and can be used to detumble the S/C and for dumping built up momentum by the

reaction wheels. This algorithm uses magnetometer data inputs to calculate the rate of change of the magnetic field (**B** derivative, **Bdot**) and commands the magnetorquers to set the S/C dipole to a gain (k) multiplied by the change in the magnetic field (**Bdot**). A control torque results, as the Earth's magnetic field acts on the S/C dipole vector. The magnitude of the control torque is calculated with equation Equation 8.22.

$$\mathbf{T}_c = \mathbf{D} \times \mathbf{B} = -k(\mathbf{B}_{k+1} - \mathbf{B}_k) \times \mathbf{B} = k(\omega \times \mathbf{B}) \times \mathbf{B} \tag{8.22}$$

8.5. RESULTS

An overview of the ADCS system is provided in the block diagram depicted in Figure 8.3.
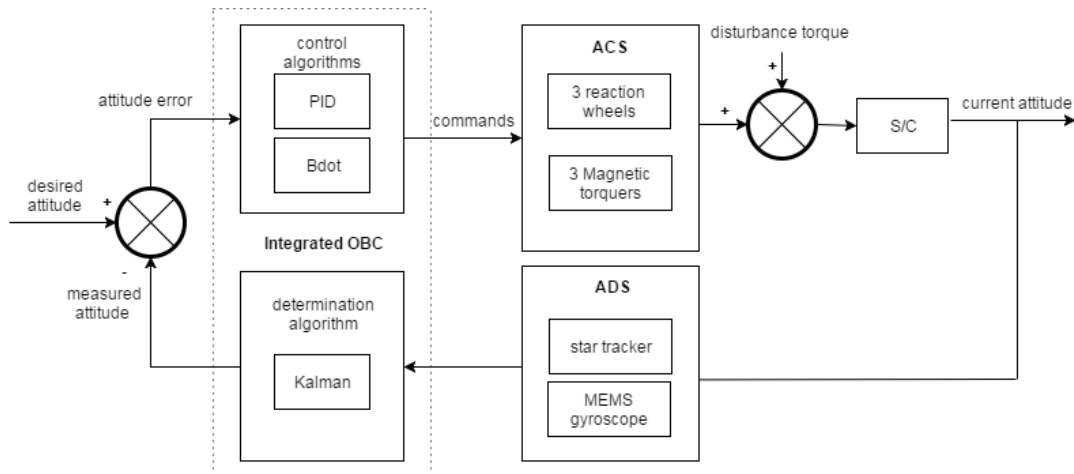

Figure 8.3: Block diagram of the EPIC ADCS.

The designed EPIC ADCS performance was then simulated in Matlab environment and the attitude control results are depicted in Figure 8.4 - Figure 8.7. The geometric properties, the disturbance torques, the selected Hyperion ADCS hardware and the control algorithms are integrated in the simulation. Note that perfect attitude knowledge is assumed, i.e. the Kalman filter is not included in the simulation. Much like the disturbance torques, the overall error is the square root of the sum of the component errors.

Figure 8.4 simulates the response of the EPIC S/C attitude with an initial tumbling rate - (ω_x, ω_y, ω_z) = (0.1, -0.05, 0.05) - to the Bdot algorithm. Results are indicated separately for the roll (ϕ), pitch (θ) and yaw (ψ) angles of the vehicle body in the spacecraft reference frame. The settling time is found to be 3251s, i.e. after this amount of time the attitude error remains within 1°. Figure 8.5 depicts the respective control torques in the x, y and z axes, exerted by the three-axes magnetic torquers.

Figure 8.6 simulates the response of the EPIC S/C attitude response to a maximum occurring disturbance torque. The settling time for 1° pointing accuracy for the PID controller has been found to be 41s. Figure 8.7 depicts the respective control torques in the x, y and z axes, exerted by the reaction wheels.

8.6. SENSITIVITY ANALYSIS

A sensitivity analysis was then performed for three variables: atmospheric density (due to change in solar activity), operational altitude and magnetic cleanliness. The results are the following:

- **Solar activity:** assuming the MSISE-90 atmospheric model, the pointing accuracy that can be achieved during solar average and solar maximum activity, at an altitude of 520km, is 2° and 51°, respectively.

- **Altitude:** under low solar activity conditions the pointing accuracy that can be achieved is 1° between 450-600km altitude and is limited by the magnetic torque. Under average solar activity this is 2.7° for 600km, 4° for 450km and 1° for 600km.
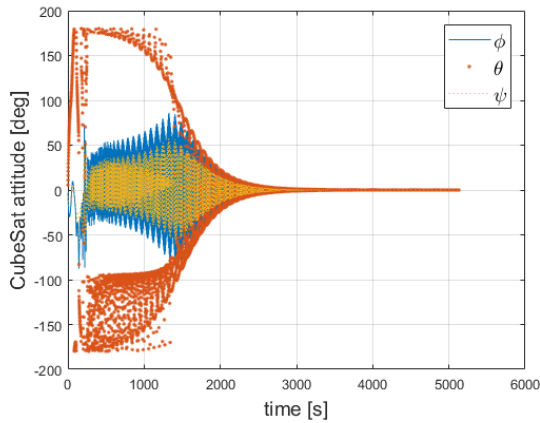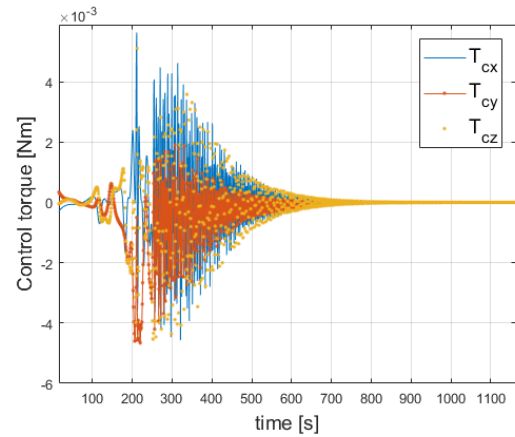
Figure 8.4: Response to BDot algorithm

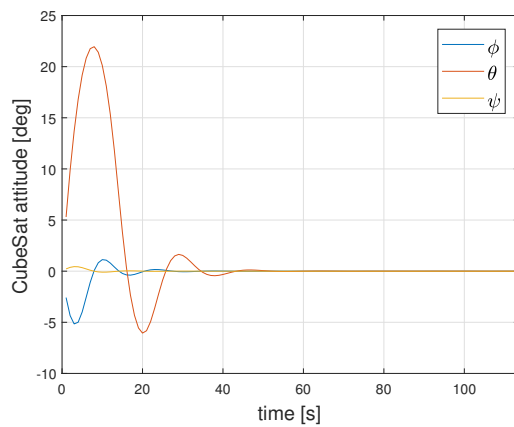Figure 8.5: Magnetorquer control torque
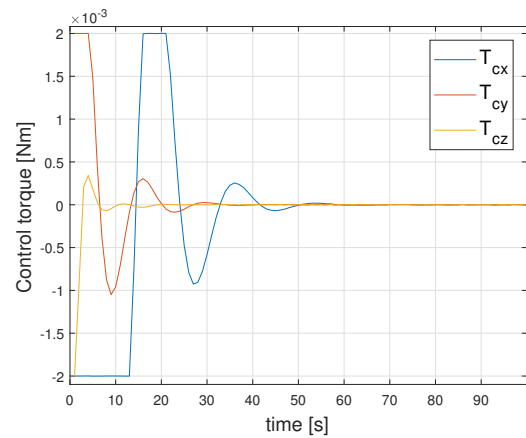

Figure 8.6: Response to PID algorithm

Figure 8.7: Reaction wheel control torque

- **Magnetic cleanliness:** for low solar activity at 520km altitude, $0.1Am^2$ and $0.2Am^2$ lead to a pointing accuracy of $7.4°$ and $14.8°$, respectively. Lowering the magnetic cleanliness had no effect, since then the aerodynamic torque became dominant.

8.7. VERIFICATION, VALIDATION & RECOMMENDATIONS

The procedures to be executed for ensuring the EPIC ADCS design meets the requirements and fulfils its purpose - the verification and validation, are discussed in this section.

VERIFICATION

Verification of the resulting calculations is done by comparing the calculated values with other low earth orbit (LEO) operational, preferably 6U, CubeSats.

- **Geometric properties:** moments of inertia in principal axes of the ARAPAIMA, a 7kg 6U CubeSat are not significantly different compared to EPIC S/C. I.e. Ixx,Iyy,Izz = (0.0541, 0.0914, 0.1054)kgm2 for ARAPAIMA versus Ixx,Iyy,Izz = (0.058, 0.104, 0.137)kgm^2 for EPIC [79].
- **Disturbance torques:** for the ARAPAIMA mission, operational at an altitude of 500km the disturbance torques were calculated for the high solar activity. The mathematical model for EPIC was then tested for the inputs values of the ARAPAIMA CubeSat. The disturbance torques that resulted from the calculations used for the EPIC model, applied to the ARAPAIMA CubeSat and its parameters were in the same order of magnitude [79]. It must be noted here that the solar constant, assumed for the ARAPAIMA mission for high solar activity at 500km, was taken as Φ = 1,366W/m2. For EPIC this was assumed to be Φ = 1,367W/m2 for 500km at low solar activity.

For the EPIC mission at low solar activity the solar torque is therefore likely overestimated. However, this shall not change the design since the magnetic torque shall then dominate and drive the design (see Table 8.3).

- **Sizing of hardware performance:** the calculated performance requirements are within the range of what the market currently has to offer (Section 8.3). Although it must be noted that it is reaching the limit of what is currently possible in terms of pointing accuracy requirements for CubeSats - a low solar activity and a magnetic cleanliness of the vehicle needed to be assumed in order to meet the requirements. No other CubeSat mission that use an active ADCS for CubeSats, for LEO orbits below 650km and that can reach a pointing accuracy requirement of 1°, have not been found.

- **Algorithms:** the simulations are performed with the assumption that certain algorithms are used by the Hyperion ADCS. This however, cannot be verified, since the algorithms used are restricted from disclosure to parties outside the company. The algorithms used by the Hyperion ADCS are however flight proven [25].

VALIDATION

Both the ADCS magnetorquers and the attitude algorithms can be validated in a Helmholtz cage. Such a facility is available at the Aerospace faculty of the TU Delft. The Helmholtz cage simulates the Earth's magnetic field. By placing a S/C within this field and changing its attitude, the force that a magnetorquer can create, can be tested using an external sensor. The Bdot algorithm can be validated by evaluating its outputs to inputs of changing magnetic field as well as the magnitude of momentum dumping that can be realised using the magnetorquers [27].

A simulation in a micro-gravity facility will enable rotation that is free of friction. This way tests can be performed on S/C oscillatory modes and on the dynamic response of the S/C to inputs of disturbance torques can be simulated [80]. Such a facility can be found in The European Space Research and Technology Centre in Noordwijk, the Netherlands [6].

The aforementioned validation methods should be applied to test the system's sensitivity to accuracy requirements and sensor and actuator settings (e.g. assess the consequences of failure of an ADCS component to overall performance) at different operational modes of the S/C.

RECOMMENDATIONS

It is concluded that reaching a 1° pointing accuracy for EPIC S/C at 520km altitude is a challenge. It is recommended that the CubeSat should operate during its lifetime above 530km - this will harbour a larger margin for solar activity in relation to the pointing accuracy achievements. Next to that, a specific statistical analysis (using e.g. Monte-Carlo simulations) of the attitude error and the error budgets should be performed in which a sensitivity analysis can be included. Finally, a simulation of the attitude response of EPIC CubeSats could be performed by Hyperion with their specific, optimised and flight proven attitude algorithms.

---

[6] http://www.esa.int/About_Us/ESTEC/New_laboratory_at_ESTEC [cited 28-06-17]

<div align="right">

9

</div>

TELECOMMUNICATIONS SUBSYSTEM

The Telecommunications subsystem is responsible for the link to the ground. It will communicate the spacecraft status, commands and scientific data to the ground and vice versa if necessary. Without the communication system the satellite cannot be reached, making it a key subsystem. This chapter will give an overview of what the telecommunications is and does based on the findings on the link budget in [31]. It will start with explaining what the system is required to do. Secondly, it will explain the ways how the requirements can be met and it will finalise by trading off all the different available parts and integrating the entire system.

9.1. REQUIREMENTS

The communications subsytem depends a lot on the date rate gathered by the payload and the amount of processing done by the on the on-board data handling subsystem. Requirement **EPIC-SYS-S01-Config.02-C.01.2** and **EPIC-SYS-S01-Config.02-C.02.2** states that the communication system should be able to send all the scientific and housekeeping data back to earth at least every 12 hours. In order to do so, the amount of data sent over a period of time should be equal or larger than the data gathered over that same period of time. This period of time should be long enough to make an actual representation because peaks must be avoided.

The system has multiple other requirements that come form third parties. These are for example the requirement that it shall not interfere with other players in space and thus has to comply with the International Telecommunication Union (ITU) regulations. This organisation gives out radio frequencies to operate on. Another important stakeholder is the ground station company. This network of ground or space based (satellite) antennas is used to capture the signals sent out by the spacecraft which are then analysed and processed. The communication system has to comply with the standards set by these organisations.

9.2. FREQUENCY BANDS

Radio communications in space are categorised into bands. These bands have different operating frequencies and are used for different purposes. In higher frequencies one can send more data. During the meeting with Hyperion [25] and the crew from the ground station from the TU Delft [81] a lot of knowledge was gained.

CubeSats usually operate in the VHF (Very High Frequency), UHF (Ultra High Frequency), S-band or X-band communication band[81]. These 4 bands have different properties, different data rates and require different equipment. In each frequency band the ITU will assign a certain bandwidth to each satellite of satellite constellation. For S-band and lower bands a bandwidth can be bought, for higher frequencies these have to be rented for certain periods of time. A brief overview of different bands used by CubeSats can be found below.

- VHF is used for low data rate communication system. It can sent up to 2400 bits per second[1]. It has a low power consumption compared to the other bands. In addition, VHF operates between 30MHz and 300MHz and is omnidirectional, because it uses dipole antennas to generate its radiowaves.

---

[1] http://www.delfispace.nl/delfi-n3xt/comms [cited 26-06-2017]

- UHF is a frequency band that is right above VHF. It operates between 300MHz and 1GHz, but usually around 440MHz [82]. UHF also uses dipoles and like VHF, is omnidirectional. The maximum data rate of UHF is 19.2kbits per second.

- S-band, unlike UHF and VHF, is a directional frequency. When implemented in CubeSats, a patch antenna [34] is used to send it's data back to Earth. S-band operates between 2 and 4 GHz and can reach a 2Mbits per second downlink.

- X-band is the most powerful frequency, making it very useful for transmitting a large amount of data. X-band is fairly occupied at this moment of time and has to be reserved for future use [25]. Furthermore it is the most power consuming of all the frequencies. The benefit of using it is that data rates up to 100Mbits per second can be achieved.

The type of frequency band which is going to be used depends on the ground station and the data rates. In 9.4 this will be evaluated to determine the type of system which will be equipped on the satellites.

9.3. GROUND STATIONS

The ground station of a satellite mission is the base on the ground which receives the data sent by the satellite. As mentioned earlier the ground station play a significant role on the processing of the data. The requirements state that the satellite should be able to transmit it's data back every 12 hours. A single ground station will not satisfy this requirement, because it can only see the satellite every 12 hours due to the Earth's rotation. The satellite then also needs to be in the right place of it's orbit to make contact with the ground station. Therefore multiple ground stations are needed.

To reduce the complexity of the ground system only ground station networks will be evaluated. This networks have the benefit of having the same software and requirements for every ground station within the network. Also inter- satellite links will be evaluated. This method uses in orbit satellites to transmit the data and these will then send the data back to earth. A list of the available ground systems can be found below.

- **GENSO**[2]: The Global Educational Network for Satellite Operations (GENSO) network is an educational network used by universities and government space agencies. The main goal is to provide easy access to space for students and universities. However, GENSO is out of operation.

- **KSAT Lite**[3]: The KSAT lite ground station network is the smaller variant of the KSAT network. This Lite version is designed especially for CubeSats or other small satellites. It uses VHF, UHF, S-band and X-band (only some ground stations) to communicate with the satellite. It has 22 ground stations and 14 within the ±55° degree latitude.

- **NEN**[4]: The Near Earth Network (NEN) is a network used by NASA. It consist of ground facilities and satellites in LEO, GEO, highly elliptical orbits and lunar orbits. This network is large and is designed to be able to communicate with all kinds of different satellites within the sphere of influence of the Earth.

- **Iridium satellite network**[5]: The Iridium network is a satellite network that consists of 66 satellites and can be used for inter-satellite links. It operates at an altitude of 780 Km and grants global coverage on the ground. To use the inter-satellite link one usually has to pay for the amount of data sent through the satellites [25]. The system is designed for ground communication relay, but also offers satellite services.

- **TDRSS**[6]: The Tracking and Data Relay Satellite System (TDRSS) is part of NASA's Near Earth Network. It consist of several satellites in GEO orbit. These satellite are designed to send data to and from satellites in LEO. They only operate in S-band or higher frequencies.

---

[2] http://www.esa.int/Education/How_GENSO_works [cited 26-06-2017]
[3] http://www.ksat.no/en/news/2016/january/ksat%20lite-network/ [cited 26-06-2017]
[4] https://www.nasa.gov/directorates/heo/scan/services/services/index.html [cited 26-06-2017]
[5] www.iridium.com [cited 27-06-2017]
[6] https://nssdc.gsfc.nasa.gov/nmc/spacecraftDisplay.do?id=2002-011A [cited 27-06-2017]

The best system for the the EPIC mission will be the KSAT Lite ground system, since this is especially designed for small satellites. It has the benefits of being available in the radio bands CubeSats usually communicate in and is cheap.

9.4. SIMULATION

To determine the best suitable communication system, a simulation was made to achieve three goals. The first is figuring out what the maximum data rate for gathering information is. The second is to determine whether the preliminary chosen system can be used without discarding to much data and the last part is to determine the maximum memory needed in order to store and send the data. The simulation makes use of the orbital propagator tool in subsection 5.3.2 to determine the location of a satellite in terms of latitude and longitude. One satellite will be used as a reference simulation for all of the satellites.

The first step of the simulation is to determine whether the spacecraft is in contact with the ground station or not. To do so the latitude and longitude at every timestep in the simulation of the spacecraft are needed. This is done by the propagator in subsection 5.3.2. Then every longitude and latitude locations of all the ground station have to be known. This is done based on information provided by the ground network provider.

Using the conversion of spherical coordinate system in the Cartesian coordinate system as seen in Figure 9.1 and in Equation 9.1, one can determine the angle between the two vectors using equation 9.2. Note that $\theta = 90° - Lat$ and $Long = \varphi$. This angle is compared to the maximum angle γ can make before the elevation angle is to low.

$$x = r \cdot \sin(\theta) \cdot \cos(\varphi), \quad y = r \cdot \sin(\theta) \cdot \sin(\varphi), \quad z = r \cdot \cos(\theta) \quad (9.1) \qquad \cos(\gamma) = \frac{\bar{A} \bullet \bar{B}}{|\bar{A}||\bar{B}|} \quad (9.2)$$
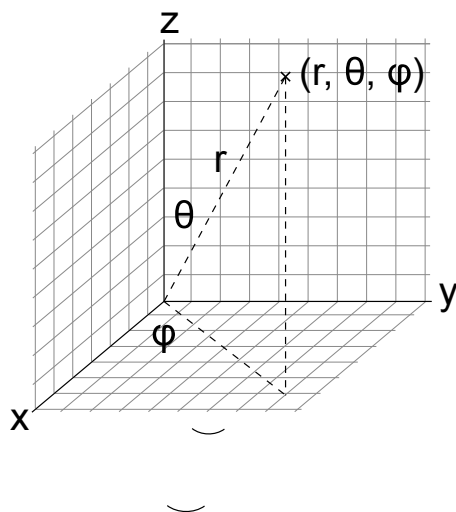
Figure 9.1: Spherical coordinate system in Cartesian space
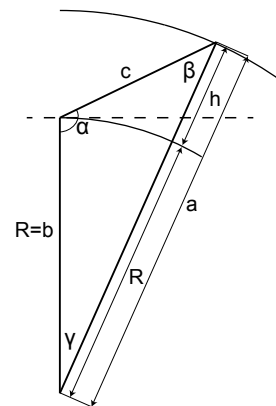
Figure 9.2: Visualisation of the elevation angle

To calculate the maximum angle γ which can be used, the law of sines is used. Since the angle of α is known to be the elevation angle (δ) plus ninety degrees ($\alpha = \delta + 90°$) as seen in Figure 9.2. The elevation angle is the angle between c and the dotted line (also known as the local horizon).

$$\frac{\sin(\alpha)}{a} = \frac{\sin(\beta)}{b} = \frac{\sin(\gamma)}{c} = C \quad (9.3)$$

Applying this equation to Figure 9.2, angle β can be derived. Since side a and b of the triangle are known to be the radius of earth and the radius of earth plus the height of the satellite respectively. Then using the triangle postulate theorem, which states that the sum of the angles of a triangle is 180°, angle γ can be derived. Rearranging Equation 9.3 to Equation 9.4, then use Equation 9.5 to find the maximum angle of γ:

$$\beta = \sin^{-1}\left(b \cdot \frac{\sin(\alpha)}{a}\right) \quad (9.4) \qquad \gamma_{max} = 180° - \alpha - \beta \quad (9.5)$$

This will be compared to the value obtained in Equation 9.2. If that value is lower than γ_{max} the space-craft is in view of the ground station and can transmit data. At this point, the time is noted and when the spacecraft is out of view again the time will be noted again. The difference between these time stamps is the time the spacecraft can sent data down. The second step in the simulation is to produce preliminary sizing results. It uses all of the 'contact times' and calculates the percentage of the time the spacecraft is in view of a ground station. This percentage should then be larger or equal to the percentage of the gathering rate to the data send rate. If this is true all data can be send down within the simulated time. If not then some data cannot make it down. As calculated in section 11.3 the gathering data rate is 5758 bits/s (bps) which includes the telemetry data. Using Equation 9.6 the required downlink rates can be found as seen in Table 9.1.

$$\frac{t_{contact}}{t_{total}} \geq \frac{bit/s_{gathering}}{bit/s_{send}} \tag{9.6}$$

Table 9.1: Ratio of time available of total time for different communication strategies and corresponding theoretical maximum data rate for gathering data.

	UHF	Nadir pointing S-Band	Ground tracking S-band
Practical maximum [Kbps]	19.2	2000	2000
$t_{contact}/t_{total}$ [%]	21.8	0.686	21.8
Maximum Bps gathering [bps]	3790	13676	435961

Since the regular S-band with ground tracking, or pointing the antenna towards the ground, has more than 75 times the capability to send all the data down, an alternate idea was brought up; use the S-band antenna antenna while remaining nadir pointed. The S-band antenna has a beamwidth of 30° [34]. In order to calculate the new contact time, the minimum angle of elevation was set to 60°, since 90° − 30° = 60°. The results can be found in Table 9.1.

The third step in the code is to use all these 'contact times' and use them to calculate whether the data gathered can be sent down. For this calculation the worst case scenario was used, which means that the CubeSat will be collecting data the entire time while operative and does not stop to send data down. The program then runs for every contact time found in step 1. For every time in contact it sends data down and during every second it collects data. The governing equation is Equation 9.7.

$$bits = bits/s \cdot t \tag{9.7}$$

Every time step the data gathered is added to the total memory and the sent data is subtracted from the total memory. The simulation ran for a total of 30 days and the result can be seen in Figure 9.3. This is during nominal operations.
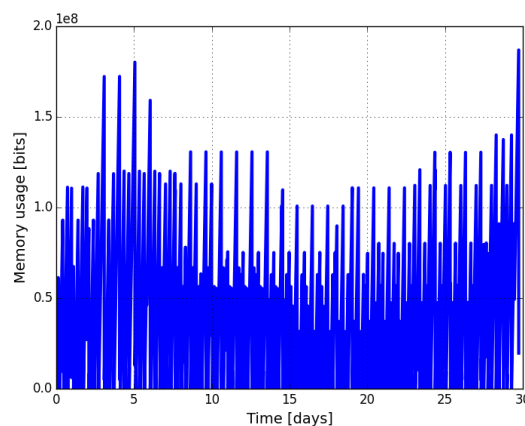

Figure 9.3: Theoretical memory capacity over 30 days. h = 520km

The fourth step was to apply the program to the most extreme case the spacecraft would be in. According to Table 5.1 the maximum and minimum orbit altitudes are respectively 670km and 350km. The

propagator in the first step was run for these new altitudes. The results for the upper and lower orbit can be found in Table 9.2.

Table 9.2: Memory needed and availability of the spacecraft for different bands

	UHF		S-band	
	In sight %	Max. memory needed	In sight %	Max. memory needed
Lower orbit	13.6	30.4	0.28	450.8
Nominal orbit	21.8	23.8	0.69	178.3
Upper orbit	28.9	23.3	0.97	169.8

9.5. REDUNDANCY

The communication system is a key element within the spacecraft. If the communication system fails the entire spacecraft will be lost in space. To ensure the redundancy multiple transmitters for the S-band will be included as well as an UHF telecommunications system. This UHF has multiple advantages for use as a back-up or secondary antenna system. First of all, it's omnidirectional, allowing communication during random tumbling. Insight into the problem can be transmitted down to and a possible solution can be transmitted back up. Either to restore the spacecraft or deorbit it. The second advantage also has comes due to the omnidirectionality of the UHF antenna. Like stated in section 9.4 the availability of the spacecraft is very high. Thus it has a low latency between telemetry messages. The third advantage is the robust of the system. It is compared to the S-band antenna a simple system with a better reliability.

9.6. COMMUNICATIONS SYSTEMS SELECTION

The communications subsystem consists consists out of 2 parts. The antenna itself and the 'radio'. The latter modulates the data onto the used frequency, such that it can be sent by the antenna. These two components can be bought apart, but it's more favourable to have these bought from the same manufacturer. The interface between the two will than the be the same.

S-BAND ANTENNA TRADE-OFF

Table 9.3: The trade-off between the communications systems

Product	1	2	3	4
Manufacturer	ISIS[7]	Gomspace[8]	Clyde Space[9]	Clyde Space[10]
Product name	S-band Tranciever	NanoCom TR-600	SPUT high-bit rate	CPUT S-band
Costs/price [euro]	8500	9500	12500	8900
Power usage [W] - nominal	3.8	1	5	5
Peak Power useage [W]	3.8	6	5	5
Voltage needed [V]	6.5	5	6-dec	6-dec
Mass [g]	62	74.2	100	100
Size [mm x mm x mm]	96x90x15	90x96x31	96x90	96x90
Maximum temperature [℃]	60	85	61	61
Minimum Temperature [℃]	-20	-40	-25	-25
Generated Data rate [bit/s]	0	0	0	0
Frequency [GHz]	2.2	2.2	2.2 - 2.45	2.2 - 2.45
Data rate downlink [bit/s]	100 kbps	25 Mbps	10 Mbps	2 Mbps
Volume [U]	0.12960	0.26784	0.1728	0.1728
Modulation	BPSK, GMSK	QPSK	OQSPK	QSPK

---

[7] https://www.isispace.nl/product/isis-txs-s-band-transmitter/ [cited 27-06-2017]

[8] https://gomspace.com/Shop/subsystems/communication/nanocom-sr2000.aspx [cited 28-06-2017]

[9] https://www.clyde.space/products/65-cput-high-bitrate-sband-transmitter [cited 27-06-2017]

[10] https://www.clyde.space/products/35-cput-sband-cubesat-transmitter [cited 27-06-2017]

Table 9.4: Trade-off table for S-band antenna system

Product	1	2	3	4	5	6	7
Manufacturer	IQ Wireless	Clyde Space	SpaceQuest	Endurosat [11]	Helical communication technologies	antdevco	Gom Space
product name	HISPICO [12] RHCP	CPUT [13]	AC-2000 [14]		Helical antenna [83]	microstrip [84] patch antenna	NanoCom[15] ANT2000
Costs/price [euro]	4600	4725	on request	3000	11000	On request	5000
Power usage [W] - nominal	8	3	N.A	4	1	8	0,6
Peak Power useage [W]	10	?	N.A	4	56	10	10,7
Mass [g]	-	50	100	64	-	120	110
Size [mm x mm x mm]	50x50x3.2	100x100x5	-	-	100x100x35	100x100x3.5	98x98x20.1
Maximum temperature [℃]	-	85	80	-	85	100	85
Minimum Temperature [℃]	-	-25	-40	-	-40	-65	-40
Pointing Accuray needed [°]	42.5	60	45	35	30	35	30
Frequency [GHz]	2.228	2.2-2.45	2-2.3	2.3-2.5	2.3	2.2	2.05 - 2.2

---

[11] https://www.endurosat.com/cubesat-store/cubesat-communication-modules/s-band-patch-antenna/ [cited 28-06-2017]

[12] https://www.cubesatshop.com/product/s-band-patch-antenna-rhcp-hispico/ [cited 27-06-2017]

[13] https://www.clyde.space/products/13 [cited 27-06-2017]

[14] http://www.spacequest.com/shop/ac-100-s-band-circular-antenna [cited 27-06-2017]

[15] https://gomspace.com/Shop/subsystems/communication/nanocom-ant2000.aspx [cited 27-06-2017]

The sizing of the S-band antenna was done with consideration of the UHF system in mind. This will be done in Table 9.6. From Table 9.3 and Table 9.4 the best option was selected. It was the Gomspace TR-600 communication radio and the Gomscape ANT-2000 S-band antenna patch. These two components are designed to work together without efford and also with the rest of the system. The Gomspace S-band antenna has a low power consumption when idle and a variable power usage when transmitting data[34]. The communication computer has the lowest nominal power consumption. With a theoretical maximum of 25Mbps it also has the highest data rate of all the communications systems.

UHF ANTENNA TRADE-OFF

Table 9.5: Trade-off table for UHF communication systems

Product	1	2	3	4
Manufacturer	ISIS	ISIS	GomSpace	Clyde Space
Product name	UHF Down/VHF Up [16]	VHF Down/UHF Up [17]	NanaCom AX100 [18]	CPUT VUTRX [19]
Costs/price [euro]	8500	8500	On request	8600
Power usage [W] - nominal	3	1.7	2,8	4
Peak Power usage [W]	4	1.7	2,8	10
Voltage needed [V]		6.5-12.5	3,3	7.2
Mass [g]	75	85	24,5	90
Size [mm x mm x mm]	96x90x15	96x90x15	6.5x40x65	96x90
Maximum temperature [℃]	60	60	85	31
Minimum Temperature [℃]	-20	-10	-30	-25
Frequency [GHz]	0.45	0.15	0.43-0.44	0.44
Data Rate Downlink [Bit/s]	9600	9600	9600	9600
Attitude det accuracy [°]	-	-	-	-
Volume [U]	0.1296	0.1296	0,0169	-
Modulation	-	-	FSK/MSK/ GFSK/GMSK	GMSK

Table 9.6: Trade-off table for UHF antenna systems

Product	1	2	3	4
Manufacturer	Gomspace	Gomspace	ISIS	EnduroSat
Product name	NanoCom Ant-6F [20]	NanoCom ANT430 [21]	Deployable turn-stile [22]	UHF/VHF an-tenna [85]
Costs/price [euro]	3500	On request	5500	3000
Power usage [W] - nominal	2	2	0.6	0.6
Peak Power useage [W]	10	10	2	2
Mass [g]	100	30	100	85
Maximum temperature [℃]	100	100	60	80
Minimum Temperature [℃]	-55	-55	-20	-25
Frequency [GHz]	0.43	0.43	0.43	0.44

For the UHF communication systems two tables were made. Like the S-band, the UHF also consists of 2 components. The radio which can be found in Table 9.5 and the antenna itself, which can be found in Table 9.6. The final choice was made on the communication of the GomSpace ANT-6F antenna [35] and the GomSpace Nanocom AX100 [36]. The reasoning behind this was the crosslink between the S-band

---

[20]https://gomspace.com/Shop/subsystems/communication/nanocom-ant-6f.aspx [cited 28-06-2017]

[21]https://gomspace.com/Shop/subsystems/communication/nanocom-ant430.aspx [cited 28-06-2017]

[22]https://www.cubesatshop.com/product/turnstile-antenna/ [cited 28-06-2017]

and UHF telecommunication systems. The radio computers of this particular system can be placed on a dock. This allows for data communication and structural integration at the same time. This means that both systems can communicate with each other while also holding the option to work separately.

The ANT-6F Antenna is the only CubeSat antenna designed for 6U CubeSats. It has a 10 by 20 cm base and can be placed either at the bottom or the top of the the CubeSat. The other antenna systems in Table 9.6 would be modified in order to fit on a 6U CubeSat.

9.7. COMMUNICATIONS FLOW DIAGRAM

The communication flow diagram gives insight to the structure used for communication. It depicts what steps are taken for both uplink and downlink. The steps are depicted in Figure 9.4.
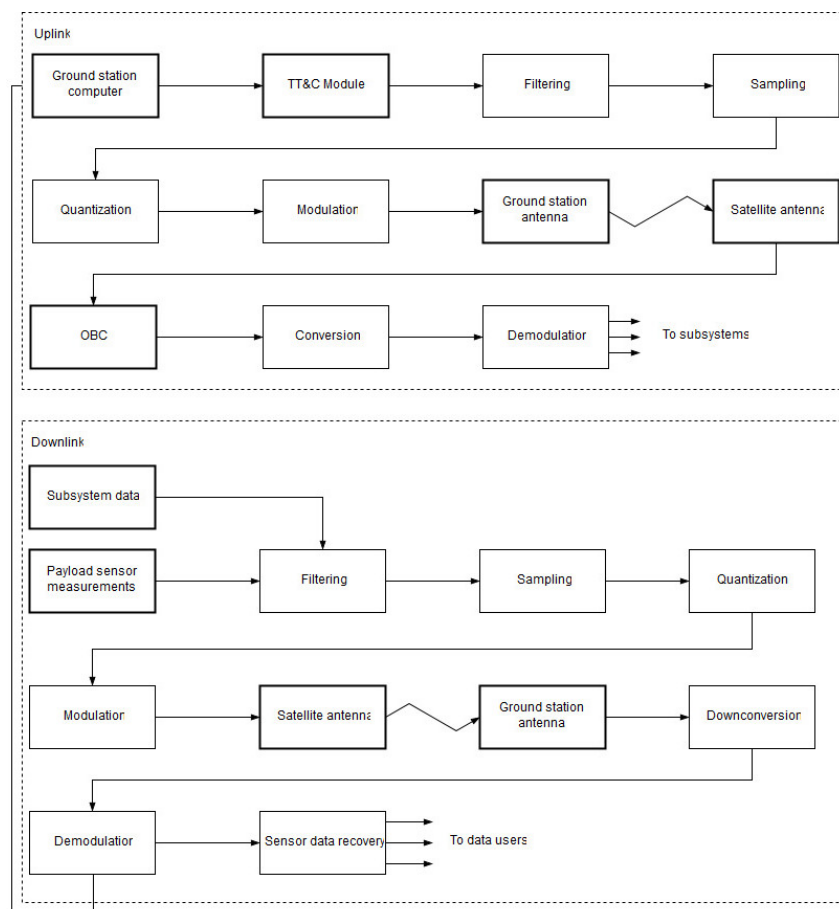
Figure 9.4: The communication flow diagram for one EPIC satellite

9.8. VERIFICATION & VALIDATION

This chapter will deal with the verification and validation of the simulation mentioned earlier in this chapter. The base of the simulation is already spoken of in subsection 5.4.2, where the propagator is validated. The rest of the program will be validated in this section.

For the validation GMAT will be used. GMAT has a package which can determine the contact times of a satellite in orbit. The input required for are the Kepler elements of the satellite and the latitudes and longitudes of all the ground stations. GMAT then calculated, based on a given initial time and date, the start time and date and the stop time and date. This information is then inputted into python where a plot is made.

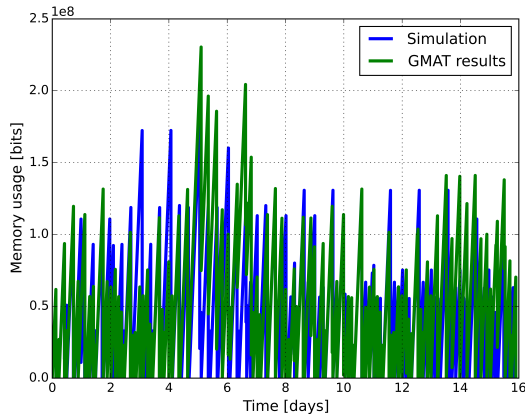Figure 9.5: GMAT results plotted over simulation results for normal operations characteristics
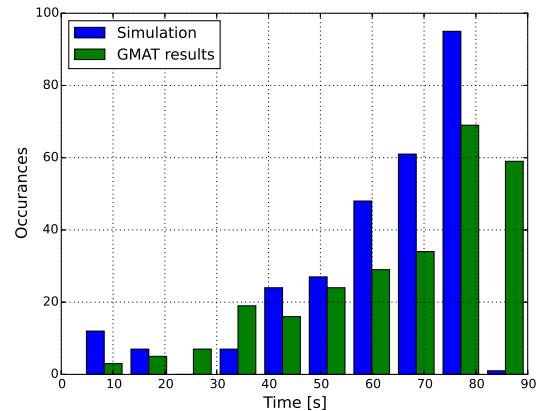

Figure 9.6: Histogram of contact time duration for the simulation and GMAT for normal operations

In Figure 9.5 one can see the GMAT results plotted over the original simulation results. The mismatch in peaks comes due the discrepancy in the simulation. It can only track the results in a 10 seconds interval where GMAT can calculate the start & stop times till 10 milliseconds accurate. The same can be found seen in Figure 9.6 The distribution of the simulation has a gap around the 55 mark. The cause is that the region is from 52 to 60 and the timestep for the simULATION is 10 seconds. The 60 mark is included in the next column. The GMAT results are more refined and thus give a more gradual result.

In Table 9.7 one can see the different parameters of the duration length of every orbit for S-band transmission. The average, percentage contact time, standard deviation and memory are listed. The average of the percentage contact time parameter defines the average of the contact times and if the orbital parameters are aligned. The standard deviation depicts the distribution of the values and the maximum memory shows if more memory should be allocated for data. In lower-orbit the GMAT simulation shows that no memory is available. This is because the memory diverges. More data is being gathered then being send. So, Equation 9.6 has not been met.

Table 9.7: Different characteristics of contact times for S-band

	Lower orbit		Normal orbit		upper orbit	
	simulation	GMAT	simulation	GMAT	simulation	GMAT
Average contact time	41.1	40.6	62.5	64.9	82.5	81.4
$t_{contact}$ / t_{total}	0.286	0.271	0.686	0.669	0.966	0.938
Standard deviation	12.8	10.8	19.1	19.2	23.7	22.6
Memory needed	508.4	N.A.	180.5	219.7	169.8	169.8

9.9. CONCLUSION

In this conclusion a small overview will be given to summarise the entire subsystem. The link budget from [31] was used as base. Then a simulation has been made to calculate the best option for this mission. This results in the communication subsystem having four components; 2 antennas and 2 communication computers. One of each for S-band transmissions and one for UHF communications. The CubeSat is equipped with a Gomspace ANT2000 and TR-600 for S-band and the Gomspace ANT-6F and AX100 for the UHF communications. The spacecraft will use the S-band communications to transmit the scientific payload and the UHF for the telemetry part receiving and transmitting. To transmit the data the spacecraft does not have to be pointed. With a nadir pointing S-band Antenna the data rate is high enough to send all the data down to earth. The ground system network used is the KSAT which is explained in section 9.3.

10

ELECTRICAL POWER SUBSYSTEM

As explained in the trade-off analysis of the EPIC [31] and as conventional for any CubeSat, the primary power source consists of the solar arrays, while the secondary energy source is the batteries (Section 10.1). The regulation of the electrical power system is done by an EPS board as elaborated in Section 10.3.

10.1. SOLAR ARRAY SIZING AND CONFIGURATION

10.1.1. SOLAR ARRAY REQUIREMENTS AND SELECTION

From the budget breakdown in Table 4.1, the nominal power required is 14.2W. Furthermore, the telecommunication demands peak power for 0.68% of the time, such that the total average nominal power is 14.5W. Also for sizing the solar arrays, the required satellite lifetime used is 3 years. The actual power that has to be generated by the solar arrays, accounting for line losses is given by Equation 10.1. The maximum eclipse time is found from Equation 10.2 to be 35.5 minutes. The path efficiencies during eclipse and daylight (η_e, η_d) are determined by the EPS to be 0.6 and 0.8 respectively. As explained in Chapter 11, the power requirement for eclipse and daylight operations is indifferent since only one data acquisition mode is present to maximise scientific yield. Accordingly, the solar power generated during daylight (P_{sa}) is 27.3W.

$$P_{sa}T_d = P_{nom}\left(\frac{T_e}{\eta_e} + \frac{T_d}{\eta_d}\right) \qquad (10.1) \qquad\qquad T_e = 2\sqrt{\frac{a^3}{\mu}}\arcsin\left(\frac{R_e}{a}\right) \qquad (10.2)$$

Next, due their high efficiency, flight heritage and COTS availability, the GaAs triple-junction 3G30C solar panels of Azurspace are chosen is specified in the concept trade-off [31]. Their beginning of life efficiency is 29.8%, however, in hot conditions near EOL, the efficiency can drop to 24.9% as determined in Section 10.1.2. Each cell has a size of 30.18cm^2 Section 10.1.3 analyses the amount and configuration of these solar arrays.

10.1.2. SOLAR POWER DEGENERATION EFFECTS

TEMPERATURE EFFECTS

The influence of temperature on the solar panel performance is given by Azurspace to be -6.7 mV/°C and 0.24 mA/°C, given a nominal temperature of 28°C. In Chapter 12, it is analysed that the maximum temperature experienced by the solar panels is 85.6°C. The degenerative effect for GaAs triple-junction cells can be approximated by a linear relationship, calculated in Equation 10.3. Therefore, the efficiency η_T can become as low as 86% (Figure 10.1).

$$\eta_T = 1 + (T_{max} - T_{ref})\frac{\partial P}{\partial T} \qquad (10.3)$$

RADIATION EFFECTS

The space environment can cause significant solar power losses near EOL due to radiation consisting of electrons and protons. Therefore, usually a silicon dioxide coverglass protection layer is applied on the solar array. The Azurspace 3G30C solar panel is equipped with a 100μm CMX 100 AR coverglass layer. To ensure this layer provides sufficient protection and estimate the degradation level due to radiation effects, the radiation shall be analysed by the SPENVIS software developed by BIRA in collaboration with ESA.
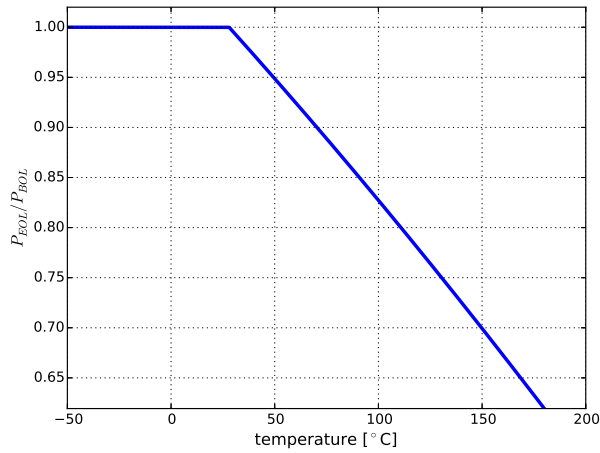
Figure 10.1: Degradation of solar panel performance due to temperature changes of a Azurspace 3G30C solar panel
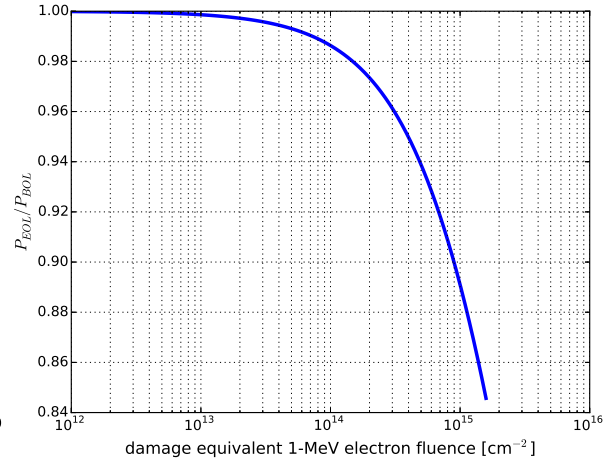

Figure 10.2: Degradation of solar panel performance due to radiation of a Azurspace 3G30C solar panel

The inputs used are the orbital parameters of EPIC, the solar cell Azur 3G28, which is very similar to the 3G30C arrays, and the 100μm coverglass protection layer. The SCREAM model is used, using radiation effects from trapped protons/electrons and solar protons. The simulation produces radiation particles using Monte Carlo simulations of radiating particles and handles a confidence level of 97%. The simulation is run for solar maximum and considering non-ionizing energy loss, which affect solar cells the most [86].

The total equivalent 1 MeV fluence experience over the 3 year lifetime is simulated to be $3.2 \cdot 10^{13}$ e^-/cm^2. From the equivalent fluence, in Figure 10.2 a performance degradation of 0.5% over the Cube-Sat lifetime is concluded. A commonly made assumption for triple junction cells results in a total 1.5% degradation [39], which however excluded altitude and inclination variances, explaining the difference.

10.1.3. SOLAR ARRAY SIZING AND CONFIGURATION OPTIMISATION
The power generation of CubeSat is often based upon estimates, hence including large safety margins. However, this resulted in power-limited Cubesats in the past [87]. For this reason, high-fidelity, numerical power estimates are employed for the EPIC mission. A computer aided design (CAD) model is imported into STK, such that the power generation is computed considering sunlight incidence angles and shadow effects. This effective solar power receiving surface is used with to calculated the generated power using Equation 10.4. A generally adopted value for the solar irradiance is 1360W/m^2 [1]. Furthermore, the solar intensity is defined to be a value between 0 and 1, where the maximum value indicates full sunlight. Any value in between indicates that the CubeSat is located in penumbra.

$$P = \eta \cdot A_{eff} \cdot \text{solar intensity} \cdot \text{solar irradiance} \tag{10.4}$$

A first design iteration determined that at least four deployable solar panels are needed to ensure the necessary solar power generation of 27.3W determined in Section 10.1. The deployables are covered on both sides with solar panels, while only not covered on the top and bottom 1U face as shown in Figure 10.3 to allow for sensor measurements (see Chapter 7). For the configurations available by ISIS [24] and accounting for holes necessary for some subsystems (Chapter 14), a total of 119 AzurSpace 3G30C solar cells are used. Furthermore, no tracking or pointing solar panels are COTS available, so the deployment angles of the solar panels are stationary. As a result, the deployable solar panel attachment position and deployment angle shall be optimised.

From the binomial theorem [88], it can be concluded that 15714 possibilities exist to attach the 4 deployable solar panels onto a Cubesat with a 6U form factor. Not all possibilities can be analysed individually
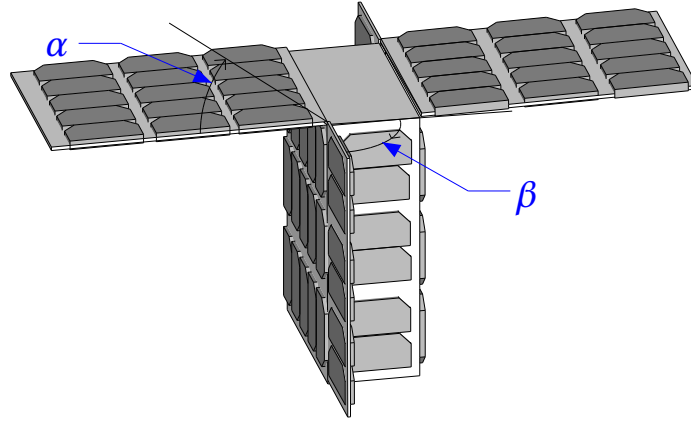
---

[1] http://lasp.colorado.edu/home/sorce/ [cited 25-05-2017]

Figure 10.3: Definition of the deployment angles α and β

due to computational time constrains. However, many options can be disregarded since the deployable panel configuration depends on EOL strategy of Section 18.2; a minimum area in direction of flight of 0.153m^2 is required. This can only be provided by two 6U deployable panels. Furthermore the solar panels will be placed in front of flight direction for stability reason. During the deployment phase, the CubeSat can fly as low as 350km. At this altitude, a reasonable amount of drag is present and placing the deployable panels in the back creates a stabilising 'weathervane' effect, in a similar way as for drag sails [89]. Initially the configuration consisted of these two deployable arrays in flight direction. However, no solution was found providing enough power for the mission. As a result, two 3U solar panels are added, which are not deployed in flight direction so the drag is not increased. Furthermore, the solar panels are deployed symmetrically to prevent excess disturbance torques.
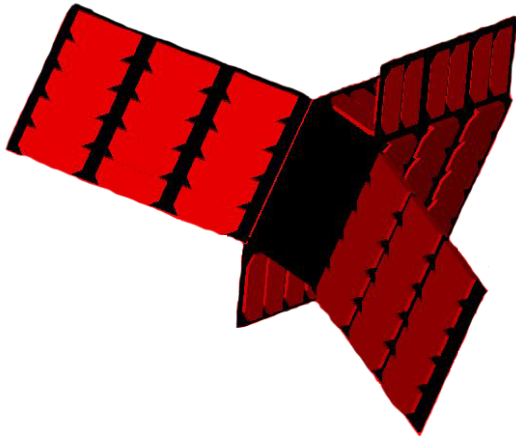
Figure 10.4: Visualisation of SketchUp model in STK using the Solar Panel tool
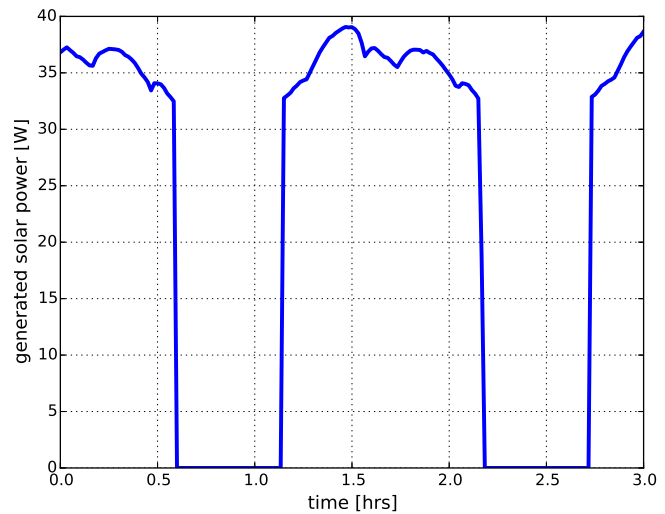
Figure 10.5: Example power generation by the solar arrays over time for α=20° and β=80°

After the solar panel attachment is determined, the angles α and β as in Figure 10.3 are left for optimisation. The minimum required area in direction of flight of 0.153m^2 can be translated into a limit for α of ±34°. For the optimisation process of the deployment angle, the objective is to maximise the minimum orbit average power during the mission lifetime. This is mathematically defined in Equation 10.5.

$$\max\left\{\min\left\{\frac{1}{P}\int_{(n-1)P}^{nP} P_{sa}\left(\alpha,\beta,t\right) dt, T = 1 \text{ orbit}, n \in \left[0, \frac{3 \text{ year}}{P}\right], |\alpha| < 34°, 0° < \beta < 270°\right\}\right\} \quad (10.5)$$

The effect of the incidence angles of the sun are modelled in the Solar Panel tool of STK. The or-

bital configuration (Chapter 5), CubeSat configuration and solar panel efficiency are used as inputs to model the average power generated. For compatibility reasons, the CubeSat configuration is modelled in SketchUp to be able to import in STK. The CubeSat seen from the sun, using a red colour indication for power generating surfaces is shown in Figure 10.4. The intensity of red visualises which areas have the best incidence angle. The output from the STK solar panel simulation is the time-wise variation of power P_{sa} from the solar panels, an example graph is shown in Figure 10.5.

To find the optimal angles, a lattice is constructed with a 10° spacing, since a finer grid would have required additional licenses for STK which are unavailable. Still, the minimal power generated for an orbit during a 3 year CubeSat lifetime could be analysed using STK. The initial configuration before the optimisation ($\alpha=\beta=0°$) produces a minimal power of 30.6W. After optimisation process it is concluded that a combination of $\alpha=15°$ and $\beta=82°$ is optimal, with an according minimal average power generation during daylight of 35.2W as shown in Figure 10.6. To obtain a finer grid, interpolation of the coarse grid is used, resulting in a maximum interpolation error of 0.46W. The optimisation process extents the initial power generation by 15%. However, this increased power does not allow to remove on the deployable solar panels; i.e. additional power is used for redundancy. Since the power demand in 28.2W, a power margin of 29% is added. The solar strings are arranged in 17 strings of 7 cells as explained in Section 10.3, such that up to 3 strings can fail before a power shortage will arise.
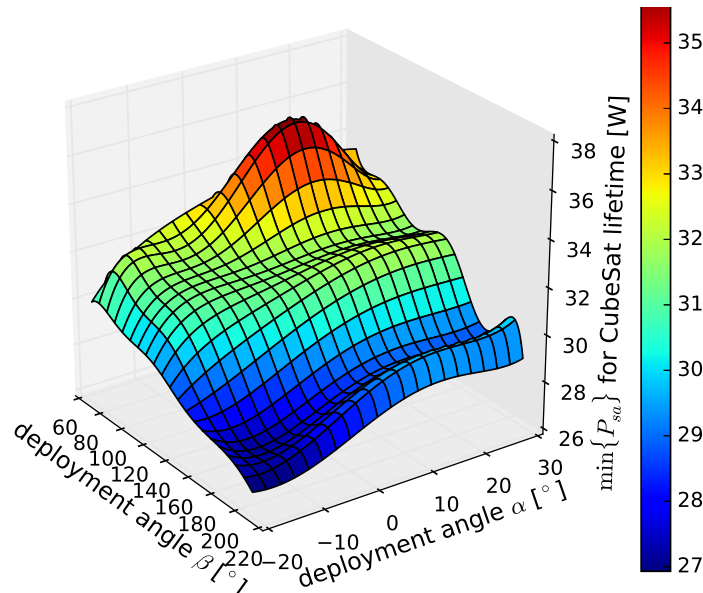
Figure 10.6: Minimum occurring power production for one orbit over a CubeSat lifetime as a function of the solar panel deployment angles

10.1.4. VERIFICATION & VALIDATION
The degeneration effect estimated by radiation was modelled in SPENVIS (Section 10.1.2). To cross-check the fluence values, the simulation output is compared to equivalent fluence values produced by Rauschenbach [90] giving a similar result of $1 \cdot 10^{14} \mathrm{e}^-/\mathrm{cm}^2$. The SPENVIS application has also been extensively compared to space flight data [86], validating the software.

To size the solar panel arrays, an optimisation model is developed in Section 10.1.3. In order to verify the optimisation model, two software units are tested: the tool calculating the solar power generation and the optimisation tool. The solar power generation tool is tested on the simplest case possible: a regular 1U CubeSat assuming the full sides are covered with solar panels. Similarly as explained in Section 10.1.3, the cube is modelled in Sketchup. At first, the simplified model is assumed to be continuously pointing at the sun. The small difference is due to the fact that the exact solar intensity used by STK is not disclosed. Besides, albedo effects could be accounted for in STK, generating a slightly higher results, however no detailed documentation on the model is available. A similar analysis is done by

A. Sirin [91], the solar power for a simple 1U cube with GaAs 3G28C solar panels was analysed for random tumbling conditions in a sun synchronous orbit at 500km. By any means, the analytical results are in close correspondence with the values generated by the STK solar panel tool, which makes the tool adequately verified (see Table 10.1).

Table 10.1: Verification of STK solar panel tool

Mode	STK solar tool result [W]	analytical result [W]	Difference [%]
One face pointing at sun	3.42	3.375	1.3
Two face, at angle of 45°	4.83	4.81	0.4
Random tumbling [91]	2.62	2.48	5.3

Next, the optimisation process is compared to a solar panel deployment angle is compared to an analysis by Lowe et al. [87]. In this work, the solar panel deployment for a 3U CubeSat is optimised. The reference paper demonstrates the solar panel deployment optimisation for a 3U CubeSat, being deployed from the International Space Station. Two deployable solar panels are considered for power generation. The paper also considers optimisation of the deployable solar panel layout. However, as discussed in Section 10.1.3, for the EPIC mission, the layout was determined based upon mission constraints and considerations. Therefore, the optimal configuration determined by Lowe is directly adopted and only the deployment angle optimisation is considered. The optimisation process by Lowe results in a maximum power of 17.15W, at an deployment angle of 90° for both panels. Using the approach described in Section 10.1.3 however, the maximum power found is 16.2W occurring at an angle of 90° and 85°,see Figure 10.7. This discrepancy can be explained by the different propagator used (STK versus custom made [87]). Also minor difference in the used CAD model could have a signification effect, since the exact dimensions of the used solar panels are not notified by the author. Still, the deviations are assessed to be minor such that the power optimisation tool is accurate enough for design purposes.

A recommendation for further work would be producing a similar simulation as the STK solar panel tool. If this seems unfeasible, a finer grid could reduce interpolation errors. Lastly, a full STK license could also enhance the power optimisation.
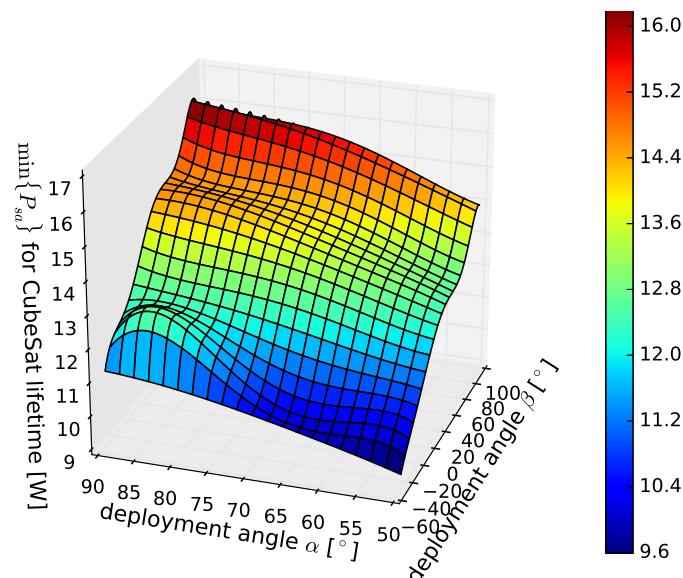

Figure 10.7: Verification of the power optimisation tool of Section 10.1.3 on a reference case [87]

10.2. BATTERY SIZING

The batteries are the secondary power source, needed for operations during eclipse time and peak power supply. The orbital altitude of 520km results in a total of 16,600 battery cycles over the 3 year

lifetime. To obtain the required cycle number, for lithium-ion batteries, a depth of discharge (DoD) of 40% is concluded from [92]. Furthermore, the EOL capacity at this DoD is typically 70% of the initial life capacity. Next, the amount of these battery arrays is determined to ensure power can be supplied during eclipse in the 3 year mission lifetime. The energy required to be stored by the batteries is given by Equation 10.6. The discharge time equals the maximum eclipse time of 36 minutes, determined by Equation 10.2. The battery to load efficiency η_{battery} can estimated to be 0.9 [39].

$$E_{\text{battery}} = \frac{P_{\text{battery}} \cdot t_{\text{discharge}}}{\text{DOD} \cdot \eta_{\text{battery}}} \tag{10.6}$$

The average power required during eclipse is 17.6W, resulting in a required energy storage of 28.9 Wh. As discussed for the concept trade-off [31], the battery type chosen for the EPIC mission is the Lithium-Ion-Polymer EXA BA0x (Figure 10.8), which is made COTS available by ISIS [93]. This Cube-Sat battery array is selected since it provides the highest energy density available on the market and has flight heritage. Each battery cell can store 900mAh or 3.325Wh and configurations with 6, 8, 12 and 16 cells are for sale [93]. Since the energy storage at EOL is only 2.33Wh for each cell, at least 13 cells are required. In order to add a power margin and add redundancy in case of failure, 2 battery packs of 16 cells are chosen, with an output voltage of 7.4V. The battery cell properties are summarised in Table 10.2.

Next to power supply during eclipse time, batteries are ought to store energy for peak power supply. The peak power that could occur during the EPIC mission is 45W (Table 4.1). The discharge rate of the BA0x battery pack is 20 times the nominal capacity within two seconds. Therefore, Lastly, the BA0x batteries has a 3C charge rate, meaning that the full capacity can be charged within 20 minutes. Eclipse times are always more than 20 minutes, so it can be deduced that no difficulties occur.

Table 10.2: Battery capacity at the EOL for the 3.325Wh BA0x high energy density battery cells [93]

Charge cycles for 3 year lifetime	16600
Battery cell capacity [Wh]	3.325 [93]
EOL battery capacity [%]	70 [92]
Depth of Discharge (DoD) [%]	40 [92]

10.3. ELECTRIC POWER SYSTEM AND ELECTRICAL BLOCK DIAGRAM

To ensure the global functioning of the electrical power system, an EPS board is incorporated into the design. This system establishes the regulation of the available power, that is, providing the power to all other subsystems. In order to optimise the total power output for the solar arrays a maximum power point tracker (MPPT) puts voltage across strings of solar cells. This is because the current of solar cells is constant. Within the EPS the voltage is then converted via DC/DC converters to the voltages of the output channels. The solar cells are arranged such that 7 solar cells are connected in series outputting power at 18.9 V. Furthermore, two 16 cell battery arrays are connected in parallel, giving 7.4V of voltage. The most suitable COTS component satisfying aforementioned needs is the NanoPower P60 (Figure 10.9) distributed by GOMSPACE. The inherent efficiency of this EPS board is 80% and already comes with 3 possible output voltages. All different voltages necessary for each component are summarised in Table 10.3. The electrical block diagram, shown in Figure 10.10, describes the interconnection of all subsystems. Following considerations are made for the electric block diagram:

- The total of 119 Azurspace solar cell are allocated in 17 strings of 7 cells, giving a solar panel output voltage of up to 18.9V. This way, one of the three ACUs has only five strings instead of six.
- Three ACUs are used such that less solar cells depend on each MPPT and to have more input channels, allowing a reduction in amount of solar cell strings. This increases the overall solar panel efficiency and redundancy in the system.
- The Langmuir probe and INMS need 2 voltages, one for the digital circuit and one for the analogue instrument.
- The RPA needs one voltage for the digital circuit (5V) and one for the voltage generator of the instrument (20V). In a similar way, the electrical field probe needs a 6.8V power supply, which

is not provided by the EPS output channels. Hence, the electric field probe and RPA require a DC/DC converter. A low power push/pull DC/DC converter is chosen as proposed by Huang [94].

- The UHF antenna is passive, thus there is no connection to the EPS in the block diagram.
- The electrical block diagram only shows positive electric connection, but every component is also connected to the ground of the CubeSat.
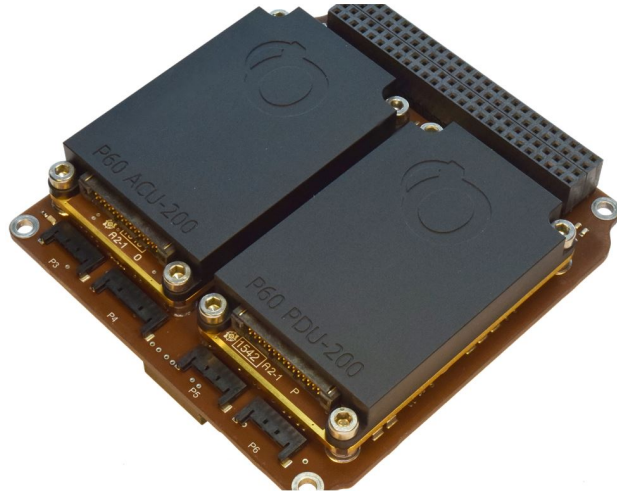
Figure 10.8: EXA BA0x high energy density battery pack, ISIS [93]

Figure 10.9: NanoPower P60 EPS component produced by GOMspace

Table 10.3: Electric components in the CubeSats and their required supply voltages. The * marks the sensors which are installed on only one of the two configurations.

Component	Manufacturer	Part number	Voltage[V]	Source
Solar cells	Azurspace	3G30C	2.7	[95]
Batteries	ISIS	BA0X	7.4	[93]
S-Band transceiver	Gomspace	TR-600	5	[33]
S-Band antenna	Gomspace	NanoCom ANT2000	8	[34]
ADCS	Hyperion	iADCS400	5	[96]
Propulsion	Hyperion	PM200	5	[25]
Magnetometer	ISIS	NSS	5	[97]
Dosimeter	SkyFox Labs	piDOSE-DCD	5	[32]
Electric Field Sensor	DIME mission	N/A	6.8	[98]
Langmuir probe	QB50 University of Oslo	N/A	3.3 and 5	[66]
INMS*	QB50 University of Oslo	N/A	3.3 and 5	[70]
RPA*	University of Texas	N/A	5 and 20	[71]
GPS antenna	SkyFox Labs	piPATCH-L1/FM	5	[99]
GPS receiver	SkyFox Labs	piNAV-NG GPS/FM	3.3	[100]
On-board computer	ISIS	iOBC	3.3	[101]
UHF transceiver	Gomspace	NanoCom AX100	3.3	[36]
UHF antenna	Gomspace	ANT6F	0	[35]
Thermal sensors	NTC	NTC thermister	3.3	[37]
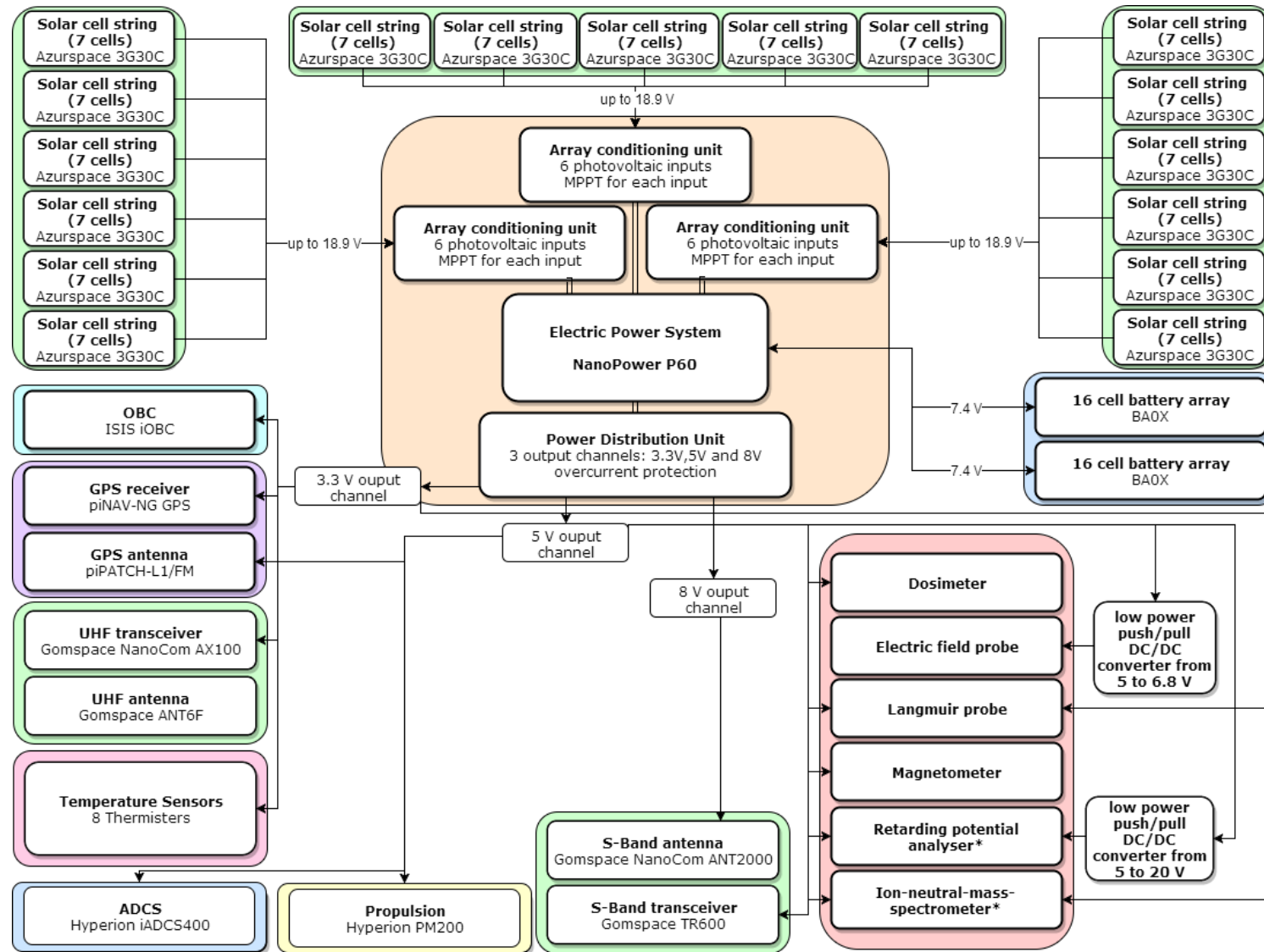
Figure 10.10: Electric block diagram of the CubeSats. The * marks the sensors which depend on the CubeSat configuration.

11

ON-BOARD DATA HANDLING SUBSYSTEM

In this chapter the on board data handling subsystem will be designed. First the data rates of all subsystems are listed. Then the different communication interfaces of all subsystems are presented. After a data handling block diagram is created and the OBC, as well as the required data memory are chosen. Those decisions are based on the results from Chapter 9. Finally the general software architecture is presented in a software block diagram.

11.1. SUBSYSTEM DATA RATES AND INTERFACES

The data rates and communication interfaces of all subsystems are presented in Table 11.1. The attitude sensor data rate and the solar cell sun sensor data rate are estimated from attitude sensor data size found for the Oslo University QB50 satellite [66] and typical sampling rates for star trackers [102].

All basic housekeeping sensors such as the output channel voltage and current sensor or the thruster valve status sensor are assumed to have a word size of 1 byte which equals 8 bits. The Gomspace NanoPower P60 EPS has 3 output channels with each one sensor. It has been decided to use 3 array conditioning units (ACUs) on the EPS system (see Section 10.3). Therefore a total of 18 input channels are present, which justifies the sensor quantity for the input channel voltage and current sensors.

The fault detection watchdog sends a signal to the data storage as soon as a component had to be reset. This information is then sent down to the ground station during the next downlink. The exact functioning of the fault detection watchdog is explained in Section 11.5. For the data rate estimation one fault detection signal is considered to be 8 bits. This way it will also be possible to determine which component encountered the problem. The sampling rate is assumed to be 0.5 Hz, because the watchdog timer will have to have a lower sampling rate than all other subsystems as explained in Section 11.5.

The fault status of each subsystem is estimated to have 8 bit words. This is because some integrated systems such as the ADCS system from Hyperion have more complex error messages. With approximately 13 subsystems operational at a time during the data acquisition phase this leads to the estimated 104 bit/s data rate. The ADCS mode selection data rate is directly estimated from the different pointing scenarios that will be encountered during the mission. It is assumed that 4 different pointing modes for the deployment phase are required when the propulsion system is active. Other than those modes there will be the detumbling mode, the safe mode, the data acquisition nadir pointing mode. Even though antenna pointing will not be necessary as shown in Chapter 9 it will be assumed that 25 ground station locations are stored within the Hyperion iADCS400 in case of unforeseen circumstances which require higher data rates. Therefore the on-board computer will have to distinguish between 32 different modes. This requires a word size of 8 bits. The sampling rate is assumed to be the same as for the star tracker. The tele command uplink data rate is assumed to be the maximum UHF uplink rate of 10 [kbit/s]

The payload ON/OFF commands are simple 1 bit commands for each of the 5 payloads installed on the two different CubeSat designs (see Chapter 7). The thruster control command includes 4 modes: wake-up, fire, stop firing and sleep. Those 4 modes require 2 bits. 10 Hz is a high enough sampling rate to achieve the required accuracy for the altitude change considering that the time per burn during a transfer manoeuvre of several hours is around 15 seconds (see Chapter 6).

The different communication interfaces will have to be accommodated by the on-board computer. As can be seen from Table 11.1 I^2C, SPI and UART interfaces will have to be supported.

Table 11.1: Data rates and communication interfaces between all subsystems including the data rates between the OBC and the data storage. If the source is indicated as an estimate the estimation method is explained in Section 11.1

Item	Comm Interface	Received by	Quantity	Sampling rate [Hz]	Word Size [bit]	Required data rate [bit/s]	Source
Power subsystem							
Overcurrent event log	I2C	OBC	1	1	8	8	Estimate
Solar cell sun sensor	voltage	ADCS	1	10	96	960	Estimate
Output channel voltage and current	I2C	OBC	3	1	8	24	Estimate
Input channel voltage and current	I2C	OBC	18	1	8	144	Estimate
Thermal subsystem							
Temperature sensors	voltage	OBC	8	1	16	128	Estimate
GN&C							
GPS time	UART 9600 8-N-1	OBC	1	10	32	320	[66]
GPS position data	UART 9600 8-N-1	OBC	1	10	48	480	[66]
Propulsion							
Thruster valve status	I2C	OBC	1	1	8	8	Estimate
ADCS							
Attitude sensor	I2C	OBC	1	10	96	960	Estimate
Communications							
Tele command uplink	I2C	OBC	1	1	10000	10000	Chapter 9
Payload							
Magnetometer	I2C	OBC	1	10	72	720	[24]
Dosimeter	UART 115200 8-N-1	OBC	1	0.1	144	14.4	[67]
Langmuir probe	UART 9600 8-N-1	OBC	1	10	200	2000	[65]
Electric field probe	UART	OBC	2	70	8	560	[68]
Ion/neutral mass spectrometer	SPI	OBC	1	1	1300	1300	[70]
Retarding potential analyser	I2C	OBC	1	1	400	400	[71]
OBDH							
Fault detection watchdog	serial	Storage	1	0.5	8	4	Estimate
Fault status of each subsystem	serial	Storage	13	1	8	104	Estimate
GPS time	serial	Storage	1	10	32	320	Estimate
GPS position data	serial	Storage	1	10	48	480	Estimate
Payload data (config 1)	serial	Storage				4594.4	sum with INMS
Payload data (config 2)	serial	Storage				3694.4	sum with RPA
Attitude data	serial	Storage	1	10	96	960	Estimate
Housekeeping data	serial	Storage				264	sum of sensors
Thruster control	I2C	Propulsion	1	10	4	40	Estimate
ADCS mode selection	I2C	ADCS	1	10	8	80	Estimate
Payload ON/OFF	serial	Payloads	5	1	1	5	Estimate
Subsystem ON/OFF	serial	Subsystems	10	1	1	10	Estimate

The thermal sensors are assumed to have a word size of 16 bit [37]. There are 8 sensors in each CubeSat as explained in Chapter 12.

11.2. MEMORY SIZING AND DATA COMPRESSION

The minimum required memory size as found in Chapter 9 is 350 Mbit, which is equal to about 44 MB. Doubling this value for redundancy and to allow space for the uncompressed data which is being collected yields a value of 88 MB. All OBC systems considered in Section 11.3 have the option to use SD cards with at least 2GB of storage capacity. Therefore memory does not pose a problem. In Section 11.3 the redundancy of the memory storage is discussed.

To optimize the amount of data that is downlinked during one contact time a compression algorithm will be used. Each time 2Mbit of uncompressed data is saved on the storage unit the LZMA (Lempel-Ziv-Markow-Algorithm) algorithm is used to compress the data. The LZMA algorithm is lossless, which allows for exact decompression of the original data. It is found that a 2Mbit binary data file can be compressed to a size of 83% of the original file (see Section 11.6).

11.3. ON BOARD COMPUTER TRADE-OFF

From Table 11.1 the total data rate that is received by the OBC as well as the data rate from the OBC towards the data storage are calculated and displayed in Table 11.2. The data rates across the I^2C, UART and SPI interfaces are also found to fix the requirements for the OBC. From the subsystem requirements it can also be found that the power consumption of the OBC shall not exceed 1W.

Table 11.2: Total data rates across interface busses to the OBC, from the OBC and to the data storage

Total data rate	Configuration with INMS [bit/s]	Configuration with RPA [bit/s]
Across SPI bus	1300	1300
Across I2C bus	12984	11944
Across UART bus	3374.4	3374.4
Across AD converter	128	128
From payload to storage	4594.4	3694.4
From telemetry to storage	2132	2132
From OBC to storage	6774.4	5874.4
To the OBC	16666.4	15766.4

Four OBC units are considered for the mission: The Hyperion CP400.85, the Gomspace NanoMind Z7000, the Gomspace NanoMind A3200 and the ISIS on board computer (IOBC). During personal conversations or email contact with the OBC suppliers it was found that all of the considered units are compatible with all types of SD cards. The costs of the units are all comparable and highly depend on the options that are taken for each unit. Therefore cost is not taken into account for the trade off. All the systems work with 32 bit processors and after talking to the suppliers it was found that the required processes can easily be handled by all OBC's [25][24]. The most capacity consuming process is considered to occur during the downlinking phase, while data is still being gathered and compressed with the LZMA algorithm. The exact performance of each unit under these conditions can only be simulated after the exact code is written. Parallel operations can heavily influence the performance of an OBC. It is therefore recommended to use a processor emulator (such as QEMU [1]) in the next design phase to exactly compare the performance of each OBC. Also the read and writing speed to and from the data storage is key. The read speed should always be above the downlinking data rate. For all OBC's considered it was found that the corresponding SD-cards' read speeds exceed the 2Mb/s of maximum downlink data rate for the S-Band system [25][24]. As an example the IOBC SD-cards have a minimal read speed of 500 KB/s [24], which equals 4Mbit/s. That is twice as high as the maximum downlink data rate.

From Table 11.3 it can easily be seen that the IOBC from ISIS is the best choice. Once the CP400.85 from Hyperion has flight heritage it is the clear winner, but since the OBC is one of the most critical

---

[1] http://www.qemu.org/download/ [cited 19-06-2017]

Table 11.3: Qualitative trade-off matrix for the OBC subsystem. Green: excellent, exceeds the expectations, Blue: good, meets the expectations, Yellow: correctable or acceptable deficiencies, red: unacceptable deficiencies.

Options	Interfaces [7.5%]	Power [10.0%]	RAM [10.0%]	clock rate [10.0%]	Flight heritage [35.0%]
CP400.85	green Customiz- able	green 0.1W[103]	green 512MB[103]	green 500MHz[103]	yellow No
NanoMind Z7000 [104]	blue SPIO, I2C SPI, SD, UART, ADC	red 2.3W [104]	green 512MB	green 800MHz	blue Yes
NanoMind A3200[10	blue SPIO, I2C SPI, SD, UART, ADC	blue 0.9W	blue 128MB	blue 32MHz	blue Yes
IOBC [101]	blue I2C, SPI, UART, ADC, SD	green 0.55W	blue 64MB	green 400MHz	blue Yes

systems on board when it comes to lifetime and reliability, the flight proven IOBC is prefered. For redundancy two IOBC's will be installed in each CubeSats to achieve a higher reliability as discussed in Chapter 16. The same principle as used on the DelfiNext CubeSat will be employed: If the primary OBC is silent on the databus for an extended period of time, then the secondary OBC will take over [2]. As data storage two 2GB SD-cards are chosen. This is done, because the data storage units are one of the most vulnerable systems on board with respect to radiation. There are mainly two types of SD-cards: single layer cells and multi layer cells. Whereas the latter have a higher data to size ratio, they are also more prone to radiation damage. Therefore two SD-cards of the single layer cell type are chosen.

11.4. DATA HANDLING BLOCK DIAGRAM

In Figure 11.3 the different interconnections and the data rates are shown graphically. The data rates created by the ON/OFF commands from the OBC to the payload or subsystems is not shown in Figure 11.3, because those data rates are comparatively small and to keep the diagram more clear. The IOBC does not have enough UART connections. This problem is mitigated by using a UART to SPI converter [106]. The S-Band transceiver maximum data rate of 2Mbit/s is only assured by using the SPI interface which has a maximum data rate of 10Mbit/s across its bus. Therefore the S-Band transceiver is connected to an I2C SPI converter before being connected to the SPI bus of the IOBC.

11.5. SOFTWARE ARCHITECTURE

In Figure 11.4 the basic software architecture of each CubeSat is shown. The possible commands to the payload or subsystems from the ground stations include the possibility to shut down or power up each subsystem and sensor individually. Attitude commands can also be send to the ADCS system and the propulsion system can be programmed for a firing sequence in connection with a timer or a GPS location input. Ground commands can also include the request to resend older data during the next downlink. Basic software updates can also be uplinked. The data storage SD-cards will be filled to the maximum. When they are full the oldest data will be overwritten with the new incoming data from telemetry and sensors.

The commissioning phase, which happens in between the two deployment manoeuvres (as shown in the functional flow diagram in section 2.3.1), does not have a separate mode. During the comissioning phase the data acquisition mode is used in combination with ground commands which allow the individual testing of different components and sensors.

---

[2] http://www.delfispace.nl/delfi-n3xt/command-and-data-handling [cited 19-06-2017]

The software architecture also includes a fault detection watchdog, which continuously works in parallel with the structure shown in Figure 11.4. The fault detection watchdog has a timer. If no command is given to a subsystem within the given time the subsystem is reset. The timer has the same frequency as the subsystems that it is controlling to prevent that the subsystems reset themselves without any critical reason. This structure allows to counteract bit flips, which can be caused by the space environment radiation [25]. If a subsystem had to be reset, this will be logged in the subsystems fault status. Subsystems that have processing capabilities, such as the Hyperion iADCS400 and the Hyperion PM400 propulsion subsystem, reset themselves when no command is received as shown in Figure 11.1. Subsystems that have not enough processing power or non at all, such as the sensors, are reset by the OBC as shown in Figure 11.2.
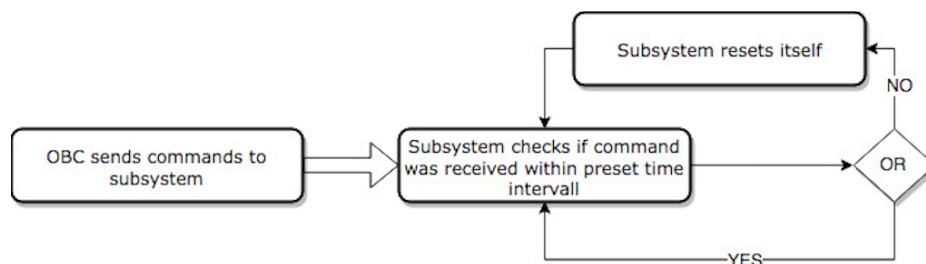

Figure 11.1: Fault detection watchdog functioning for autonomous subsystems
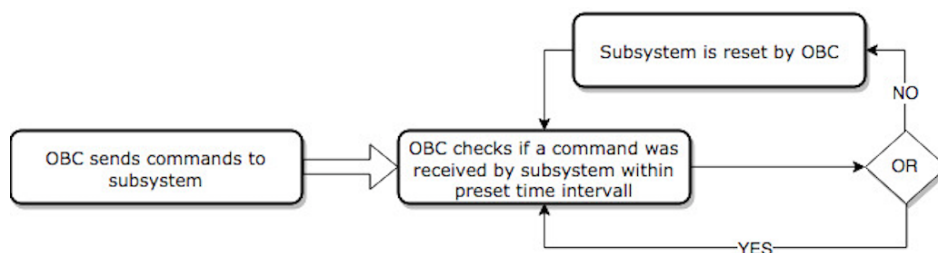

Figure 11.2: Fault detection watchdog functioning for subsystems with limited processing capacity

The safe mode as shown in Figure 11.4 is not only triggered by a mode selection but is also automatically entered if one of the following conditions apply:

- One of the thermal sensors detects a temperature lower than 0 degrees Celsius or higher than 40 degrees Celsius within the CubeSat.
- A series of over-current events within a short period of time. This indicates a problem with the electrical power system.
- The slew rate is close to the maximum slew rate allowed to maintain structural integrity.
- A subsystem has been reset multiple times within 10 seconds by the fault detection watchdog.

Those conditions have to be analysed in more detail during the next design phase. To find the maximum allowable slew rate it will be necessary to find the rotational rate, which will create accelerations that produce stresses higher than the yield stresses of the materials used in the CubeSat. The ADCS itself does not have a maximum slew rate from which it can recover. The ADCS only requires more time to stabilise the CubeSat from a high rotational rate.

To determine the number and magnitude of over-current events which could damage the CubeSats electrical power system and subsystems a detailed electrical analysis will have to be carried out in combination with testing.

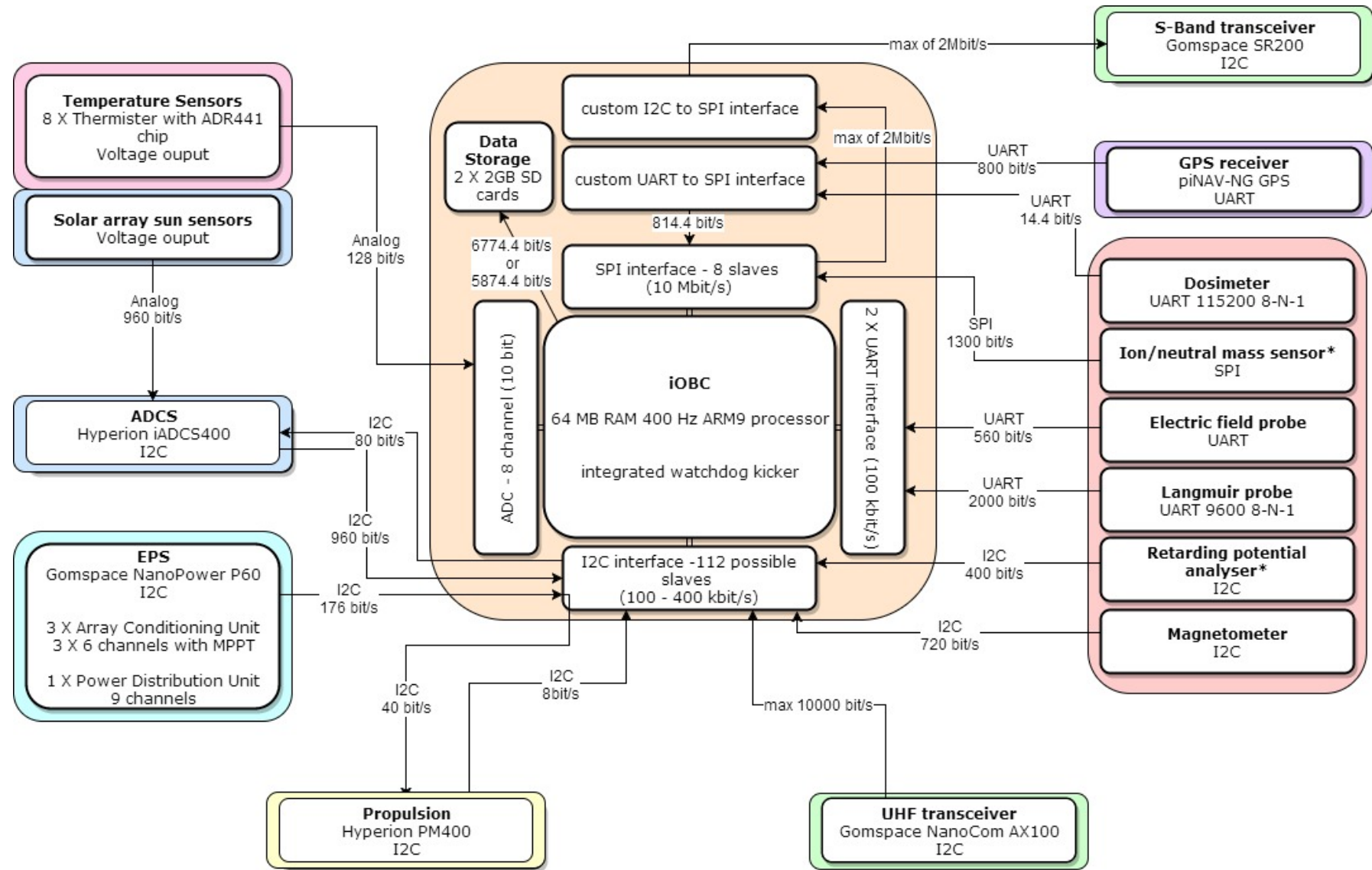The temperature limits are determined by the PM200 propulsion system.

Figure 11.3: Data block diagram showing the data rates and the interfaces between the different components.
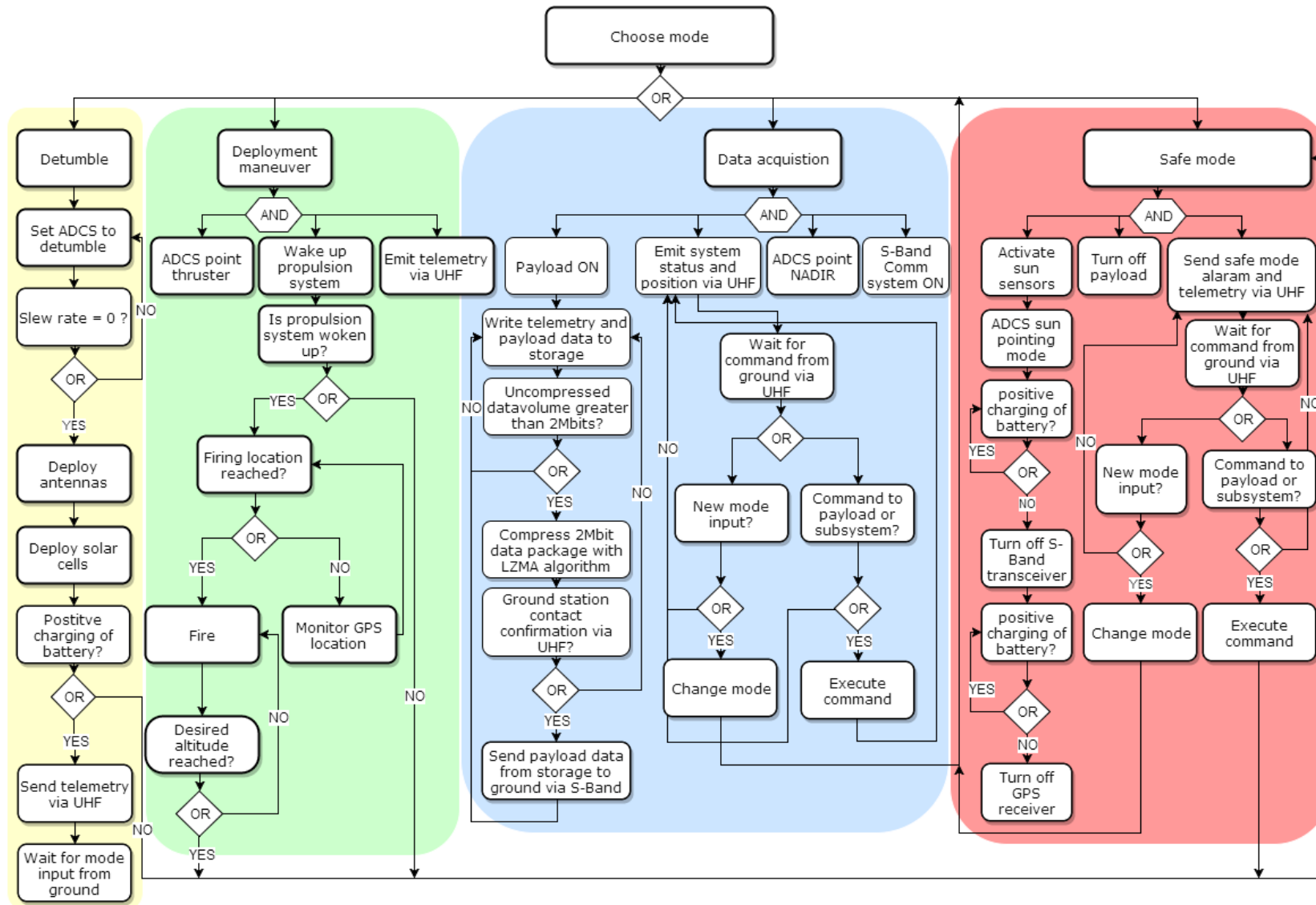
Figure 11.4: Software block diagram showing the basic software architecture of the CubeSats in the constellation

11.6. VERIFICATION & VALIDATION

A Python program was written to generate data files, which contain the same type of data as would be output by the sensors [66] [32] [24][67] [71] [68]. In this program data is generated as pseudo random floats, which has the same amount of significant digits as would be generated by the respective sensors. Those floats are then 32bit binary IEEE encoded. The data is then written to a data file, which most closely represents the data that would have to be compressed by the OBC. Each generated line of data represents one discrete time step. The data file is then compressed by using the LZMA algorithm. This process was repeated with different file sizes with a range from 150KB to 350KB. 250KB corresponds to about 2Mbit, which is the data volume which will be compressed at regular intervals. The python program was unit tested as well as system tested. Two trials with two different pseudo random data sets were performed. The results are presented in Figure 11.5 and 11.6.
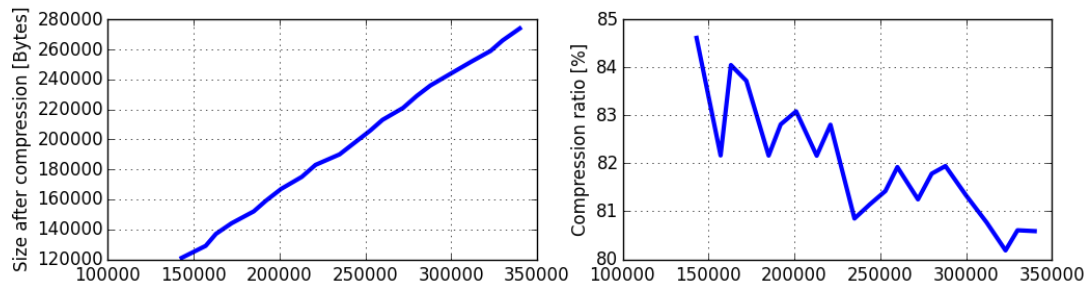
Figure 11.5: Second data compression performance of the LZMA algorithm for representative pseudo random binary data files
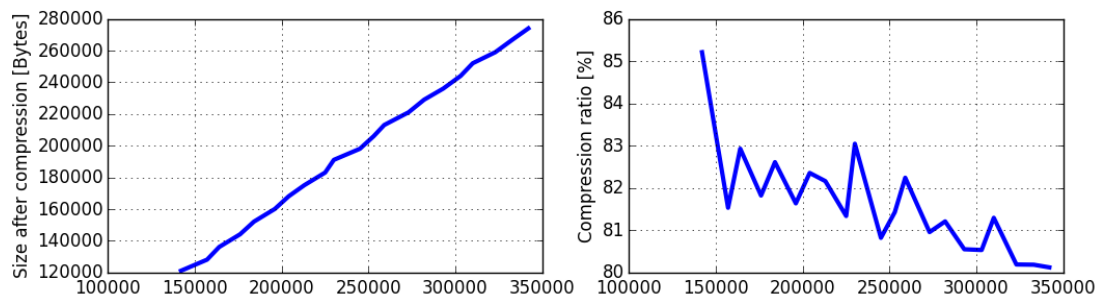
Figure 11.6: Second data compression performance of the LZMA algorithm for representative pseudo random binary data files

As can be seen in Figures 11.5 and 11.6, it can be concluded that a compression ratio of 83% can be expected

As further verification of the results of this Chapter it is recommended to implement a software which comes as close as possible to the real instructions performed by the CubeSats. This software should be tested first using an emulator for a 32-bit ARM9 processor as found in the IOBC. Possible emulators include QEMU as well as ARMSIM# of the University of Victoria [3]. Then, upon successful completion of this verification the software and computer performance should be validated through testing on an engineering model as provided by ISIS.

---

[3] http://armsim.cs.uvic.ca/ [cited 19-06-2017]

<div align="right">

12

</div>

<div align="right">

THERMAL CONTROL

</div>

Thermal control is the control of spacecraft equipment and structural temperatures [29]. The current chapter presents a detailed analysis of the interaction between the spacecraft and its heating environment. First, the temperature requirements are discussed in Section 12.1. Next, the methodology of the thermal analysis is given in Section 12.2. This section also presents the results of the analysis and the verification and validation procedures. Then the thermal design based on the results of the analysis is presented in Section 12.3. Lastly, the thermal stresses within structural members are checked in Section 12.4.

12.1. SPACECRAFT TEMPERATURE REQUIREMENTS

Every spacecraft component has its own temperature requirements which determine the temperature operating limits of the spacecraft. It is necessary for the thermal control system (TCS) to maintain this thermal environment to avoid component failure and loss of mission. The operational temperature limits for all spacecraft platforms are listed in Table 4.1. From this table it is seen that the temperature of the spacecraft is constrained within 0°C and +40°C. A thermal analysis is then performed to facilitate the design of a TCS that meets the temperature requirements.

12.2. THERMAL ANALYSIS

In the following section the thermal analysis of the EPIC mission is presented. First, the methodology of creating a thermal model is explained. The model is tailored to the specifications of the EPIC satellites and applied. Next, the results of the analysis are displayed and the design as a consequence thereof is presented. Lastly, the verification and validation procedures are outlined.

METHODOLOGY

There are two types of thermal control - active control and passive control. Active control techniques are generally complex while consuming power and telemetry resources, making them relatively heavy [29]. In comparison, passive control techniques consist of selecting surface finishes and using insulation, making them lighter. The satellites being designed are small CubeSats which shall have low mission costs and low power consumption. Since passive control offers optimal compliance with these mission requirements, it is opted for.

The subsequent thermal analysis models the spacecraft equilibrium temperature for a variety of 22 surface finishes. From the results of the analysis a surface finish that meets the operational temperature limits of the spacecraft can be selected. It is noted that the thermal analysis was programmed and performed in MATLAB software. Before proceeding with the method of the analysis, the applied assumptions are stated:

- The thermal analysis shall be based on the interaction of heat from the environment to a single node (the spacecraft). The spacecraft is assumed to be an isothermal node.
- It is assumed that planetary infrared radiation emanates uniformly from the cross-sectional area of Earth [29].
- Convective and conductive interaction are neglected due to very low levels of molecules in space, even in low earth orbit.
- Aerodynamic heating is neglected due to very low level of drag present in space.

- Heat transfer through the hinges connecting the deployable surfaces to the spacecraft, is negligible [27].

The only way for the spacecraft to interact with its environment in space is through heat exchange, namely in the form of radiation. The thermal modelling is carried out by requiring thermal equilibrium. The heat input to the spacecraft must equal the heat output $Q_{in} = Q_{out}$. In the list below the terms contributing to the thermal balance are described, and their interactions are illustrated in Figure 12.1.

- J_s Direct solar radiation
- J_a Albedo radiation which is solar radiation reflected by nearby planets
- J_p Planetary radiation which is infrared energy radiated by nearby planets
- Q_{rad} Heat radiated to space by spacecraft
- Q_{int} Internally dissipated power by spacecraft components

The terms are elaborated in Equations 12.1, 12.2, 12.3, and 12.4. Where a is the albedo factor, R_e is the radius of Earth, R_{orbit} is the orbit radius of the satellite, σ is the Stefan-Boltzmann constant equal to $5.67 \cdot 10^{-8}$ Wm^{-2}K^{-4}, and T is the equilibrium temperature of the spacecraft. The parameters A_{surf} and ϵ are explained shortly in the following text. The internal heat dissipation of the spacecraft is estimated with Equation 12.4, where the subscripts indicate heat dissipation of different satellite components.

$$J_a = J_s a \left(\frac{R_e}{R_{orbit}} \right)^2 \quad (12.1) \qquad J_p = 237 \left(\frac{R_e}{R_{orbit}} \right)^2 \quad (12.2) \qquad Q_{rad} = A_{surf} \sigma T^4 \epsilon \quad (12.3)$$

$$Q_{int} = Q_{thruster} + Q_{transceiver} + Q_{eps} + Q_{battery} + Q_{obc} + Q_{adcs} + Q_{payload} \quad (12.4)$$
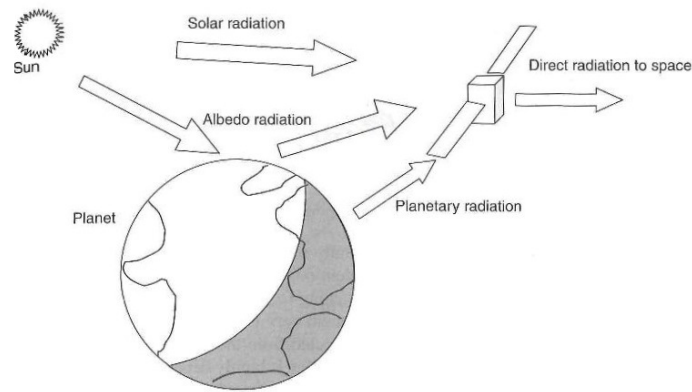
Figure 12.1: Spacecraft thermal environment [29]

From the parameters given in Equations 12.1 to 12.4, the thermal balance $Q_{in} = Q_{out}$ then translates to Equation 12.5. The parameters α and ϵ are properties that represent the absorptivity and emissivity of a surface. On the right hand side of Equation 12.5, A represents the normally projected area on the spacecraft from the incoming source of radiation. The subscripts s, a, and p, indicate the sources of radiation - solar, albedo, and planetary. On the left hand side of Equation 12.5, A_{surf} stands for the total radiating surface of the spacecraft, which emits as a grey body. From Equation 12.5, the equilibrium temperature of the spacecraft T can be solved for.

$$A_{surf} \sigma T^4 \epsilon = A_s J_s \alpha + A_a J_a \alpha + A_p J_p \epsilon + Q_{int} \quad (12.5)$$

It is noted that Equation 12.5 is only applicable to a spacecraft surface covered with a single material. This is not the case for the EPIC satellites, whose surfaces are partially covered by Azurespace solar cells (for reasoning behind this choice of solar cells, see Section 10.1). This means that the surface of one satellite is covered by two materials - by solar cells and by a surface paint which is designed by the thermal engineer. For this reason, Equation 12.5 is refined to account for a spacecraft surface covered by two different materials. The refined formulation is displayed by Equation 12.6.

$$\sigma T^4 (A_{spt} \epsilon_{sp} + A_{leftt} \epsilon_v) = J_s (A_{sp} \alpha_{sp} + A_{left} \alpha_v) + J_a (A_{sp} \alpha_{sp} + A_{left} \alpha_v) + J_p (A_{sp} \epsilon_{sp} + A_{left} \epsilon_v) + Q_{int} \quad (12.6)$$

In Equation 12.6, the areas A_{sp}, A_{spt}, A_{left}, and A_{leftt}, stand for projected solar panel area, total solar panel surface area, leftover uncovered projected area, and total leftover uncovered surface area. For visual support, Figure 12.2 and Figure 12.3 are referred to. The surface properties of the Azurespace solar panels are given as $\alpha_{sp} = 0.91$ and $\epsilon_{sp} = 0.89$ [107]. Furthermore, the subscript v indicates the variability of the surface properties. In the MATLAB program, a block of code loops through a collection of 21 different surface finishes, each time using a different α and ϵ. By this way the program computes 21 equilibrium temperatures for the spacecraft. A flowchart of the program logic is given in Figure 12.4.
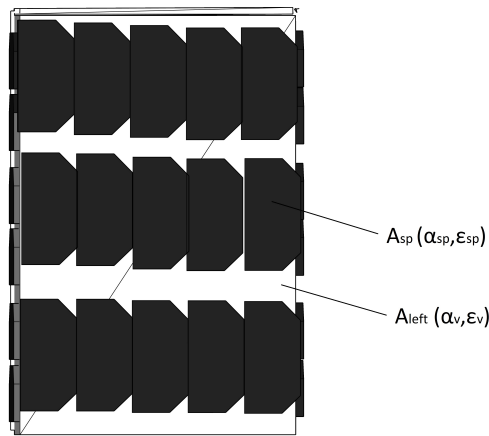
Figure 12.2: Visualisation of parameters related to projected areas
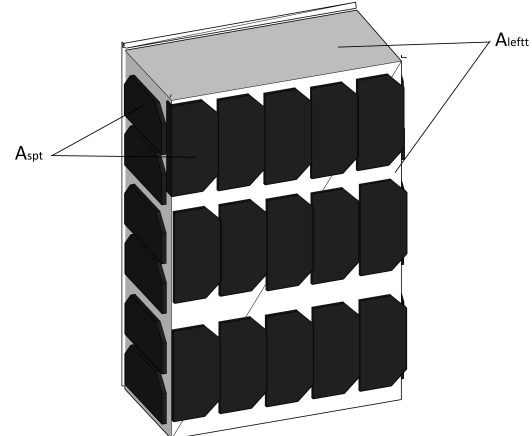
Figure 12.3: Total solar panel surface area and total leftover surface area
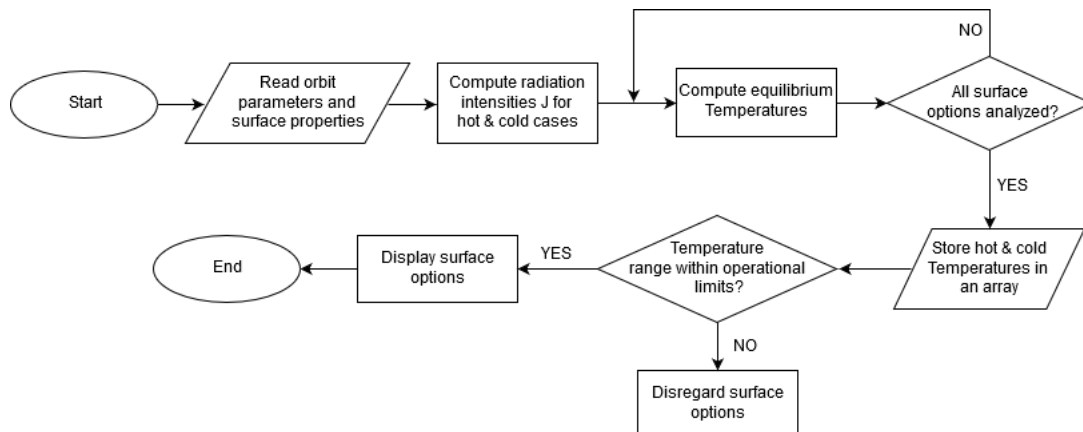
Figure 12.4: Program flowchart for thermal model

Lastly, equilibrium temperatures have been computed for both worst case scenarios (hot case and cold case). By analysing both extremes the operational range of the spacecraft can be determined within the temperature constraints discussed in Section 12.1. It is noted that the worst case scenarios are computed for the nominal mode of the spacecraft (one side perpendicular to sun, other side perpendicular to earth, i.e. Nadir pointing). This is done because the EPIC satellites are Nadir pointing 99% of the time. The results of the thermal analysis are provided in the next section.

RESULTS

The results of the thermal analysis are displayed in Table 12.1. Next to the equilibrium temperatures for both hot and cold cases, the α/ϵ ratios and maximum changes in temperature are also displayed. The list of surface finishes with their corresponding absorptivities and emissivities are retrieved from Fortescue et al [29]. From Table 12.1, it is seen that higher α/ϵ ratios help retaining spacecraft heat, while lower ratios help emitting spacecraft heat.

Furthermore, the results from Table 12.1 correspond to the mission's nominal operation altitude of 520km and inclination of 55°. However, during the lifetime of the mission, each CubeSat is planned to experience orbit altitudes as low as 350km and as high as 670km for constellation deployment purposes. Details about the constellation deployment can be found in Table 5.1, Section 5.2. Performing a sensitivity analysis on the spacecraft temperatures from a range of 350km to 670km, has revealed that the most critical altitude for thermal control is 350km. From the entire list of surface finishes, there are 3 options which meet the temperature requirements from Section 12.1. The results of these 3 options are displayed in Table 12.2.

Table 12.1: Spacecraft equilibrium temperatures for worst cases for 21 different surface finishes, each combined with AzureSpace solar cells. Computed for operational altitude of 520km and inclination 55°.

	Surface Finish	Hot Case [°C]	Cold Case [°C]	α/ϵ	ΔT
1	Polished beryllium	85.3	64.8	44.0	20.5
2	Goldized kapton	80.3	60.4	12.5	19.9
3	Gold	78.9	59.1	6.25	19.8
4	Aluminium tape	78.0	58.3	5.25	19.7
5	Polished aluminium	76.1	56.4	3.0	19.6
6	Aluminized kapton (alu. outside)	75.7	56.3	2.8	19.4
7	Polished titanium	56.1	37.4	1.0	18.6
8	Black paint (epoxy)	52.4	33.7	1.12	18.7
9	Black paint (polyurethane)	50.6	32.0	1.06	18.6
10	Black paint (polyurethane, EC[1])	54.3	35.4	1.18	18.8
11	Silver paint	58.8	40.2	0.84	18.6
12	White paint (silicone)	40.4	23.1	0.31	17.2
13	White paint (silicone, 1000hr UV rad.[2])	40.9	23.6	0.35	17.3
14	White paint (silicate)	35.1	18.4	0.13	16.6
15	White paint (silicate, 1000hr UV rad.)	35.5	18.7	0.16	16.7
16	Solar cells (GaAs, typical values)	53.1	34.4	1.1	18.7
17	Solar cells (Silicon, typical values)	50.0	31.6	0.91	18.3
18	Aluminized kapton (kapton outside)	50.9	32.8	0.63	18.1
19	Aluminized FEP[3]	52.9	35.0	0.34	17.9
20	Silver coated FEP (SSM[4])	38.5	21.6	0.1	16.8
21	Optical solar reflector	39.8	22.8	0.09	16.9

Table 12.2: Spacecraft surface options meeting temperature requirements at 350km

	Surface Finish	Hot Case [°C]	Cold Case [°C]	α/ϵ	ΔT
14	White paint (silicate)	36.0	18.8	0.13	17.2
15	White paint (silicate, 1000hr UV rad.)	36.4	19.2	0.16	17.2
20	Silver coated FEP (SSM)	39.5	22.1	0.1	17.4

The coating that provides the highest contingency margin with respect to the operational limits is chosen. For the spacecraft, the limits are constrained between 0°C and 40°C. From Table 12.2 it is clear that the highest margin to the next operational limit (of 4°C), is provided by silicate white paint. It is also favourable because it shows minimal degradation in space after 1000 hours of UV radiation.

In addition, the thermal analysis is applied to the deployable solar panels of the spacecraft. This is done to check the maximum temperature that the solar panels experience. It is important to minimise the temperature of the solar panels as much as possible, in order to maximise the solar panel efficiency. The results of the thermal analysis show that the lowest achievable maximum temperature of the deployables

[1]EC = electrically conducting
[2]UV = Ultraviolet
[3]FEP = fluorinated ethylene propylene
[4]SSM = second surface mirror

is 85.6°C. The coating that provides this, is again white paint. This is a convenient result, since it reduces the complexity of the coat application during production procedures, thus saving time and costs. For more details on the specifications and manufacturer of the coating, Section 12.3 is referred to.

Verification and Validation

Verifying the model will ensure that there are no mistakes in the code, which may cause the model to behave differently than what is expected. To determine whether the thermal program performs correctly, unit testing is applied. This entails running blocks (or units) of code using special inputs for which the results are already known or can be expected, and checking the outputs. The results of the verification are given in Table 12.3. As can be seen, for the second and third unit tests, the actual outcomes match the expected outcomes. For the first unit test, the actual outcome also matches the expected outcome, considering that it is a MATLAB feature that division by 0 is treated as a limit. It can thus be concluded that the code is verified.

Table 12.3: Verification of thermal model

Special input	Expected outcome	Actual outcome
$A_{spt} = A_{leftt} = 0$	Error	Infinity
$\alpha_{sp} = \alpha_v$ $\epsilon_{sp} = \epsilon_v$	561.93 °C	561.93 °C
$J = 0$ $Q_{internal} = 0$	0 K	-273.15 °C

The verified code is then proceeded with a system validation. This is necessary to ensure that the results of the program resemble the reality of the physical process that is modelled. The validation data presents thermal cases for different spacecraft. The cases and their respective parameters are a courtesy of a course given by Professor Zandbergen of the TU Delft Faculty of Aerospace Engineering [108]. The integrity of the validation data is thereby guaranteed. For each case, the equilibrium temperature of the spacecraft is computed with the model and compared to the validation data. The results of this comparison and the percentage error between the numbers is presented in Table 12.4. It can be seen that all results are less than 1% error. This confirms the accuracy of the model, and concludes that it reasonably models the physical reality.

Table 12.4: Validation of thermal model

Case	Model Data [°C]	Validation Data [°C]	% Error
1	33.28	33.0	0.84
2	127.77	128.0	0.18
3	119.29	119.35	0.05

12.3. Design of Thermal Control System

In this section the design of the thermal control system is presented. First, the specifications of the coatings for the spacecraft and deployable solar panels are given in Section 12.3. Then, the choice of the thermal sensors is presented in Section 12.3.

Spacecraft Surface Finish

In the previous section the spacecraft coating was selected to be white paint. The optimal white coating is a combination of 2 white thermal control paints provided by AZ Technology Corporation. The white paints selected are the non-organic AZW/LA-II paint and the organic AZ-400-LSW[5]. It is noted that the AZW/LA-II has proven flight heritage in the Materials International Space Station Experiment (MISSE). First, a thin layer of AZW/LA-II is applied to a prepared outer surface of the S/C. Then, a thick layer of the organic AZ-400-LSW is applied on top. As one can see from the spectral reflectance graphs in

---

[5] http://www.aztechnology.com/materials-coatings-AZ-400-LSW.html [cited 26-06-2017]

Figure 12.5 and 12.6, this combination guarantees thermal control for a range of radiation.

Furthermore, by applying a thin layer of non-organic coating, and a thick layer of organic coating, a high degree of sustainability is maintained. Additionally, the AZ-400-LSW thermal coating meets the NASA Handbook (NHB) flammability and toxicity requirements NHB 8060.1C[6]. Furthermore, the organic coating has very low outgassing properties. The upgraded equilibrium temperatures for the spacecraft bus and deployables can be found in Table 12.5. For weight and cost estimates of the thermal coating, Table 4.1 is referred to.

Table 12.5: Upgraded equilibrium temperatures using combination of non-organic AZW/LA-II and organic AZ-400-LSW white thermal coatings

	Temperature [°C]
S/C hot case	35.2
S/C cold case	18.6
Maximum for deployable solar panels	86.1
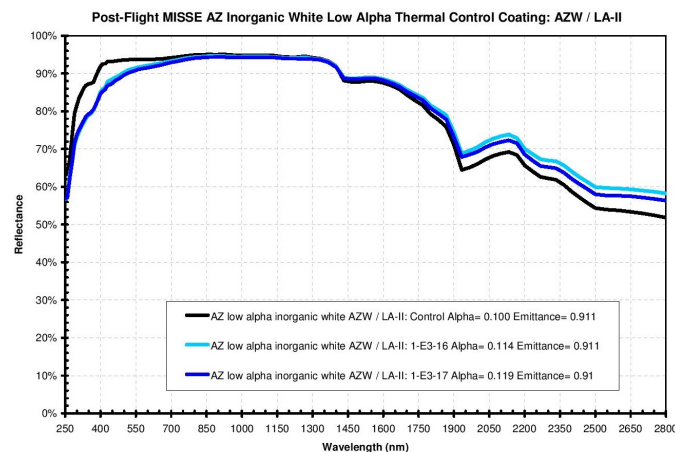
Figure 12.5: Marshall Space Flight Center (MSFC) analysis of AZW/LA-II coating on MISSE[7]

THERMAL SENSORS

To be able to monitor the spacecraft's temperature, thermal sensors are applied. The thermal sensors themselves are thermistors; they are resistors whose resistance changes with temperature. The product selected is the NASA/GSFC S-311P827/01 thermistor from QTI Sensing Solutions. These thermistors are certified by NASA for space programs specifying quality level Grade 1 parts[9].

Eight thermistors will be applied to each EPIC CubeSat - one on each of the 6 outer sides, and 2 on the inside walls experiencing the highest temperature extremes. Thus one inner thermistor is placed on the wall facing perpendicular to the sun, and another is placed on the wall facing perpendicular to Earth (nominal nadir pointing mode). For weight and cost estimates of the thermistors, Table 4.1 is referred to.

---

[6] http://www.aztechnology.com/materials-coatings-AZ-400-LSW.html [cited 26-06-2017]
[7] http://www.aztechnology.com/materials-coatings-AZW-LA-II.html [cited 26-06-2017]
[8] http://www.aztechnology.com/materials-coatings-AZ-400-LSW.html [cited 26-06-2017]
[9] https://www.thermistor.com/nasagsfc-s-311-p-82701-02-03-04 [cited 26-06-2017]

Figure 12.6: Hemispherical spectral reflectance for AZ-400-LSW white coating[8]

12.4. THERMAL STRESSES IN THE STRUCTURE

To analyse whether temperature differences cause critical expansions or contractions to structural elements, calculations are made. For a single structural element, the displacement due to a change in temperature is given in Equation 12.7 [109]. The variable ΔT is positive for expansion and negative for contraction. The constant α_c stands for the linear coefficient of thermal expansion, and L stands for the length of the structural member in millimetres.

$$\delta_T = \alpha_c \Delta T L \qquad (12.7)$$

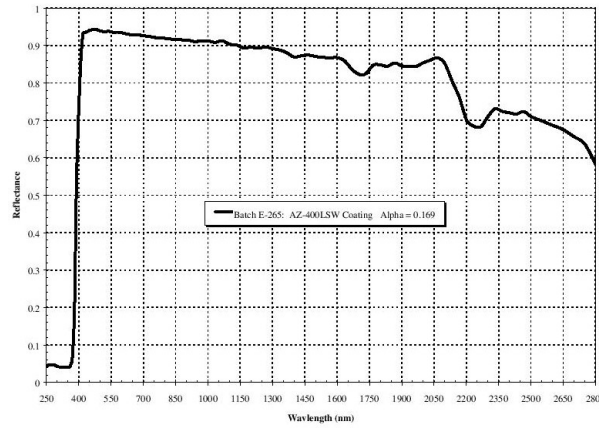A critical sub-assembly in the CubeSat is analysed. The sub-assembly has three different structural members: a printed circuit board (PCB), connection rods, and connection members. They are depicted in Figure 12.7. It is assumed that the structure will be assembled at 20°C room temperature. From Section 12.2, it is known that the CubeSats will operate in the temperature range from a minimum of 17.5°C to a maximum of 34.0°C. Thus, for expansion ΔT = +14 and for contraction ΔT = -2.5. The results of the displacements for the three members are displayed in Table 12.6. The rod and member are much longer in the axial direction than circumferential direction, therefore any displacements in their circumferential planes are negligible. The PCB on the other hand has in-plane dimensions which are much longer than in the axial direction, and therefore the displacement in the PCB's axial direction can be neglected.

Table 12.6: Displacements in the three members of the critical sub-assembly

	$PCB_{x\text{-}dir}$	$PCB_{y\text{-}dir}$	$Rod_{axial\text{-}dir}$	$Member_{axial\text{-}dir}$
Expansion [mm]	0.0188	0.0176	0.0300	0.0353
Contraction [mm]	-0.0034	-0.0031	-0.0054	-0.0063

Furthermore, the stresses at two critical locations in the sub-assembly are analysed. The stress due to expansion or contraction at a connection can be found by equating the thermal strains. This is shown in Equations 12.8 and 12.9. The method used is from Megson [110]. In addition, since no external loads are applied, Equation 12.10 holds.

$$\epsilon_a = \epsilon_b \quad (12.8) \qquad \frac{\sigma_a}{E_a} + \alpha_a \Delta T = \frac{\sigma_b}{E_b} + \alpha_b \Delta T \quad (12.9) \qquad \sigma_a A_a + \sigma_b A_b = 0 \quad (12.10)$$

Now there are two equations (Equations 12.9 and 12.10) and two unknowns which can each be solved simultaneously for the stresses acting in structural members a and b, as can be seen in Equation 12.11. Isolating for the stresses:

$$\sigma_a = \frac{\Delta T (\alpha_b - \alpha_a) A_b E_b E_a}{A_b E_b + A_a E_a} \qquad\qquad \sigma_b = -\frac{\Delta T (\alpha_b - \alpha_a) A_a E_b E_a}{A_b E_b + A_a E_a} \qquad (12.11)$$
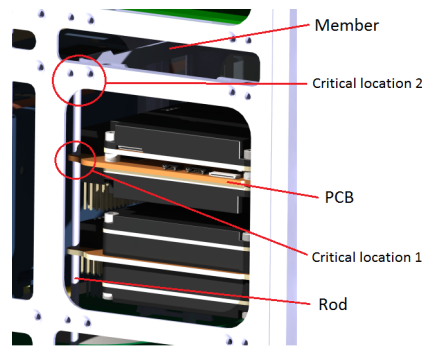
Figure 12.7: Critical sub-assembly in CubeSat. Connection between PCBs and structure via rods

Two critical locations are analysed. One at the connection of the PCB with the rod, and the other at the connection of the rod and the member. The stresses are presented in Table 12.7. It can be seen that for one connection, at either expansion or contraction, both members experience equal and opposite stresses. So one member is in tension, whereas the other is in compression. From the table it can be seen that the stresses are so small, that the structural design with gap tolerances of 0.2mm in the connections, suffice to sustain thermal stresses.

Table 12.7: Thermal stresses at critical locations

	Member	Expansion	Contraction
Critical location 1	σ_{PCB} [Pa]	37	-208
	σ_{rod} [Pa]	208	-37
Critical location 2	σ_{PCB} [Pa]	19	-104
	σ_{member} [Pa]	104	-19

12.5. DISCUSSION AND RECOMMENDATIONS: THERMAL STRATEGY AND DESIGN

Looking back, there are several remarks that can be made about the thermal analysis. For one, the external surfaces on which scientific instruments are mounted, have been neglected and assumed available for coatings. This was done incidentally to simplify the problem. However in reality this might have a significant influence on the analysis, especially if large areas of the spacecraft are covered by sensors. For future considerations it is thus recommended to take areas covered by sensors into account.

Furthermore, the analysis has been conducted assuming the spacecraft to be 1 isothermal node, thereby neglecting heat transfer between different surfaces or different equipment within the spacecraft. The reasoning behind the simplification was due to time constraints. Modelling more than 1 isothermal node would have consumed considerably more time with the setup in MATLAB. Nonetheless, modelling with multiple isothermal nodes would substantially increase the value of the results of the thermal analysis. It is therefore highly recommended for further investigation. Also in this case a dedicated software such as ThermXL from ESATAN-TMS is recommended for verification since it is able to model multiple nodes.

Lastly, it is worth noting that deployed solar panels or surfaces would reflect additional irradiation to the spacecraft bus. This would affect the heat transferred to the spacecraft Q_{in}. For future work, it would be interesting to investigate this effect.

<div align="right">

13

</div>

MATERIAL AND STRUCTURAL CHARACTERISTICS

Following the thermal stresses analysis, this Chapter discusses the material and structural characteristics of the CubeSats. In Section 13.1 the characteristics of a number of materials are given while in Section 13.2 a radiation dosage analysis in performed. Finally, in Section 13.3 the natural frequency and maximum von Mises stresses are calculated by means of a Finite Element Method and verified with a simplified analytical approach.

13.1. MATERIAL CHARACTERISTICS

Table 13.1 lists the properties of a number of materials that are used in the CubeSat. The 6U structure is made of Aluminum 7075-T6 which is a commonly used material for space applications. The PCBs are made of Fr-4 while copper is typically used for the wiring. Furthermore, the triple junction solar cells are made of Gallium arsenide.

Table 13.1: The properties of a number of materials used in the CubeSat.

Young's Modulus [GPa]
Yield strength [Mpa]
Poisson's ratio [-]
Thermal expansion coefficient [K^{-1}]
Density [kg/m^3]

13.2. RADIATION DOSAGE ANALYSIS

The complete set of side solar panels which will be made by ISIS is also going to be used as radiation shielding for the structure. These panels are made of an aluminum substrate and their total thickness is 2.5mm[1]. To get an indication on the radiation dosage during total operational time of the mission, the SHIELDOSE-2 model implemented in SPENVIS was used [2]. The analysis shows the dose-depth curves for different radiation sources. Currently the model allows the analysis to be performed with respect to pure aluminum finite slab shield which has a density of 2700kg/m^3. This implies that some accuracy is expected to be lost. Furthermore, cut-outs for the star tracker, propulsion nozzle and the payload are made on the surface of the side panels, meaning that the total dosage will be higher in reality. More information on the layout of the CubeSats can be found in Chapter 14.

In order to run the radiation models, the orbit generator program was used to define the orbital parameters. To simulate the deployment scenario, the mission was defined into 6 segments starting from the launch date, which was assumed to be in 2019. Each of the first 5 segments has a period of 30 days representing the time that the CubeSats will spend for the deployment, starting from the initial launch altitude of 530km as specified in Chapter 5 up to an altitude of 670km and back to the operational altitude of 520km which is at the last segment. The last segment has the period needed for the CubeSats

---

[1] https://www.isispace.nl/product/custom-solar-panels/ [cited 24-06-2017]
[2] https://www.spenvis.oma.be/ [cited 24-06-2017]

to complete the 5 year mission.

Once the orbit was defined, a number of radiation sources were considered. These are the following:

- **Trapped protons and electrons:** These particles which mainly originated from the solar wind, are captured by the magnetic field of Earth in the so called Van Allen radiation belts.

- **Bremsstrahlung:** This form of radiation is emitted when high energy particles suffer rapid deceleration in the vicinity of an atomic nucleus of the shielding material [111].

- **Solar protons:** As the name suggests this type of radiation originates from the Sun. These high energy particles might cause the formation of electron-hole pairs which in turn cause the performance of micro-electronics devices and solar cells to degrade [3].

SPENVIS allows the user to choose from a variety of radiation models. For the current analysis, the solar minimum models of trapped protons (AP-8) and electrons (AE-8) made by NASA's Space Science Data Coordinated Archive (NSSDCA) were used. The models are very popular for engineering applications since they are the only ones to completely cover the region of the radiation belts and also offer a wide range of energy for both protons and electrons[4]. In addition the ESP-PHYSIC long term particle model developed by NASA was added to the analysis in order to investigate the effect of the solar particles on the total dosage. The dose-depth curves for a range of aluminum thicknesses were then computed and shown in Figure 13.1.
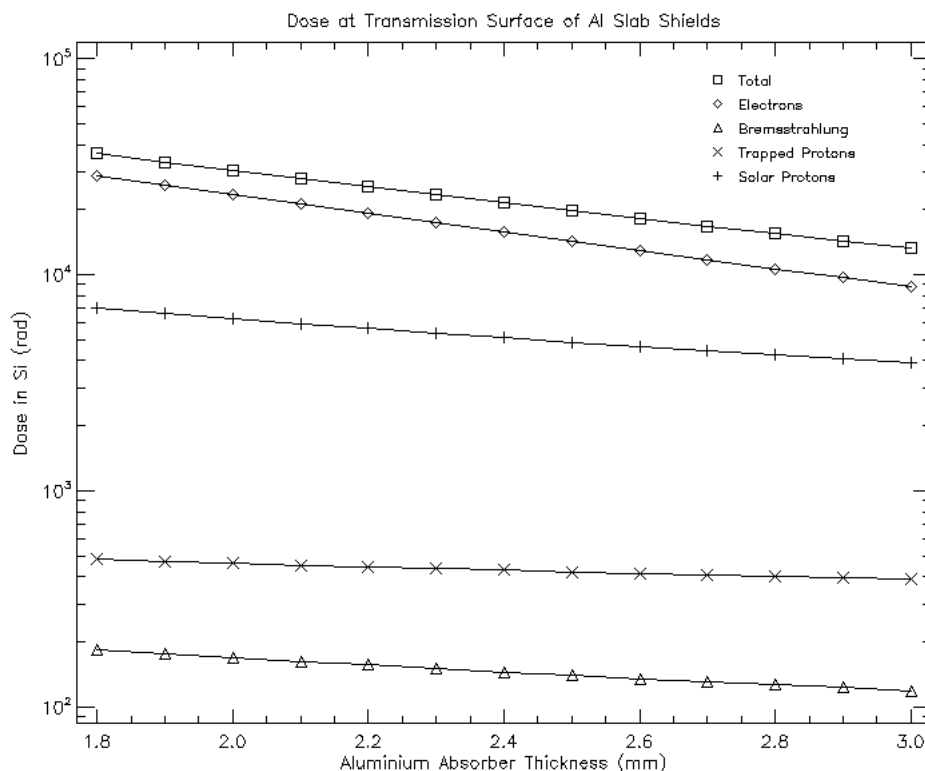
Figure 13.1: Dose-depth curve for a 520km circular orbit using SPENVIS.

According to the plot, with an aluminium thickness of 2.5mm the total dose of radiation is estimated to be 19krad. This result is then compared with the radiation requirements for a number of critical components of the CubeSat. Note that obtaining information on radiation requirements for all subsystems was not

---

[3] https://www.spenvis.oma.be/help/background/flare/flare.html#INTRO [cited 03-07-2017]

[4] https://www.spenvis.oma.be/help/background/traprad/traprad.html [cited 24-06-2017]

feasible because not all manufacturers provide the required data. Table 13.2 lists a number of critical components that are used, together with their dosage requirement. For the ISIS on-board computer, data on the dosage levels were not available and since it is a critical component a reference value obtained from the Hyperion CP400.85 processing platform was used.

Table 13.2: Allowable radiation for various subsystems.

Component	Dosage [krad]
On-board computer [103]	25
Electrical power system [5]	20
ADCS [96]	45
GPS receiver [6]	30

For the components that have data on maximum allowed radiation dosages, it can be concluded that they will meet the requirements on the total dose of radiation that will be experienced during the operational lifetime of the mission.

13.3. STRUCTURAL CHARACTERISTICS

The section discusses the method used to investigate the structural characteristics of the CubeSats. The loads experienced by the CubeSat are first derived and a finite element model is then tested according to the loads specified by the launcher. The results are then verified using an analytical approach.

13.3.1. ENVIRONMENTAL LOAD CASES

During the launch phase the CubeSats will experience various types of loads. The source of these loads mainly arises from the vibrations produced by the rocket engines, which propagate through the structure of the launcher and are transmitted to the CubeSats through the mechanical interface of their deployers. During lift-off the engines also produce high levels of acoustic noise and broadband random vibrations. These loads also arise during the interaction of the launch vehicle with the atmosphere during the transonic phase of the flight. Besides the vibro-acoustic loads the CubeSats also experience shock loads which emerge by the use of pyrotechnic devices for stage separation. Of course it can happen that the CubeSats are loaded simultaneously by a number of these loads and therefore it is critical to assess the ability of the structure to withstand the launch environment. Information about the loads that the CubeSats will have to withstand is generally provided by the launch vehicle user's manual [112].

QUASI STATIC LOADS

As more propellant is consumed during each stage of the launch, the axial acceleration of the rocket increases reaching a maximum value at the end of the burn. When the stage has reached burn-out, the acceleration drops and increases again when the next stage is ignited. The magnitude of these loads are given in terms of load factors by the launch vehicle providers. Rocket Lab's Electron launcher acceleration loads are given in Table 13.3 for each flight phase. It can be seen that the most load intensive phase is at the burn-out of the second stage. These loads will be used in Section 13.3.2 to perform the analysis of the structure.

SINE LOADING

The structure will also experience low frequency dynamic loading during the launch. These loads are typically in the range of a few Hz up to 20Hz [112]. To avoid amplification of these loads due to the resonance phenomenon, the CubeSat's fundamental frequencies for both modes of vibration (axial and lateral) need to be determined and compared with the minimum values provided by the launch vehicle manual. Rocket Lab currently does not provide frequency data for the Electron launcher, so reference values are used. Typical frequencies for a number of launchers are given in Table 13.4.

---

[5] https://gomspace.com/Shop/subsystems/power-supplies/nanopower-p60.aspx [cited 24 June 2017]
[6] http://www.skyfoxlabs.com/product/15-pinav-ng-gps [cited 24-06-2017]

Table 13.3: Rocket Lab's Electron flight acceleration loads [38].

Event	Axial [g]	Lateral [g]
Lift-off	+/- 0.2	+/- 0.9
Max q	+/- 2.0	+/- 0.9
Stage 1 Separation	+/- 5.3	+/- 0.7
Stage 2 Ignition	+/- 1.0	+/- 0.7
Fairing Separation	+/- 1.2	+/- 0.5
Stage 2 Burn-out	+/- 6.6	+/- 0.2
Stage 2 Apogee Kick	<5	+/- 0.2

Table 13.4: Spacecraft stiffness requirements for different launchers [113].

Launch Vehicle	In lateral direction	In axial (thrust) direction
Dnepr	>15 Hz	20 Hz - 45 Hz
Delta II 7320	>12 Hz	>35 Hz
H-IIA	>10 Hz	>30 Hz
PSLV	>18 Hz	>40 Hz
Soyuz BAI/KOU	>15 Hz	>35 Hz
Zenit 2 SLB	>6 Hz	>20 Hz

ACOUSTIC AND RANDOM VIBRATION LOADING

As mentioned earlier, the structure also experiences acoustic and random vibrations. One source of acoustic noise is the expansion of the gas in the nozzle and its interaction with the launch platform. Another source is the interaction of the vehicle with the atmosphere in the form of turbulence during the transonic phase. These loads also produce vibrations which extend from a range of low frequencies up to 10000Hz [114]. These vibrations have the characteristics of random signals and therefore are not possible to predict [113]. Nevertheless, launch vehicle providers define them in terms of a power spectral density profile for the launchers. Due to lack of data from Rocket Lab, a proper analysis for these types of loads is left for future work.

SHOCKS

Shocks are produced by mechanisms used to separate various stages, fairings and the CubeSat themselves. The mechanisms generate a very rapid transient load that can be characterised by acceleration loads in the order of few thousands g's and very high frequencies which are highly damped [113]. Due to their highly damped nature, shocks generally do not pose concerns for the primary structure of the CubeSat, but they can produce defects in more sensitive equipment such as relays and transformers. According to [113] analytical methods to demonstrate the ability of a structure to withstand shock loads are unreliable and the only approach is to perform tests. More information on the type of tests can be found in Chapter 17.

13.3.2. STRUCTURAL & VIBRATIONAL ANALYSIS

In this section the structural and vibrational analysis of the CubeSat structure is performed. The analysis consists of two parts. In the first part a finite element analysis is done with the CATIA V5 software. The maximum von Mises stress as well as the natural frequency is determined. This way it is determined whether the CubeSats can withstand the loads during the launch phase. In the second part the analysis is carried out analytically in order to verify the results obtained from the finite element method.

SELECTION OF COMMERCIAL OFF-THE-SHELF 6U STRUCTURE

A market research has been performed on the COTS available 6U structures. ISIS and Gomspace are the only companies based in Europe that provide these and their two structures have very similar characteristics. The ISIS structure has a mass of 1100g[7] while the Gomspace variant has a mass of 1060g [8]. Both of the structures have been used in past missions and both of them can easily be

---

[7]https://www.isispace.nl/product/6-unit-cubesat-structure/ [cited 24-06-2017]
[8]https://gomspace.com/Shop/subsystems/structures/6u-structure.aspx [cited 24-06-2017]

configured to fit subsystems from other companies. In terms of costs, ISIS gives a price range of 7,350€ to 7,850€ while prices from Gomspace are not available. Since both the products have similar characteristics , it is expected that they will not differ in price either. The selection is therefore based on the location of the company, such that the transportation time and costs are minimised. ISIS being Dutch and located in Delft is therefore chosen.

FINITE ELEMENT METHOD

For the finite element method a 6U ISIS CubeSat CAD structure is populated with all the components. The components are simplified but have the approximate same volume, the exact same mass and the approximate material characteristics as the real components. The components have been placed in locations as determined in Chapter 14. The 6U CubeSat CAD structure has the same dimensions as the structure sold by ISIS [24].

ASSUMPTIONS

- All components containing a PCB are assumed to consist entirely of the FR-4 material and to be isotropic, with the worst case characteristics as shown in Chapter 13.1.
- Due to BA0X batteries' FR-4 substrate, they are assumed to have the same characteristics as the PCBs.
- All sensors and antenna substrates are assumed to possess the material characteristics of an isotropic FR-4 material.
- The solar panels are assumed to have the material characteristics of Aluminium 7075-T6, since their substrate is made from aluminium [115]
- All components are fastened directly onto the 6U structure. Normally the PCBs are stacked on rods, which in turn are connected to the structure. The rods are thus neglected.
- The CubeSats are only clamped at one of the smaller sides to the launcher. They are assumed to be placed horizontally within the launcher. This is considered to be the worst case scenario. In reality the CubeSats will be much more constraint since they are within a dispenser within the launcher.
- Both CubeSat configuration will not differ significantly in their configuration since one sensor is exchanged for another with similar mass and material properties. Therefore only one configuration will be analysed, which is regarded as representative for both configurations (see Figure 13.2).

The fifth assumption is made due to the complexity of such an analysis. In the detailed design phase it is recommended to take the connection rods as shown in Figure 12.7 in Chapter 12 into account. During this design phase the main goal is to show that the 6U main structure can withstand the loads.

VON MISSES STRESS ANALYSIS

A linear tetrahedral mesh was used for the analysis of the CAD model. This is deemed to be sufficiently accurate, since the margin between the yield strength of the materials and the von Mises stresses acting on the CubeSat, is expected to be very large. A parabolic mesh was also used to verify this method and the estimated error for the linear tetrahedral mesh is analysed. The mesh size is adapted to accurately fit the shape and contours of each component of the CubeSat model such that a high overall accuracy is obtained.

The launch phase of the stage 2 burn-out (see Table 13.3) has been identified as the most load intensive. This result was established by calculating the von Mises stresses in a simplified analytical model for each launch phase. This model is later also used to verify the results of the finite elements method. The overall mass of the model, including the solar panels (which are hidden in Figure 13.3 for illustrative purposes) is 8.7kg. To include the design margins for the mass, the acceleration loads are adapted. Since the actual CubeSats are expected to have a mass of 12kg after including cables, bolts and unforeseen additional components, the acceleration loads were increased proportionally. This can be done since force equals mass times acceleration (F = ma). The loads applied to the model are shown in the last row of Table 13.5.

The axial acceleration is applied across the shortest length of the CubeSat (in Figure 13.2 this is in y direction). This is done since the second area moment of inertia in that direction is the smallest
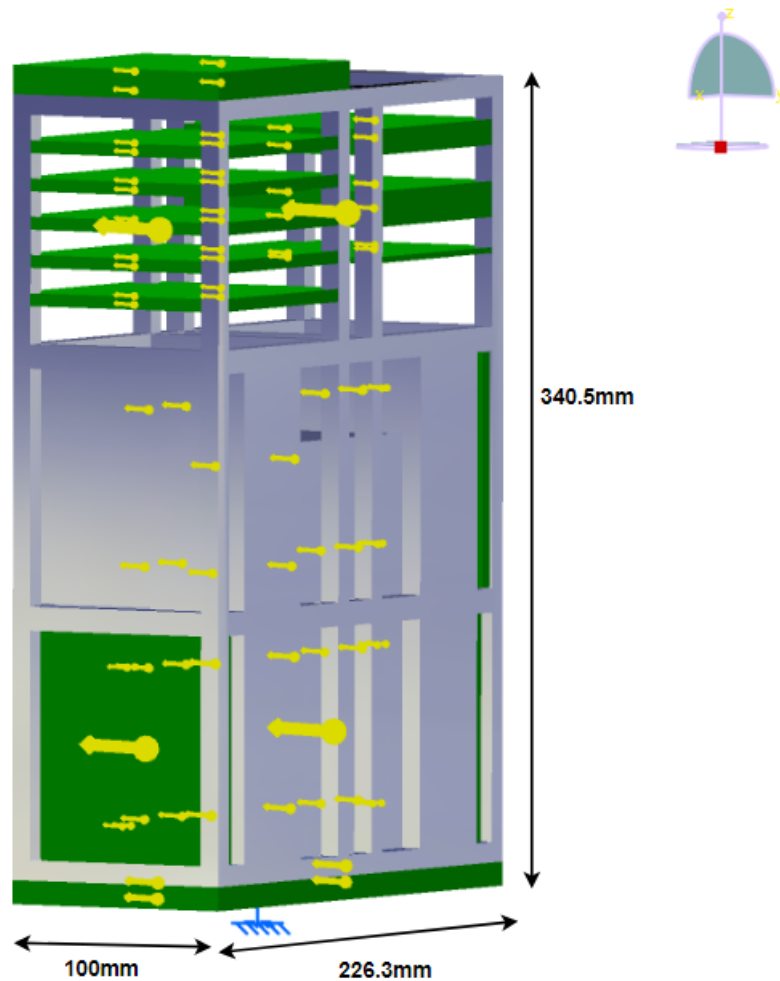
Figure 13.2: CAD model for FEM analysis. The FR-4 material is displayed in green, the rest is Aluminum 7075-T6. The solar panels are not displayed for illustrative purposes.

Table 13.5: Acceleration loads on CubeSat including the safety factor as well as an adaptation for the difference in final mass from 8.7kg of the model to 12kg

	Axial [m/s^2]([g])	Lateral [m/s^2]([g])
Electron's stage 2 burnout loads	+/-64.75 (6.6)	+/-1.96 (0.2)
Including safety factor of 1.5	+/-97.12 (9.9)	+/-2.94 (0.3)
Adapted for expected 12kg mass	+/-133.96 (13.7)	+/-4.06 (0.41)

and thus the stresses there will be the highest. The lateral acceleration is applied along the z-axis of the CubeSat. Figure 13.3 shows the results for the stage 2 burn-out phase. It can be seen that the maximum Von Mises stress is 1.9 MPa, which is far below the yield stress of the Aluminum 7075-T6 and FR-4 materials, as shown in Section 13.1. The estimated precision of the analysis was also computed. The magnitude for the estimated local error is 10^{-7}. Considering the already low stresses experienced this is very acceptable.

NATURAL FREQUENCY ANALYSIS

The natural frequency of the CubeSats is calculated with a frequency analysis with the same mesh as for the Von Misses stress analysis. For the analysis 10 modes are used. In Figure 13.4 it can be seen that the maximum stresses occur at around 709Hz. The stresses occurring at this frequency are well
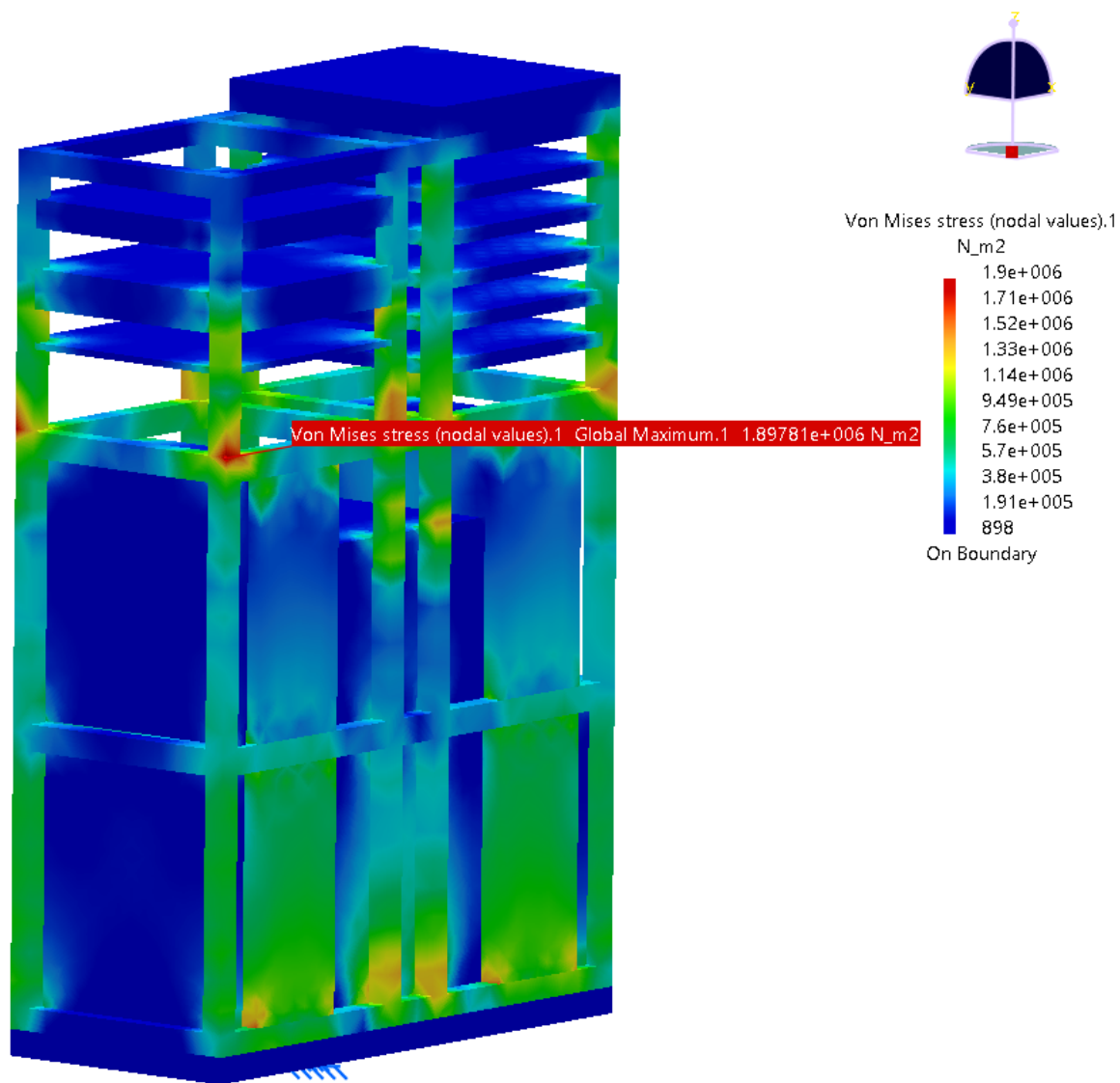
Figure 13.3: Von Mises stress for the stage to burnout loads of Rocket Lab's Electron

beyond the yield stresses of the materials used. But since the minimum natural frequencies required by the launchers shown in Table 13.4 are well below the natural frequency of 709Hz, the stresses shown in Figure 13.4 will not be experienced by the CubeSats.

13.3.3. VERIFICATION THROUGH ANALYTICAL METHOD

ASSUMPTIONS

In order to propose an analytical model certain assumptions need to be made. These assumptions will cause the model to deviate from real life values but they will reduce the complexity of the problem. The assumptions made are the following:

- The CubeSat structure is modelled as a hollow beam. Normally the structure is more complicated with several cut-out and thickness variations.

- The mass of the beam is equal to the maximum allowable mass for the CubeSat design specifications equal to 12kg [116]. This means that the acceleration loads that the structure will have to withstand are going to be higher, representing the worst case scenario in terms of loading.
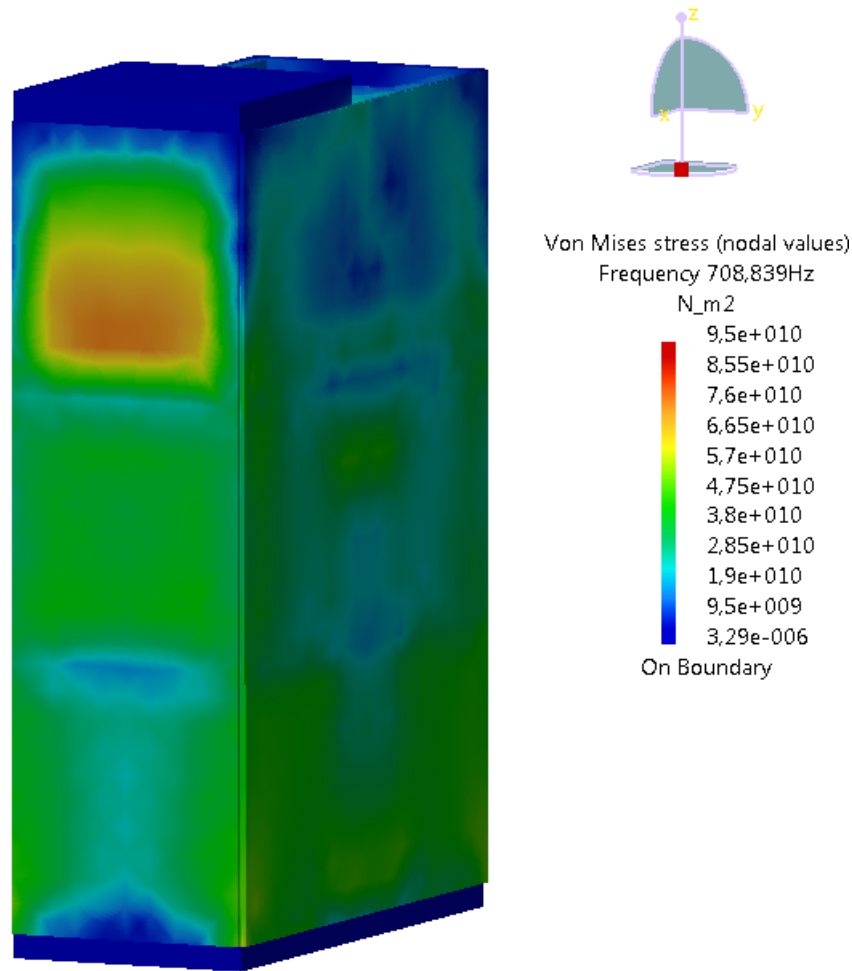
Figure 13.4: Frequency analysis

- The acceleration loads are modelled as point loads which act through the centre of gravity of the structure [108]. In real life this might not be the case. These loads can be distributed along the structure so that all structural members are loaded. For the current analysis this implies that only a section of the beam is going to be loaded.

- The contact area of the CubeSats' rails is adjusted to the thickness of the modelled beam.

- The thickness of the beam accounts for the surface area of the rails and the side panel thickness.

CROSS SECTIONAL PROPERTIES

The cross section of the beam is shown in Figure 13.5. Due to symmetry about both x and y-axis, the centroid is located at centre of the cross section. Recalling the assumption fifth assumption from above, the thickness of the structure was adjusted so that it accounts for both the surface area of the rails and the thickness side solar panel which has a thickness of 2.5mm. The original structure consists of 4 rails which are in contact with the deployer during launch. Their surface dimensions are [8.5mm x 8.5mm] so that their total area is equal to $2.89 \cdot 10^{-4} m^2$. The width (w) and height (h) of the beam are 226.3mm and 100mm respectively. The total thickness is therefore approximated to be equal to 2.95mm.

The moments of inertia of the cross section are calculated using Equations 13.1 and 13.2 respectively. Due to symmetry, I_{xy} is neglected.

$$I_{xx} = \int y^2 dA = \frac{1}{12} w h^3 - \frac{1}{12}(w-2t)(h-2t)^3 = 3.551 \cdot 10^{-6} m^{-4} \tag{13.1}$$
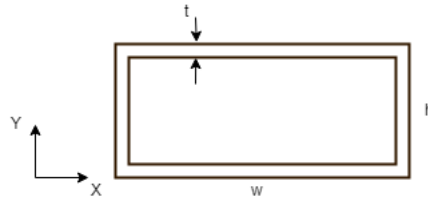
Figure 13.5: The cross section of the beam.

$$I_{yy} = \int x^2 \, dA = \frac{1}{12} hw^3 - \frac{1}{12}(h-2t)(w-2t)^3 = 1.261 \cdot 10^{-5} \, m^{-4} \tag{13.2}$$

CRITICAL BUCKLING LOAD

Now the properties of the cross section have been identified, the next step of the analysis involves finding the load at which the structure will buckle. The critical buckling load, P_{cr} is given by Equation 13.3, where E is the Young's modulus of the material, I is the moment of inertia of the cross section and L^* is the effective length of the beam.

$$P_{cr} = \frac{\pi^2 E I}{(L^*)^2} \tag{13.3}$$

Beams buckle about the axis with the lowest moment of inertia so I_{xx} is taken in this case. Furthermore, since the beam is clamped in on and free to move in the other end the effective length is equal to 2L [39]. The total length of the structure is equal to 340.5mm. Using assumption **AS-STR-03**, the axial load is acted at the centre of gravity of the structure, therefore L is equal to 170.25mm. Therefore the critical buckling load for the beam is calculated to be equal to $21.6 \cdot 10^6 N$ a much larger load than the maximum axial force of 1165N acted during the second stage burn out.

MOMENT AND DISPLACEMENT

Figure 13.6 shows how the acceleration loads are assumed to be acted on the beam. It is evident that the lateral force will cause the beam to deflect by producing a moment along the z-direction. This moment will be maximum at the root of the beam while the deflection will be maximum at the tip. The deflection of the beam can be determined using Equation 13.4 which is derived from the well known moment-curvature relationship [109].
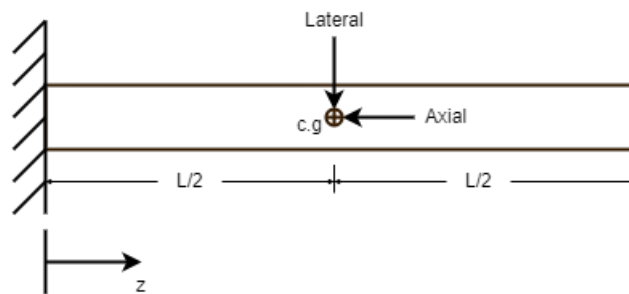
Figure 13.6: The acceleration loads acted on the beam.

$$\frac{d^2 v}{dz^2} = -\frac{M}{EI} \tag{13.4}$$

Where the moment distribution is given by Equation 13.5:

$$M(z) = \begin{cases} P(\frac{L}{2} - z), & \text{for } 0 \leqslant z \leqslant \frac{L}{2} \\ 0, & \text{for } \frac{L}{2} \leqslant z \leqslant L \end{cases} \tag{13.5}$$

In order to find an expression for the deflection of the beam the following derivation is used. For $0 \leq z \leq \frac{L}{2}$, Equation 13.4 is integrated twice:

$$-EI\frac{dv}{dz} = \frac{PLz}{2} - \frac{Pz^2}{2} + C_1$$

Where $\frac{dv}{dz} = 0$ at $z = 0$ so that $C_1 = 0$,

$$-EIv = \frac{PLz^2}{4} - \frac{Pz^3}{6} + C_2$$

Where $v = 0$ at $z = 0$ so that $C_2 = 0$ and therefore:

$$v = -\frac{Pz^2}{EI}\left(\frac{L}{4} - \frac{z}{6}\right) = -\frac{Pz^2}{12EI}(3L - 2z)$$

For $\frac{L}{2} \leq z \leq L$, the following expression is used:

$$v = v\,|_{\frac{L}{2}} + \theta\,|_{\frac{L}{2}}\frac{L}{2}$$

Where $\theta = \frac{dv}{dz}$ and is the slope of the beam. It follows then,

$$v = \frac{PL^3}{12EI} + \frac{dv}{dz}\,|_{\frac{L}{2}}\frac{L}{2} = \frac{PL^3}{12EI} + \frac{6Pz}{12EI}(L - z)\,|_{\frac{L}{2}}\frac{L}{2}$$

Which reduces to Equation 13.6:

$$v = -\frac{PL^2}{48EI}(6z - L) \tag{13.6}$$

According to Table 13.3, the most load intensive phases of the launch are during the separation of the first stage and the burn-out of the second stage. The maximum bending moments and deflections of the beam at these load cases are given in Table 13.6. It can be seen that the assumed model can well withstand the lateral loads in both of the load cases. For the calculation of the load a safety factor of 1.5 was also considered. Safety factors are typically given to describe the structural capacity of a system beyond the applied load in order to increase its reliability [108].

The maximum stress due to bending is then calculated using Equation 13.7 where y_{max} is the distance furthest away from the the neutral axis.

$$\sigma_{z,max} = -\frac{My_{max}}{I_{xx}} \tag{13.7}$$

Table 13.6: The maximum bending moment and thus bending stress occurs at the root of the beam while the maximum deflection occurs at the tip.

Launch phase	Bending moment [Nm]	Deflection [m]	Bending stress [MPa]
Stage 1 Separation	-159.33	$-1.51 \cdot 10^{-5}$	+/- 2.2
Stage 2 Burn-out	-198.41	$-1.88 \cdot 10^{-5}$	+/- 2.8

SHEAR

The lateral load also induces shear stresses along the beam. These stresses will have a constant value form the root of the beam till the centre of gravity where the load is applied. To determine the shear stresses the shear flows in the cross section need to be found. To do so, a cut is first made as shown in Figure 13.7 in order to determine the basic shear flow of the open section. The basic shear flow is given by Equation 13.8 where subscript i denotes the section in the cross section under consideration.
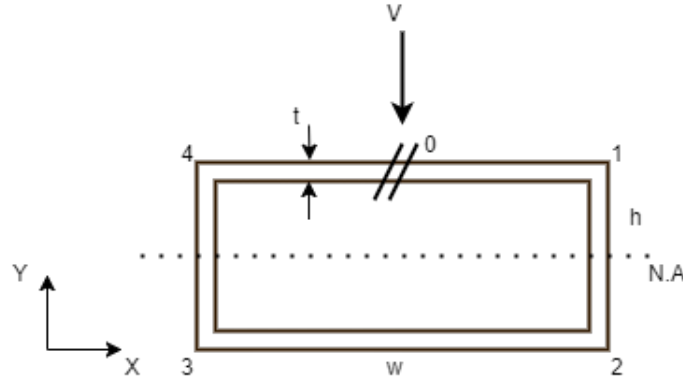
Figure 13.7: The cross section of the beam shown where the cut has been made for the calculation of the basic shear flows.

$$q_{b_i} = -\frac{V}{I_{xx}} \int_0^s y \, ds \tag{13.8}$$

The cut is then closed and the constant shear flow $q_{s,0}$ is determined using moment equivalence as shown in Equation 13.9. The moment centre is placed on point 0 which coincides with the line of action of the lateral load. p is the moment arm and A represents the enclosed area. The total shear flow is then the sum of the basic shear flow and the constant shear flow, Equation 13.10. The shear stress can is found using Equation 13.11 [110].

$$0 = \oint p q_{b_i} \, ds + 2 A q_{s,0} \tag{13.9}$$

$$q_{s_i} = q_{b_i} + q_{s,0} \tag{13.10}$$

$$\tau_i = \frac{q_{s_i}}{t} \tag{13.11}$$

VON MISSES STRESSES

The bending and normal stresses are combined using the Von Misses stress formula (Equation 13.12) to determine the yield stress of the beam [110]. For failure not to occur, the yield stress needs to be lower than the yield stress of the material.

$$Y = \sqrt{\frac{1}{2}\left[(\sigma_x - \sigma_y)^2 + (\sigma_y - \sigma_z)^2 + (\sigma_z - \sigma_x)^2\right] + 3\tau_{xy}^2 + 3\tau_{yz}^2 + 3\tau_{xz}^2} = \sqrt{\sigma_z^2 + 3\tau_{xy}^2} \approx 716 kPa \tag{13.12}$$

NATURAL FREQUENCY

To calculate the natural frequencies in both the axial and lateral directions of the beam, Equations 13.13 and 13.14 obtained from SMAD were used [39]. The results are given in Table 13.7.

$$f_{nat,lateral} = 0.560\sqrt{\frac{EI}{mL^3}} \tag{13.13}$$

$$f_{nat,axial} = 0.250\sqrt{\frac{AE}{mL}} \tag{13.14}$$

Table 13.7: The natural frequencies of the beam

	Axial beam	Lateral beam
Natural frequency [Hz]	502.7	1762.5

STRESS ANALYSIS OF FASTENERS AND BOLTS

As the smallest structural member of the CubeSat structure a bolt will be analysed for the found maximum von Mises stress of 4.8MPa from Section 13.3.3, since this is the highest stress calculated from both approaches. The bolt diameter connecting the CubeSat structural elements is found to be 2.5mm by inspecting the ISIS CAD model [24]. It will be assumed that an Aluminium 7075-T6 bolt is used. This way the materials of the structure and the bolt are the same and additional thermal stresses and thus fatigue stresses are avoided during the orbital lifetime. To assume the worst case scenario, the bolts

will be analysed in shear. According to the Tresca criterion [117] the bolts will be able to carry 0.5 times the tensile yield strength when loaded in shear. Since the tensile yield strength of Aluminium 7075-T6 is 503MPa the shear yield strength is approximated to be 251.5MPa, which is still far above the 5MPa experienced during launch.

As a second analysis a finite element analysis was done on a single bolt with the dimensions as derived from the ISIS Cad model [24]. The length of the bolt was found to be 10mm. This allows for a 5mm nut to fasten the bolt. For the finite element analysis it is assumed that the 5MPa von Mises stress acts purely in uni-lateral direction through the bolt. The affected cross sectional area of the bolt times this stress yields the applied force of 98.17N. Since this force is applied as a pure shear force and the bolt is assumed to be clamped at both ends, this is considered to be the worst case scenario. The result is presented in Figure 13.8. As can be seen, the highest von Mises stress experienced within the bolt lies far below the Aluminium 7075-T6 yield stress of 503MPa.
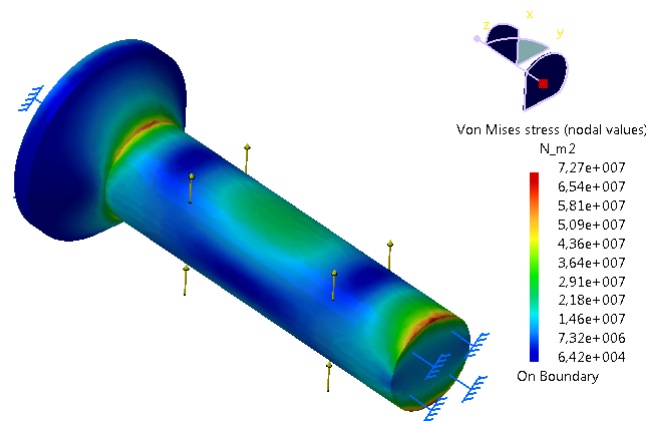
Figure 13.8: Analysis of bolt in shear

13.3.4. DISCUSSION

Both the analytical and the finite element approach predict much lower stresses than the yield stresses of the structural materials used in the CubeSats. Both predicted natural frequencies which are much higher than the frequencies of the launchers. Yet there are significant differences between the two approaches.

The finite element method predicts a maximum of 1.9MPa. The analytical method predicts a maximum of approximately 5MPa as well at the clamped end. The order of magnitude is the same, the actual difference between the two values is more than 50%. This difference is attributed to a difference in area moment of inertia between the two models. The CAD model has a higher area moment of inertia, due to the relatively large components placed on the inside of the model. The analytical model assumes a continuous thickness of 2.95mm of a hollow beam. This thickness does not simulate the area moment of inertia accurately. Nonetheless the results are satisfying since the order of magnitude as well as a large margin are predicted by both models. The natural frequency foreseen by the finite element method is 709 Hz, whereas the natural frequency of the analytical model is 500.8Hz. This difference of about 200Hz can also be explained in terms of the differences in the moment of inertia. Since the hollow beam has a lower moment of inertia than the finite element method, its natural frequency will also be lower.

The large margin of a factor of about 100 between actually experienced stresses and the yield stresses can be explained by the fact that COTS components are used. The structure itself withstands the loads applied to it, but when adding components in the interior the area moments of inertia increase a lot. Also, high safety factors are used for CubeSats. If a CubeSat were to cause the failure of an entire launch as a secondary load, that could jeopardise future launch opportunities or make launch companies reluctant to accept CubeSats as secondary payload.

An important factor that was not taken into account in the analytical model is the material of the PCBs. The FR-4 material has a much lower Young's modulus than the Aluminium 7075-T6 (21GPA versus 71.7GPa), which is the only material used in the analytical model making the model less reliable. The natural frequency is dependent on the assumed spring stiffness, which in turn is dependent on the elasticity of the materials. There is of course a much more complex interaction between cross sectional area, length and Young's modulus of the CubeSat and its different components, but the above explanation still holds to explain the principle behaviour of the two models. Overall both models predict a much higher natural frequency of the CubeSats than is required by the launchers. With this comfortable margin it can safely be assumed that the CubeSats' natural frequency will never be excited during the launch phase.

Acoustic loads and random vibrations as well as the frequencies generated by the propulsion system shall be analysed but due to lack of data from both Rocketlab and Hyperion Technologies the analysis could not be performed and shall be done in the future. The analysis can be validated by performing structural tests as described in Chapter 17. Finally, on a later design stage a thermal fatigue analysis should be conducted to investigate the number of cycles the structure can withstand at the environmental thermal stresses.

<div align="right">

14

</div>

<div align="center">

CONFIGURATION AND LAY-OUT

</div>

In this chapter the layout of the different subsystems in both of the CubeSats configuration will be shown. As explained in Chapter 7, the mission consists of two types of configurations. The only difference arises form the use of one different payload. More specifically, the EPIC-A configuration has the INMS instrument while the EPIC-B configuration has a RPA instead. The rest of the subsystems are exactly the same, but their configuration within the structure will slightly change for the EPIC-B configuration in order to fit the larger RPA instrument. This is discussed further in Section 14.2. Isometric representations for the EPIC-A and EPIC-B configuration are given in Figures 14.1 and 14.2 respectively. The coordinate system used throughout the chapter complies with the system specified in the 6U design specification document [116]. Sections 14.1 and 14.2 discuss the different configurations while in Section 14.3 a draft drawing is presented. Lastly, during the configuration design, the volume regulations of the dispenser (Figure 14.5) are taken into account [116].
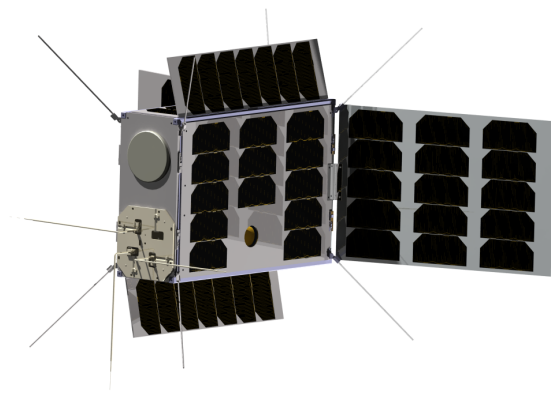
Figure 14.1: Isometric view of EPIC-A
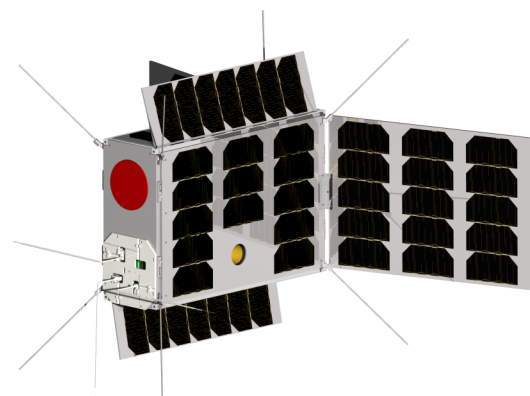
Figure 14.2: Isometric view of EPIC-B

When looking the outside envelope the only difference between the two configurations is the use of a different payload on the upper side of the +Z surface. To avoid confusion between the two, a red surface is given for the retarding potential analyser. The INMS, Langmuir probe and RPA are placed on the ram facing side of the CubeSat in order to generate more reliable data. For both configurations, three types of antennas can be identified. These are three Langmuir probe antennas, four E-field antennas and four UHF antennas as shown in Figures 14.1 and 14.2.

14.1. INNER LAY-OUT OF EPIC A

The inner lay-out of the EPIC-A is depicted in Figure 14.3. The components that are visible from this view, are given numbers and are identified in Table 14.1. The PCBs are first stacked together and the 4 rods (not visible) of the 6U structure are used to constrain them. The propulsion system is place in the middle towards the -Z surface such that the line of action of the thrust force coincides with the centre of gravity of the structure. Furthermore, a small opening has been made on the back-face cover for the gases expelled by the nozzle. To symmetrically distribute the weight of the propellant the two extra propellant tanks (no. 12 and 14) are placed on either side of the thruster. The only available space left in the structure is the space currently occupied by the ADCS and the electric sensor. The ADCS being

heavier, was placed near to the centre of mass of the CubeSat and the electric sensor (no. 5) was then mounted on the remaining space available. As discussed in Chapter 7, the magnetometer is affected by noise from the S/C electronics and for optimal measurements the sensor needs to be mounted away from the electronics. A boom deployment mechanism would be difficult to implement since that would affect the power generation of the side solar panel and therefore a different approach was implemented. The magnetometer is mounted on the outer region of the -Y surface big solar panel as shown in Figure 14.6. In order to accommodate the instrument during stowed configuration, a cavity was made which has the same dimensions as the instrument. The available space left in the CubeSat is approximately equal to 0.8U.
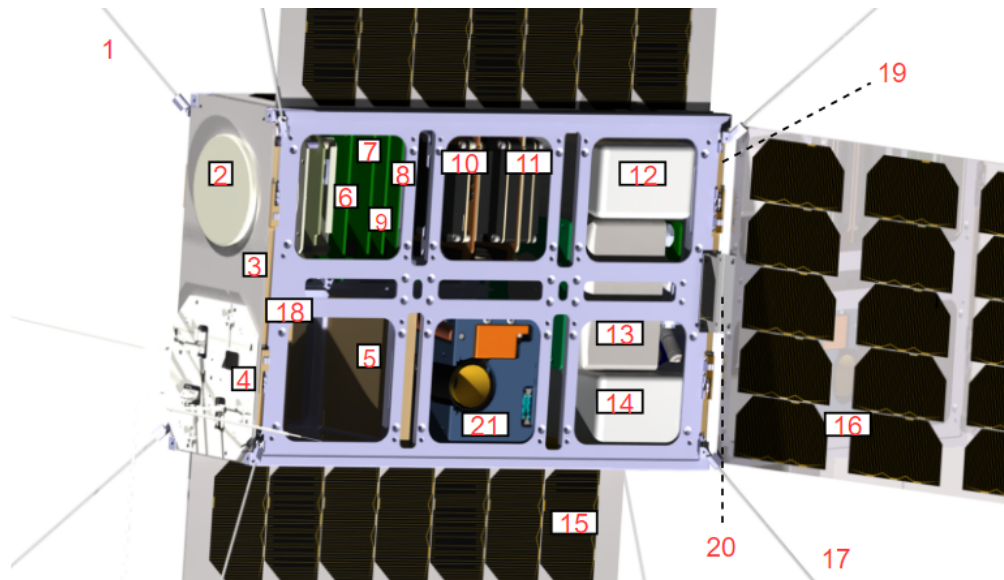
Figure 14.3: The subsystem lay-out in EPIC-A

Table 14.1: List of components shown in Figure 14.3

Number	Component	Number	Component
1	Electric sensor antennas	12	Extra propulsion tank
2	INMS	13	Hyperion propulsion system
3	Langmuir probe	14	Extra propulsion tank
4	Front-face cover	15	Side-solar panel assembly
5	Electric sensor	16	Big-solar panel assembly
6	GPS receiver PCB	17	UHF antenna
7	Docimeter PCB	18	ISIS 6U structure
8	ISIS On-board computer	19	Back-face cover
9	ISIS On-board computer	20	Big-solar panel hinge
10	Gomspace EPS	21	Hyperion ADCS
11	Communication subsystem (3x S-band receivers, 1x UHF receiver)		

14.2. INNER LAY-OUT OF EPIC B

The inner lay-out of the EPIC-B is depicted in Figure 14.4. The lay-out is very similar to the one in Figure 14.3 with the only difference being the configuration of the GPS receiver, the Dosimeter and the two on-board computers. Due to the large size of the RPA (no. 1), it was decided to place the four PCB plates (no. 2) between the Langmuir probe and the E-field probe. Again the set of PCBs are stacked together and constrained using the four rods on that location of the 6U structure. The configuration of the remaining components has stayed the same resulting in a volume of 0.3U that is left available.

Figure 14.6 shows the inner lay-out of the EPIC-B but now from a different view. The components, including numbering, are listed in Table 14.2.
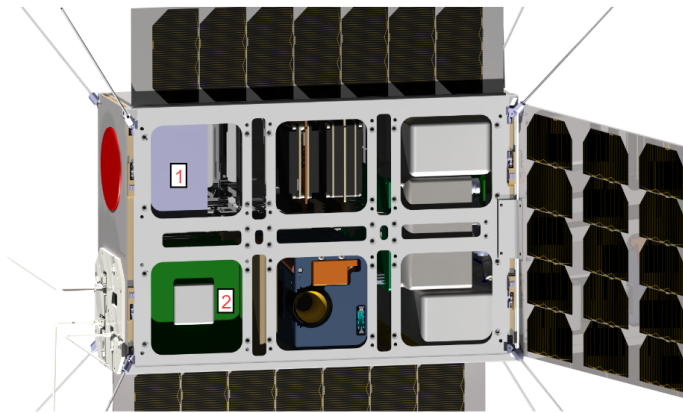
Figure 14.4: The lay-out of the subsystems in the EPIC-B configuration.
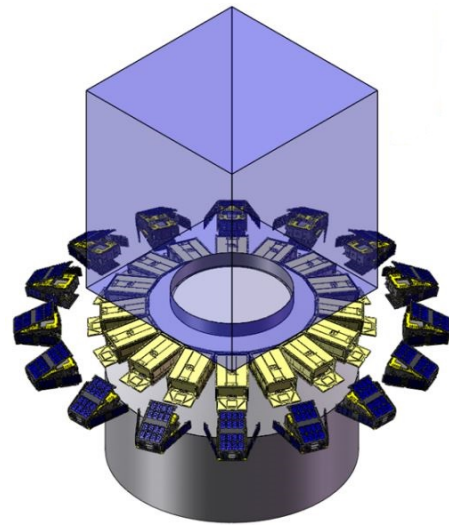
Figure 14.5: Configuration of dispensers for 16 CubeSats
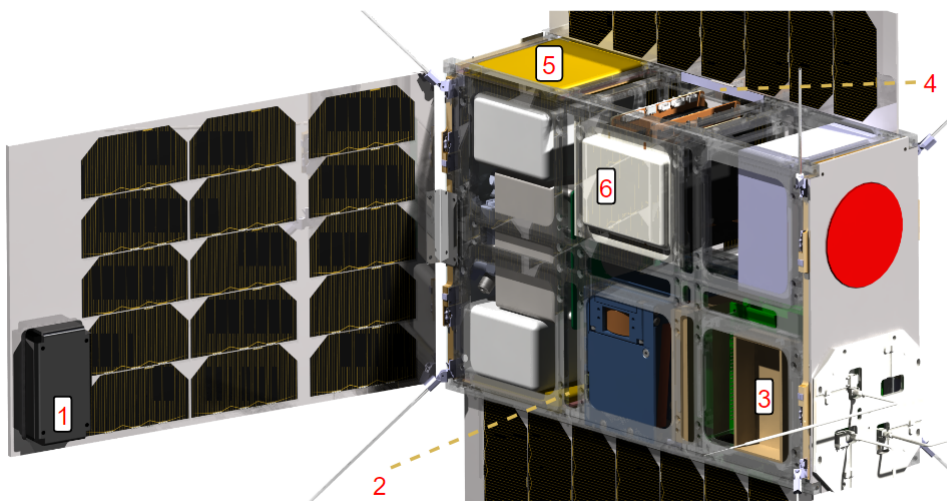
Figure 14.6: The lay-out of the subsystems in the EPIC-B configuration.

Table 14.2: List of components shown in Figure 14.6.

Number	Component	Number	Component
1	Magnetometer	4	Side panel hinge
2	Battery pack	5	Battery pack
3	Magnetometer cavity	6	S-band patch antenna

14.3. DRAFT DRAWINGS

+Z surface view
Scale: 1:1

+Y surface view
Scale: 1:1

77.31

40

213.7

732.02

71

321.6

226.3

383.73

340.5

4.63

30

TECHNICAL RISK MANAGEMENT

Risk management is the process of forecasting and evaluating risks and their root causes, together with mitigating or avoiding their impact [118]. Risk assessment improves the chance of mission success and as such, is a vital aspect in the design of any spacecraft mission. Firstly, critical subsystems are identified (Section 15.1). Then the risks and their causes are identified and described. Next, they are categorised according to the likelihood of occurrence and criticality of consequences (Section 15.2). The risks are then visualised based on these categories in a risk map. Finally, risk mitigation strategies are applied and a new risk map is presented (Section 15.3).

15.1. CRITICAL SUBSYSTEMS IDENTIFICATION

The first step to the technical risk management is identifying the risks on subsystem level. The subsystems which are prone to failure are identified by analysing the historical failure data of S/C. Different failure datasets have been analysed by a number of authors on a subsystem level. Figure 15.1 depicts the contributions of subsystems to the satellite failures. Three primary contributors have been identified: the EPS, the on-board computer (OBC) and the communications system (including antennas) (COM). Another survey conducted by [119] indicates the communication systems (49%) as a major contributor, followed by the electrical power subsystem (19%) and the on-board computer (7%). A large amount of the root causes in both surveys could not be identified and were allocated to the "unknown" category.
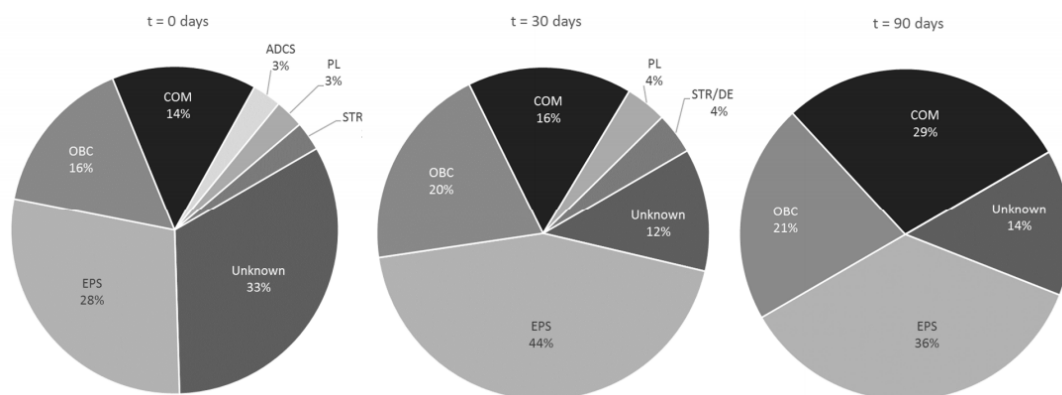
Figure 15.1: Subsystem contributions to CubeSat failure after ejection (including DOA) [120].

The critical subsystems, according to historical data, are the on-board computer, the electrical power system and communications. The following mission risk categories have been defined: command & data handling (C&DH), EPS and telemetry, tracking and command (TT&C)/GN&C. These must be analysed with care for optimal risk identification and mitigation. Other mission risk categories include payload, structure and propulsion.

15.2. SUBSYSTEM RISK ASSESSMENT

The following sections focus on an in depth risk analysis for the following mission risk categories: C&DH, EPS and TT&C/GN&C, payload, structure and propulsion. The failure modes are given in Table 15.1. In this table the mission risk category, failure modes and their respective root cause is given. The risks are also labelled by an identification number (ID) for further reference. Next, each risk is categorised with

respect to its probability of occurrence and criticality. The likelihood, or probability of occurrence of a risk, is categorised according to Table 15.2. At this stage it is not possible to assign a discrete probability to each risk. Thus an educated guess is made about which level is most appropriate. The criticality of the risks is divided into the following levels: negligible, minor, significant, critical and catastrophic. Moreover, the analysis does not account for all the possible risks. Table 15.1 shows a number of possible risks and has identified one of the many possible root causes per failure mode.

Table 15.1: Subsystem risk identification and ranking

Category	ID	Failure mode	Root cause	Likelihood	Criticality
C&DH	1	Software does not fulfill its purpose	Memory management errors	Near certainty	Critical
	2	Bit-flip occurence	Cosmic radiation	Highly likely	Critical
	3	Data cannot be stored to the SD card	SD card degradation due to radiation	Likely	Significant
EPS	4	Solar array cannot perform anymore	Short or open circuit failure	Highly likely	Catastrophic
	5	Damaged battery cannot store energy anymore	High charge voltage, degradation	Highly likely	Catastrophic
	6	Power distribution does not provide energy to sub-components	Electrostatic discharge, degradation of cables	Likely	Catastrophic
TT&C/GN&C	7	During manoeuvring or orbit maintenance critical loads are reached	Wrong commands cause S/C to overload (human error)	Low likelihood	Significant
	8	Spacecraft loses orientation temporarily	Geomagentic storm interference	Low likelihood	Minor
	9	Antenna was unable to deploy	Deployment damaged during launch	Highly likely	Critical
Payload	10	Magnetometer unable to retreive accurate data	Electromagnetic interference with other components	Likely	Critical
	11	Booms of the electrical field sensor do not deploy	Deployment mechanism failure	Likely	Significant
	12	The sensors prove to have a low scientific yield	Earthquake prediction not well understood	Likely	Critical
Structural	13	Damaged mechanical structure	Collision of space debris	Low likelihood	Critical
	14	Degradation of solar panels or coating	Long exposure to radiation	Highly likely	Critical
	15	Excitation of eigenmotions during launch	Acoustic waves, vibrations	Likely	Catastrophic
	16	Deployment mechanism does not work	Hinges get stuck	Likely	Critical
Propulsion	17	Propulsion system explodes and entire spacecraft is lost	High levels of oxygen density are reached within the fuel tank	Low likelihood	Catastrophic

Table 15.2: Likelihood criteria for risk ranking.

Likelihood level	Probability of occurrence [-]
Near certainty	0.8-1.0
Highly likely	0.6-0.8
Likely	0.4-0.6
Low likelihood	0.2-0.4
Not likely	0.0-0.2

15.3. RISK MAP AND RISK MITIGATION

Using Table 15.1, the risks are visually represented in a risk map as can be seen in Figure 15.2. Risk levels have been identified and assigned to each risk based on the likelihood and criticality. A four level risk ranking has been established from low, moderate, high to extreme. Low level risks would require little to no mitigation measures. Other risk levels will be assigned the appropriate measures in order to reduce the risk magnitude.

Figure 15.2: Risk map before mitigation

In order to mitigate the mission risks one of the following mitigation techniques may be applied [118]:

1. Avoid risk by eliminating root cause and/or consequence.

2. Control the cause or consequence.

3. Transfer the risk to a different party or project.

4. Assume the risk and continue in development.

The best way is to mitigate the risk is through eliminating the root cause. If this is not possible, one should try to control the consequence. For this project no risk transfer to different parties or projects is considered. Lastly, if nothing else is possible, one would have to accept the risk and continue. The following measures have been applied to mitigate the mission risks:

1. Software does not fulfil its purpose: include a watchdog timer to restart the system. Have a safe mode in case of repeated crashes to wait for uplinking of updated software.

2. Bit-flip occurrence: apply redundant coding (copies of bits) and error-detecting code.

3. Data cannot be stored to the SD card: add a second SD card.

4. Solar array cannot perform anymore: test for manufacturing flaws (for short circuits) on the ground, and add redundant strings on cell level (for open circuits).

5. Damaged battery cannot store energy anymore: ensure that extensive testing is done on the ground and add a redundant battery in case the primary battery fails during operation.

6. Power distribution does not provide energy to subcomponents: apply radiation shielding and extensive testing on ground.

7. During manoeuvring or orbit maintenance critical loads are reached: ensure that experienced staff send commands to the satellites, add an inertial measurement unit.

8. Spacecraft loses orientation: the risk level is very low, thus no to small measures are required. Geomagnetic storms are temporary and commands from ground controllers can adjust the course of the satellite if necessary.

9. Antenna was unable to deploy: check for manufacturing flaws and apply extensive testing on ground.

10. Magnetometer unable to retrieve accurate data: testing on ground and adjusting the distance between the relevant components, turn off other components when the magnetometer is on.

11. Booms of the electrical field sensor do not deploy: use deployment mechanisms which have been extensively tested or proven reliable in the space environment.

12. The sensors prove to have a low scientific yield: have as many as possible flight proven sensors which were used on previous earthquake precursor missions.

13. Damaged mechanical structure: apply redundancy concept to constellation so mission may continue.

14. Degradation of solar panels or coating : apply the redundancy concept to the constellation (adding spare satellites), use the appropriate coating for the desired spacecraft lifetime.

15. Excitation of eigenmotions during launch: failure of materials during launch can be mitigated by getting materials from certified suppliers (minimise residual stresses, meeting required tolerances). Use simulations of launch loads and vibrations.

16. Deployment mechanism does not work: extensive testing on ground.

17. Propulsion system explodes and entire spacecraft is lost: design for a larger fuel tank, by applying a safety factor, to avoid dangerous oxygen density levels.

Figure 15.3 shows the risk map after the implementation of mitigation measures. Applying the measures reduced the risk levels significantly. There are no extreme risk levels. However, careful care should be taken into the remaining risks. If an event of catastrophic level occures, the satellite is immediately lost. This risk is then accepted. Redundancy is applied throughout the constellation for optimal availability, which is discussed in Chapter 16.

	green	yellow	orange	red
	Low	Moderate	High	Extreme

Likelihood		Negligible	Minor	Significant	Critical	Catastrophic
	Near certainty	yellow	orange	orange	red	red
	Highly likely	green	yellow	orange	red	red
	Likely	green	yellow	3	orange	5	orange	red
	Low likelihood	green	green	8, 13	yellow	11	orange	1, 2, 9, 16	orange	4, 6, 15
	Not likely	green	green	yellow	7	yellow	10, 12, 14	orange	17

Criticality Of Consequence →

Figure 15.3: Risk map after mitigation

<div align="right"># 16</div>

RELIABILITY, AVAILABILITY, MAINTAINABILITY AND SAFETY ANALYSIS

This chapter focuses on the reliability, availability, maintainability and safety aspects of the EPIC mission. The definitions are described in Section 16.1. Section 16.2 analyses the reliability through historical failure data and a Markov model. Section 16.3 discusses the deployment, maintenance and availability of the constellation. Finally Section 16.4 describes the safety aspects of the mission.

16.1. DEFINITION

To assure that a product will operate as expected, a Reliability, Availability, Maintainability and Safety (RAMS) analysis is performed. The definition of each of these characteristics is shortly discussed in the list below:

1. Reliability[1]: "The ability of a system, subsystem, component or part to perform its required functions under stated conditions for a specified period of time. Reliability is the probability, assuming the system was operating at time zero, that it continues to operate until time t and is also sometimes known as the probability of mission success."

2. Availability[1]: "A characteristic which expresses the quality of a device or system for being at hand when needed. The most common measure of availability is the probability that the unit is operational."

3. Maintainability[1]: "A characteristic of design and installation which inherently provides for an item to be retained in, or restored to a specified condition within a given period of time, when the maintenance is performed in accordance with prescribed procedures and resources."

4. Safety [121]: "A system is said to have an adequate safety if it does not cause harm to people, the environment, or any other assets during its life cycle - during normal use and also for foreseeable misuse."

16.2. RELIABILITY

The reliability of the EPIC mission can be derived from historical S/C flight data to which the method of distribution fitting is applied. With this procedure a valid model for mission reliability can be generated. There are two approaches available to derive the system reliability. The focal point of the first approach is deriving the Weibull reliability model based on previous satellite failure data. The second approach focuses on the Markov model of the satellite system. The Markov model uses failure rates from numerous subsystems, based on historical spacecraft failure data, to represent the operable states.

16.2.1. WEIBULL MODEL

Most commonly, the Weibull distribution is used to simulate S/C reliability. However, CubeSat reliability differs from the one of traditional S/C, since it is heavily influenced by the dead-on-arrival (DOA) cases. Therefore, the 2-Weibull mixture function is chosen as a simulation tool. This function can account for both the DOA's and the wear-out life. Furthermore, in order to address the DOA's, the Percent Non-Zero

---

[1]http://www.lr.tudelft.nl/organisatie/afdelingen/space-engineering/space-systems-engineering/expertise-areas/fundamentals-of-rams-engineering/ [cited 23-05-2017]

(PNZ) parameter is introduced which handles the out-of-the-box failures. PNZ represents the ratio of non-zero failure items. Equation 16.1 describes the 2-Weibull mixture parametric model with Maximum Likelihood Estimation (MLE). In here, the first term accounts for the wear-out life and the second term accounts for the DOA's.

$$R(t) = \alpha \cdot \exp\left[-\left(\frac{t}{\theta_1}\right)^{\beta_1}\right] + PNZ \cdot (1-\alpha) \cdot \exp\left[-\left(\frac{t}{\theta_2}\right)^{\beta_2}\right] \qquad (16.1)$$

The parameters for CubeSats in Equation 16.1 are suggested by Langer [120] to be: $PNZ = 0.8146$, $\alpha = 0.2115$, $\beta_1 = 0.4797$, $\beta_2 = 1.0710$, $\theta_1 = 57.9715$ and $\theta_2 = 4837.3947$. Dubos [122] and Guo [123] suggest reliability models for different S/C mass categories as depicted in Figure 16.1. For the EPIC mission, Langer's reliability model is assumed to have the best fit. His model is derived from a CubeSat Failure Database of 178 S/C and includes educational missions, which have a relatively lower reliability. All S/C in this database were lauched before 2014. According to the assumed model the CubeSat reliability is reduced to 52.4% after 3 years.
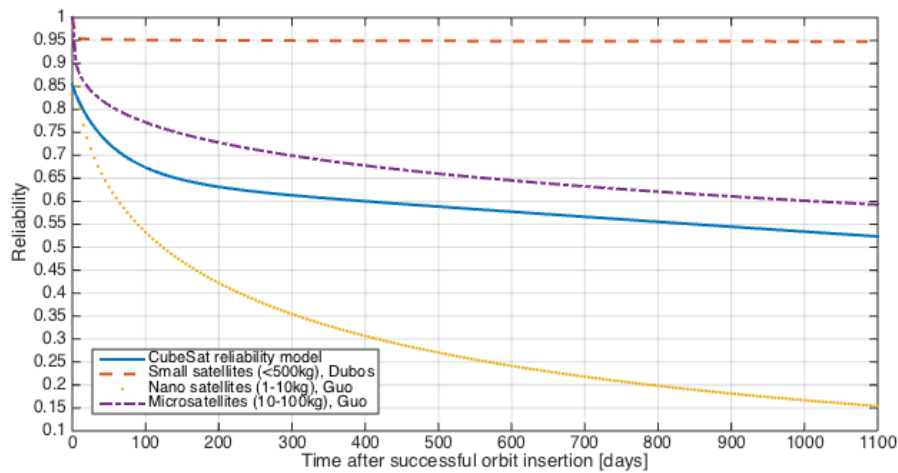
Figure 16.1: Reliability models for different S/C mass categories.

The EPIC constellation shall consist of at least 12 operational CubeSats, orbiting in 6 different planes (2 operational CubeSats, per plane) (Chapter 5). The formation flight provides redundancy and performance benefits to the system. By adding spare satellites, the reliability is further increased. Using equation 16.2 [119], the reliability of one formation can be computed. Where n is the total amount of CubeSats, k is the number of CubeSats required for operations and p the reliability of one CubeSat (equivalent to the reliability computed by the Weibull model).

$$R_{k;n,p} = \sum_{r=k}^{n} \binom{n}{k} p^r (1-p)^{n-r} \qquad (16.2)$$

Figure 16.2 shows the reliability of formation flight for different numbers of spare satellites, of which at least two satellites must be operational, and compares this to the reliability of a single satellite. From this figure the following results are derived: adding a single spare satellite increases the reliability by approximately 53% after 3 years, adding two results in an increase of about 72% and adding three in approximately 84%. Thus, from a reliability perspective it is concluded that the constellation design should strife for adding as many spare satellites as possible in each orbit. Whether this is feasible with the available cost budget shall be determined (see Section 16.3).

Optimisation of reliability can also be acquired through improving the reliability of the satellites themselves. As mentioned in Chapter 15, the contributions per subsystem to satellite failures was analysed. To improve the reliability of a single satellite, the focus should be put on the following subsystems: EPS, OBC and COM. Subsystem reliability improvements can be attained through extensive testing and adding redundancy. To reach a design life of three years, it is advised to have at least selected
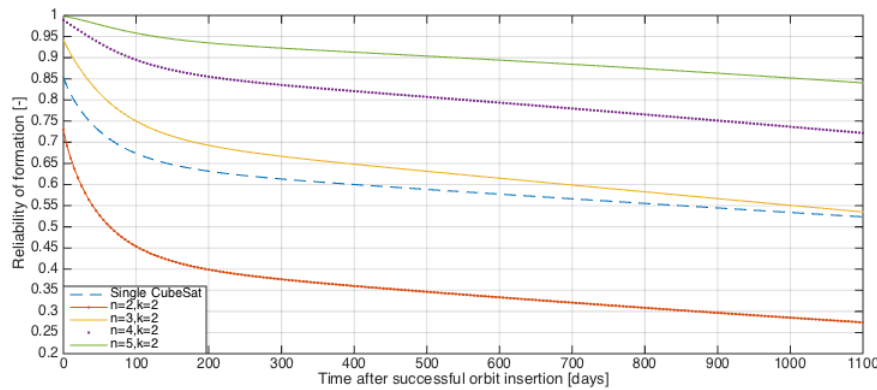
Figure 16.2: CubeSat formation reliability for different amount of spare satellites.

redundancy for the critical subsystems. This will however influence the mass, cost and design risk of the system.

Care should be taken that redundancy actually improves reliability [39]. Firstly, in case of a design flaw, a copy of the component will have the same flaw. Therefore functional redundancy should also be considered, where two redundant systems perform the same task through different designs. Finally, also the switching circuitry between redundant systems should be at least more reliable than the single system, as it may cause both components to fail. Each option should therefore be analysed with respect to mass, cost, reliability and design risk.

16.2.2. MARKOV MODEL

A satellite consists of multiple subsystems. Select subsystems are allowed to fail in succession, before a satellite is considered to have failed as a whole. By analysing the individual failure rates, a Mean Time To Failure (MTTF) of the complete system can be computed. Susceptible components are identified as well as an estimate for the operational time of one satellite is acquired. In order to analyse this, a Markov model is used. The Markov model is a powerful tool which represents a list of the possible states of that system, the possible transition paths between those states, and the rate parameters of those transitions[2].

A Markov model for the EPIC satellites is shown in Figure 16.3.
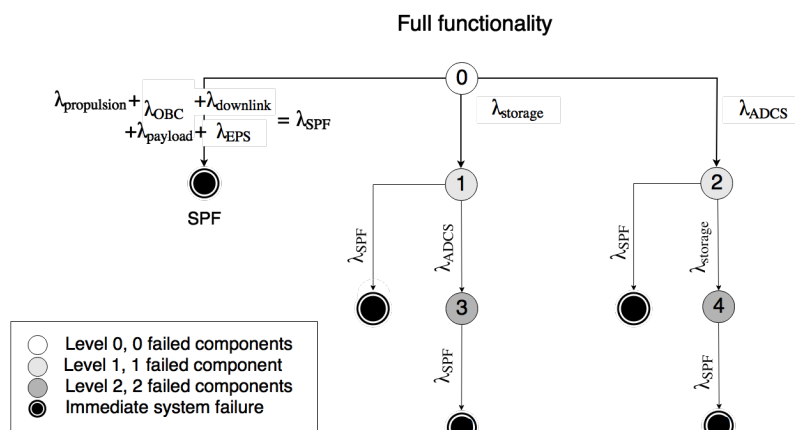
Figure 16.3: Markov model for a single satellite (based on the model by S. Engelen [124])

The branches given by the Markov chain are represented by a set of partial differential equations. Given

[2] http://www.mathpages.com/home/kmath232/part2/part2.htm [cited 16-06-2017]

the initial state of the Markov chain, the set of partial differential equations is based on the continuity equation [125]:

$$\text{rate of buildup = rate of flow in - rate of flow out}$$

The set of differential equations can be written in matrix form as shown in equation 16.3 [126].

$$\mathbf{P}^{'}(t) = \mathbf{P}(t)\mathbf{Q} \tag{16.3}$$

$\mathbf{P}^{'}(t)$ is the row vector of derivatives of the state probabilities with respect to time. $\mathbf{P}^{'}(t)$ is the row vector of all the state probabilities. $\mathbf{Q}$ is the transient matrix whose elements are defined by the rate parameters of the transitions. The elements are shown by Equation 16.4 and Equation 16.5 where λ_{ij} is the rate between the transitions.

$$q_{ij} = \lambda_{ij}, \quad i \neq j \tag{16.4}$$

$$q_{ii} = -\sum_{i \neq j} \lambda_{ij}, \quad i = j \tag{16.5}$$

The EPIC satellites are modeled as data-centric satellites (as seen in Figure 16.4), which will be applied to the Markov model. The thermal subsystem has been omitted from the model as it acts in a passive manner, thus its influence would be negligible to the reliability model. The same reasoning holds for the mechanical structure.
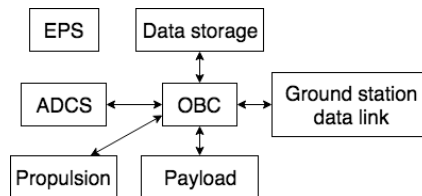
Figure 16.4: Data-centric model used in the Markov analysis (adapted from [124])

As mentioned earlier, the Markov model emphasises the operable states of the satellite. Figure 16.3 shows the Markov model. The first state being nominal, where the system is fully opertional, is indicated as state "0". Five critical components are the OBC, the payload, the downlink, the propulsion and the EPS. These are labeled as "Single Points of Failure" (SPF) and result in immediate failure of the satellite. Without the OBC, no data flow is possible and control is lost over the satellite. The satellite is considered lost if the payload cannot function, as this results in a mission failure. This also applies for the downlink, if no data can be transmitted to the ground, no data is retrieved thus the mission is a failure. The propulsion system is crucial within the first six months for deployment. Without a functioning EPS, none of the other subsystems can perform. The other states represent a reduced operability of the satellite. Up to 2 components, as indicated in the Markov model, may fail before the satellite is considered lost.

The failure rates per subsystem are attained through analysis from previous satellite failures. Guo [123] has gathered and analysed previous nano-satellite failure data up to 2012. It is assumed that the failure data of nano-satellites corresponds to failure data of CubeSats. However, the quality of the data is not considered high. As more data is gathered over time, the quality will increase. The failure data is fitted to a Weibull distribution as defined by equation 16.6.

$$R(t) = \exp\left(-\left(\frac{t}{\eta}\right)^{\beta}\right) \tag{16.6}$$

The failure rate is derived from the Weibull parameters: $\lambda = 1/\eta$. Not all failure rate data exists for the identified satellite components. The storage failure rate is assumed to be equal to the OBC failure rate. Also, the propulsion is assumed to fail at the same rate as the ADCS [124]. The subsequent failure rates are shown in Table 16.1.

The Markov model consists out of 4 transient states and several absorbing states. This is due to the fact that the satellite components are unrepairable. Once the system reaches a failure or absorbing state, transitions are not allowed. The transient states are represented as a set of partial differential

Table 16.1: Weibull parameters [123] and failure rates per subsystem

Subsystem	β	η [days]	λ [years]
EPS	0.311	83575	1/229
OBC	0.430	989536	1/2709
ADCS	0.429	166123	1/455
Storage	0.430	989536	1/2709
Downlink	0.262	297130	1/814
Payload	0.430	989536	1/2709
Propulsion	0.429	166123	1/454

equations. The differential equations for states 0, 1, 2, 3 and 4 are shown in equation 16.7. The satellite starts in state 0, hence the initial conditions are $\mathbf{I} = [P_0(0), P_1(0), P_2(0), P_3(0), P_4(0)] = [1, 0, 0, 0, 0]$.

$$
\begin{aligned}
\frac{\partial P_0}{\partial t} &= -(\lambda_{\text{SPF}} + \lambda_{\text{storage}} + \lambda_{\text{ADCS}})P_0 \\
\frac{\partial P_1}{\partial t} &= \lambda_{\text{storage}}P_0 - (\lambda_{\text{SPF}} + \lambda_{\text{ADCS}})P_1 \\
\frac{\partial P_2}{\partial t} &= \lambda_{\text{ADCS}}P_0 - (\lambda_{\text{SPF}} + \lambda_{\text{storage}})P_2 \\
\frac{\partial P_3}{\partial t} &= \lambda_{\text{ADCS}}P_1 - \lambda_{\text{SPF}}P_3 \\
\frac{\partial P_4}{\partial t} &= \lambda_{\text{storage}}P_2 - \lambda_{\text{SPF}}P_4
\end{aligned}
\tag{16.7}
$$

The set of partial differential equations are converted in matrix form, the transient matrix $\mathbf{Q}$. The mean time spent in a state until absorption, z, is computed using equation 16.8. The MTTF of the complete system is given by equation 16.9 [125].

$$\mathbf{z}\mathbf{Q}^T = -\mathbf{I} \tag{16.8}$$

$$\text{MTTF} = \sum_{i \in Q} z_i \tag{16.9}$$

The time spent per state is given by Table 16.2 and are represented in Figure 16.5. The total MTTF of the system is approximately 158 days, of which the largest portion of time is spent in the nominal state, followed by state 2. This follows from the larger failure rate for the ADCS than the failure rate of the storage component.

Table 16.2: Time spent per state

Level	State	Time spent [days]
0	0	112.2914
1	1	4.8554
	2	36.8115
2	3	1.6844
	4	2.1439
Total		157.7866

Figure 16.5: Bar chart representing the time spent per operable state

SENSITIVITY ANALYSIS

The Markov model is prone to changes. The propulsion system is not required after six months. A Markov model is set up where the propulsion system is allowed to fail, provided that the propulsion system does not fail during the time of deployment.

Figure 16.6: Updated Markov model where the propulsion system is not considered a SPF

The Markov model as seen in Figure 16.6 results in a total system MTTF of approximately 163 days. This is an increase of 5 days or an increase of 3% compared to the first Markov model. Hence, considering other components as non-crucial will have an effect on the overall reliability. However, in this case, the effect of the propulsion system is not significant. Another Markov model was analysed in case one of the two downlink options (UHF- or S-band) is allowed to fail. The results are shown in Table 16.3.

Table 16.3: Resultant MTTF of each Markov model

Single point of failures	Non-crucial elements	MTTF [days]
OBC, EPS, downlink, payload, propulsion	Storage, ADCS	158
OBC, EPS, downlink, payload	Storage, ADCS, propulsion	163
OBC, EPS, payload, propulsion	Storage, ADCS, downlink	166

16.2.3. DISCUSSION

The Weibull model depicts the chance of one satellite being operable at a certain point in time. The Weibull model exhibits two limitations. Firstly, the Weibull model does not account for wear-out phenomena. According to the current model the reliability slowly decreases after the first year. The Weibull function does not describe the "bath-tub curve" for typical failure phenomena. Furthermore, the dataset (collected by Langer) used to describe the Weibull model uses failure data from 2003-2014. Thus the current model is considered a conservative estimation of the actual reliability of CubeSats.

The Markov analysis was able to give an estimate on the operational time spent in a (reduced) operable state. The dataset collected by Guo is not considered of high quality, as it does not contain data from recent years. To improve the Markov analysis, a failure dataset for CubeSats on a subsystem level should be used. As this is not yet possible, it is assumed that the resulting MTTF is below the actual MTTF.

The Markov model assumes an exponential probability distribution of the systems failure rates. However, as stated by several authors, including Langer and Guo, the satellite failure data may be best described by a Weibull function. The Markov model does not account for infant mortalities. Several measures exist to improve the Markov model. The first is to have an up to date failure dataset for all the

subcomponents. The Markov model allows for analysing the effect of the redundant components. However, the state space, will increase explosively. The Markov model is therefore limited to the analysis of only a few components.

16.3. DEPLOYMENT & MAINTAINABILITY & AVAILABILITY

From the Weibull model, discussed in the Section 16.2, the effect of different deployment and maintenance approaches on the availability of the constellation can be calculated. The availability of three different cases are analysed. In the following paragraph the requirements and assumptions are discussed. Section 16.3.1 describes the three cases, and the methodology used to analyse the case. Section 16.3.2 shows the results of each case. Next, the conclusions and recommendations, derived from the results, are found in Section 16.3.3. Finally, the verification and validation approach for the availability calculations is found in Section 16.3.4.

Deployment and maintenance is constrained by the budget. The budget dictates that a maximum of 52 satellites and 5 launches can be used. From the constellation design, it is found that full operation is achieved when six groups with 60° RAAN in between, of two satellites, are operative. Lastly, throughout this section the type of satellite, configuration A or B, is ignored. The approach described in this section can be expanded to include differentiation between both types. But due to time constraints and the limited impact on the performance of having two different configurations per group, the type is not considered.

16.3.1. METHODOLOGY

For the analysis of the availability, three different cases have been simulated. In the first case, all spacecraft are launched simultaneously and simulated over the entire operational life of the constellation. The second and third case analyse different deployment methods, both using two launchers with twelve satellites each. Due to a lack of engineering resources, these cases have only been simulated up to the start of the operational life. The second case deploys and distributes the satellites per launcher, over the three nearest groups. The third case sends two satellites to each group (the minimum required for operability) while redundant satellites are kept in a parking orbit to replace failed satellites.

Each case has been analysed using a Monte Carlo simulation. In this simulation multiple distinctive situations are generated by assigning a unique lifetime to each satellite. The lifetime of the S/C is determined by taking random samples from the inverse Weibull distribution. Each situation will perform differently using the same maintenance and development approach. Through the law of large numbers however, a mean and distribution of the availabilities for each case is found. With this distribution the different cases can be compared.

The simulations for each use similar scripts. Each script starts in an initialisation phase. In this phase the spacecraft are given their initial location, intended location, lifetime, expected lifetime, status (on ground, reserve, operational, dead), propellant, drift magnitude and direction. Next, the script enter a loop where the time is propagated by a day in every cycle. Each cycle the parameters described above are updated based on the time passed and the case specific actions taken. Lastly, the script continues until a condition, determined by the specific case, is met. When the loop is stopped, the relevant results are stored in a file and the script terminates. In the following paragraphs the specific methodology for each case is described.

CASE I: SIMULTANEOUS DEPLOYMENT

The first maintenance and deployment case analysed, is the simultaneous launch of all satellites. This method has no maintenance planned and instead relies on redundancy to provide sufficient availability. This approach is analysed as a reference case to compare with other, more complicated, methods. The logic used in the simulation of this case is visualised in Figure 16.7.

The simulation starts by deploying 52 S/C from 5 launchers simultaneously, the maximum allowed by the budget. Each launcher deploys the S/C in between the RAAN of two neighbouring groups. Since only five launches are available, two groups have just one launch to receive S/C from. Hence these

launches have the maximum allowed S/C on a single launcher, twelve as discussed in Section 5.1. Once deployed by the launcher, the S/C, not dead on arrival, are immediately distributed over the six intended groups. Even though each S/C is only allowed to manoeuvre to the two nearest groups, in over 99% of the cases, the S/C can be evenly assigned to each group. Next, time is propagated. When the constellation reaches operational status, the simulation reports the availability on a daily basis. Finally, at the end of its intended operational life, these reports are consolidated to the availability of the constellation over this period.

The second maintenance and deployment case uses two initial launches with twelve satellites to deploy the constellation. Each satellite, not DOA, is immediately distributed over the three groups within 60° RAAN of the launch location. This case is simulated until the constellation is operational. If the constellation is unable to reach this state the program is terminated. The logic used in the simulation is visualised in Figure 16.8. However, because each S/C is directly assigned to each group, no spares are available for replacement. Hence, when a replacement is needed to be operational, the program directly terminates. The piece of code dedicated to sending a replacement, found in Figure 16.8, is therefore not used for this case.

CASE III: DOUBLE LAUNCH DEPLOYMENT WITH PARKING ORBIT
The third and final case uses, like the second case, two launches with twelve satellites initially. However, only two of the non DOA satellites are assigned to each group. The other S/C remain in the initial launch orbit as spares. Once a satellite fails intended for one of the groups, a replacement for this satellite is sent. This system is less prone to deployment failures as satellites can be replaced. However, because it takes a long time to drift to an assigned group, the deployment time is increased significantly. The algorithm behind this case is visualised in the same way as the second case, see Figure 16.8. However when a replacement is needed, it is possible to send a spare satellite. This case is simulated up to the point where the constellation is operational.

16.3.2. RESULTS
The simultaneous deployment case is analysed from deployment through the end of its intended operational lifetime. Hence the availability over its operational life can be calculated. The results of the Monte Carlo simulation with four thousand cycles can be found in Table 16.4. Three results of the analysis are particularly interesting. Firstly, in 77% of the situations analysed, the constellation is fully operational throughout its life. Furthermore, in 90% of the situations, the constellation is fully operational for more than 69% of the time. Lastly, 90% of the cases have no more than one group fail partially throughout its life.

Table 16.4: Availabilities calculated by a 4000 cycle Monte Carlo simulation of case I

Failure	Mean [%]	90th percentile [%]	Cases [%]
No failure	-	-	77.07
>1 Partial group failure	7.27	31.06	22.93
>2 Partial group failure	0.61	0	2.77
>3 Partial group failure	0.01	0	0.20
>1 Group failure	0.89	0	3.33
>2 Group failure	0.01	0	0.13
>3 Group failure	<0.01	0	0.10

In Table 16.5 the performance of the deployment for case II and III are compared. These cases have only been simulated up until successful operations. Hence, no data of the availability over its operational life can be presented. Instead the success rate of reaching operational status with only two launches, and the time it took is presented. From these results it is found that the second case has a constant time to successful operations of 183 days. This follows from the time it takes for the furthest travelling S/C (60° RAAN) to reach its intended location. In comparison case III has a higher success rate but needs a longer time to reach operational status. When a satellite, heading to a particular group, fails before reaching the intended group, a replacement has to make the same journey again. Hence the time to deployment increases significantly.
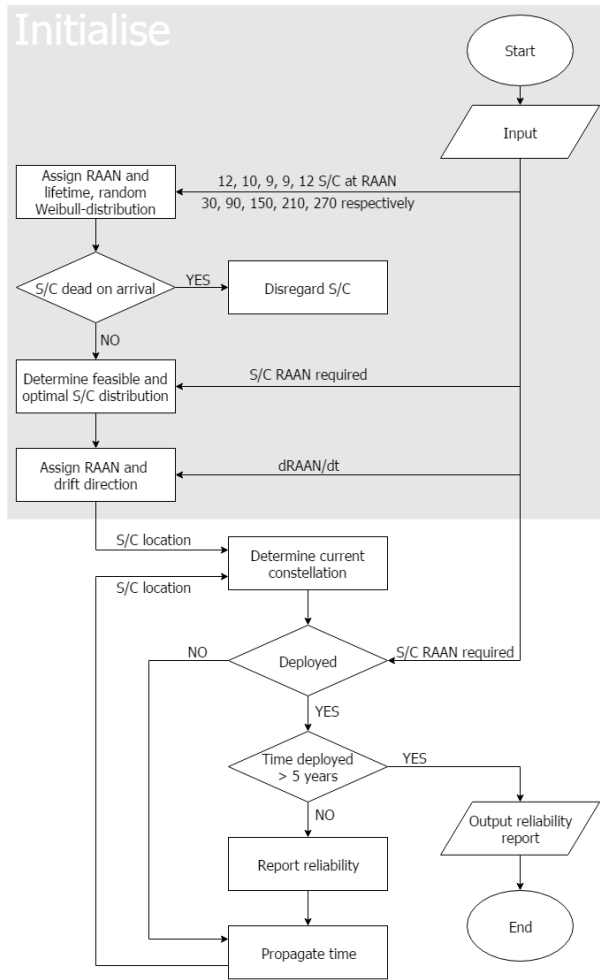
Figure 16.7: Logical flow of script for case I
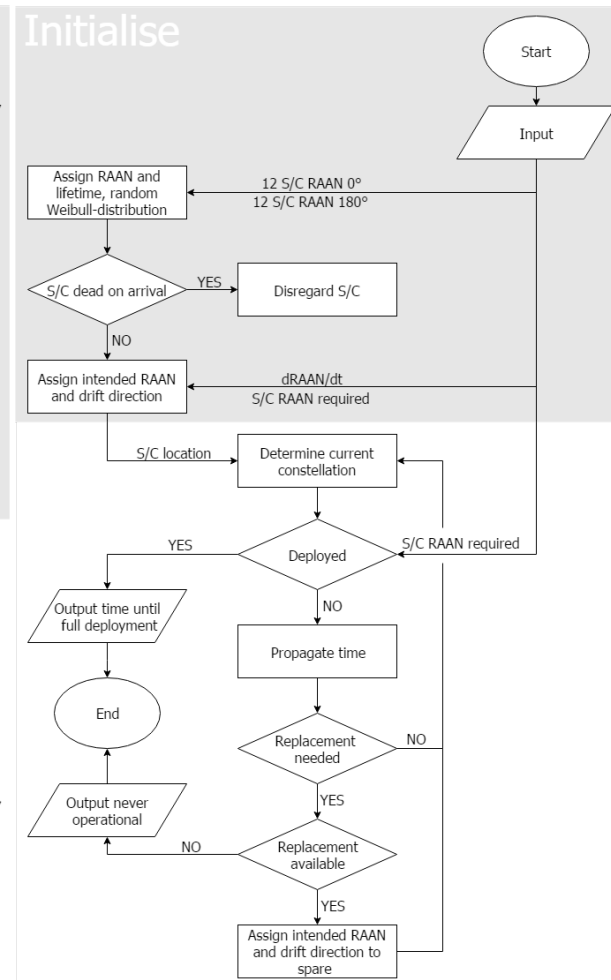
Figure 16.8: Logical flow of script for case II and III

Table 16.5: Success rate and time to operations calculated from 1000 cycle of a Monte Carlo simulation for case II and III

Case	Success rate [%]	Time to successful operations	
		mean [days]	90th percentile [days]
II	48	183	183
III	83	251	362

16.3.3. CONCLUSION AND RECOMMENDATION

From the results of the first case it is found that, using a relatively simple deployment and maintenance approach, high availabilities can be attained. In more than 90% of the cases the worst state of the constellation would be a single partial group failure. This failure would only be present 31% of the intended operational life. This method has however also significant drawbacks.

Firstly, each satellite will be at least five years old at the end of its lifetime. The S/C are not designed to operate for such a long time, hence the solar panels will degrade more than intended, reducing the potential performance of the S/C. Next, by launching all spacecraft at the same time, design flaws, unnoticed on the ground, can be present on all S/C in the constellation. This could have a catastrophic impact on the system, without any possibility to correct them. Furthermore, all funds for the mission have to be available and spent from the start of the mission. This is a large risk for the customer who needs to pay for an unproven constellation upfront. Launching a constellation with a limited number

of satellites and lower performance instead could be more attractive. Once this limited constellation is proven to work, the lifetime and performance of the constellation can than be extended and improved through maintenance.

For the reasons described above cases II and III are analysed. These case only have two initial launches and 24 S/C. This is expected to reduce the funds required at the start of the mission by half. This reduces the risk for the customer significantly. As discussed before, the effect of potential subsequent launches has not yet been analysed. Hence, data over the whole intended lifetime of the constellation is currently unavailable. Instead, the results compare the performance of both cases between deployment and operational status of the constellation. From this comparison it can be concluded that there is a trade-off between deployment time and success rate. For a full trade-off however, also location and health of the remaining S/C should be taken into account.

In future design phases, this analysis should be expanded. Different maintenance and deployment approaches should be analysed over the entire lifetime of the constellation. These approaches can vary in launch scheduling methods, number of satellites per launch, and deployment strategies. For the future it is recommended to start with a design option tree to identify all options. Next, promising options should be analysed using the same tools as described in this section. Finally a trade-off can be made based on the risk, performance, and sustainability of each option. Because analysing each option takes significant engineering resources, attention should be taken to only consider promising options.

16.3.4. VERIFICATION AND VALIDATION

The verification and validation possibilities for a Monte Carlo simulations is very limited [127]. Monte Carlo simulations are almost always made for a specific problem. The program can therefore not be verified through comparison with other simulations. Neither is it viable to validate the results with real world examples. Even if the constellation would be launched, there is no method to determine whether the simulations are accurate. Instead the V&V focuses on the inspection of individual pieces of code and its results.

Firstly, the Weibull distribution functions are verified through comparison with the source of the distribution [120]. From Figure 16.9 and Figure 16.10 one can see that the parametric models correspond exactly. Also the mean of 4000 samples of the Weibull distribution is close to the original parametric model, a consequence of the law of large numbers. Finally also the 95% confidence interval boundaries are similar. This verifies the correct implementation of the Weibull, inverse Weibull, and lifetime assignment functions used in the analysis.
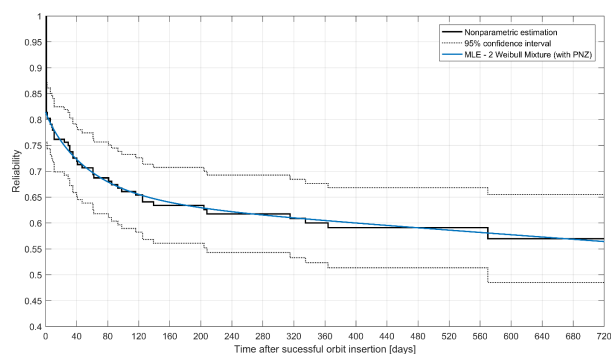
Figure 16.9: Plot of MLE 2-Weibull mixture parametric fit by M. Langer [120]
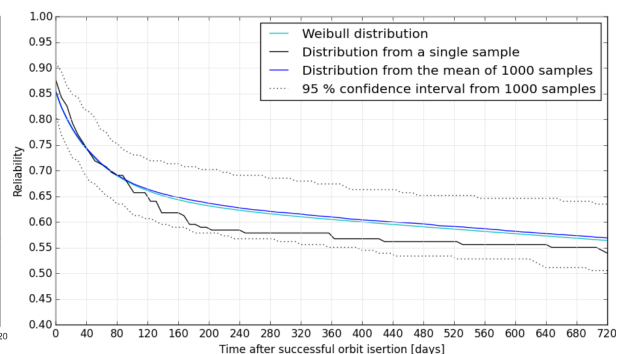
Figure 16.10: Reproduction of the plot by M. Langer through custom Weibull functions

Next the propagation of time and the corresponding drift of S/C is verified to work correctly through the result of the deployment time of case II. As calculated in Chapter 5 the deployment time to change 60° RAAN corresponds to half a year or 183 days. The other sections of code could not be verified analytically or comparatively as the code makes decision specific to the EPIC mission. These sections were therefore only verified through inspection of the program logs and visualisations. From this visualisation,

the effect of the decisions made by the program can be seen. For a discrete amount of samples, these effects were carefully monitored and checked for unintended behaviour.

16.4. SAFETY

The safety of a system is defined by L. Yu. [121], in the following way: "A system is said to have an adequate safety if it does not cause harm to people, the environment, or any other assets during its life cycle - during normal use and also for foreseeable misuse." In this project the definition of safety is extended to also include mission and investment safety.

To minimise the potential harm of the constellation to people, the environment and other assets, the design will not contain radioactive materials. Furthermore, in each trade-off, the safety of each option is considered. The propulsion system uses potentially explosive bi-propellant but is still chosen in the trade-off due to a lack of feasible alternatives. Next, during the material and component selection of the S/C, the melting temperature is checked. The melting temperature should be low enough to fully burn up in the atmosphere[3]. Finally, in the sustainability analysis (Chapter 18), an EOL and collision avoidance strategy is proposed to minimise litter in LEO.

Mission safety is ensured through extensive verification and validation efforts. Every tool, simulation and calculation is checked for mistakes, incorrect assumptions, and its applicability to the specific problem. Each satellite will also be tested individually according to the CubeSat design specification (CDS) [30], as indicated in the requirements [40]. This includes random vibration, shock, thermal vacuum bake-out, and visual testing. The EPIC systems should also be resilient against hacking attempts. Losing control due to hacking could impact mission success and the safety of other satellites.

Finally to ensure funding for the project, it is important to consider funding safety. By lowering the initial investment, the system can prove its capabilities before committing to the full price of the constellation. This is considered in the design through the use of COTS components, which do not require initial development. Furthermore gradual deployment of the constellation is considered.

---

[3]http://www.aerospace.org/cords/all-about-debris-and-reentry/spacecraft-reentry/ [cited 18-05-2017]

17

PRODUCTION PLAN

This Chapter discusses the sequence of activities that make up the production process of the CubeSats. Chapter 7 shows that not all of the CubeSats will carry the same payload on board. Therefore different production processes need to occur per CubeSat configuration. Nevertheless, the general flow of activities related to such processes are the same for each type of CubeSat. This is shown in Figure 17.1 where the activities to be executed during the production phase are identified. Two types of activities can be distinguished from Figure 17.1, these are the non-recurrent and recurring processes which are discussed below.
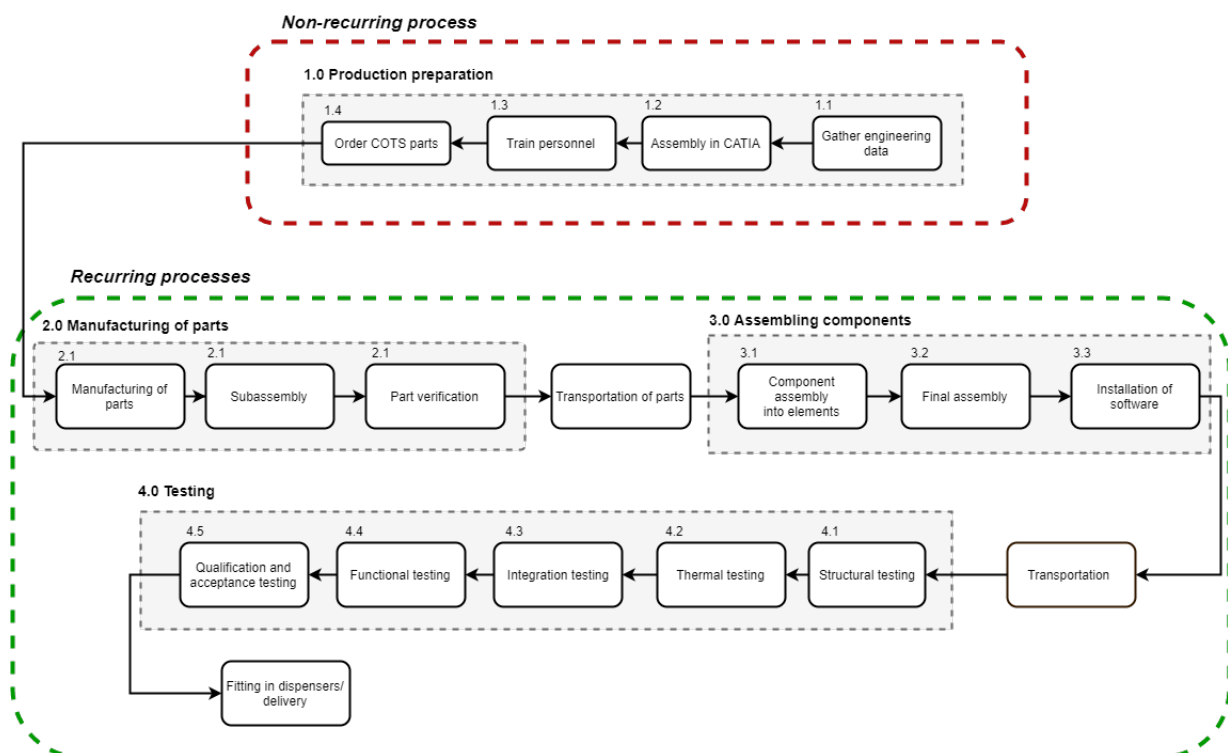
Figure 17.1: The production plan of the CubeSat

17.1. NON-RECURRING PROCESS

Non-recurrent processes are processes that are executed once per product type. These processes determine to a high degree the effectiveness of the recurring processes and are therefore executed early in the life cycle of the mission [128]. The preparation for production is the first non-recurrent process that can be identified for the EPIC mission. It is a crucial process since it forms the baseline to develop the CubeSat. The first step involves the gathering of engineering data such as dimensions for each subsystem and payload which are used to develop a model in CATIA. The subsystems or payloads will not have to be designed since CAD versions are available from their manufacturers but the order in which they need to be installed has to be investigated in order to save time and costs during the real assembly. Once the assembly process has been identified and a complete model per CubeSat type has been constructed a users manual can be made in order to train the personnel responsible for the manufacturing and assembly of the CubeSat components. Meanwhile, the COTS components can be

ordered.

Requirement **EPIC-SYS-S11-Cs.01.1** states *"If a choice between a new design and a commercial of the shelf component has to be made and both options meet all other requirements, the COTS component shall be chosen."* [40]. CubeSats are part of a standardisation in space and thus have standard sizes and masses. Due to those standardised rules parts for CubeSats have been designed to fit into the CubeSat's structure. COTS parts are also verified and tested and thus are more reliable than new designs.

Several companies have found their way into the market of CubeSat part production. Some are smaller and focus more on specific parts, while other broaden their vision and offer a variety of products and services, like ISIS [24] and Clyde Space. The CubeSat.org site has a list of companies which can help developers of small satellites perform their mission. Once the COTS parts are ordered a series of recurring process will take place.

17.2. RECURRING PROCESSES

Recurring processes are processes which are repeated for every product type [128]. The first process for this mission consists of the manufacturing of the CubeSat's components. The COTS parts have their own production processes in which specialised machines and tools are used by the manufacturer's facilities. A number of these parts might not exactly meet the dimensions of the structure and therefore will need to be modified. Furthermore, parts which are not COTS will have to be manufactured. Once the parts are assembled into sub-assemblies, verification methods are used to ensure that these sub-assemblies do not contain any errors. After that they are transported to the facility where the assembly will take place. During assembly, the sub-assemblies are connected together making up a larger structure. Once assembly has taken place, the CubeSats need to be programmed to perform their functions. Therefore, all necessary software will be installed. Verification methods will also be used here in the form of simulations to ensure that the software runs smoothly. The next step involves a series of tests for each CubeSat to ensure smooth running operations and compliance with requirements such as **EPIC-STK-09** regarding the launch contractor's requirements. More information regarding the testing can be found in Section 17.2.3. Having completed all the activities described above, the CubeSats are ready to be delivered to the launch facility.

17.2.1. MANUFACTURING

The majority of the components that make up the CubeSat are commercially off the shelf available and have their own manufacturing processes. As mentioned earlier, some components are not COTS available or the COTS need to be modified. These are the following:

- +Z surface cover (front-face)
- Retarding potential analyser
- -Z surface cover (back-face)
- Langmuir probe (modification)
- -Y surface magnetometer cavity

The manufacturing processes applied to these components, can take place either in university laboratories or space companies located in the Netherlands. The manufacturing process should strive for waste reduction in order to comply with the sustainable philosophy of the entire mission.

17.2.2. ASSEMBLY AND INTEGRATION

The assembly will take place in a clean room. This is a room, which has a controlled level of airflow and contamination and is characterised by the amount of particles per cubic meter of space. The International Standardisation for Organisation (ISO) has developed several classes which are used to characterise the clean rooms. The faculty of aerospace engineering of TU Delft has a registered ISO 8 clean room in which research for small satellites is being conducted. The CubeSats Delfi-C3 and Delfi-N3xt were built and tested in those fascilities as well[1]. But due to the high number of CubeSats

---

[1] https://www.tudelft.nl/en/ae/organisation/departments/space-engineering/space-systems-engineering/facilities/ [cited 18-05-2017]

that need to be assembled other locations in the Netherlands will be preferred. Possible candidates include, among others, the ISIS assembly facility and the ESA/ESTEC facilities in Noordwijk.

In order to make the assembly of the CubeSats as efficient as possible, the assembly workbench will be organised such that all equipment can easily be accessed. This includes all the screws, screwdrivers, components, wires, etc. A user guide manual will be provided to the people responsible for the work containing all necessary information about the assembly sequence. Before entering the clean room facility, the assembler will wear the required protection gear to avoid contamination of the clean room environment. While working on the workbench measures for static electricity protection will be taken. To do so, a bracelet is usually used which is attached to the assembler and the table.

The main assembly activities are as follows. The 6U structure provides rods for the mounting of the PCBs. First a baseline plate will be placed and then the PCBs will be stacked one on top of the other. Four spacers will be used per PCB (one for each rod) to constrain the PCBs and to give structural integrity during vibrations. Once stacked, the wiring to and from both of the ISIS on-board computers will be completed. After that, the payload sensors and the two antennas will be attached to the structure and connected to the computer and their respective receivers. The ADCS and the propulsion unit being the two largest subsystems will be installed last such that all the wiring of the other systems is completed. Once the inner harness is finished the solar panels surfaces (excluding the solar cells) will be covered with white thermal paint and then installed and connected to the EPS.

17.2.3. TESTING STRATEGY

Testing is performed to meet the launch provider requirements as well as to ensure the safe operation of the CubeSat and the dispensers. The testing requirements and testing levels will be derived from Rocketlab's user guide manual and NASA's General Environmental Verification Standard GSFC-STD-7000 [38]. Furthermore, in order to reduce the time spent on transportation of the CubeSats, testing facilities located in the Netherlands will be chosen. Different types of testing are discussed below.

STRUCTURAL TESTING

Structural testing is performed to simulate the mechanical loads that the spacecraft will experience. During the development of the structure, different structural tests wil take place to check for each type of load. Information regarding the mechanical environment of the CubeSat was given in Chapter 13. Structural testing will also be used to validate the finite element model built for structural performance prediction.

THERMAL TESTING

Thermal testing is performed to simulate the operational thermal conditions that the spacecraft will need to handle. According to [108], thermal balance testing is often performed on space systems to ensure system integrity. These test can also provide validation means for the mathematical models from Chapter 12 used for thermal performance prediction. Another type of thermal test that will be performed is the thermal vacuum test, where the full system is tested in a vacuum environment and at different temperature ranges.

INTEGRATION TESTING

This type of testing is mainly performed to find out whether the elements that make up the assembly fit and work together. Three types of tests fall within this category. Mechanical integration testing is performed to check the mechanical interfaces of the components as well as their mass properties. Electrical integration tests allow to investigate the electrical signal and power interfaces of the components as well as their power consumption. Finally, software testing is performed using simulated environments to investigate whether the software will run smoothly.

FUNCTIONAL TESTING

These tests are performed to prove that the spacecraft can perform all types of functions. These include:

- Solar panel and antenna deployment test
- Close-loop control tests for the attitude control system
- Radio frequency test
- Magnetic cleanliness and electromagnetic field test

QUALIFICATION AND ACCEPTANCE TESTING
The 6U CubeSat design specification document mentions three types of tests that CubeSats typically undergo during the qualification and acceptance stage [116]. These are the following:

- Random vibration testing to simulate the launch environment of the CubeSat.

- Thermal vacuum bake-out testing to ensure proper out-gassing of the components.

- Visual inspection testing to detect possible surface defects.

According to the CubeSat design specification the following approach is implemented for this phase [116]. First, qualification testing will take place on the engineering models. For this mission there will be two models, one for each configuration. Information from the outcome of these tests will be used to modify the flight model which in turn will be tested to acceptance levels first with a 6U test dispenser and then on the 6U flight dispenser. Once this is completed, protoflight testing will be performed on the flight models again based on the testing requirements of the launcher and the GSFC-STD-7000. First, the models will be tested to protoflight levels in the 6U test dispenser and then in the flight version for a final acceptance random vibration test. Lastly, after having integrated the CubeSat into its dispenser, additional testing will be performed to ensure proper integration. Figure 17.2 shows the testing flow diagram as given by the design specification document.
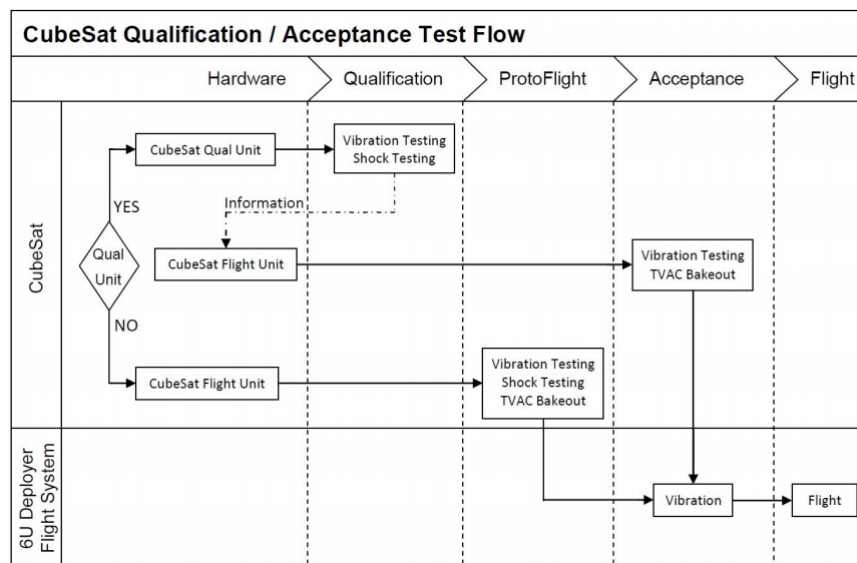

Figure 17.2: General testing flow diagram for CubeSats [116].

<div align="right">**18**</div>

SUSTAINABLE DEVELOPMENT STRATEGY

Since the beginning of the design process of this mission steps were taken to make the EPIC mission as sustainable as possible. The framework of sustainability was first defined in the Project Plan. In the baseline phase a sustainable development strategy was introduced which focuses on the three aspects of sustainability, namely the social, economical and environmental factors surrounding the mission. During the Mid-term phase the strategy was analysed further resulting in its current state in this report. In Section 18.1 the approach towards a sustainable production process is presented while in Section 18.2 the end of life strategy is discussed. Finally in Section 18.3 the risk of in-orbit collisions with space debris and meteoroids is estimated.

18.1. PRODUCTION PROCESS

A crucial aspect on the sustainability of the mission lies in the production process, for which a detailed discussion has been given in Chapter 17. The Lowell Center for sustainable production defines sustainable production as the creation of goods and services using processes and systems that are non-polluting, conserving of energy and natural resources, economically viable, safe for workers, communities consumers and socially rewarding for all working people [1].

MATERIAL USE

The choice on the materials used for the design of the CubeSats will be based on their impact on the environment. Typically the structure of the CubeSat is made of aluminium alloys and during operations the faces are covered with solar panels. Since most of the parts are available COTS, limited choice for material use is possible. Nevertheless, COTS products made of hazardous materials are avoided. In addition radioactive or toxic materials will not be carried on board thus meeting requirement **EPIC-STK-07.1**, which states that *"The small satellite constellation shall not use any radioactive materials".*

PRODUCTION EFFICIENCY

The framework applied to enhance the production efficiency is related to waste minimisation. It is therefore important to evaluate the assembly and test processes in terms of value added and non-value added activities. Controlling the non-value added activities can drive waste elimination. The number of inspections during the production phase will be reduced if the output of these inspections can be predicted or by choosing to inspect a lower number of satellites [39]. Another aspect to take into consideration is the amount of testing. Although testing cannot be avoided, it is possible to reduce the redundant testing [39]. For example no supplementary tests are necessary if after the first test the component was not affected by any process. Testing also drives the satellite's delivery time and the process shall be designed to aim at a minimised cycle time [128]. The time spent for the transportation of the parts also influences the development time, so space companies located in Europe are preferred.

18.2. END OF LIFE STRATEGY

According to the Inter-Agency Space Debris Coordination, it is found that post mission orbital lifetime shall not be more than 25 years [129]. This implies that after the mission is completed, an EOL strategy must be implemented. According to ISO 16164:2015 which focuses on the post-mission disposal of spacecraft operating in or crossing LEO, six disposal options in order of preference shall be used to meet the debris mitigation requirements[2]:

---

[1] http://www.sustainableproduction.org/abou.what.php [cited 20-05-2017]
[2] https:www.iso.org/standard/55741.html [cited 25-04-2017]

1. Retrieval followed by controlled re-entry and safe recovery on the Earth

2. Controlled manoeuvre in to a targeted re-entry with a well-defined impact footprint on the surface of the Earth

3. Controlled manoeuvre to an orbit with a shorter orbital lifetime

4. Augmentation of orbital decay using a deployable device

5. Natural orbital decay

6. Raising orbit perigee altitude sufficiently above the LEO protected region that perturbations do not cause re-entry to this region within 100 years

From this list, options 3,4 and 5 seem feasible for this particular mission. Option 1 will not be considered due to the complexity and the budget constraints. A new mission would have to be designed just for this task. The fact that the constellation consists of many CubeSats makes it even more difficult. Furthermore, missions to demonstrate active debris removal are currently only under development (e.g e.Deorbit[3], RemoveDEBRIS[4]). Option 2 is mostly related to spacecraft of larger sizes in which complete burn during re-entry is not feasible. If that was the case for this mission, a controlled set of manoeuvres would have to be performed to decrease the orbital lifetime of the satellite and consequences of incomplete burn in the atmosphere would also have to be assessed in order to minimise the risk of ground impact due to surviving fragments [130]. Lastly, option 6 is also discarded, since it would require an unfeasible Δv of approximately $700 m/s$ to increase the orbital altitude above the LEO region [39]. For the remaining three options a trade-off analysis was conducted during the mid-term phase. The criteria chosen to evaluate these options were the cost, weight and the complexity added to the system. It was then concluded that letting the CubeSats naturally decay is the most optimal option even though the rest of the feasible options meet the 25 year requirement [31].

The CubeSats are left in their orbits after the end of operations and atmospheric perturbations cause the decrease of the orbital velocity. This option is the easiest to implement since it will not affect any design options for the subsystems and the payload. Evidence exists in literature showing that it is feasible for a 6U CubeSat to meet the 25 year de-orbiting requirement. More specifically, Qiao Li et al. have conducted an analysis on the orbital decay of different sized CubeSats [131]. In order to make their model more accurate factors such as initial orbit altitude, surface area, drag coefficient, atmospheric model and solar flux were taken into account. It was found that at an altitude of approximately $550 km$ the CubeSat will meet the 25 year requirement even if other factors were significantly altered; e.g. the atmospheric model or the drag area of the CubeSat. These results can therefore be used as verification means for the orbital decay of the CubeSats of mission.

To support the aforementioned finding and to assure that the EPIC mission will meet the sustainability requirements, a preliminary analysis on the orbital decay of the CubeSats in this mission was conducted during the mid-term phase using the Semi-analytical Tool for End of Life Analysis (STELA). The software receives certain inputs from the user and propagates the given orbit using semi-analytical models and assessment of criteria such as third body perturbations. The output of the software is a report which summarises the computation and provides the initial and final orbital parameters [5]. The analysis showed that it is feasible to meet the 25 year requirement.

ESTIMATION OF NATURAL DECAY TIME

Since at this point more data is available on the design a more elaborate analysis can be conducted using STELA. The input parameters are given in Table 18.1 together with their corresponding significance on the results. The drag area is defined as the area perpendicular to the velocity vector and is equal to the area of the +Z surface of the CubeSat. For optimum power generation purposes, in Section 10.1 it was decided to place the big solar panels at an angle of $\beta = 82°$. This leads to a drag area of $0.175 m^2$. In addition as described in Chapter 5 some CubeSats will be deployed at an altitude of 670km for the constellation deployment. Since this is the highest altitude achieved in the mission and thus has

---

[3] http://www.esa.int/Our_Activities/Space_Engineering_Technology/Clean_Space/e.Deorbit [cited 8-05-2017]

[4] https://www.surrey.ac.uk/ssc/research/space_vehicle_control/removedebris/ [cited 8-06-2017]

[5] https://logiciels.cnes.fr/content/stela?language=en [cited 13 June 2017]

the lowest orbital decay, the worst case scenario in which the propulsion system fails and the CubeSat cannot perform a transfer orbit to a lower altitude will be analysed. Another critical input required by the software is the atmospheric model used in the simulation. In the current version of the tool, the user can choose between three models, US76, JACCHIA 77 and NRLMSISE-00 where the latter is used since it is the most recent. Apart from the atmospheric contributions to the orbital decay the solar activity also needs to be taken into account. The solar radio flux at 10.7 cm (2800 MHz) is an excellent indicator of solar activity and has been measured constantly since 1947 [6]. On average the solar cycle has a period of eleven years which can be seen in Figure 18.1. Since it is difficult to estimate the solar activity for the coming years and because 2 solar cycles will have occurred during the maximum de-orbiting time of 25 years, it is decided that a mean value, as provided by STELA, of 140 sfu is a reasonable estimate for the simulation process. Figure 18.2 shows the variation in the orbital altitude throughout time. It takes approximately 20 years for the CubeSats to de-orbit thus meeting the requirement.

Table 18.1: The parameters that were used during the simulations and their significance.

Parameters	Value	Unit	Significance in the results
Right Ascention of ascending node	50	°	Negligible
Argument of perigee	50	°	Negligible
Mean anomaly	50	°	Negligible
Reflecting area	0.5	m^2	Negligible
Reflectively constant	1.2	-	Fixed
Inclination	56	°	Medium
Perigee	670	km	High
Apogee	670	km	High
Drag coefficient	2.2	-	High
Drag area	0.175	m^2	High
Mass	12	kg	High
Atmospheric model	NRLMSISE-00	-	High
Solar activity	Mean constant F10.7=140 & AP = 15	-	High

For an operational altitude of 520km and a launch date somewhere in 2019, the value for the solar activity is chosen to be equal to 65 sfu for the first five years and a mean value of 140 sfu for later years. This is a reasonable estimate since according to Figure 18.1, the constellation operates at solar minimum conditions. The calculated time to de-orbit is then reduced to 8 years.
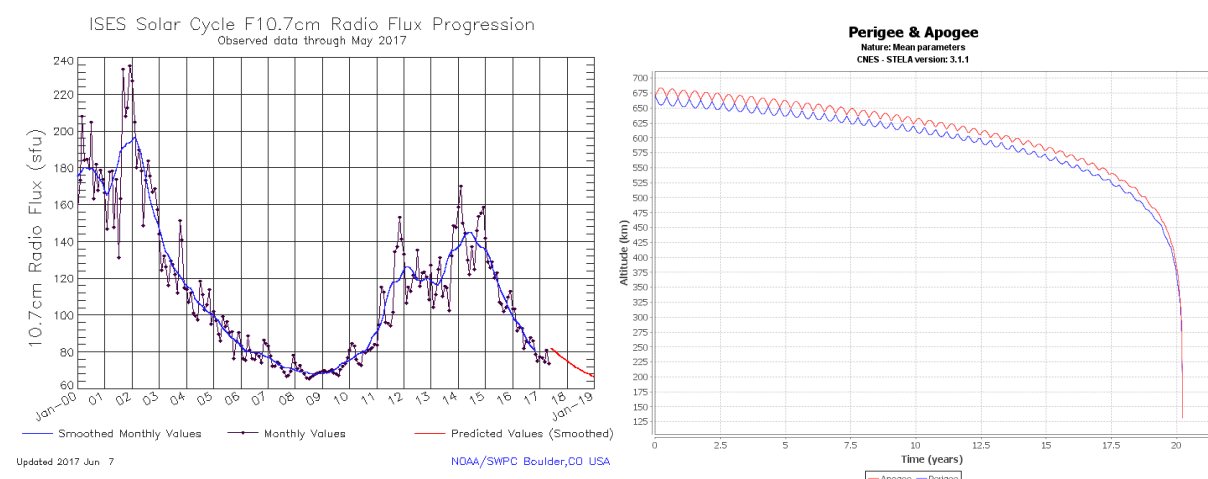

Figure 18.1: The solar cycle activity of the previous years together with a prediction for the coming 2 years [7].

Figure 18.2: The simulated orbital decay of the CubeSats starting from an altitude of 670km [132].

---

[6]http://www.swpc.noaa.gov/phenomena/f107-cm-radio-emissions [cited 13-06-2017]

18.3. SPACE DEBRIS ASSESSMENT

An important aspect that needs to be taken into consideration while designing the mission is the risk behind in-orbit collisions with space debris. Currently, the United States maintains a catalogue of about 20000 objects larger than 10cm in diameter orbiting earth and the majority of these are debris. NASA uses special ground-based sensors and performs inspections of returned satellite surfaces to statistically determine the population of debris. An estimated number of 500000 objects of a diameter of 1 to 10cm orbit Earth at this point in time [133]. These objects can travel with speeds up to $10km/s$, and even the smallest piece can create severe damage to satellites and consequently generate even more debris [8].

For this mission an investigation on the risk behind in orbit collision has been conducted using ESA's Meteoroid and Space Debris Terrestrial Environment Reference tool [134]. The 2009 model of the tool covers all debris and meteoroids of sizes larger than $1\mu m$ and includes predictions of the space debris environment until 2050 [9]. The software allows the user to perform an analysis on the debris or meteoroid flux for a given orbit.

Figure 18.3 shows the two dimensional flux distribution of debris at a range of altitudes. For an operational altitude of 520km the semi-major axis for each orbital plane is equal to 6891km which corresponds to a value of $0.1849 \cdot 10^{-4} m^{-2} yr^{-1}$. Figure 18.4 shows the dimensional flux distribution for a range of inclinations. It is found that at an inclination of 55° the total flux is equal to $0.2176 \cdot 10^{-7} m^{-2} yr^{-1}$. As suggested by ECSS-E-ST-10-4C, the flux (F) can be transformed to a number of impacts (N) by assuming a linear increase with respect to the exposed area (A) and time (T) of the CubeSat (Equation 18.1). The probability of n impacts is then calculated by applying Poisson statistics, as shown by Equation 18.2 [135].

$$N = F \cdot A \cdot T \qquad (18.1)$$

$$P_n = \frac{N^n}{n!} e^{-N} \qquad (18.2)$$
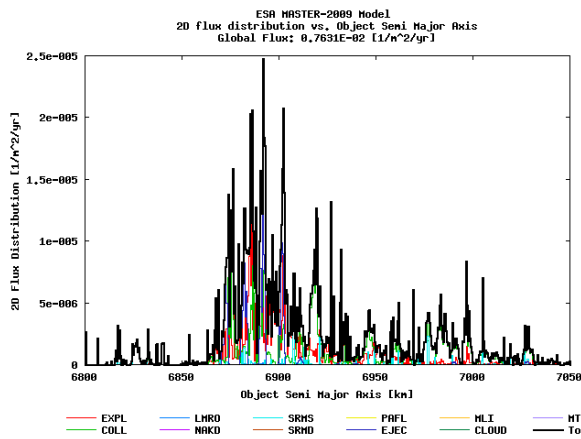
Figure 18.3: The two dimensional flux distribution of debris at a range of altitudes [134].
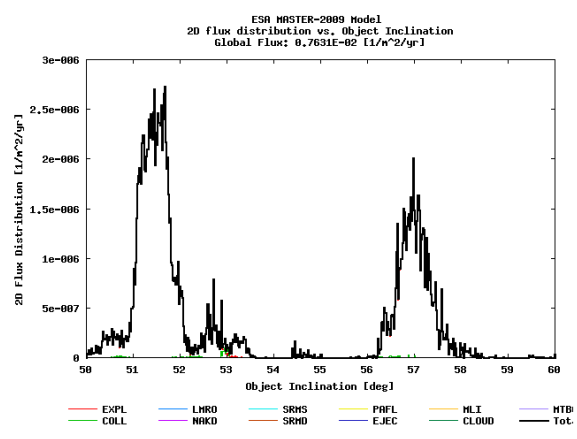
Figure 18.4: The two dimensional flux distribution of debris at a range of inclinations [134].

For a total surface area of the CubeSat equal to $0.49m^2$, it is found that the probability of a single impact at the operational altitude is $9.1 \cdot 10^{-6}$ while for the orbital inclination a probability of $1.42 \cdot 10^{-15}$ was estimated. These values suggest that the risk of collision with orbital debris is very low.

---

[7] http://www.swpc.noaa.gov/phenomena/f107-cm-radio-emissions [cited 13-06-2017]

[8] https://www.nasa.gov/mission_pages/station/news/orbital_debris.html [cited 22-06-2017]

[9] http://m.esa.int/Our_Activities/Operations/Space_Debris/Analysis_and_prediction [cited 22-06-2017]

19

COMPLIANCE MATRICES & FEASIBILITY

In this chapter the compliance matrices and an analysis of the feasibility is presented. In Section 19.1 the compliance matrices, and the feasibility to meet these requirements is discussed. Next, Section 19.2 determines the feasibility of the design to major changes in system parameters.

19.1. COMPLIANCE MATRICES

In this section the compliance of the designed system to the requirements set in the baseline report is checked [40]. The references are divided in stakeholder requirements, system requirements, subsystem requirements and budget requirements. All requirements are evaluated, and in case a requirement is not met, the rationale why the design does not meet the requirements is discussed. If a requirement is met, this is indicated with a tick mark (✓) and if this is not the case, this is indicated with an x-mark (✗). Finally, the results of the compliance matrices shall be concluded.

19.1.1. COMPLIANCE TO STAKEHOLDER REQUIREMENTS

The stakeholder requirements have a unique identifier, EPIC-STK-XX. The compliance matrix of the stakeholder requiremets can be found in Table 19.1. Stakeholder requirements **EPIC-STK-02** to **EPIC-STK-04** cannot be verified yet, since the mission has not been executed. But the design presented in this final report suggest that these requirements will be complied to completely.

Table 19.1: Compliance matrix for the stakeholder requirements of the EPIC mission

Identifier	Requirement	✓ / ✗
EPIC-STK-01	The small satellite constellation shall provide information to validation the coupling of ionosphere physics and seismic activity.	✓
EPIC-STK-02	The small satellite constellation shall alleviate the impact of major earthquakes on human life.	✗
EPIC-STK-03	The small satellite constellation shall alleviate the economic impact of major earth-quakes.	✗
EPIC-STK-04	The small satellite constellation shall provide a warning before a major earthquake with a time margin, which is sufficient to evacuate the affected area.	✗
EPIC-STK-05.1	The small satellite constellation shall abide by the regulations as stated by the Inter-Agency Space Debris Coordination Committee.	✓
EPIC-STK-07.1	The small satellite constellation shall not use any radioactive materials.	✓
EPIC-STK-08.1	The small satellite constellation shall not disturb frequency bands that are already in use.	✓
EPIC-STK-09	The small satellite constellation shall comply with specifications as stated by the launching contractor.	✓
EPIC-STK-10	The small satellite constellation shall not inflict any damage on the launcher during the launch and insertion to orbit phase.	✓
EPIC-STK-11	The total mission cost shall not exceed 50 million euros including development time, launch and operations.	✓
EPIC-STK-12	The small satellite constellation design shall be completed by the 7th of July 2017.	✓
EPIC-STK-13	The small satellite constellation shall serve as an educational tool for DSE students.	✓

19.1.2. COMPLIANCE TO SYSTEM REQUIREMENTS

This section evaluates the compliance to the system requirements, which are numbered using the requirement identifier as EPIC-SYS-SXX-system.YY. The numbering XX refers to the according stakeholder requirement and YY is the system requirement in order of importance. In Table 19.2 and Table 19.3 the compliance matrix can be found. The following requirements are not met.

- **EPIC-SYS-S05-Config.06** The CubeSat propulsion system only provides sufficient Δv for the Hohmann transfers, which is necessary for the constellation deployment. The team decided to do no orbital maintenance, since the orbital decay at mission altitude during the short satellite lifetime, will not influence other mission aspects.
- **EPIC-SYS-S11-OP.02** The CubeSats in the EPIC constellation are designed to be functional and available for three years. However, it is taken into account that part of the satellites fail. This is why a strategy is designed to replace the failed satellite.
- **EPIC-SYS-S02-Qf.03 & EPIC-SYS-S02-Qf.04** The compliance to these two requirements cannot be investigated, since the earthquake precursor concept has yet to be verified.
- **EPIC-SYS-S04-OP.04** Since the EPIC mission uses a constellation, one ground station, i.e. the TU Delft, will not be sufficient. Since the GENSO project is terminated, the team decided to make use of a commercial ground system service, provided by the company KSAT. [136]

19.1.3. COMPLIANCE TO SUBSYSTEM REQUIREMENTS
This section evaluates the subsystem requirements. Every subsystem requirement has an unique identifier in the form EPIC-SYS-SXX-system.YY-subsystem.ZZ. In this identifier, XX refers to the associated stakeholder requirement, YY is the system requirement and ZZ is the number of the subsystem requirement. The subsystem compliance matrix can be found in Table 19.4 and Table 19.5. The requirements that are not met or not yet have been met by the EPIC design are listed below.

- **EPIC-SYS-S10-Func.08-SV.02** This manual includes every specification the CubeSat has to comply with. This can only be verified after all mandatory testing has been done and the S/C is ready for launch. At this point in the design this is not applicable.
- **EPIC-SYS-S10-Func.08-SV.07, EPIC-SYS-S10-Func.08-SV.09,EPIC-SYS-S10-Func.08-SV.10** and **EPIC-SYS-S10-Func.08-M.02** These requirements cannot be checked, since there is no information available from Rocket Lab. This will be discussed with Rocket lab after the launch service agreement is signed by all parties. [38].
- **EPIC-SYS-S01-Config.04-GN.05** It has been decided, that there is no need for communication between the CubeSats. Every CubeSat communicates the location to the ground stations, where their relative location and coverage will be determined.
- **EPIC-SYS-S01-Config.07-T.04** The satellite is modelled as an isothermal node, so this requirement cannot be evaluated. However the temperature varies between 18.8°C and 36°C, hence the difference will not exceed 17.2°C.
- **EPIC-SYS-S01-Config.01-RP.08** The changes in electron temperature of the INMS can be measured between 0.1eV to 28eV. Although this does not meet the requirement set in the baseline report, this is still considered accurate enough to provide reliable data.
- **EPIC-SYS-S01-Config.01-RP.09** The measurement of total electron content will not be done during the EPIC mission. This sensor was eliminated in the trade-off. [31]
- **EPIC-SYS-S01-Config.01-RP.11** The sensors can measure magnetic oscillations with a sensitivity of 6.5nT. Although this does not meet the requirement set in the baseline report, this is still considered accurate enough to provide reliable data.
- **EPIC-SYS-S01-Config.04-GN.01** to **EPIC-SYS-S01-Config.04-GN.04** This is done by the ADCS.

19.1.4. BUDGET COMPLIANCE
In Table 19.6 the compliance to the available budget is summarised. From the table it can be seen that the design of the EPIC CubeSats fits within the budgets.

19.1.5. CONCLUSION
From the requirements compliance matrices and feasibility analysis presented in the previous sections, it can be concluded, that the EPIC earthquake precursor small satellites constellation meets the bigger part of the requirements set in the baseline report. [40] The requirements that are not complied to, cannot be checked yet, but will be verified during the test phase. In this final report a solid design is presented, that fits the budgets and constraints.

Table 19.2: Compliance matrix for the system requirements of the EPIC mission, part 1

Identifier	Requirement	✓ / ✗
Functional		
EPIC-SYS-S01-Func.01	The small satellite constellation shall measure changes in the ionosphere to confirm a link with seismic activity on earth.	✓
EPIC-SYS-S02-Func.02	The small satellite constellation shall search for signatures for earth-quakes of magnitude M > 7.	✓
EPIC-SYS-S02-Func.03	The small satellite constellation shall detect the earthquakes at least 36 hours in advance.	✓
EPIC-SYS-S01-Func.03.2	The CubeSats shall be deployed by a proven deployment mechanism.	✓
EPIC-SYS-S01-Func.04.1	Each CubeSat shall command its own subsystems by an on board data handling unit.	✓
EPIC-SYS-S05-Func.05	Each CubeSat shall de-orbit after the operational lifetime is over.	✓
EPIC-SYS-S01-Func.06	Each CubeSat shall determine its position with respect to the earth's surface.	✓
EPIC-SYS-S01-Func.07	Each CubeSat shall be able to control its attitude to comply with the payload pointing accuracy requirements.	✓
EPIC-SYS-S05-Func.08	Each CubeSat shall maintain its orbit for at least three years.	✓
EPIC-SYS-S01-Func.09	The small satellite constellation shall provide its own power supply.	✓
EPIC-SYS-S01-Func.10	Each CubeSat shall control its internal temperature to stay within the operational limits of all subsystems.	✓
Configuration		
EPIC-SYS-S01-Config.01	Each CubeSat shall accommodate a scientific payload able to measure the electrical and magnetic fields and their perturbations in the ionosphere.	✓
EPIC-SYS-S01-Config.02	The CubeSats shall have a command and communications subsystem capable of establishing a data link with ground stations on Earth.	✓
EPIC-SYS-S01-Config.03	The CubeSats shall have an electrical power supply subsystem capable of supplying enough power for all on board systems.	✓
EPIC-SYS-S01-Config.04	The CubeSats shall have a guidance navigation and control subsystem that determines the CubeSats position with respect to the earth's surface.	✓
EPIC-SYS-S01-Config.05	The CubeSats shall have an attitude determination and control subsystem	✓
EPIC-SYS-S05-Config.06	The CubeSats shall have a propulsion system that is capable of orbit insertion, orbit maintenance and de-orbiting.	✗
EPIC-SYS-S01-Config.07	The CubeSats shall have a thermal control subsystem.	✓
Interface		
EPIC-SYS-S09-Inter.01	Each CubeSat shall be connected to the launcher by a CubeSat-launcher interface.	✓
EPIC-SYS-S09-Inter.02	The CubeSats shall fit within the launcher dispensers.	✓
EPIC-SYS-S09-Inter.03	The CubeSats shall have a structure which withstands the structural loads specified by the launch contractor plus a safety factor of 1.2.	✓
EPIC-SYS-S09-Inter.04	The CubeSats shall have a structure which withstands the vibrational loads specified by the launch contractor plus a safety factor of 1.2.	✓
EPIC-SYS-S04-Inter.05.1	The small satellite constellation's housekeeping data shall be monitored by ground stations.	✓
EPIC-SYS-S01-Inter.06	The small satellite constellation shall send the acquired scientific data to the ground stations.	✓
EPIC-SYS-S01-Inter.07	The scientific data shall be distributed to the scientific institutes and authorities.	✓
Environmental		
EPIC-SYS-S14-Env.03.1	The CubeSats shall not pose a health threat during manufacturing due to toxicity of materials	✓
Quality factor		
EPIC-SYS-S02-Qf.01.1	Each CubeSat shall have a operational reliability of at least 52% for the intended lifetime.	✓
EPIC-SYS-S02-Qf.02.2	The duty cycle of the sensors shall be at least 50%.	✓
EPIC-SYS-S02-Qf.03	The probability of false negatives (undetected earthquakes) shall be lower than <tbd> for earthquakes of a magnitude M> <tbd>.	✗
EPIC-SYS-S02-Qf.04	The probability of false positives (false alarms) shall be lower than <tbd> for earthquakes of a magnitude M> <tbd>.	✗

Table 19.3: Compliance matrix for the system requirements of the EPIC mission, part 2

Identifier	Requirement	✓ / ✗
Operational		
EPIC-SYS-S11-OP.01	The full operative lifetime of the small satellite constellation shall be at least5 years	✓
EPIC-SYS-S11-OP.02	The lifetime of each CubeSat of the constellation shall be at least 3 years.	✗
EPIC-SYS-S04-OP.03	The satellite constellation shall cover all regions prone to earthquakes as defined by data of the International Seismological Centre.	✓
EPIC-SYS-S04-OP.04	The ground operations shall be managed by the TU Delft ground station or GENSO. Only if down link time provided by these is not sufficient, other ground stations can be considered	.✗
EPIC-SYS-S04-OP.05	The small satellite constellation shall be operated by qualified personnel	✓
EPIC-SYS-S08-OP.06	The small satellite constellation shall comply with ITU regulations.	✓
EPIC-SYS-S09-OP.07	The small satellite constellation shall have a revisit less than 4 hours for the covered area.	
Physical		
EPIC-SYS-S09-Phy.01	Each CubeSat shall have a maximum size of 10 x 20 x 30 cm (6U).	✓
EPIC-SYS-S09-Phy.02	Each satellite shall have a maximum mass that complies with the dispenser requirements.	✓
EPIC-SYS-S09-Phy.03.1	Each subsystem shall fit within or be attached to the CubeSat's structure.	✓
Support		
EPIC-SYS-S11-Sup.01	The CubeSats shall be launched with currently available launch systems.	✓
EPIC-SYS-S11-Sup.02	The small satellite constellation shall be designed using low cost available software.	✓
EPIC-SYS-S10-Sup.03	The CubeSats shall be tested in certified testing facilities	✓
Verification		
EPIC-SYS-S11-Ver.01	All requirements shall be verifiable.	✓
EPIC-SYS-S11-Ver.03	A verification plan for all subsystems shall be specified.	✓
Cost & schedule		
EPIC-SYS-S11-Cs.01.1	If a choice between a new design and a commercial of the shelf component has to be made and both systems meet the requirements, the COTS component shall be chosen.	✓
EPIC-SYS-S11-Cs.02	Each subsystem shall have an allocated mass budget.	✓
EPIC-SYS-S11-Cs.03	Each subsystem shall have an allocated cost budget.	✓
EPIC-SYS-S12-Cs.04	The draft version of the project plan shall be completed by the 28th of April 2017.	✓
EPIC-SYS-S12-Cs.05	The final version of the project plan shall be completed by 8th of May 2017.	✓
EPIC-SYS-S12-Cs.06	The draft version of the baseline report shall be completed by the 5th of May 2017.	✓
EPIC-SYS-S12-Cs.07	The Baseline review shall be completed by 8th of May 2017.	✓
EPIC-SYS-S12-Cs.08	The final version of the baseline report shall be completed by $1>^{th}$ of June 2017.	✓
EPIC-SYS-S12-Cs.09	The draft version of the midterm report shall be completed by the 26th of May 2017.	✓
EPIC-SYS-S12-Cs.10	The midterm review shall be completed by 29th of May 2017.	✓
EPIC-SYS-S12-Cs.11	The final version of the midterm report shall be completed by $8>^{th}$ of June 2017	✓
EPIC-SYS-S12-Cs.12	The jury summary shall be completed by 22th of June 2017.	✓
EPIC-SYS-S12-Cs.13	The draft version of the Final report shall be completed by 23th of June 2017.	✓
EPIC-SYS-S12-Cs.14	The Final review shall be completed by 26th of June 2017.	✓
EPIC-SYS-S12-Cs.15	The poster of the DSE project shall be completed by 29th of June 2017.	✓
EPIC-SYS-S12-Cs.16	The final version of the Final report shall be completed by 4th of July 2017.	✓
EPIC-SYS-S12-Cs.17	The executive summary shall be completed by 5th of July 2017.The final presentation shall be completed by 6th of July 2017.	✓
EPIC-SYS-S12-Cs.18	The final presentation shall be completed by 6th of July 2017.	✓
EPIC-SYS-S12-Cs.19	Status meetings with the principle tutor and project coaches shall be performed weekly.	✓
EPIC-SYS-S12-Cs.20	A logbook outlining all important decisions and meeting minutes shall be maintained during the project.	✓
EPIC-SYS-S12-Cs.21	A personal appendix containing feedback about the design, the team process and personal contribution shall be made available to the principle tutor and coaches at the moment of the midterm and final report.	✓

Table 19.4: Compliance matrix for the subsystem requirements of the EPIC mission, part 1

Identifier	Requirement	✓ / ✗
Launch		
EPIC-SYS-S09-Inter.01-L.01	The CubeSats shall be designed to accommodate ascent venting per ventable volume/area <2000inch.	✓
EPIC-SYS-S09-Func.08-L.02	Random vibration testing shall be performed to the levels and duration as defined by the launch contractor.	✓
EPIC-SYS-S09-Inter.01-L.03	The dispensers shall be acceptance and quality tested.	✓
EPIC-SYS-S09-Inter.02-L.05	No components on the CubeSat faces shall exceed 10mm normal to the surface.	✓
EPIC-SYS-S09-Func.08-L.06	The launch vehicle shall command deployment of the dispenser's CubeSats.	✓
EPIC-SYS-S09-Func.08-L.07	The launch vehicle shall not deploy the CubeSats in a trajectory that will contact the primary mission in case of piggy backing or the launch vehicle itself.	✓
EPIC-SYS-S09-Func.08-L.08	No debris shall be generated that will inhibit separation.	✓
Structural/Vibrational		
EPIC-SYS-S10-Func.08-SV.02	The CubeSat shall meet the structural requirements outlined in NASA's GSFC-STD-7000A.	✗
EPIC-SYS-S10-Func.08-SV.03	The maximum mass of each CubeSat shall be 12kg.	✓
EPIC-SYS-S10-Func.08-SV.04	The CubeSat shall withstand an acceleration load of at least 9.9g in axial direction and 0.3g in lateral direction (this includes a safety factor of 1.5).	✓
EPIC-SYS-S10-Func.08-SV.05	The CubeSat shall have a natural frequency higher than 45Hz.	✓
EPIC-SYS-S10-Func.08-SV.06	The CubeSat shall withstand a thermal gradient across its longest cross section of 40°C where 0°C is the minimum and 40°C is the maximum.	✓
EPIC-SYS-S10-Func.08-SV.07	The CubeSat shall withstand a random vibration level of at least <tbd>.	✗
EPIC-SYS-S10-Func.08-SV.08	Deployables shall be constrained by the CubeSat, not the dispenser.	✓
EPIC-SYS-S10-Func.08-SV.09	The CubeSat shall withstand a mechanical shock level of at least <tbd>.	✗
EPIC-SYS-S10-Func.08-SV.10	The CubeSat shall withstand a vibro-acoustic level of at least <tbd>.	✗
Material		
EPIC-SYS-S14-Env.03-M.01.2.1	Any toxic material during production of the CubeSat shall con-form to the regulations of the University of Southern California Environmental Health and Safety.	✓
EPIC-SYS-S10-Func.08-M.01.3	The least flammable materials shall be used.	✓
EPIC-SYS-S10-Func.08-M.01.4	Materials that will not burn readily upon ignition shall be used	✓
EPIC-SYS-S10-Func.08-M.01.5	Materials, including leakage, shall not come in contact with a non-compatible material that can cause a hazard.	✓
EPIC-SYS-S10-Func.08-M.01.6	Hazardous materials shall not retain a static charge that presents an ignition source to ordnance or propellants or a shock hazard to personnel.	✓
EPIC-SYS-S10-Func.08-M.02	Materials used in the structure shall feature the same coefficient of thermal expansion as the deployer.	
EPIC-SYS-S10-Func.08-M.03	The CubeSat rails and standoffs, which contact the dispenser rails and ejector plate, shall be hard anodised aluminium to prevent any cold welding within the dispenser.	✓
EPIC-SYS-S14-Env.03-M.04	No radioactive materials shall be used.	✓
EPIC-SYS-S10-Func.08-M.05	Typically, Aluminium 7075, 6061, 6082, 5005, and/or 5052 are used for both the main CubeSat structure and the rails. If materials other than aluminium are used, the Mission Integrator or dispenser manufacturer shall be contacted	✗
EPIC-SYS-S10-Func.08-M.06	CubeSat materials shall have a total mass loss <1.0%.	✓
EPIC-SYS-S06-Func.08-M.08	The materials used shall withstand a temperature range of 0°C to 0°C.	✓
Payload		
EPIC-SYS-S01-Func.01-RP.01	The CubeSat shall fly lower than 1,000km.	✓
EPIC-SYS-S01-Func.01-RP.02	The CubeSat shall fly within 800km from the future epicentre.	✓
EPIC-SYS-S01-Config.01-RP.04	The CubeSats measurements shall be taken for latitudes of $60°C$.	✓
EPIC-SYS-S01-Config.01-RP.06	The electric field sensor shall have an accuracy of at least 10 μV/m.	✓
EPIC-SYS-S01-Config.01-RP.07	The CubeSats shall measure the changes in the electron density within the range of $1 \cdot 10^8$ - $5 \cdot 10^{11}$ m $^{-3}$.	✓
EPIC-SYS-S01-Config.01-RP.08	The CubeSats shall measure the changes in the electron temperature within the range of 0.052eV and 0.86eV.	✗
EPIC-SYS-S01-Config.01-RP.09	The CubeSats shall measure the changes in the total electron content with an accuracy of <tbd>.✗	
EPIC-SYS-S01-Config.01-RP.11	The CubeSats shall be capable of measuring magnetic oscillations within the range of 0.2-3nT.	✗

Table 19.5: Compliance matrix for the subsystem requirements of the EPIC mission, part 2

Identifier	Requirement	✓ / ✗
GN&C		
EPIC-SYS-S01-Config.04-GN.01	The GN&C subsystem shall measure the spacecraft's position of centre of mass.	✗
EPIC-SYS-S01-Config.04-GN.02	The GN&C subsystem shall maintain the spacecraft's position of centre of mass.	✗
EPIC-SYS-S01-Config.04-GN.04	The GN&C subsystem shall provide less than 1° position accuracy.	✗
EPIC-SYS-S01-Config.04-GN.05	The GN&C subsystem shall estimate the relative state of other CubeSats in the constellation.	✗
ADCS		
EPIC-SYS-S01-Config.05-A.01.1	The ADC subsystem shall provide the pointing accuracy required by the sensors.	✓
EPIC-SYS-S01-Config.05-A.02	The ADC subsystem shall provide less than 1° pointing accuracy.	✓
EPIC-SYS-S01-Config.05-A.03	The ADC subsystem shall provide less than 1° control accuracy.	✓
EPIC-SYS-S01-Config.05-A.04	The ADC subsystem shall provide less than 1° pointing stability.	✓
Communication		
EPIC-SYS-S01-Config.02-C.01	The communication subsystem shall be able to transmit data to the ground system.	✓
EPIC-SYS-S01-Config.02-C.02.1	The CubeSat shall be able to sent its housekeeping data to the ground system.	✓
EPIC-SYS-S04-Inter.05-C.03	The ground system shall be able to track the spacecraft	✓
EPIC-SYS-S04-Inter.06-C.04	The ground system shall be able to receive and transmit data to the satellites	✓
EPIC-SYS-S01-Config.02-C.05	The ground system shall be an already existing system.	✓
EPIC-SYS-S01-Config.02-C.07	The communication subsystem shall communicate in S-band.	✓
EPIC-SYS-S01-Config.02-C.08	The communication subsystem shall have a BER of less than 10^{-5}.	✓
EPIC-SYS-S01-Config.02-C.09	The communication subsystem shall have a bandwidth of a least <tbd>.	✓
Power/propulsion		
EPIC-SYS-S05-Config.03-P.01	The CubeSat power subsystem shall provide a nominal power of at least 14W.	✓
EPIC-SYS-S05-Config.03-P.02	The battery life shall be at least three years.	✓
EPIC-SYS-S05-Config.03-P.03	The CubeSat shall have at least a 5V rechargeable battery.	✓
EPIC-SYS-S05-Config.03-P.04	The CubeSat shall incorporate battery circuit protection for charging/discharging to avoid unbalanced cell conditions.	✓
EPIC-SYS-S05-Config.06-P.05	The propulsion subsystem of the CubeSat shall provide a Δv of 235m/s.	✓
Thermal/radiation		
EPIC-SYS-S01-Config.07-T.01	The CubeSat shall have a passive thermal control system.	✓
EPIC-SYS-S01-Config.07-T.02	The CubeSat shall maintain a temperature between 0°C and 40° when operational	✓
EPIC-SYS-S01-Config.07-T.03	he CubeSat shall maintain a temperature between 0°C and 40°C when non-operational.	✓
EPIC-SYS-S01-Config.07-T.04	The difference between the hot side and cold side shall not exceed 30°C	✗
EPIC-SYS-S01-Func.08-T.05	The CubeSat shall withstand a radiation level of 15krad.	✓

Table 19.6: Compliance of the EPIC mission to budget constraints

Budget	Required value	Designed value
Cost [M€]	50	49.2
Volume [U]	6	6
Weight [kg]	12	11.24
Δv [m/s]	235	270

19.2. SENSITIVITY ANALYSIS

To determine the feasibility of the design, a sensitivity analysis is made. The sensitivity of the design to major changes in the system parameters are examined. The analysis is limited to the change in parameters which have an impact on multiple subsystems.

The system parameters, analysed in this section, and their current value can be found in Table 19.7. These parameters are analysed based on their influence on the design. For each sensitivity parameter, the effect on the performance of each aspect of the mission is determined. A list of the affected aspects and performance parameters can be found in Table 19.8. The aspects and performance parameters, not affected by any of the sensitivity parameters, are left out.

Table 19.7: Sensitivity parameters including design value

Sensitivity parameters	Design value	Unit
Orbital height	520	km
Budget	50	M€
Propulsion-less mass	5.6	kg
Increased sampling rate and data to OBC	16.7	kbits/s
Power generation	14	W
Inclination	55	°
Solar flux	65	SFU

Table 19.8: Effected parameters including design value

Aspects	Effected parameters	Design value	Unit
Payload	Scientific yield/duty cycle	Optimal conditions	-
ADCS	Pointing accuracy	1	°
Constellation	Constellation performance	Optimal conditions	-
Launcher	Take-off weight	11.2	kg
OBDH	Processing Power	Over designed	-
TT&C	Down-link	6.4	W
Thermal	Temperature range	17.52 - 34.05	℃
Availability	Number of satellites	46	-
Sustainability	Orbital Lifetime	15.7	years

In the analysis, quantitative changes to the performance parameters are preferred. However, not every effect of a change can be quantified. Hence also qualitative comparisons are made. Most system parameters have been varied by 20%. The solar flux however, has been considered at solar minimum in the report. Therefore the parameter has instead been increased to high, and max solar activity.

The result of the sensitivity analysis can be found in Table 19.9. From the table it is derived that the project is unfeasible during periods of high solar activity. Inclination has a negligible impact on all affecting categories, except for the constellation where the performance would be decreased from 99% to 96%. An increase in available power would allow for a higher down-link rate while a reduction in power would reduce the down-link rate and scientific yield. Next, boosting the sampling rate would increase scientific yield but increase transmission power. Reducing the sample rate would have the same but opposite effect. Changing the budget would have a minimal, or no effect, on most systems, except for the number of satellites and the resulting availability. Finally, changing the altitude would negatively impact deployment time. Furthermore, reducing the height to 450km would be detrimental to the orbital lifetime.

To conclude, the design remains feasible with 20% change to the sample rate, generated power, inclination and budget. In comparison, reducing the height by 15%, is detrimental to the mission, and is therefore critical. Similarly increasing the propulsion-less mass by 20% causes an unacceptable increase to the launch mass. Most critical, is the solar flux. The mission can only be launched during minimal solar activity, to guarantee sufficient orbital life, and pointing accuracy. During the planned operational phase, see Section 3.2, a solar minimum is expected, hence without delays no problems are expected.

Table 19.9: Sensitivity analysis matrix. Cells highlighted in red indicate unfeasible changes for the subsystem to meet its requirement. Yellow indicates a reduction in performance of the subsystem. A cell is coloured blue, when the impact of the change on the subsystem is negligible, or no design changes are needed. Finally the greens cells are used for subsystems which improve performance due to the change.

Parameters	Iteration	Scientific yield/duty cycle	Pointing accuracy [°]	Constellation performance	Take-off weight [kg]	Processing Power	Down-link	Temperature range [°C]	Number of satellites [-]	Oribital Lifetime [years]
Height	600 km	No effect	Changes less than 0.1	Deployment time becomes 7.8 month	No effect	No effect	More power required	17.72 - 34.47	No effect	15.8
	450 km	No effect	Changes less than 0.1	Deployment time of 9.6 months	No effect	No effect	Less power required	17.30 - 33.56	No effect	3.72
Budget	60 M€	No effect	No effect	No effect	No effect	No effect	Negligible	No effect	58	No effect
	40 M€	No effect	No effect	No effect	No effect	No effect	Negligible	No effect	35	No effect
Propulsionless mass	6.8 kg	No effect	Negligable	No effect	13.6	No effect	No effect	No effect	No effect	17.8
	4.5 kg	No effect	Negligable	No effect	9.4	No effect	No effect	No effect	No effect	12.5
Increased sampling rate and data to OBC	20 kbits/s	More data collected	No effect	No effect	No effect	Capable of handling	More power required	No effect	No effect	No effect
	13 kbits/s	Insufficient data collected	No effect	No effect	No effect	Capable of handling	Less power required	No effect	No effect	No effect
Power generation	16 W	Optimal condition	No effect	No effect	No effect	No effect	More power available	No effect	No effect	No effect
	10 W	Lower duty cycle	No effect	No effect	No effect	No effect	Less power available	No effect	No effect	No effect
Inclination	60°	No effect	Negligable	Lower coverage	No effect	No effect	Negligable	Not applicable	No effect	15.8
	50°	No effect	Negligable	Lower coverage	No effect	No effect	Negligable	Not applicable	No effect	15.5
Solar flux	140 SFU	Considerable effect of anomolies	2	No effect	No effect	No effect	No effect	Not applicable	No effect	2.2
	240 SFU	Effect anomolies unacceptable	51	No effect	No effect	No effect	No effect	Not applicable	No effect	0.72

<div align="right">

20

</div>

CONCLUSION AND RECOMMENDATIONS

In this chapter, the conclusions and recommendations of the preliminary design are discussed. From the preliminary design, major aspects of the mission were determined. Firstly, the EPIC satellites have a 6U form factor. Their payload consists of a magnetometer, dosimeter, Langmuir probe, electric field sensor and either an ion neutral mass spectrometer or retarding potential analyser. The scientific data gathered by the payload, is sent using S-band to the KSAT lite ground system. Power is provided by 35 solar cells mounted on the side of the spacecraft bus, and by 84 cells mounted on deployable panels. The spacecraft are launched to an altitude of 520km and 55.5° inclination, using the Rocket Lab dedicated launchers. Next the satellites are distributed to form a Walker 55.5 6/6/2 constellation with natural orbital perturbations. These perturbations are controlled by changing the orbital height to 670km or 432km with the propulsion system. More detail will be added to the design during future design phases.

The spacecraft are designed to continuously measure with 99% coverage and a four hour revisit time. The data is available with 30 arcsec pointing knowledge, 1° pointing accuracy, and down-linked within at least 12 hours. Additionally, the on-board computer is capable of continuous data acquisition, compression, and transmission of all data gathered. To electrically support these systems, the electric power system provides 14.2W nominal power and has a battery capacity of 106Wh. Thermal control ensures an operating temperature between 18.6°C and 35.2°C. Finally, the constellation is deployed within 6 months, and is expected to have an availability of 75% over its operational life. From these performance parameters, it can be concluded that the constellation provides a unique, unprecedented service to measure earthquake precursors.

Several steps are taken to provide confidence that the design is worth the investment, and is proficient, accurate, and feasible. Firstly, the market analysis shows that the yearly economic loss due to earthquakes is on average 45 billion USD. Hence, the value of earthquake prediction could reach well beyond the 50 million euro cost of the constellation. The group organisation, project design, development logic, and approach to sustainability provide confidence that the design philosophy has resulted in a proficient design. To ensure that decisions and calculations are logical and accurate, extensive verification and validation is performed. Furthermore, the project has made extensive use of expert opinions.

Feasibility is assured through risk management, compliance matrix and sensitivity analysis. The risk map shows that through risk mitigation the potential risks have been reduced significantly. The compliance matrix has identified the requirements which are not yet met. It is however expected that in following design phases, these requirements will be met. The sensitivity analysis shows that the design is limited by a minimum altitude, propulsion-less mass and solar minimum. Other concerns are the launcher reliability (Rocket Lab) and the unknown limitations of earthquake precursors. Despite these limitations, the design is considered feasible, good, accurate and worth the investment.

With the preliminary design completed, an outline for the continuation of the project is made. The next phase of the project is the detailed design, and is expected to take one year. In this phase the design is completed, bandwidth is reserved, public relations are set up, funding is sought and the commercial off the shelf (COTS) components are ordered. This is followed by nine months of production and qualification where the manufacturing, assembly, integration and testing of the satellites takes place. Next the utilisation phase begins where the constellation is expected to launch March 2019, followed by six months of deployment. The phase continues with the operations of the constellation until the end of life.

For the detailed design phase, the following recommendations are made:

- By the end of the detailed design, a full simulation of the operational life time with optimal maintenance strategy shall be performed.

- Build a working prototype of the spacecraft, by the end of the detailed design.

- Throughout the detailed design, create an up to date failure database to update the spacecraft reliability, using data from satellites of similar quality.

- Make a thermal fatigue analysis for the ISIS structure, before the start of the qualification process.

- Receive and verify performance of COTS components during the first half of the detailed design phase.

- Once the code of the satellite is complete (expected before the end of the detailed design), the code shall be simulated on hardware emulator.

BIBLIOGRAPHY

[1] Pulinets, S., and Boyarchuk, K., *Ionospheric Precursors of Earthquakes*. Springer, 1st ed., 2004.

[2] Erbest, M., and Anderson, M. A., "The Dynamics of Faulting," *Geological Society*, vol. 367, pp. 231 – 246, 1905.

[3] Kanamori, H., "The energy release in great earthquakes," *Journal of Geophysical Research*, vol. 82, no. 20, pp. 2981–2987, 1977.

[4] Dobrovolsky, I. P., Zubkov, S. I., and Miachkin V. I., "Estimation of the Size of Earthquake Preparation Zones," *Pure and Applied Geophysics*, vol. 117, no. 5, pp. 1025–1044, 1979.

[5] Utkin, V. I., and Yurkov, A. K., "Radon as a "Deterministic" Indicator of Natural and Industrial Geodynamic Processes," *Doklady Earth Sciences*, vol. 427, no. 5, pp. 833–836, 2009.

[6] Liperovsky, V. A., Pokhotelov, O. A., Meister, C. V., and Liperovskaya, E. V., "Physical Models of Coupling in the Lithosphere-Atmosphere-Ionosphere System before Earthquakes," *Geomagnetism and Aeronomy*, vol. 48, no. 6, pp. 795–806, 2008.

[7] Kuo, C. L., Lee, L. C., and Huba, J. D., "An Improved Coupling Model for the Lithosphere-Atmosphere-Ionosphere System," *Journal of Geophysical Research: Space Physics*, vol. 119, no. 4, pp. 3189–3205, 2014. 2013JA019392.

[8] Chmyrev, V. M. , Isaev, N. V., Bilichenko, S. V., and Stanev, G.", "Observation by Space-Borne Detectors of Electric Fields and Hydromagnetic Waves in the Ionosphere over an Earthquake Centre," *Physics of the Earth and Planetary Interiors*, vol. 57, no. 1, pp. 110–114, 1989.

[9] Parrot, M., Achache, J., Berthelier, J. J., Blanc, E., Deschamps, A., Lefeuvre, F., Menvielle, M., Plantet, J. L., Tarits, P., and Villain, J. P., "High-Frequency Seismo-Electromagnetic Effects," *Physics of the Earth and Planetary Interiors*, vol. 77, no. 1, pp. 65–83, 1993.

[10] M. Cahyadi and K. Heki, "Ionospheric Disturbances of the 2007 Bengkulu and the 2005 Nias Earthquakes, Sumatra, Observed with a Regional GPS Network," *Journal of Geophysical Research: Space Physics*, vol. 118, no. 4, pp. 1777–1787, 2013.

[11] Astafyeva, E., and Heki, K., "Dependence of Waveform of Near-Field Coseismic Ionospheric Disturbances on Focal Mechanisms," *Earth, Planets and Space*, vol. 61, no. 7, pp. 939–943, 2009.

[12] Pulinets, S. A., and Legen'ka, A. D., "Spatial–Temporal Characteristics of Large Scale Disturbances of Electron Density Observed in the Ionospheric F-Region before Strong Earthquakes," *Cosmic Research*, vol. 41, no. 3, pp. 221–230, 2003.

[13] Liu, J. Y., Chen, Y. I., Chen, C. H., Liu, C. Y., Chen, C. Y., Nishihashi, M., Li, J. Z., Xia, Y. Q., Oyama, K. I., Hattori, K., and Lin, C. H., "Seismoionospheric gps total electron content anomalies observed before the 12 may 2008 mw7.9 wenchuan earthquake," *Journal of Geophysical Research: Space Physics*, vol. 114, no. A4, pp. n/a–n/a, 2009. A04320.

[14] Daniell, J. E., Khazai, B., Wenzel, F., and Vervaeck, A., "Remote Sensing Technologies and Global Markets," *BCC research*, 2012.

[15] Shearer, P. M., and Stark, P. B., "Global Risk of Big Earthquakes has not Recently Increased," *Proceedings of the National Academy of Sciences*, vol. 109, no. 3, pp. 717–721, 2012.

[16] Evans, N., "The earthquake's impacts on buildings and infrastructure," in *proceedings of a workshop on Recovery following the Gisborne Earthquake*, (Wellington, New Zealand), Opus International Consultants, 2009.

[17] Wilson, J., "The Worldwide Economic Impact of Historic Earthquakes," *World Conference on Earthquake Engineering*, 2016.

[18] Porter, M. E., "The Five Competitive Forces That Shape Strategy," *Harvard Business Review*, vol. 86(1):78-93, 137, February 2008.

[19] Akhoondzadeh, M., Parrot, M., and Saradjian, M. R., "Electron and ion density variations before strong earthquakes (m>6.0) using demeter and gps data," *Natural Hazards and Earth System Sciences*, vol. 10, no. 1, pp. 7–18, 2010.

[20] Verhagen, W., and Mooij, E., "PMSE Workshop 2," in *Project Management and Systems Engineering in DSE*, (Delft, Netherlands), April 2017.

[21] Curran, R., and Verhagen, W., "Lecture 9, Concurrent Engineering & Design for Lifecycle," in *Systems Engineering and Aerospace Design course by Delft University of Technology*, March 2017.

[22] Di Domizio, D., and Gaudenzi P., "A Model for Preliminary Design Procedures of Satellite Systems," *Concurrent Engineering: Research and Applications*, vol. 16, no. 2, pp. 149–159, 2008.

[23] Decker, Z. S., "A Systems-Engineering Assessment of Multiple CubeSat Build Approaches," unpublished master's thesis, Massachusetts Institute of Technology, Cambridge, USA, June 2016.

[24] ISIS - Innovative Solutions In Space, *Private conversations with ISIS - Innovative Solutions In Space*, (Delft, Netherlands), May 2017. Report available as private document.

[25] *Private conversation with the Hyperion engineers*, June 2017. Report available as private document.

[26] *Private conversations with Dr. A. Menicucci - Delft University of Technology*, June 2017. Report available as private document.

[27] Faculty of Aerospace Engineering, *Private conversations with M.Ş. Uludağ -* , (Delft, Netherlands), May 2017. Report available as private document.

[28] Heizer, J., and Render, B., *Operations Management*. Pearson, 2014.

[29] Fortescue, P., Stark, S., and Swinerd, G., *Spacecraft Systems Engineering*. Wiley, 3rd ed., 2003.

[30] The CubeSat Program, "6U CubeSat Design Specification Rev. Provisional," *California Polytechnical State University*, 2016.

[31] Bayer, H. E., Kool, B., Maene, J. C., Marsman, C. P., Neuteboom, Y. L., Polydorou, S., Ricke, C. M., Nevinskaia, A. S., and Vakaet, C. E. I., "DSE - Small Satellites Constellation for Earthquake Precursors, Midterm Report," *Delft University of Technology*, 2017.

[32] *Private conversations with J. Laifr - SkyFox Labs*, June 2017. Report available as private document.

[33] GomSpace ApS, *NanoCom TR-600*. GomSpace ApS, 1.1 ed., 2016.

[34] GomSpace ApS, *NanoCom ANT2000*. GomSpace ApS, 1.0 ed., 2016.

[35] GomSpace ApS, *NanoComANT-6F Antenna System*. GomSpace ApS, Aalborg East, Denmark, 2016.

[36] GomSpace ApS, *NanoCom AX100 Datasheet*. GomSpace ApS, Aalborg East, Denmark, 2016.

[37] Seto-Mook, T. K., "Kumu a'o CubeSat: Thermal sensors on a CubeSat," *University of Hawaii at Mānoa*, 2009.

[38] Rocket Lab, *Payload User's Guide*, 4.0 ed., december 2016.

[39] Wertz, J. R., and Larson, W. J., *Space Mission Analysis and Design*. Microcosm Press and Springer, third edition ed., 2007.

[40] Bayer, H. E., Kool, B., Maene, J. C., Marsman, C. P., Neuteboom, Y. L., Polydorou, S., Ricke, C. M., Nevinskaia, A. S., and Vakaet, C. E. I., "DSE - Small Satellites Constellation for Earthquake Precursors, Baseline Report," *Delft University of Technology*, 2017.

[41] International Seismological Centre, *On-line Bulletin*. International Seismological Centre, Thatcham, United Kingdom, 2014.

[42] Nishenko, S. P., and Buland, R., "A Generic Recurrence Interval Distribution for Earthquake Forecasting," *Seismological Society of America*, vol. 77, no. 4, pp. 1382–1399, 1987.

[43] Indrikis, J., and Cleave, R., "Proceedings of the Fifth Annual Conference on Small Satellites," in *25th AIAA/USU Conference on Small Satellites*, AIAA/ Utah State University, Academic Press, 1991.

[44] Robusto, C. C., "The Cosine-Haversine Formula," *The American Mathematical Monthly*, vol. 64, no. 1, pp. 38–40, 1957.

[45] Beech, T.W., "A Study of Three Satellite Constellation Design Algorithms," in *International Symposium on Space Flight Dynamics*, ESA-ESTEC, Noordwijk., 1999.

[46] Rummel, R., and Peters, T., "Reference Systems in Satellite Geodesy," in *TUM Summer School*, Institut für Astronomische und Physikalische Geodäsie Technische Universität München , 2001.

[47] Nunes, M. A., "Satellite Constellation Optimization Method for Future Earth Observation Missions Using Small Satellites," in *13th International Space Conference of Pacific-basin Societies (ISCOPS)*, (Space Flight Laboratory, Mechanical Engineering Department, University of Hawaii at Manoa), 2012.

[48] Walker, J. G., "Satellite Constellations," *Space Technology*, vol. 37, pp. 559 – 572, 1984.

[49] Lansard, E., Frayssinhes, E., and Palmade, J. L., "Global Design of Satellite Constellations: a Multi-Criteria Performance of Classical Walker Patterns and New Design Patterns," *Acta Astronautica*, vol. 42, no. 9, pp. 555–564, 1998.

[50] Wertz, J. R., *Mission Geometry; Orbit and Constellation Design and Management*. Springer, 1st ed., 2001.

[51] Kim, I.Y., and de Weck, O.L., "Adaptive weighted-sum method for bi-objective optimization: Pareto front generation," *Structural and Multidisciplinary Optimization*, vol. 29, no. 2, pp. 149–158, 2005.

[52] Gen, M., and Cheng, R., *Genetic algorithms and engineering optimisation*. Wiley, 1st ed., 2006.

[53] Chmyrev, V., Smith, A., Kataria, D., Nesterov, B., Owen, C., Sammonds, P., Sorokin, V., and Vallianatos, F., "Detection and Monitoring of Earthquake Precursors: TwinSat, a Russia–UK Satellite Project," *Advances in Space Research*, vol. 52, pp. 1135–1145, September 2013.

[54] Crisp, N.H., Smith, K., and Hollingsworth, P., "Launch and deployment of distributed small satellite systems," *Acta Astronautica*, vol. 114, no. 3, pp. 65–78, 2015.

[55] C. J. Fong and W. T. Shiau and C. T. Lin and T. C. Kuo and C. H. Chu and S. K. Yang and N. L. Yen and S. S. Chen and Y. H. Kuo and Y. A. Liou and S. Chi, "Constellation Deployment for the FORMOSAT-3/COSMIC Mission," *IEEE Transactions on Geoscience and Remote Sensing*, vol. 46, no. 11, pp. 3367–3379, 2008.

[56] Lang, T. J., "Symmetric circular orbit satellite constellations for continuous global coverage," in *Proceedings of the AAS/AIAA Astrodynamics Conference*, (Kalispell, MT), 1988.

[57] Lang, T. J., "Spacecraft Observations of Electromagnetic Perturbations Connected with Seismic Activity," *Advances in the Astronomical Sciences*, vol. 114, no. 2, pp. 1127–1142, 2003.

[58] AMR Propulsion Innovations, *IFM Nano Thruster*. AMR Propulsion Innovations, 1.0 ed., 2016.

[59] GOMSpace, *NanoProp 6U propulsion system*. GOMSpace, 1.0 ed., 2016.

[60] Hyperion Technologies, Delft, Netherlands, *PM400 Series Propulsion Module*, 2016.

[61] Powell, S., Knop, T. and Engelen, S., "Experimental Evaluation of a Green Bi-Propellant Thruster for Small Satellite Applications," in *30th annual AIAA/USU Conference on Small Satellites*, (Logan, USA), AIAA, 2016.

[62] Zakirov, V., Sweeting, M., Lawrence, T. and Sellers, J., "Nitrous Oxide as a Rocket Propellant," *Acta Astronautica*, vol. 48, no. 5-12, pp. 353–362, 2001.

[63] Wicks, R. T., "QB50 Science Operations," *University of Oslo*, 2015. QB50-INMS-MSSL-PL-15001.

[64] *Private conversations with Dr. Masutti - Project Manager QB50*, June 2017. Report available as private document.

[65] *Private conversations with Mr Picozza - Principle Investigator CSES*, May 2017. Report available as private document.

[66] Bekkeng, T. A., "QB50 m-NLP Science Unit Interface Control Document," *University of Oslo*, 2016. QB50-UiO-ID-0001 M-NLP ICD.

[67] SkyFox Labs, *Digital CubeSat Dosimeter (piDOSE-DCD): Product Datasheet*, 2017.

[68] Fish, C.S., Swenson, C.M., Crowley, G., Barjatya, A., Neilsen, T., and Gunther, J., "Design, Development, Implementation, and Onorbit Performance of the Dynamic Ionosphere CubeSat Experiment Mission," *Space Dynamics Lab Publications*, 2014.

[69] Rodriguez, M., Paschalidis, N., Jones, S., Sittler, E., Chornay, D., Uribe, P., and Cameron, T., "Miniaturized Ion and Neutral Mass Spectrometer for CubeSat Atmospheric Measurements," in *30th AIAA/USU Conference on Small Satellites*, 2016.

[70] Chaudery, R. A., "QB50 INMS Science Unit Interface Control Document," *University College London*, 2015. QB50-INMS-MSSL-ID-12001 Issue 13.

[71] Earle, G. D., Davidson, R. L., and Perdue, M. D., "Thermal Plasma Instrumentation for CubeSat missions," in *24th Annual AIAA/USU Conference on Small Satellites*, (William B. Hanson Center for Space Sciences The University of Texas at Dallas), 2010.

[72] Sample, J. G., "The Stein Particle Detector," *Regents of the University of California The University of California, Berkeley*, 2015. AFRL-RV-PS-TR-2015-0094.

[73] Macdonald, M., and Badescu, V., *International Handbook of Space Technology*. Springer, 2014.

[74] Starin, S.R., and Eterno, J., "Attitude Determination and Control Systems."

[75] Wertz J.R., *Spacecraft Attitude Determination and Control*. Kluwer Academic Publishers, 1978.

[76] Rawashdeh, S.A., "Passive Attitude Stabilisation for Small Satellites," Master's thesis, University of Kentucky, United States of America, 2010.

[77] Riwanto, A.B., "CubeSat Attitude System Calibration and Testing ," Master's thesis, Aalto University, Helsinki, 2015.

[78] Pal, P. K., and Fox, S.M., "The Effects of Momentum Bias on a Gravity Gradient Stabilised Spacecraft with Active Magnetic Control," *Itahco, Inc.*

[79] Udrea, B., Nayak, M., and Ankersen, F., "Analysis of the Pointing Accuracy of a 6U CubeSat Mission for Proximity Operations and Resident Space Object Imaging."

[80] Clarke, M., Guo, J., Sanders, B and Gasiewskie, A., "Affordable and Accessible Attitude Control Validation Test Methods for CubeSats," in *67th International Astronautical Congress*, 2016.

[81] *Private conversation with TU Delft Ground Station crew*, June 2017. Report available as private document.

[82] GomSpace ApS, *NanoCom ANT430*. GomSpace ApS, 1.0 ed., 2016.

[83] Helical Communication Technologies, *L-band series*. HCT, Paterson Air Force Base, Ohio, 2016.

[84] Antenna Development Corporation, *Microstrip Patch Antennas*. Antenna Development Corporation, Las Cruces, Mexico, 2013.

[85] EnduroSat, *UHF/VHF Antenna – User Manual*. EnduroSat, Sofia, Bulgaria, 2016.

[86] Messenger, S. R., Walters, R. J., Summers, G. P., Morton, T. L., LaRoche, G., Signorini, C., Anzawa, O., and Matsuda, S., "Displacement damage dose analysis of the comets and equator-s space solar cell flight experiments," in *16th European Photovoltaic Solar Energy Conference*, 2000.

[87] Lower, C., Macdonald, M., and Greenland, S., "Through-life modelling of nano-satellite power system dynamics," in *64th International Astronautical Congress*, (Beijing, China), September 2013.

[88] Stewart, J., *Calculus: Early Transcendentals*. Cengage Learning, seventh edition ed., 2012.

[89] Kedare, S. S., and Ulrich, S., "Advances in the Astronautical Sciences Astrodynamics," *Applied Thermal Engineering*, vol. 156, no. 2, pp. 1231–1249, 2015.

[90] Rauschenbach, H. S., *Solar Cell Array Design Book*. Jet Propulsion Laboratory, 1st ed., 1976.

[91] Sirin, A., "Power System Analysis of J3 CubeSat and RATEX-J High Voltage Power Supply Calibration," master's thesis, Luleå University of Technology, Luleå, Sweden, September 2015.

[92] Saft, *Lithium-ion battery life*. Saftbatteries, 2016.

[93] Agencia Espacial Civil Ecuatoriana, *BA0X: 1U high capacity battery arrays*. Agencia Espacial Civil Ecuatorianas, 2016.

[94] Daocheng Huang, "How to Design an Isolated, High Frequency, Push-Pull DC/DC Converter," *LT Journal of Analog Innovation*, vol. 25, no. 2, pp. 25–29, 2015.

[95] Azurspace Solar Power GMBH, *30% Triple Junction GaAs Solar Cell Type: TJ Solar Cell 3G30C - Advanced*. Azurspace Solar Power GMBH, 2016.

[96] Hyperion Technologies, *iADCS400 Attitude Determination And Control System*, 2016.

[97] Innovative Solutions In Space, *Magnetometer Performance*. NewSpace Systems, Somerset West, South Africa, 2014.

[98] Crowley, G., Fish, C., Pilinski, M., and Azeem, I., "Constellation of CubeSats for Realtime Ionospheric E-Field Mearurements for Global Space Wheater," in *31st Space Symposium, Technical Track*, (Colorado Springs, Colorado, United States of America), 2015.

[99] SkyFox Labs, *Space-Friendly Active GPS-L1 Patch Antenna piPATCH-L1 Product Datasheet*. SkyFox Labs, Prague, Czech Republic, 2017.

[100] SkyFox Labs, *Space-Friendly CubeSat GPS Receiver/Next Generation piNAV-NG Product Datasheet*. SkyFox Labs, Prague, Czech Republic, 2017.

[101] Innovative Solutions In Space, *On Board Computer (iOBC)*, 2016.

[102] John L. Crassidis , *Angular Velocity Determination Directly from Star Tracker Measurements*. University at Buffalo, 2002.

[103] Hyperion Technologies, *CP400.85 Processing Platform*, 2016.

[104] Gomspace, *NanoMind Z7000 Datasheet On-board CPU and FPGA for space applications*, 2016.

[105] Gomspace, *NanoMind A3200 Datasheet On-board Computer System for mission critical space applications*, 2016.

[106] Microsemi cooperation, *UART-to-SPI interface - design example*, 2012.

[107] Boxtel, T. V., "Thermal Modelling and Design of the DelFFi Satellites," master thesis, Delft University of Technology, Delft, Netherlands, January 2015.

[108] Zandbergen B.T.C., *Aerospace Design & Systems Engineering Elements I Part: Spacecraft (bus) Design and Sizing*. Delft University Press, 3rd ed., 2015.

[109] Hibbeler R. C., *Mechanics of Materials*. Pearson, 9th ed., 2014.

[110] Megson T.H.G., *Aircraft Structures for Engineering Students*. Elsevier, 4th ed., 2011.

[111] Stabin G. M., *Radiation Protection and Dosimetry: An Introduction to Health Physics*. Sptinger, 1st ed., 2007.

[112] Gugliemo S. A., Richardson G., Quill P., "Launch Environment," *Encyclopedia of Aerospace Engineering*, 2010.

[113] Adriano Calvi, "Spacecraft Loads Analysis An Overview," in *University of Liege Satellite Engineering Class*, (ESA/ESTEC, Noordwijk, The Netherlands), 2011.

[114] Wijker J., *Spacecraft Structures*. Springer, 2008.

[115] Innovative Solutions In Space, *Solar Panels*. Innovative Solutions In Space, Delft, Netherlands, 2013.

[116] California Polytechnic State University, *6U CubeSat Design Specification Rev. PROVISIONAL*, x1 ed., May 2016.

[117] Hibbler, R. C., *Mechanics of Materials, 9th Edition*. Pearson, 2013.

[118] Brumbaugh, K. M., and Lightsey, E. G., "A Risk Management Plan for Cubesats," in *Conference Paper*, (Austin, Texas), American Insitute of Aeronautics and Astronautics (AIAA), 2012.

[119] Rabasa, G. O., *Methods for Dependability Analysis of Small Satellite Missions*. PhD thesis, Politecnico di Torino, 2015.

[120] Langer, M., and Bouwmeester, J., "Reliability of Cubesats – Statistical Data, Developers' Beliefs and the Way Forward," in *30th AIAA/USU Conference on Small Satellites*, 2016.

[121] L. Yu, "Probabilistic Verification of Satellite Systems for Mission Critical Applications, PhD thesis," *University of Glasgow*, 2016.

[122] Dubos, G. F., Castet, J. F., and Saleh, J. H., "Statistical Reliability Analysis of Satellites by Mass Category: Does Spacecraft Size Matter?," *Acta Astronautica*, vol. 67, no. 5–6, pp. 584–595, 2010.

[123] Guo, J., Monas, L., and Gill, E., "Statistical Analysis and Modelling of Small Satellite Reliability," *Acta Astronautica*, vol. 98, pp. 97–110, 2014.

[124] Engelen, S., *Swarm Satellites: Design, Characteristics and Applications*. TU Delft, 2016.

[125] Bobbio, A., "Dependability and Maintainability Theory and Methods: 5. Markov Models," in *IFOA Lecture Slides*, (Reggio Emilia, Italy), 2003.

[126] Kramer, Z., "Reliability Analysis and Artificial Intelligence: Markov Modelling," in *San Francisco Power & Energy Society Past Technical Presentations*, August 2011.

[127] *Private conversations with W. Verhagen - Delft University of Technology*, June 2017. Report available as private document.

[128] Hamann, R. J., and Tooren van, M. J. L., "Systems Engineering & Technical Management Techniques Part II: Issue 1," January 2006.

[129] Inter-Agency Space Debris Coordination Commitee, "IADC Space Debris Mitigation Guidelines," September 2007. IADC-02-01.

[130] Cornara, S., Beech, W. T., Bello-Mora, M., and Martinez de Aragon, A., "Satellite Constellation Launch, Deployment, Replacement and End-of-Life Strategies," in *13th Annual AIAA/USU Conference on Small Satellites*, 1999.

[131] Qiao, L., Rizos, C., and Dempster, G. A., "Analysis and Comparison of CubeSat Lifetime," in *Proceedings of the 12th Australian Space Conference, Sydney, Australia*, pp. 249–260, Citeseer, 2013.

[132] Centre National D'Etudes Spatiales, "Semi-analytic Tool for End of Life Analysis (STELA)," December 2010.

[133] Baiocchi D., Welser W., *Confronting space debris : strategies and warnings from comparable examples including deepwater horizon*. RAND Corporation, first edition ed., 2007.

[134] European Space Agency, "Meteoroid and Space Debris Terrestrial Environment Reference (MASTER)," December 2009.

[135] ECSS-E-ST-10-04 Working Group, "ECSS-E-ST-10-04C ," November 2008.

[136] Koningsberg Satellite Services, *KSAT lite*. Tromsø, Norway, 2015.

A

SPACECRAFT SYSTEM AND ASTRODYNAMIC CHARACTERISTICS

Table A.1 present the spacecraft system and astrodynamic characteristics of the EPIC mission.

Table A.1: Spacecraft System and Astrodynamic Characteristics

Characteristic	Value	Comments
Mass	11.2 [kg]	Including 20% contingency
Volume	6U	
Power	14.2 [W]	
Number of solar cells	119	
Battery capacity	106.4 [Wh]	
Propellant budget (liquid propellant)	880 [g]	
Telemetry data rate	UHF: 19.2 [kbits/s], S-band: [2 Mbits/s]	
Communications link budget	UHF: 8.75 [dB], S-band: 6.15 [dB]	
Memory size	2 x 2GB	
Pointing accuracy	1°	for ρ<2.7·10^{-13}kg/m^3 and D<0.013Am^2
Thrust, Nominal	0.3-0.8 [N]	Varies with temperature (-5℃ - 30 ℃)
Coverage	99%	Of earthquake prone area's
Revisit time	4 [hr]	
Mission duration	5+ [yr]	
Number of operational satellites per plane	2	
Number of planes	6	
Total number of satellites produced	46	
Ground station selection	Educational/scientific	
Launcher selection	Electron by Rocket Lab's	12 6U CubeSats per launch
EOL	Natural decay	Within 25 years
Inclination	55°	
Orbital period	5699 [s]	
Altitude	520 [km]	
Orbit	Circular	
Δv budget	270 [ms^{-1}]	Including 15% contingency
Deployment time	1 Launch: 6 [months]	
Temperature operating range	18.6°C - 35.2°C	
Temperature limits	0°C - 40°C	